Sheep Liver Cytosolic Aldehyde Dehydrogenase; A fresh perspective

A thesis presented in partial
fulfilment of the requirements
for the degree of

Master of Science in Chemistry

at

Massey University
New Zealand

Richard Malcolm Sime
1995

Abstract

The pre-steady-state mechanism of aldehyde dehydrogenase has been further investigated using synthesised deuterated 4-*trans*-(N,N-dimethylamino) cinnamaldehyde as a substrate.

Reporter groups of the active site of ALDH have indicated the presence of a divalent or trivalent metal electrophile, shown in chapter 3 as being either $Fe^{(II)}$ or $Fe^{(III)}$.

Studies of the spectral properties of NADH bound to aldehyde dehydrogenase have revealed the presence of at least two spectrally different enzyme-NADH species. The consequences of this information are important in interpretation of the kinetic data and understanding apparently contradictory experimental results from different research workers.

The steady-state kinetics of ALDH have been further investigated.

A sensitive substrate for use in enzyme immunoassays has been designed and synthesised. The preliminary kinetic behaviour observed using this substrate has been studied with three enzymes.

Aldehyde dehydrogenase has been used as a model system for studying the effects of electromagnetic radiation on biological systems.

Acknowledgements

I wish to thank my supervisors, Len Blackwell for his enthusiasm for science, from who I developed a lively interest in enzyme immunoassays, and Paul Buckley for his teaching and advice during this study.

I would also like to thank Jeremy Hill and Geoffery Barnes who also worked with me in an almost supervisory role, and were a source of much inspiration. Thanks are extended to all members of Chemistry-Biochemistry for helpful comments and also Bernardette Kilsby of the Department of Plant Biology and Biotechnology for useful references.

Finally I wish to thank my wife Lis, for her patience and encouragement.

Table of contents

Introduction 1

Chapter 1

Kinetic Isotope Effect on Acyl-Enzyme Formation During Oxidation of 4-*trans*-(N,N-dimethylamino) Cinnamaldehyde by Aldehyde Dehydrogenase

1.1 Introduction 3
1.1.1 4-*trans*-(N,N-dimethylamino) cinnamaldehyde as a substrate for aldehyde dehydrogenase 3
1.1.2 Investigation of the pre-steady state reaction of ALDH with DACA and its deuterated analogue as substrates. 8
1.1.3 Kinetic isotope effects 9
1.2. Materials 10
1.3. Methods 11
1.3.1 Preparation of sheep liver cytosolic aldehyde dehydrogenase. 11
1.3.2 Enzyme assays 13
1.3.3 Protein determinations 13
1.3.4 Spectroscopic determinations 14
1.3.5 Computer simulations 14
1.3.6 Pre-steady state studies of the formation of the 464 nm ALDH 4-*trans*-(N,N-dimethylamino) cinnamoyl - cysteine moiety from deuterated DACA. 14
1.3.7 Synthetic schemes for the preparation of deuterated

DACA 14
1.4 Results and Discussion 18
1.4 .1 Attempts to synthesise deuterated DACA 18
1.4.2 Synthesis of 1-[2H]-4-*trans*-N,N-dimethyl cinnamaldehyde by acid catalysed condensation of N,N-dimethyl benzaldehyde with ethanal 18
1.4.3 Isotope effects on the pre-steady-state burst during the formation of the DACA acyl-enzyme intermediate 26
1.4.4 Kinetic modeling of the isotope effects on the pre-steady-state burst during the formation of the DACA acyl-enzyme intermediate 35
1.4.5 Ethanamoyl 4-*trans*-(N,N-dimethylamino) cinnamoate 44
1.4.6 Conclusion 48

Chapter 2

Formation of 4-*trans*-(N,N-dimethylamino cinnamaldehyde complexes as models for the acyl intermediate

2.1 Introduction 49
2.2 Materials and Methods. 51
2.2.1 Formation of chromophore complexes 51
2.2.2 Determination of difference spectra 53
2.2.3 Formation of the ALDH furylacryloyl cysteine moiety using thioNAD 56
2.3 Results 56
2.3.1 DACA complexes formed with non-metal electrophiles 56
2.3.2 DACA complexes formed with metal electrophiles 60
2.3.3 Furylacrolein complexes formed with metal and non-metal electrophiles 64
2.3.4 Absorption spectra of the ALDH furylacryloyl cysteine moiety. 65
2.4 Discussion 67
2.4.1 Introduction to the discussion 67

2.4.2 Basic concepts in colour chemistry 68
2.4.3 Calculation of the approximate maximum possible red-shift for a DACA moiety 71
2.4.4 Consequences for DACA aldehyde dehydrogenase interactions 74
2.4.5 Modelling experiments 77
2.4.6 Biological examples of red-shifted spectra induced by enzymes not containing metal electrophiles. 80
2.4.7 Model experiments for the non-metal electrophiles 84
2.4.8 Possible improvements for modelling non-metal electrophiles. 90
2.4.9 Metal electrophiles 93
2.4.10 Comparison of the ALDH 4-*trans*-(N,N-dimethylamino) cinnamoyl - cysteine moiety and Alcohol dehydrogenase - DACA intermediates. 94
2.5 Conclusion 97

Chapter 3

Effects of metal ions on ALDH

3.1 Introduction 98
3.2 Materials 99
3.3 Methods 99
3.2.1 Determination of the number of magnesium binding sites using dialysis 99
3.2.2 Effect of calcium, magnesium and zinc ions on the ALDH activity at pH 5.22 100
3.2.3 Determination of the Metal ion content of highly purified ALDH 102
3.2.4 Examination of the iron profile of ALDH from the pH gradient column 103
3.2.5 Time dependent effects of EDTA 103
3.2.6 The pH dependence of EDTA inhibition 103
3.3 Results 104
3.3.1 Number of metal binding sites 104

3.3.2 Effect of Calcium Magnesium and Zinc on ALDH activity at pH 5.22. 105
3.3.3 Iron, copper and zinc determination of highly purified ALDH using atomic absorption 110
3.3.4 Examination of the iron profile of ALDH from the pH gradient column 110
3.3.5 Time dependent effects of EDTA 112
3.3.6 pH dependence of the ALDH inactivation by EDTA. 113
3.4 Discussion 114
3.4.1 Effects of metal ions on ALDH 114
3.4.2 Effects of EDTA on the ALDH activity 116
3.4.3 What is the active site metal electrophile? 117
3.5 Conclusion 117

Chapter 4

The Interactions of NADH on the ALDH Pathway

4.1 Introduction 119
4.2 Materials 120
4.3 Methods 121
4.3.1 Spectral properties of NADH bound to ALDH 121
4.3.2 Effect of pyrophosphate on ALDH activity 122
4.3.3 Activation and inhibition of ALDH by NAD 122
4.4 Results and Discussion 123
4.4.1 Spectral properties of NADH bound to ALDH 123
4.4.2 Probable cause of the ENADH red-shifted spectra 127
4.4.3 Calculation of the equilibrium constant for the two ENADH species. 128
4.4.4 Effects of propanal on the ENADH species 132
4.4.5 The 364 nm species in the kinetic pathway. 135
4.4.6 Effect of the acyl species on the absorption and fluorescence lag phases. 144
4.4.7 Relationship between decreased amplitudes and the

observed rate. 146
4.4.8 Explanation for the difference results observed by the two research groups. 150
4.4.9 Effects of pyrophosphate on activity of ALDH 151
4.4.10. Steady-state kinetics. 154
4.5 Conclusion 155

Chapter 5

Synthesis of a sensitive substrate for use in homogeneous enzyme immunoassays

5.1. Introduction 156
5.1.2 Desirable features when designing a substrate for a homogeneous EIA 158
5.2 Materials 160
5.3 Methods 160
5.3.1 Synthesis of 4-((bis 4-N,N-dimethylaminophenyl) methylinium ethanoate) phenol 160
5.3.2 Synthesis of 4-((bis 4-N,N-dimethylaminophenyl) methylinium ethanoate) phenyl ethanoate. 162
5.2.3 Measurement of the rate of hydrolysis of DMPE with rabbit liver esterase and porcine liver esterase. 164
5.3.4 Measurement of the rate of hydrolysis of DMPE with ALDH 164
5.3.5 Inhibition of the DMPE esterase reaction by ALDH 4- trans (N,N-dimethylamino) cinnamoyl - cysteine moiety. 164
5.4 Results and Discussion 165
5.4.1 Synthesis of dDMP 165
5.4.2 Synthesis of DMPE 168
5.4.3 The comparison of the spectral properties of DMPE with other structurally related compounds 173
5.4.4 Measurement of the rate of hydrolysis of DMPE with rabbit liver esterase and porcine liver esterase. 174
5.4.5 Measurement of the rate of hydrolysis of DMPE

with ALDH 175
5.4.6 Inhibition of the DMPE esterase reaction by ALDH 4-trans (N,N-dimethylamino) cinnamoyl - cysteine moiety. 176
5.4.7 Long term stability of DMPE 177
5.4.8 Safety of DMPE 179
5.4.9 Potential of DMPE in homogenous enzyme immunoassays 180
5.5 Conclusion 181

Chapter 6

ALDH as biological model for the effects of electromagnetic fields

6.1 Introduction 182
6.1 Methods 184
6.3 Results and Discussion 185
6.4 Conclusion 190

List of Tables

Table 1.4.4.1 Kinetic parameters for simulation of scheme 1.4.4.4 39
Table 1.4.4.2 Summary of kinetic parameters obtained by computer fits to scheme 1.4.4.4 40
Table 1.4.4.3 Kinetic parameters for simulation of scheme 1.4.4.5 (B) 42
Table 1.4.4.4 Summary of kinetic parameters obtained by computer fits to scheme 1.4.4.5 (B). 43

Table 2.2.1.1 DACA complexing solutions 52
Table 2.2.1.2 Furylacrolein complexing solutions 53
Table 2.3.1.1 Summary of the red-shifts induced in DACA by non-metal complexing agents. 57
Table 2.3.2.1 Summary of the red-shifts induced by metal complexing agents in DACA 64
Table 2.3.3.1 Summary of the red-shifts induced by metal and non-metal complexing agents in furylacrolein. 65
Table 2.4.3.1 73
Table 2.4.4.1 Stabilities of the ALDH 4-*trans*-(N,N-dimethylamino) cinnamoyl - cysteine moieties. 76
Table 2.4.5.1 Comparative hypsochromicity of hydrogen, sulphur and oxygen. 79
In Figure 2.4.6.2 the complexing conditions were 82
Table 2.4.6.1 Calculated red-shifts induced by non-metallo enzymes in a 4-*trans*-(N,N-dimethylamino) cinnamoyl moiety 83
Table 2.4.7.1 Comparison of modelling techniques 87
Table 2.4.10.1 Red-shifts induced in DACA by human and horse liver alcohol dehydrogenase 95

Table 2.4.10.1 Comparison of aldehyde dehydrogenase and alcohol dehydrogenase. 96

Table 4.4.3.1 Calculation of the approximate equilibrium constant of the ENADH species. 130
Table 4.4.3.2 Calculation of the approximate equilibrium constant of the ENADH species in different buffers. 130
Table 4.4.4.1 Correlation between ALDH-NADH-acyl and ALDH-NADH-aldehyde. 134
Table 4.4.5.1 Parameters used for the NADH burst simulations 142

Table 5.4.3.1 Spectral properties of tri-aryl carbonium dyes 173
Table 5.4.4.1 Measurement of kcat for porcine esterase and rabbit esterase 175

Table 6.3.1.1 Effects of parallel combinations of a.c. and d.c. magnetic fields on the activity of ALDH.....

Introduction

Sheep liver cytosolic aldehyde dehydrogenase is an enzyme which is involved in the metabolism of aldehdyes. It has been suggested that aldehyde dehydrogenase has a multifunction purpose, its broad substrate specificity allowing it to oxidise a wide variety of aldehydes to the corresponding carboxylic acids. Hence the physiological role of aldehyde dehydrogenase appears to be that of a general detoxifier (Weiner, 1989).

Aldehyde dehydrogenase was first purified by Kathy Kitson (nee Crow, thesis), and she has continued her involvement in the improvement enzyme quality thoughout. Kathy Kitson has been predominantly researching the physiological factors that control the rate alcohol metabolism, of which aldehyde dehydrogenase is one (Crow and Hardman, 1989).

The steady state and pre-steady state kinetics of sheep liver aldehyde dehydrogenase was first studied by MacGibbon (thesis). The significant outcomes of this work was that the product NADH was shown to be released from ALDH in a biphasic manner. The biphasic release of NADH was found to be the rate limiting process for many aldehyde substrates. MacGibbon also showed that ALDH could catalyse the hydrolysis of unstable esters. Later a group at Hull University, under the leadership of Mark Dickinson also started research on this enzyme. It was found that NADH could reduce the ALDH-acyl species (the reverse reaction) formed by reaction of the enzyme active site nucleophile with an anhydride. This group contributed much pre-steady state and steady information (Hart and Dickinson, 1982)

The rate of acyl enzyme hydrolysis (for many substrates) using proton release was predominantly studied by Bennett (thesis). Bennett also studied the effect of magnesium ions on the enzyme, magnesium ions being

available in abundance in vivo (Soman et al, 1970). Motion (thesis) studied the kinetic effects of pH, buffers and furthered the studies on the reverse reaction. Dunn and Buckley (1982,1985), studied the formation of a coloured quassi-stable ALDH-acyl species formed as an intermediate in the oxidation of 4-trans-(N,N-dimethylamino) cinnamaldehyde. Jeremy Hill examined the enzyme structural equilibrium between the tetrameric state and the dissociated state (Buckley et al., 1991).

Trevor Kitson made the first stable ALDH-acyl species (Kitson T., 1989) which was found to have been incorporated with the residue cysteine 302 (Kitson et al.,1991). In conjunction with Kerry Loomes, Kitson studied the effects of a variety of sulfhydral modifiers on the kinetics of aldehyde dehydrogenase (Kitson T., (1989,b)).

A major focus of the research work presented in this thesis is to further increase the kinetic understanding of aldehyde dehydrogenase.

Chapter 1

Kinetic Isotope Effect on Acyl-Enzyme Formation During Oxidation of 4-*trans*-(N,N-dimethylamino) Cinnamaldehyde by Aldehyde Dehydrogenase

1.1 Introduction

1.1.1 4-*trans*-(N,N-dimethylamino) cinnamaldehyde as a substrate for aldehyde dehydrogenase

The conjugated aldehyde 4-*trans* -(N,N-dimethylamino) cinnamaldehyde (DACA) is a substrate for aldehyde dehydrogenase (ALDH) being slowly oxidised to N,N-(dimethylamino) cinnamic acid (Dunn et al, 1982). DACA is a highly coloured aldehyde, which in phosphate buffer at pH 7.4, absorbs in the visible region at 400 nm with an extinction coefficient of 31000 $mol^{-1}cm^{-1}$.

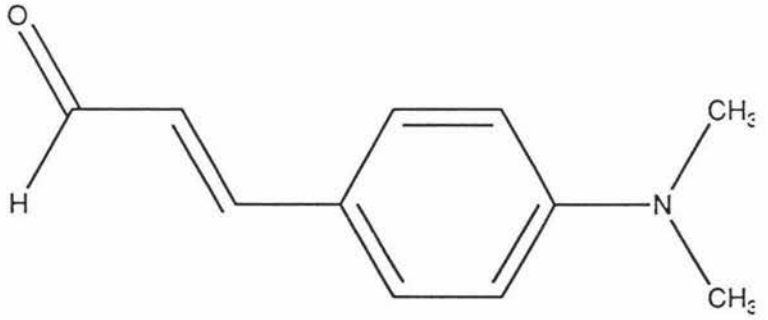

Figure 1.1.1 4-*trans*-(N,N-dimethylamino) cinnamaldehyde

DACA belongs to a general class of conjugated donor-acceptor molecules. The absorption of light by this group of molecules depends on the extent of conjugation, the polarity of the solvent environment and on the nature of the 'donor' and 'acceptor' groups. For DACA the 'donor' group is the N,N-dimethylamino group which has an electron donating

(+M) functionality, while the 'acceptor' functionality comes from the aldehyde group which is electron withdrawing (-M). For the studies reported in this chapter use will be made mainly of the spectral changes associated with changes in the 'acceptor group'.

It is believed that aldehydes react with a nucleophile (X) on the enzyme surface forming the tetrahedral species (a), schematically represented below. Species (a) then transfers a hydride ion to NAD, forming a thio-acyl enzyme NADH intermediate species (b). The acyl-enzyme intermediate is unstable and undergoes hydrolysis releasing the product carboxylic acid salt as shown in scheme 1.1.1.

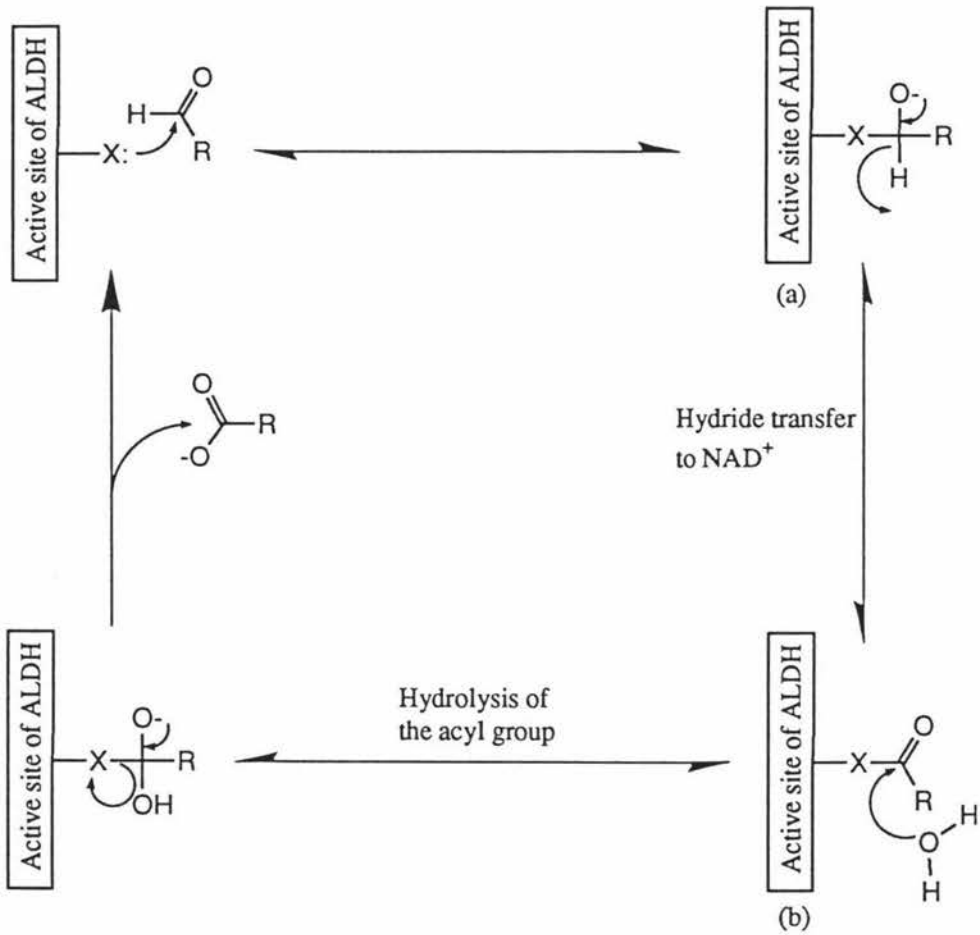

scheme 1.1.1

It has been shown by Buckley and Dunn (1982, 1985) that during the enzyme catalysed oxidation of DACA, an acyl-enzyme intermediate species with an absorption maximum at 464 nm is formed. An example of the formation and decay of the acyl-enzyme intermediate on monitoring the absorption at 464 nm is shown in Figure 1.1.2.1.

Figure 1.1.2.1 Formation and decay of the DACA acyl-enzyme intermediate

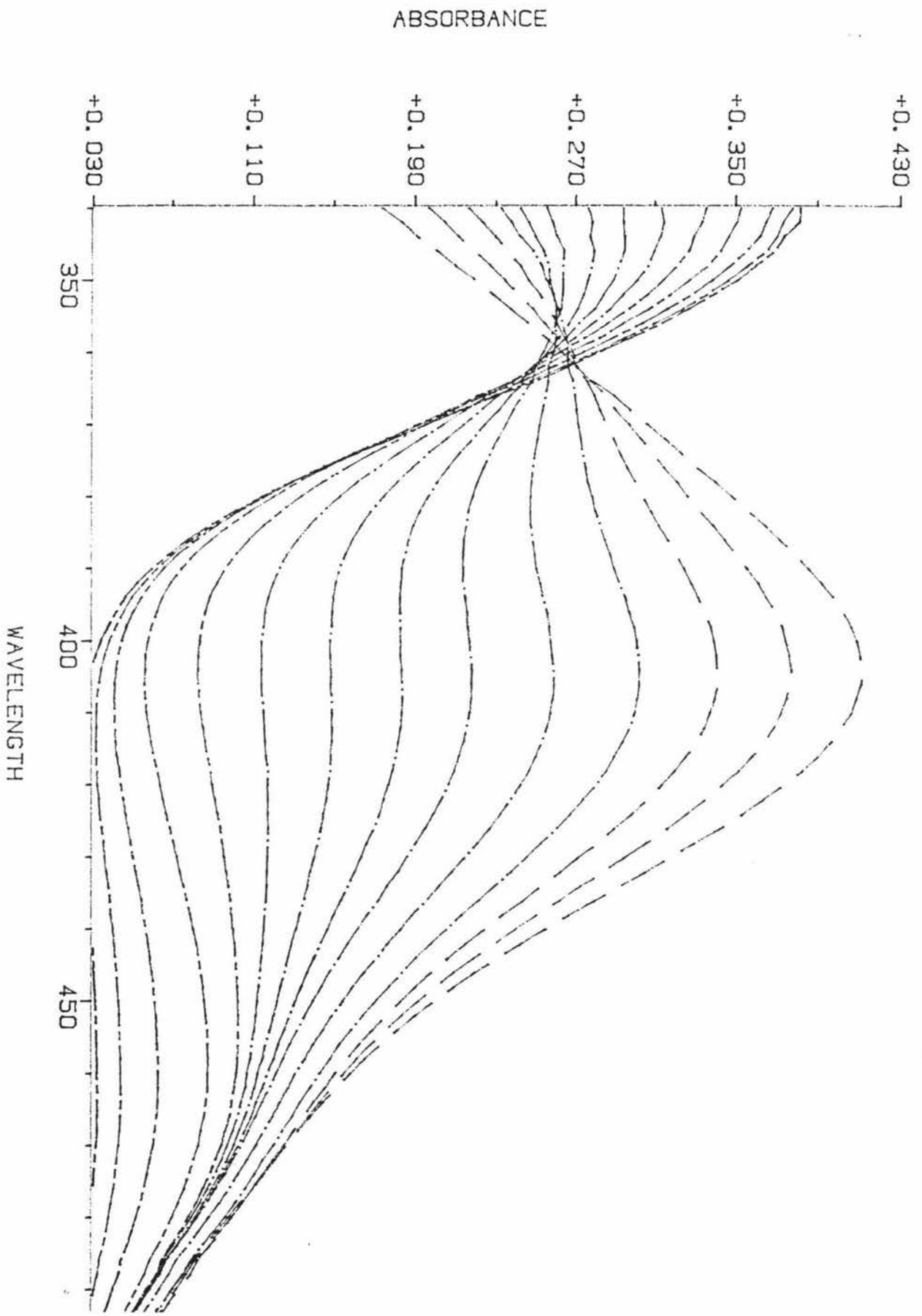

A detailed kinetic study of the formation of the 464 nm species using stopped flow techniques has been reported by Buckley and Dunn (1982, 1985). The formation of the 464 nm species appears to be biphasic and since thio-NADH (which does not absorb around 464 nm) forms with approximately the same biphasic rates it was proposed that the 464 nm species is due to the formation of the ALDH-DACA acyl species.

Denaturation of the sheep liver cytosolic aldehyde dehydrogenase shifted the absorption maximum of the ALDH-DACA acyl species to 408 nm (Loomes et al., 1990). Pietruszko et al. (1992) also formed intermediate DACA acyl-enzymes with the human mitochondrial and cytosolic aldehyde dehydrogenases. They then rapidly denatured the enzyme using trichloroacetic acid. After redissolving the denatured enzyme in 50 mM sodium acetate/2.0% (w/v) SDS pH 5.2 buffer, they were able to show that two molecules of the acyl species were incorporated per molecule of fully active enzyme. The absorption maxima of the denatured DACA acyl enzyme species were also blue shifted to 409 nm and 408 nm respectively.

The 409 nm species for the mitochondrial aldehyde dehydrogenase (Pietruszko et al, 1992) was specifically labelled at cysteine-302. This identification was accomplished by using [^{3}H]-DACA to form the acyl species and then digesting the labelled mitochondrial aldehyde dehydrogenase with trypsin. The amino acid sequence analysis showed that the sequence 273-307 had been labelled, with the radioactive label associated with cysteine residues 301-303. However, cysteine-302 is the only cysteine residue conserved in all aldehyde dehydrogenases sequenced. Furthemore in site directed mutagenesis studies when cysteine-302 has been replaced by tyrosine all ALDH activity of the enzyme (Weiner et al.) was removed. Therefore it is now accepted that cysteine-302 is the active site nucleophile. It would follow then that the acyl-enzyme species must be a 4-*trans* (N,N-dimethylamino) cinnamoyl - cysteine-302 moiety represented schematically below.

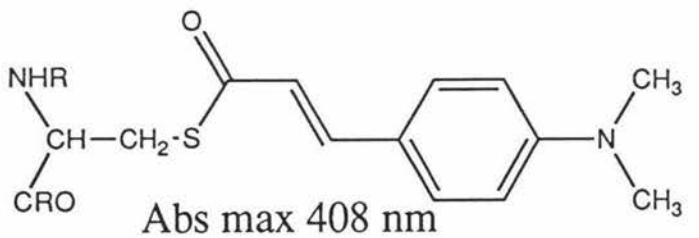

Figure 1.1.1.3 Denatured ALDH 4-*trans* (N,N-dimethylamino) cinnamoyl - cysteine-302 moiety

4-*Trans* (N,N-dimethylamino) cinnamoyl-N,N-dimethyl cysteamine is a synthetic analogue of the DACA acyl-enzyme moiety and has been prepared by Dunn and Buckley, (1985). The structure is given in Figure 1.1.1.4.

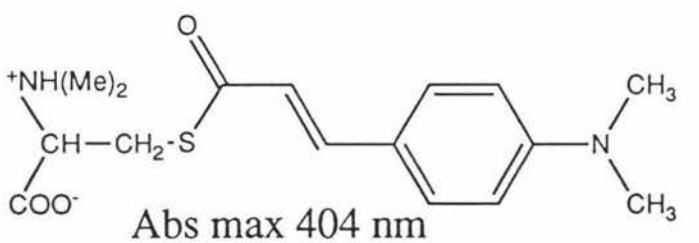

Figure 1.1.1.4 4-*trans* -(N,N-dimethylamino)cinnamoyl-N,N-dimethylcysteamine

The synthetic analogue has an absorption maximum at 404 nm which is similar to that of the denatured ALDH 4-trans (N,N-dimethylamino) cinnamoyl - cysteine-302 moiety (408 nm) suggesting a close structural similarity. In the native enzyme the DACA acyl-enzyme species has an absorption maximum red shifted to 464 nm. Clearly this spectrum is quite different from that of the model compound and suggests that the active site of aldehyde dehydrogenases must contain an additional structural feature which causes a large shift in the absorption maximum of the ALDH 4-*trans*-(N,N-dimethylamino) cinnamoyl - cysteine-302 moiety in the native enzyme.

Dunn and Buckley (1982), concluded that the special microenvironment provided by the enzyme catalytic site almost certainly involves chemical activation of the acyl enzyme, via the interaction of a strong electrophile (perhaps a proton) with the carbonyl oxygen of the 4-*trans* (N,N-dimethylamino) cinnamoyl moiety (Figure 1.1.1.5).

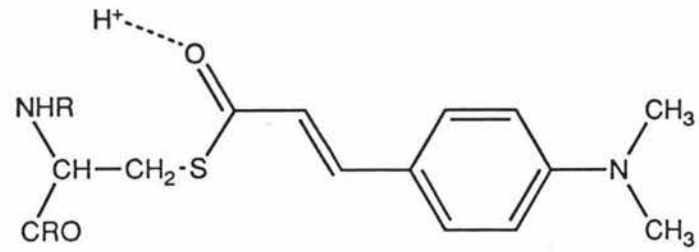

Figure 1.1.1.5 Proton interaction with carbonyl oxygen

1.1.2 Investigation of the pre-steady state reaction of ALDH with DACA and its deuterated analogue as substrates.

The formation of the 464 nm acyl-enzyme species is biphasic and must be fitted by at least two rate constants (Buckley and Dunn, 1982, 1985). By using thio-NAD as the co-enzyme they were also able to show that the rate of thio-NADH formation was controlled with approximately the same two rate constants. Because of this it was suggested that hydride transfer was a key step in the formation of the acyl-enzyme species. The fact that, for human classes (I) and (II) ALDH's, two molecules of 4-*trans*-(N,N-dimethylamino) cinnamoyl - cysteine moiety are incorporated per ALDH tetramer (Pietruszko et al., 1992) indicates that ALDH has at least two functional active sites per tetramer. One explanation of the biphasic pre-steady state reaction is that the two phases are representative of two active sites which are unequal in their catalytic activity. However preliminary work by Buckley (personnal communication) showed that only the fastest of the two rates had a DACA concentration dependence. A concentration dependence for both processes, would be expected if the biphasicity represented two unequal active sites.

It appeared probable that the fastest rate corresponded to the rates of DACA binding and subsequent hydride transfer to the NAD to form NADH and the ALDH acyl species. The slower of the two rates, having no DACA concentration dependence was more difficult to account for.

1.1.3 Kinetic isotope effects

In reactions which involve the rate limiting transfer of a hydride ion, substitution of the hydrogen by deuterium can reveal details about the mechanism of this process. The isotope effect arises because of the mass difference between the two isotopes which gives rise to a difference in the zero point energies of the C-H and C-D bonds (Wiberg et al., 1955). If the transition state involving the transfer of the hydride (or deuteride) ion is symmetrical then the zero point energy cancels in the transition state and the isotope effect is given by the difference in the zero point energies of the C-H and C-D bonds. At 25 C, this difference corresponds to a difference in the rates for the non-deuterated and deuterated compounds of about 7.0 - 10. Hence if a rate difference of this magnitude is encountered then it can be said that the hydrogen in question is in motion in the transition state.

The situation is more complex in multistep reactions such as enzyme catalysed reactions where more than one step may be involved in determining the rate of change of the process which is observed experimentally. For example, in principle every intermediate which builds up on the reaction pathway should be observable during transient kinetic studies. However, in practice this is not the case since the amplitudes of many of the intermediates will be too small to observe or there may be no physical change associated with a given process. Nevertheless, if the processes are coupled there will be a reflection of the "invisible" intermediates in the measurable transients which therefore cannot be simply equated with the rate of a single step.

In order to investigate further the two processes seen in formation of the DACA acyl-enzyme intermediate the kinetic isotope effect on both these processes was determined. Because deuterated DACA is not commercially available it had to be synthesised. This synthesis therefore constituted a major part of this chapter.

1.2. Materials

The following chemicals were used, each was of quality grade. All other materials used are described in the text.

Chemical	Company
sodium dihydrogen phosphate	Sigma
sodium acetate	Ajax
bistris	USB
NAD	Sigma
propanal	BDH
2-thioethanol	Sigma
4-dimethylamino benzaldehyde	no company label
nitric acid	Univar
potassium dichromate	Koch-Light Laboratories
ethanoic anhydride	May & Baker
D_1-chloroform	Aldrich
acrylamide	Serva
bis-acrylamide	Serva
lauryl sulphate	USBC
glycine	Sigma
hexane	Univar
chloroform	Univar
dithiothreitol	Serva
EDTA	Pronalys
4-hydroxy acetophenone	BDH
DACA	Sigma
polyethylene glycol (8000)	Sigma
D_6-ethanol	CIBA
ethanol	Univar
brilliant blue G	Sigma
acetic acid	Pronayls
sodium methoxide	no company label
sodium azide	BDH
sulphuric acid	Pronalys
sodium hydroxide	Unilab
ethyl ethanoate	Univar
hydrochloric acid	Pronayls
methanol	BDH

1.3. Methods

1.3.1 Preparation of sheep liver cytosolic aldehyde dehydrogenase.

Cytosolic ALDH from sheep livers was prepared essentially as described by Motion (thesis, 1986). Livers obtained from freshly slaughtered sheep were cooled with ice during transportation from the Freezing Works. Immediately after arrival the livers were frozen for later use.

All preparative proceedures were carried out at 4 C where possible. After semi-defrosting two livers in water 750 g of liver was sliced into small pieces. 1 litre of 0.25 M sucrose buffer (5 mM phosphate, 0.1 % 2-thioethanol, pH 7.4) was added. The mixture was then homogenised in either a blender or an ultra-turrux for approximately 60 seconds. The homogenate was then centrifuged for 15 minutes at 13800 g. The precipitate was discarded and the supernatant was strained through glass-wool, then re-centrifuged for 40 minutes at 27300 g to sediment the mitochondria. The precipitate was again discarded and the supernatant was filtered through glass wool.

The supernatant volume was then made up to 1500 ml with sucrose buffer and 180 g of polyethylene glycol 8000 (PEG) was added over 30 minutes with stirring. This was followed by centrifugation for 15 minutes at 13800 g. The precipitate was discarded and a further 120 g of PEG was added with stirring over 30 minutes, and then recentrifuged for 15 minutes at 13800 g. The precipitate was then redissolved in 400 ml of 5 mM phosphate buffer (pH 7.4) and loaded on to a DE 32 column pre-equilibrated with phosphate buffer. After washing the column with a further 500 ml of phosphate buffer the ALDH was then eluted with 20 mM phosphate buffer at a rate of 0.75 ml min^{-1}.

The fractions were then assayed for aldehyde dehydrogenase activity and those containing activity were combined. The combined fractions were dialysed into 10 mM bistris buffer (pH 6.5) and loaded onto a 2 x 10 cm column of Pharmacia DEAE sephacel which had been pre-equilibrated with the same buffer. The ALDH was eluted using 10 mM sodium acetate buffer pH (4.6). The fractions containing ALDH were then stored in the refrigerator until required. The yield up to this stage was typically

300 - 1000 mg, calulated from V_{max} assays and assuming 1.5 active sites per tetramer.

If further purification was neccessary the enzyme solution was dialysed into 20 mM phosphate buffer pH 7.0 containing 1 mM EDTA and loaded on to a 4-acetyl phenoxy sepharose affinity coloumn (≈ 300 ml wet volume), and then eluted with 1 mM 4-hydroxyacetophenone. The pure enzyme solution was then dialysed into 20 mM phosphate buffer and stored in the fridge. An example of the activity profile from the affinity column is shown in Figure 1.3.1.1.

Figure 1.3.1.1 Activity profile from the affinity column

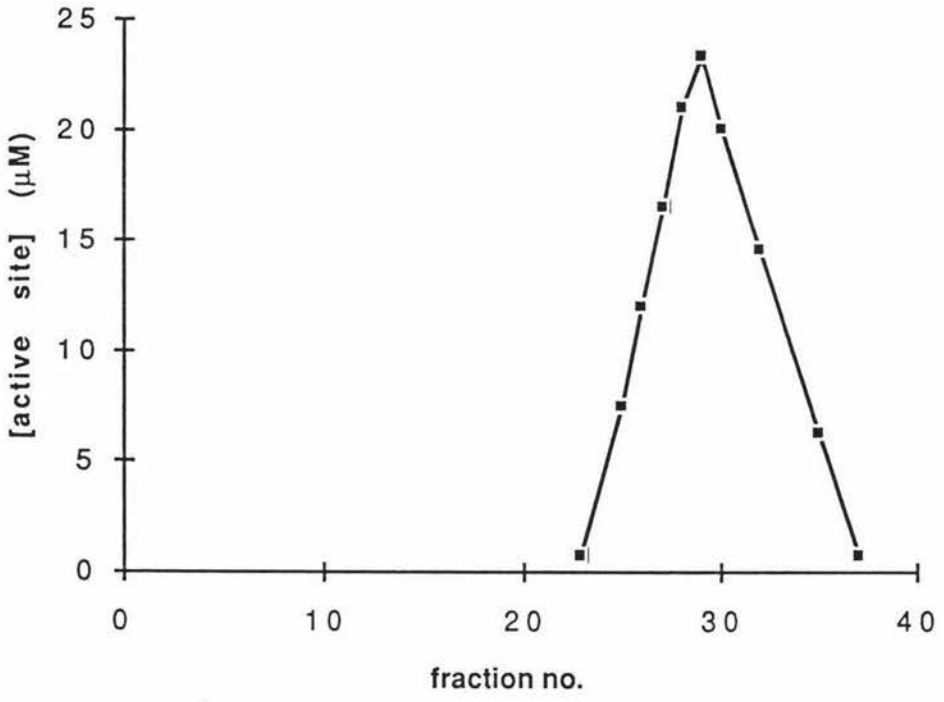

The total ALDH loaded was 537 mg, but 191 mg did not bind but washed imediately through, leaving 346 mg bound to the column. After eluting with the 4-hydroxyacetophenone the combined fractions contained 304 mg of ALDH, calulated from V_{max} assays and assuming 1.5 active sites per tetramer. The yield for this separation step was therefore 88%.

Figure 1.3.1.2 shows a gel for ALDH in various stages of purification, (a) is after the DE32 column, (b) is after the pH gradient column and (c) is after the affinity column.

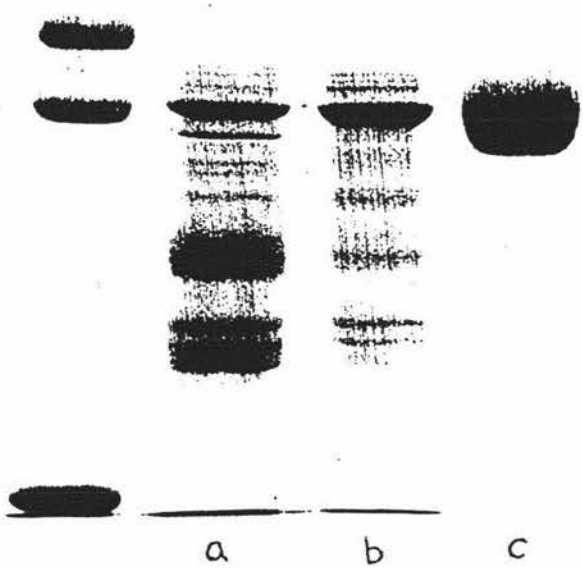

1.3.2 Enzyme assays

ALDH active site concentration were determined by the following assay mixture:

50 µl of propanal (20 mM, final)
50 µl of NAD (1 mM, final)
50 µl of ALDH solution
0.85 ml of sodium phosphate buffer pH 7.4

The assay was iniated by the addition of propanal and the formation of NADH was followed spectrophotometrically by the absorption changes at 340 nm. The k_{cat} was assumed to be 0.56 s^{-1} (Blackwell et al,1987).

1.3.3 Protein determinations

The determination of the protein concentration in ALDH samples was measured from the absorbance at 280 nm using a value of 11.3 for the absorbance of a 1% solution of ALDH (Dickinson et al., 1981).

1.3.4 Spectroscopic determinations

Spectrophotometric studies were done using a Hewlett Packard rapid scanning diode array spectrophotometer. Presteady-state kinetics were done using a Hitech Scientific stopped-flow spectrometer. Data fitting was carried out using the software applications available on the spectrometers. Nuclear magnetic resonance was done using a JEOL GX270 spectrometer and a Hitachi R-1200 spectrometer.

1.3.5 Computer simulations

Computer simulations of enzyme kinetic models were carried out using a modification of an analogue program written in Quick Basic developed by Adrian Bennett and the data were fitted using a Prism version 1.03 curve fitting package to obtain the apparent rate constants.

1.3.6 Pre-steady state studies of the formation of the 464 nm ALDH 4-*trans* (N,N-dimethylamino) cinnamoyl - cysteine moiety from deuterated DACA.

Solutions containing ALDH (6.7 μM) and NAD (2 mM) in 50 mM phosphate buffer (pH 7.4) were rapidly mixed with deuterated DACA (at variable concentrations) in a Hitech Scientific stopped-flow spectrometer at 25.6 C. The formation of the acyl species was followed at 475 nm with a slit width of 2 nm and a time constant of 3.3 μs. The data obtained were fitted using the software available on the stopped-flow spectrophotometer

1.3.7 Synthetic schemes for the preparation of deuterated DACA

Four main synthetic routes were considered for the synthesis of deuterated DACA for the transient kinetic studies.

1.3.7.1 Synthesis via a crossed aldol condensation
p-(N,N-dimethylamino) benzaldehyde is condensed with deuterated ethanal under basic conditions as shown in scheme 1.3.7.1.

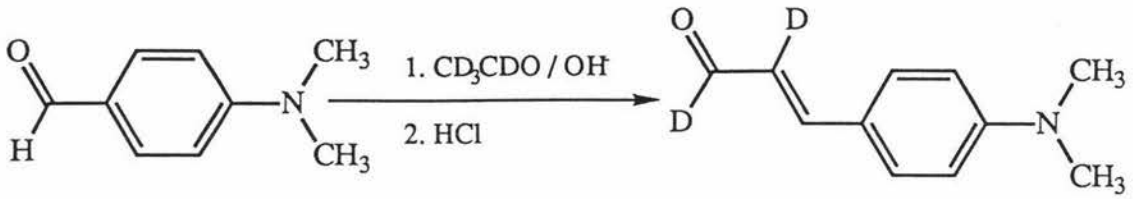

Scheme 1.3.7.1

In scheme 1.3.7.1 the methyl group of the deuterated ethanal is deprotonated by the base which then serves as a nucleophile undergoing a nucleophilic attack on the carbonyl group of the substituted benzaldehyde. After a dehydration of the intermediate aldol DACA deuterated at C-1 and C-2 results.

1.3.7.2 Partial oxidation of deuterated 4-trans-(N,N-dimethylamino) cinnamyl alcohol using pyridiniumchlorochromate

Deuterated 4-(N,N-dimethylamino) cinnamyl alcohol was synthesised previously in these laboratories by esterification of 4-(N,N-dimethylamino) cinnamic acid to the methyl ester using diazomethane and subsequent reduction with $LiALD_4$ to the deuterated 4-(N,N-dimethylamino) cinnamyl alcohol (see scheme 1.3.7.2). Partial oxidation of this compound using pyridiniumchlorochromate (PCC) is expected to produce deuterated 4-*trans* (N,N-dimethylamino) cinnamaldehyde.

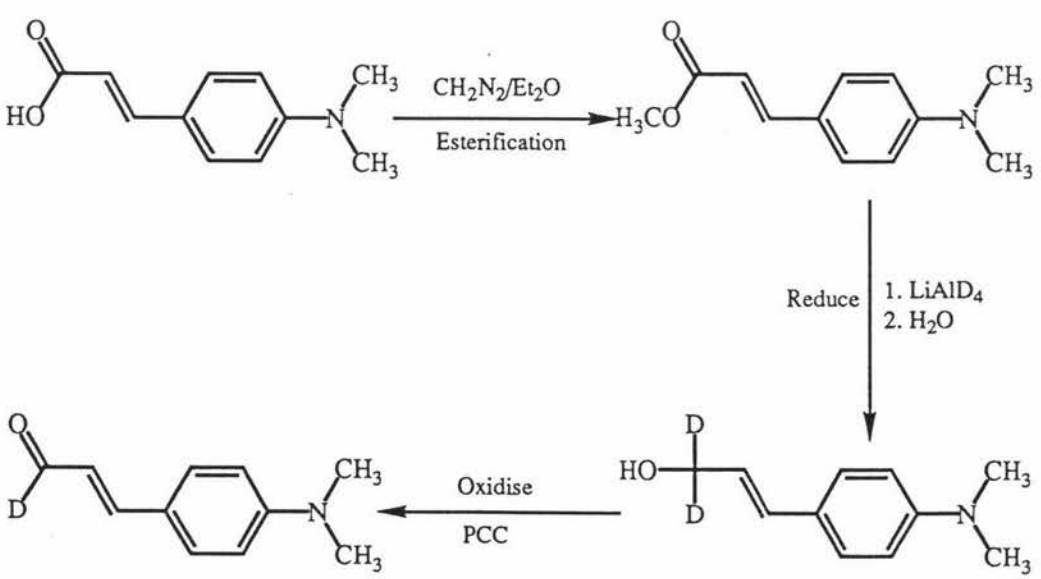

Scheme 1.3.7.2

1.3.7.3 Oxidation of deuterated 4-trans-(N,N-dimethylamino) cinnamyl alcohol with alcohol dehydrogenase

The deuterated 4-*trans*-N,N-dimethyl cinnamyl alcohol prepared by scheme 1.3.7.2 can be used as a substrate for the enzyme alcohol dehydrogenase which has a broad substrate specificity. The product of this oxidation reaction is 1-[^{2}H]-4-*trans*-N,N-dimethyl cinnamaldehyde (deuterated DACA) as shown in scheme 1.3.7.3

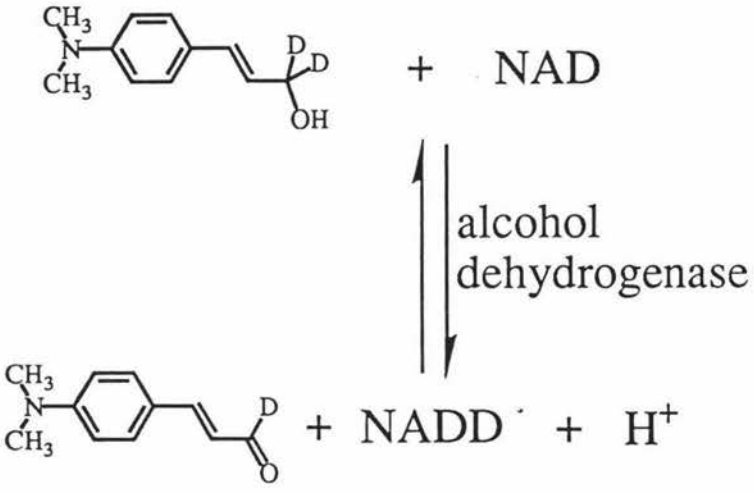

scheme 1.3.7.3

1.3.7.4 Synthesis of 1-[^{2}H]-4-trans-N,N-dimethyl cinnamaldehyde by acid catalysed condensation of N,N-dimethyl benzaldehyde with ethanal

A synthetic method dating from 1920 was also investigated (Konig et al., 1928). This method (shown in scheme 1.3.7.4) involves condensation of 4-N,N-dimethylamino benzaldehyde with excess enol (hydroxyethene) in the presence of concentrated sulphuric acid.

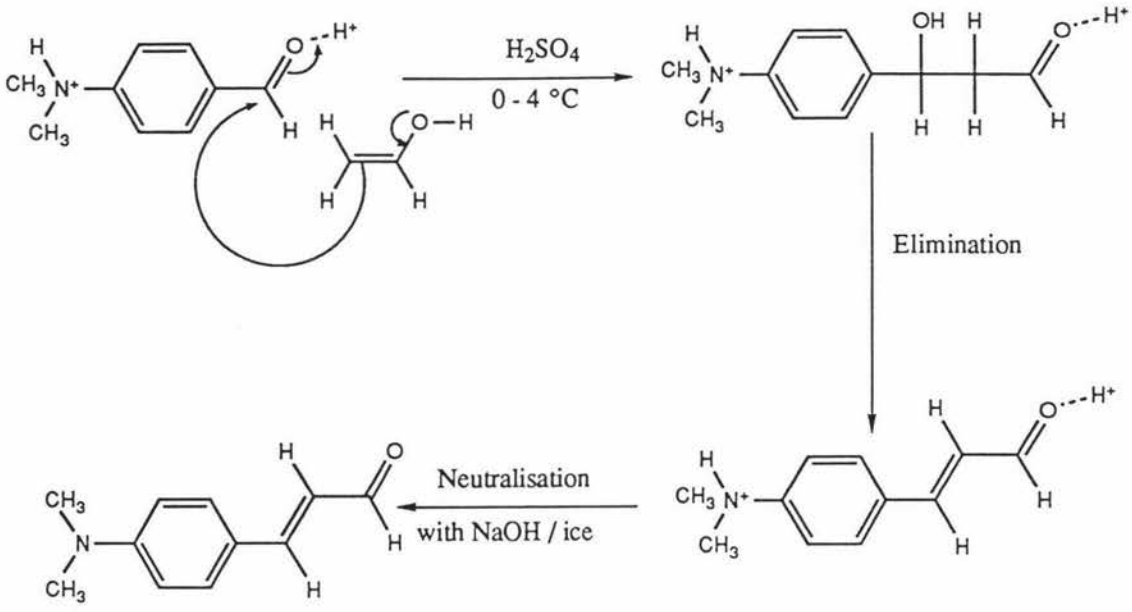

scheme 1.3.7.4

The enol of ethanal (hydroxyethene) was produced *in situ* from paraldehyde which in concentrated mineral acids is in equilibrium with ethanal.

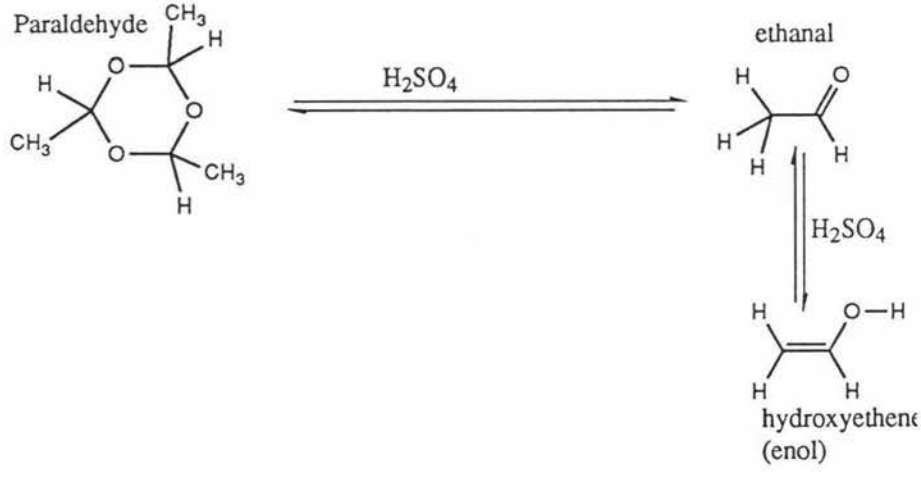

By using deuterated ethanal (CD3CDO) in the scheme instead of paraldehyde deuterated DACA should be produced. Deuterated ethanal can be purchased commercially, but there is a long delay time in obtaining it hence it was synthesised by partial oxidation of deuterated ethanol (CD3CD2OD) using a standard laboratory method employing acidic potassium dichromate as an oxidant. The deuterated ethanal was obtained in 57 % yield.

1.4 Results and Discussion

1.4 .1 Attempts to synthesise deuterated DACA

Preliminary studies were carried out with the first three synthetic routes as described in methods. The crossed aldol condensation reaction was examined by Kimmo Wiltshire during the research carried out for a B.Sc (Hons) project. The reaction gave a mixture of products which could not be separated from the product DACA and the yield was estimated to be less than 5% so the method was abandoned and not repeated here. It was thought that the N,N,-dimethyl amino group being a strong electron donator deactivated the carbonyl carbon of the aldehyde group towards nucleophilic attack.

While repeating the previous work done on scheme 1.3.8.2 it became obvious that there were problems with the oxidation step. The 4-*trans*-(N,N-dimethylamino) cinnamyl alcohol was very unstable under acidic conditions making isolation of the product difficult. An alternative partial oxidant that was only mildly acidic, chromium trioxide-3,5-dimethylpyrazole, was tried but this was also unsuccessful so this method was discontinued. Deuterated DACA was produced successfully by the alcohol dehydrogenase catalysed oxidation of deuterated 4-(N,N-dimethylamino) cinnamyl alcohol with NAD at pH 9.0. However, this reaction was very slow as 4-(N,N-dimethylamino) cinnamyl alcohol was a very poor substrate and the yield was low (4%) since the alcohol dehydrogenase lost activity during the reaction.

Synthesis of the deuterated DACA was achieved however with the acid catalysed condensation reaction shown in scheme 1.3.7.4.

1.4.2 Synthesis of 1-[^{2}H]-4-trans-N,N-dimethyl cinnamaldehyde by acid catalysed condensation of N,N-dimethyl benzaldehyde with ethanal

In a 10 ml round bottomed flask surrounded by ice, 4-(N,N-dimethylamino) benzaldehyde (295 mg) was slowly stirred (using a magnetic stirrer) into 1.5 ml of H_2SO_4 (at $\approx$ 0 °C) until it was completely

dissolved. Deuterated ethanal (300 µl of CD_3CDO) was added in 6 x 50 µl additions every 20 minutes. The red-brown colour indicative of a successful condensation did not develop as quickly as in previous runs using non-deuterated ethanal.

After the last addition of CD_3CDO the solution was stirred (15 min), then the light red brown mixture was poured onto sufficient ice so that the enthalpy of hydration of the sulphuric acid did not melt all of the ice. The acid was then 60 % neutralised with NaOH and ice, and left to stand over night. In the morning the filtrate which contained mostly the starting material was removed. Enough NaOH was then added to the solution to neutralise 95 % of the remaining sulphuric acid. The solution was then left to stand for two hours following which the precipitate was then removed by filtration and redissolved in chloroform. After the chloroform had been removed with the rotovac an orange oil weighing 230 mg remained.

Since the starting material (4-N,N-dimethylamino benzaldehyde) and the product (deuterated-DACA) had very similar polarity separation using column chromatography was unsuccessful. Careful sublimation was also tried but both the starting material and the product sublimed together. Therefore a portion of the crude product was purified twice by thin layer chromotography on silica plates, using a 4:1 hexane : ethyl acetate mixture. Each time up to 5 mg of crude oil was loaded onto a tlc plate (20 cm x 20 cm), the product was scraped off and stripped from the silica scrapings with methanol.

Because not all of the crude deuterated-DACA product was purified the overall yield was calculated from the visible absorption spectrum of the product at 430 nm, where the starting material does not absorb. This corresponded to 25 mg of DACA (7% yield). Although this was low it was sufficient for the stopped-flow measurements which only required about 0.5 mg of deuterated DACA for all the measurements

In preliminary runs using undeuterated ethanal to synthesise DACA the yields obtained were approximately 30 - 40 %, which compared very well

with the literature yield (approximately 40 %) given by Konig et al. (1928).

For the deuterated DACA however the colour developed at a noticeably slower rate than for the non deuterated case. In addition the proportion of products other than deuterated DACA was increased relative to the deuterated DACA. It appears from these results that there is an adverse isotope effect as a result of the deuterium atoms present in the methyl group and which are involved in the chemistry of the condensation reaction. In the synthesis of DACA on the other hand the carbonyl hydrogen (or deuterium) is uninvolved in the chemistry. A method of avoiding this adverse isotope effect on the formation of deuterated DACA is to use CH_3CDO for which there should be no adverse isotope effect. This product was not available during the course of this thesis.

It is important to confirm that the product from this condenstion reaction (Scheme 1.3.7.4) is DACA and that the aldehyde proton has been replaced by deuterium. The nmr spectra of the starting material 4-N,N-dimethylamino benzaldehyde (Figure 1.4.2.1), DACA (Figure 1.4.2.2) and deuterated DACA (Figure 1.4.2.3) were run in deuterated chloroform. The key features of the the nmr spectra were as follows:

For 4-N,N-dimethylamino benzaldehyde (Figure 1.4.2.1) the N,N-dimethyl groups (3.09 ppm, 6H), aromatic hydrogens (6.7 ppm, J= 9.16 Hz, 2H; 7.75 ppm, 2H) and the aldehyde hydrogen (9.74 ppm) are clearly visible. The two aromatic hydrogens at 6.7 ppm are in the 3 position (C-3) of the benzene ring (relative to the aldehyde group) whereas the two at 7.75 ppm are the C-2 aromatic protons since they are next to the electron withdrawing aldehyde group.

In the DACA spectrum (Figure 1.4.2.2) the most noticable features are that the aldehyde proton is shifted upfield to 9.59 ppm, and the C-2 aromatic protons are shifted upfield to 7.46 ppm. The extra signals at 7.41 and are 6.55 are due to the side chain alkene (CH=) groups. Since the proton at 6.6 ppm is also coupled to the aldehyde proton (J = 8 Hz) this must be the C-2 side chain carbon proton.

Figure 1.4.2.1 n.m.r of 4-N,N-dimethylamino benzaldehyde in $CDCl_3$

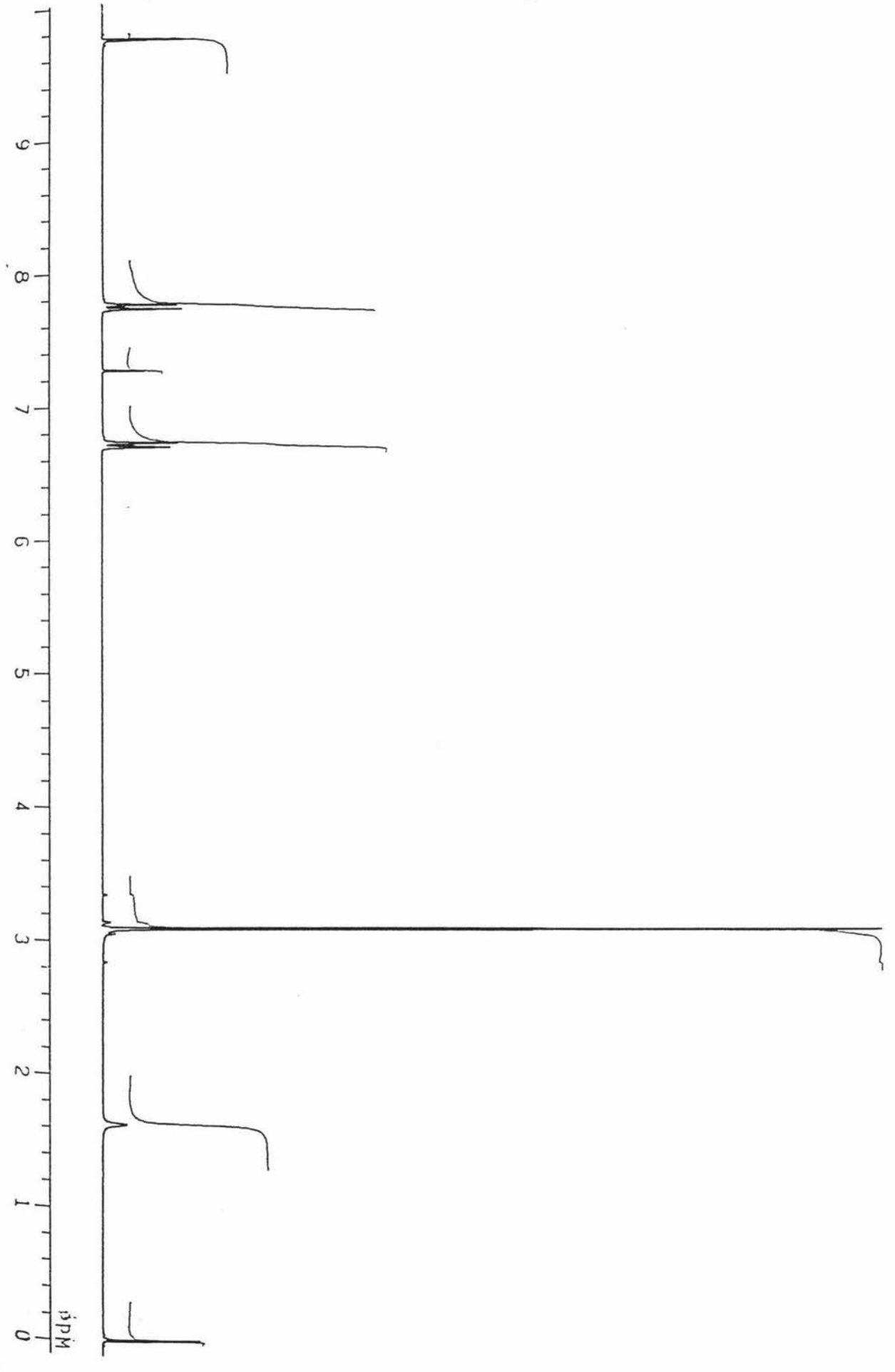

Figure 1.4.2.2 n.m.r of DACA in $CDCl_3$

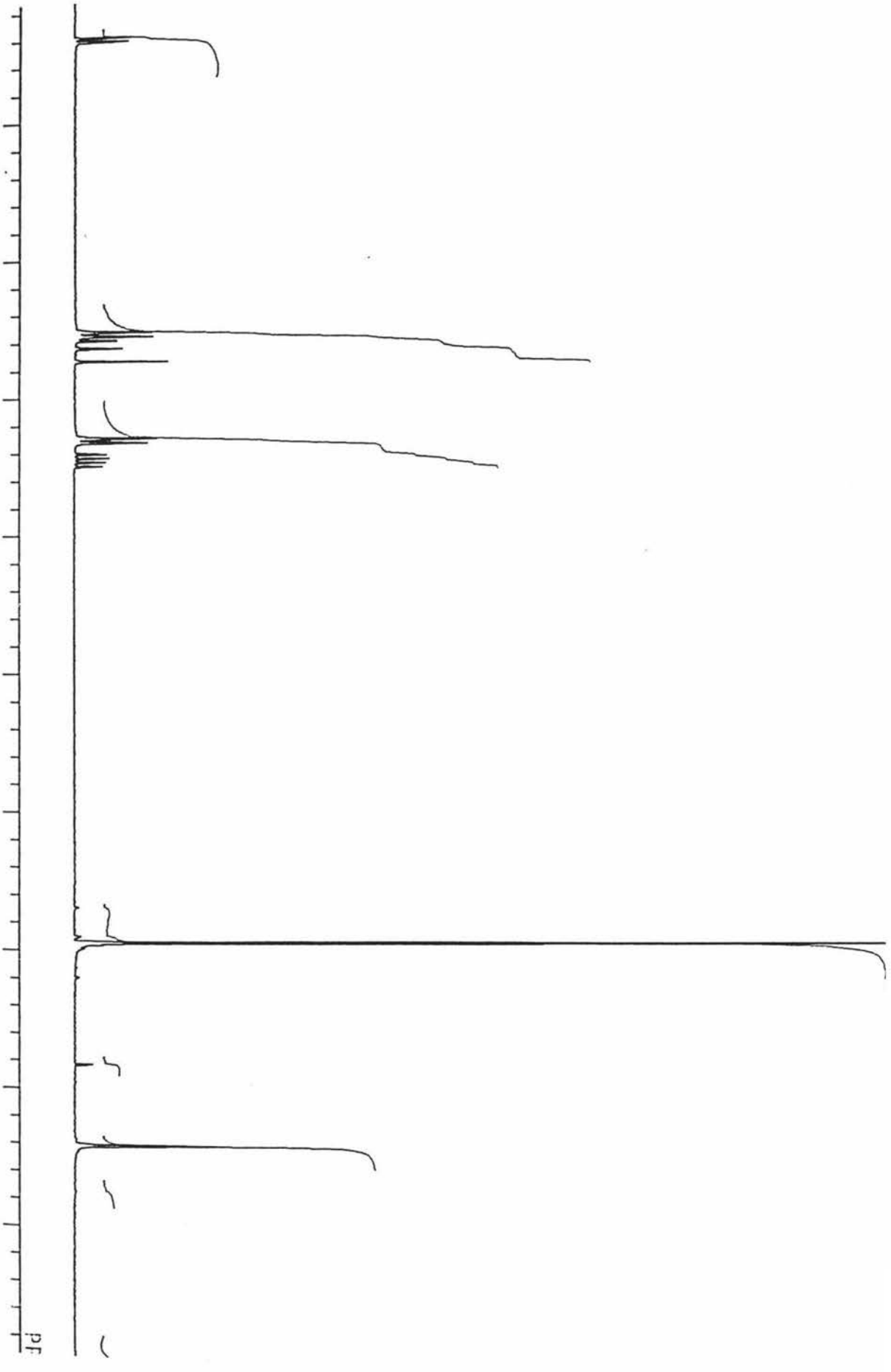

Figure 1.4.2.3 n.m.r of deuterated DACA in $CDCl_3$

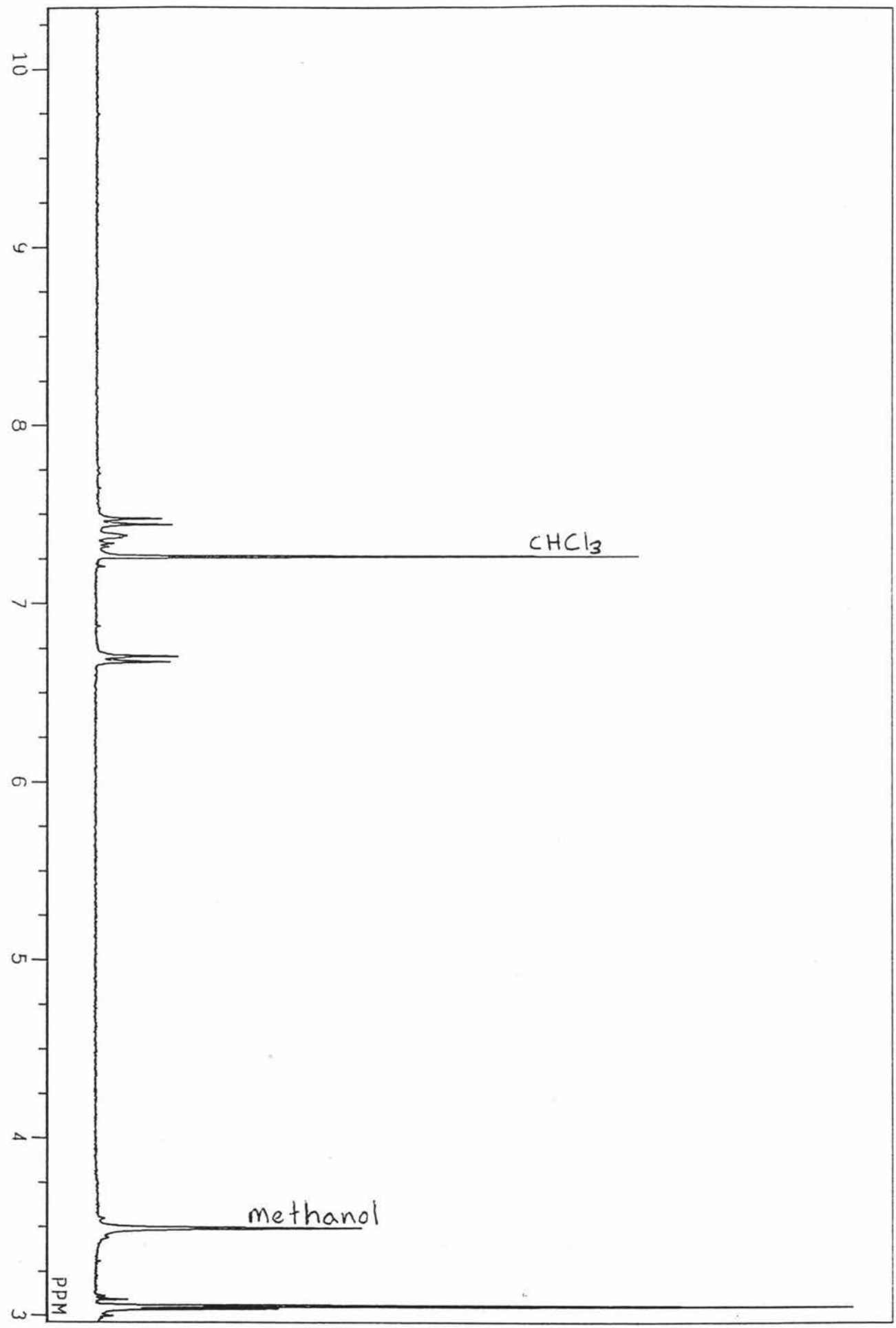

In agreement with these assignments the deuterated DACA spectrum (Figure 1.4.2.3) while showing the two sets of aromatic protons (6.7 ppm, d, 2H and 7.5 ppm, d, 2H) as in DACA does not show a signal in the aldehyde region (9-10 ppm) and the multiplet at 6.6 ppm in DACA is missing since the side chain C-2 position is also deuterated. The integration shows that the NMe_2 signal and the side chain C-3 signals are in the ratio 6:1. Hence the material produced by the condensation reations although in low yield is DACA deuterated at the side chain C-1 and C-2 positions and of sufficient purity for use in the kinetic isotope experiments.

The appearance of the 464 nm acyl intermediate formed with the synthesised deuterated DACA is shown in Figure 1.4.2.5. The time slice was recorded late in the reaction.

Figure 1.4.2.5 shows the appearance of the 464 nm acyl intermediate formed with the synthesised deuterated DACA.

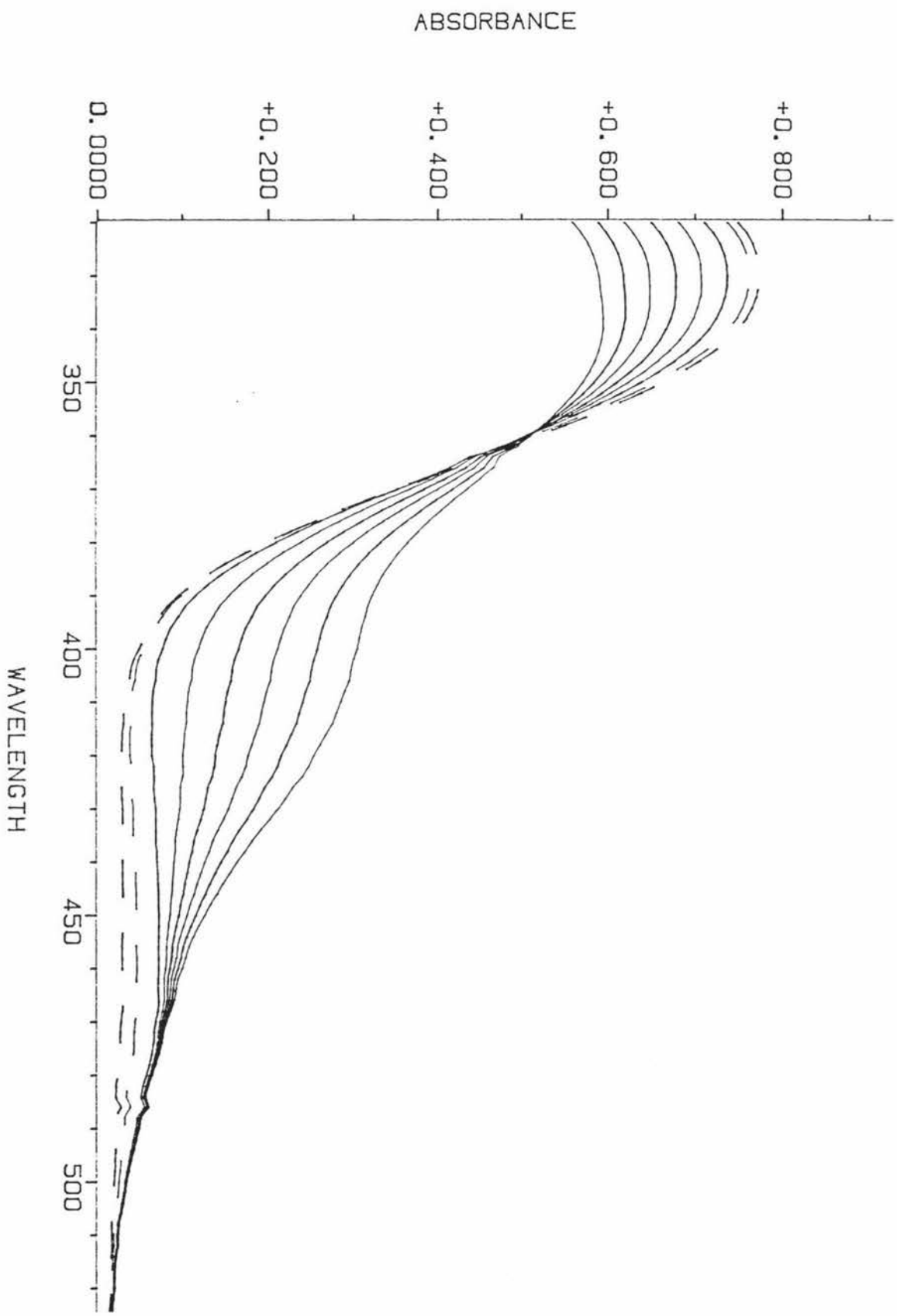

1.4.3 Isotope effects on the pre-steady-state burst during the formation of the DACA acyl-enzyme intermediate

When the DACA oxidation reaction was monitored in the stopped flow spectrometer at 475 nm there was a multiphasic rise to the steady state as shown in Figure 1.4.3.1.

The data were fitted to a two exponential model giving the rate constants shown in the figure. In principle all that is required to calculate the isotope effect is to repeat the experiment with non deuterated DACA.

However the results obtained for each stopped flow trace were dependent on the total time interval to which the burst was fitted, with smaller values for the rate constants being obtained at longer time intervals (Figure 1.4.3.2). Also, at low concentrations of deuterated DACA the time interval required was longer than at high concentrations of DACA, since the rate of reaction was slower. Hence, comparison of the rate constants for the slower deuterated DACA reaction with the faster DACA reaction constituted a problem in determining the isotope effect.

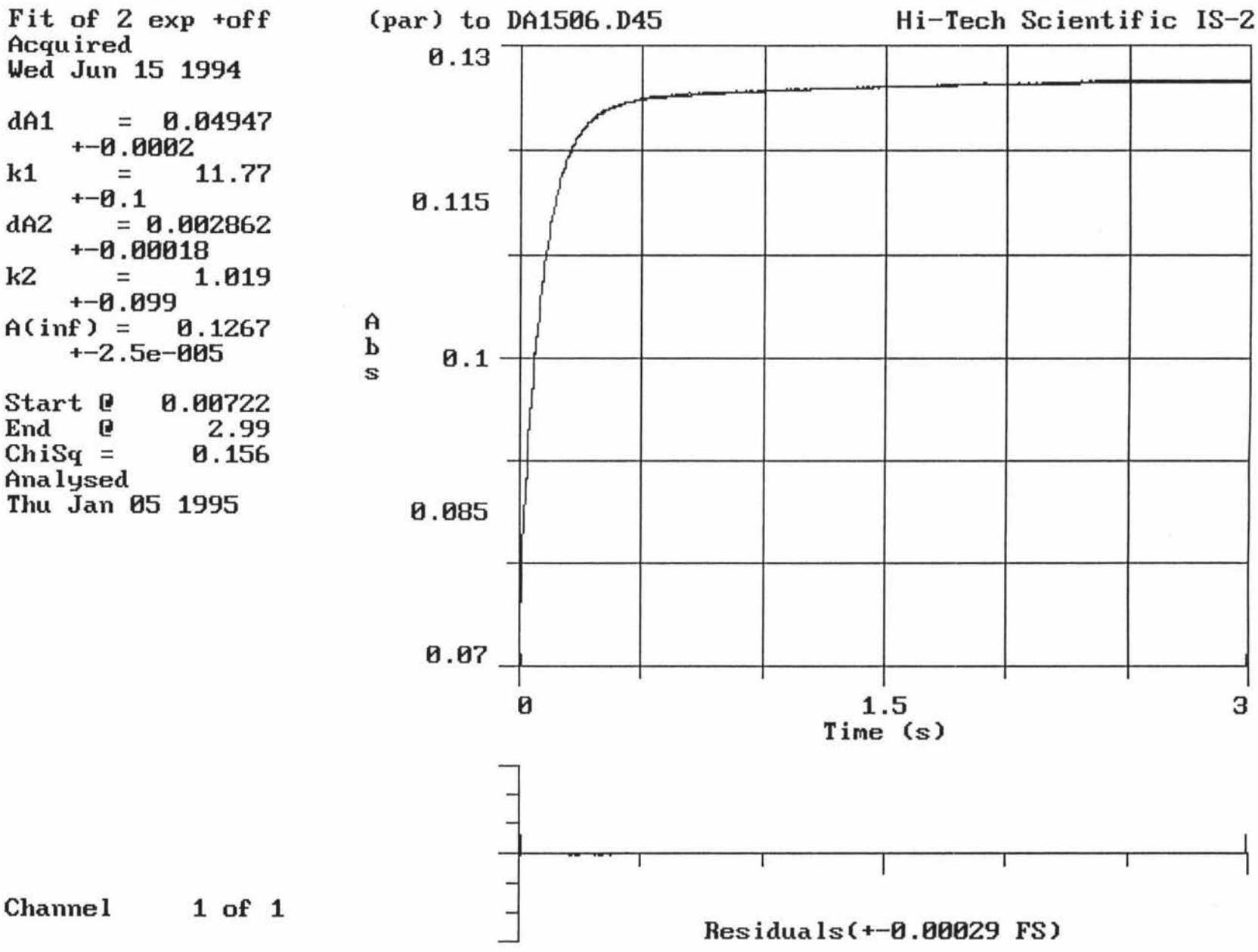

Figure 1.4.3.1 Multiphasic pre-steady-state curve for the oxidation of DACA by ALDH.

Figure 1.4.3.2 Dependence of apparent rate constants on time interval of computer fits.

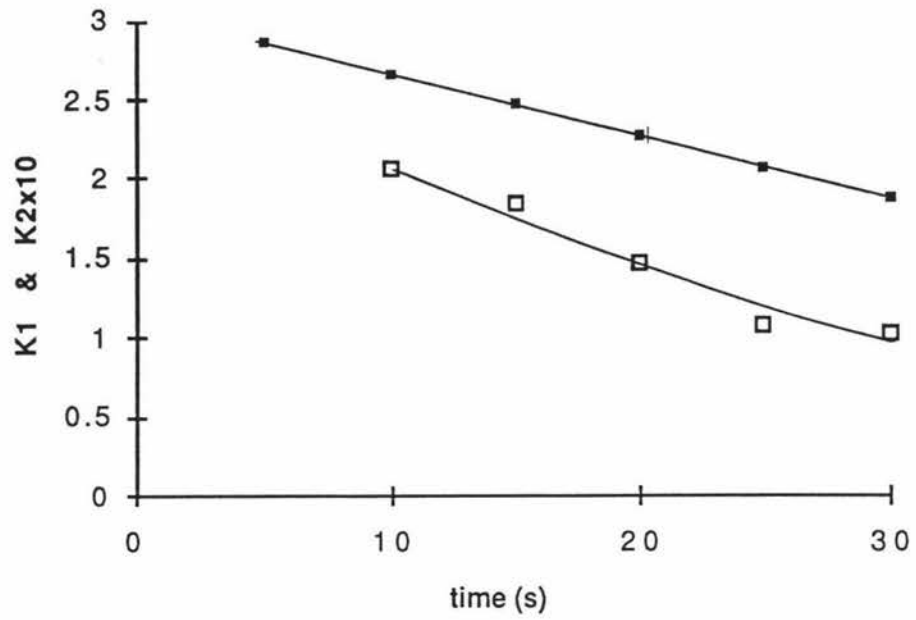

(■) Fast process *(□) Slow process*

To enable a comparison to be made between the two sets of data for the non deuterated and deuterated DACA a constant time was selected for the computer fits. Unfortunately the non deuterated DACA data were collected over a shorter time interval (15-20 seconds). Hence, the deuterated DACA data were fitted over 20 and 30 seconds since it was felt that this gave a better estimate for the slow phase. The concentration dependence of the two processes were then determined by repeating the stopped flow experiments over a range of deuterated DACA concentrations (5-32 μM). The results are given in Figure 1.4.3.3.

Figure 1.4.3.4 shows the preliminary data obtained by Paul Buckley showing the DACA concentration dependence of the faster process K1, averaged over a 15 to 20 second time interval.

Figure 1.4.3.3 Concentration dependence of rate constants for the fast process for deuterated DACA.

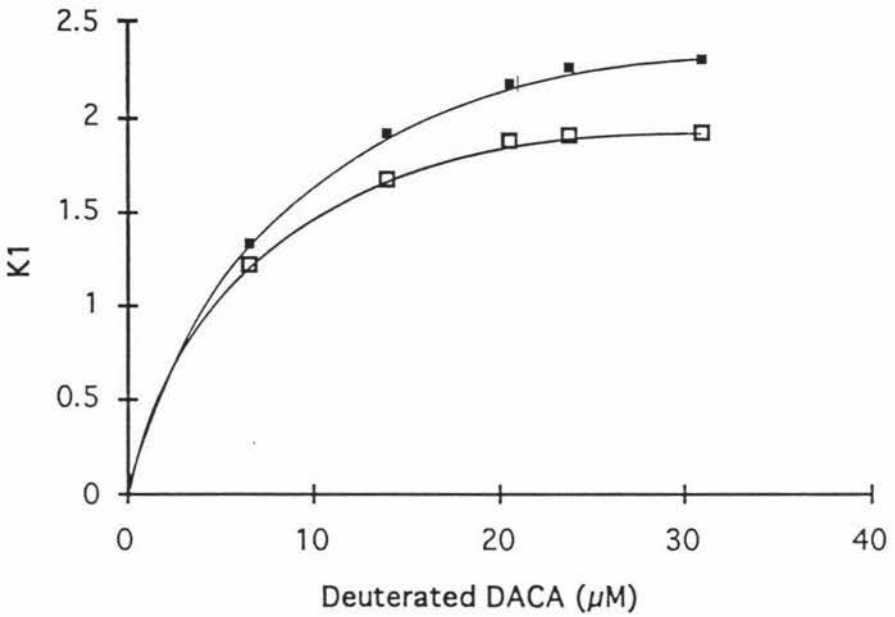

Data were fitted for 20 (■) and 30 (□) seconds at each deuterated DACA concentration.

The corresponding data for non-deuterated DACA are shown in Figure 1.4.3.4.

Figure 1.4.3.4 Concentration dependence of rate constants for the fast process for non-deuterated DACA.

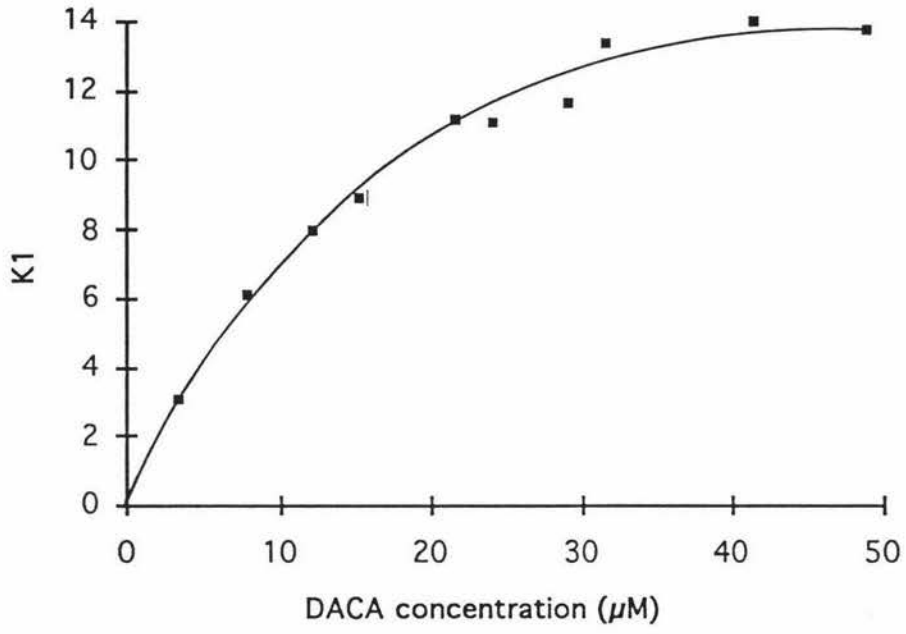

Data obtained for non deuterated DACA (P. Buckley, personal communication) were averaged over 15-20 seconds for each DACA concentration

Replots of the data as Lineweaver-Burk plots gave the apparent K_m value and maximum rate constant for both deuterated and non-deuterated DACA (Figure 1.4.3.5) and allowed the maximum isotope effect to be calculated.

Figure 1.4.3.5 Lineweaver-Burke plot for fast process for deuterated and non-deuterated DACA.

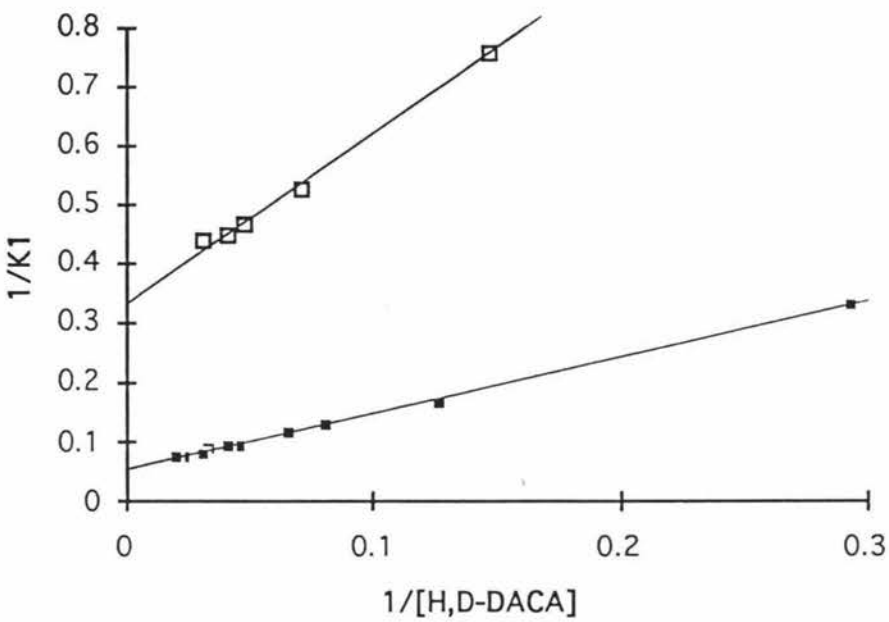

The line for DACA (■) has a slope of 1.871 and an intercept of 0.04984 seconds, giving a calculated K_m value of 18.7 μM. The line for deuterated DACA (□) on the other hand gave a slope of 2.798 and an intercept of 0.3322 seconds, giving a calculated K_m value of 8.4 μM. For each data point the ratio of the inverse slopes gives the isotope effect for the particular concentration of DACA (or DACA-d) over the range 0-50 μM and the intercepts of the Lineweaver-Burke plots give the maximum isotope effect at saturating concentration of DACA. The values for the isotope effect are shown in Figure 1.4.3.6. At infinite dilution of DACA the isotope effect was 3.0 and at saturating concentrations of DACA the isotope effect was 6.65.

Figure 1.4.3.6 Isotope effect for the fast phase process as a function of the DACA concentration.

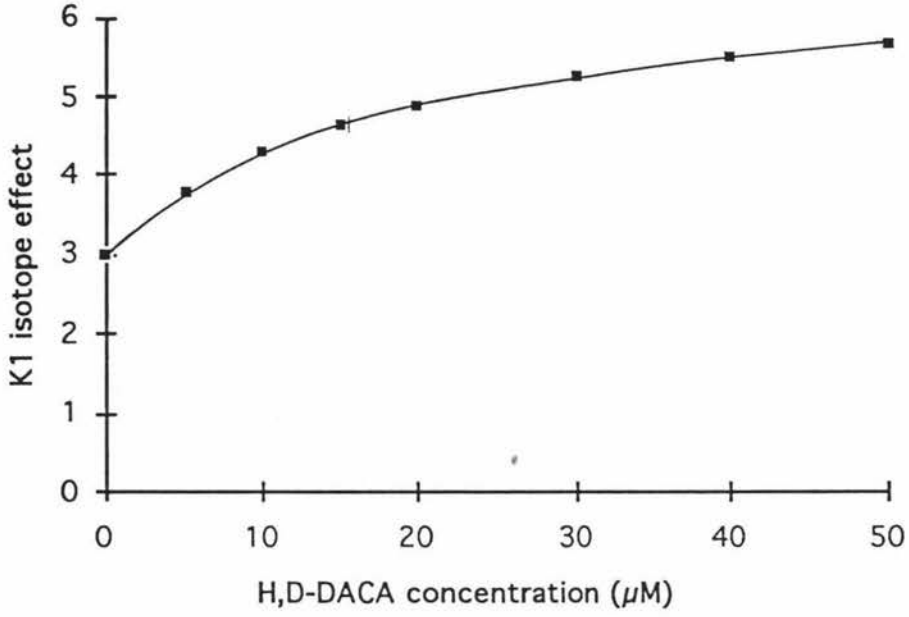

The data from Figure 1.4.3.5 were used to calculate the isotope effect at each DACA concentration.

The apparent rate constants for the slow process (K2) as a function of the deuterated-DACA concentration are shown in Figure 1.4.3.7. For calculation of the kinetic isotope effect the data obtained previously by Buckley (personal communication) are also shown (Figure 1.4.3.8).

Figure 1.4.3.7 Apparent rate constatns for the slow process as a function of deuterated DACA concentration.

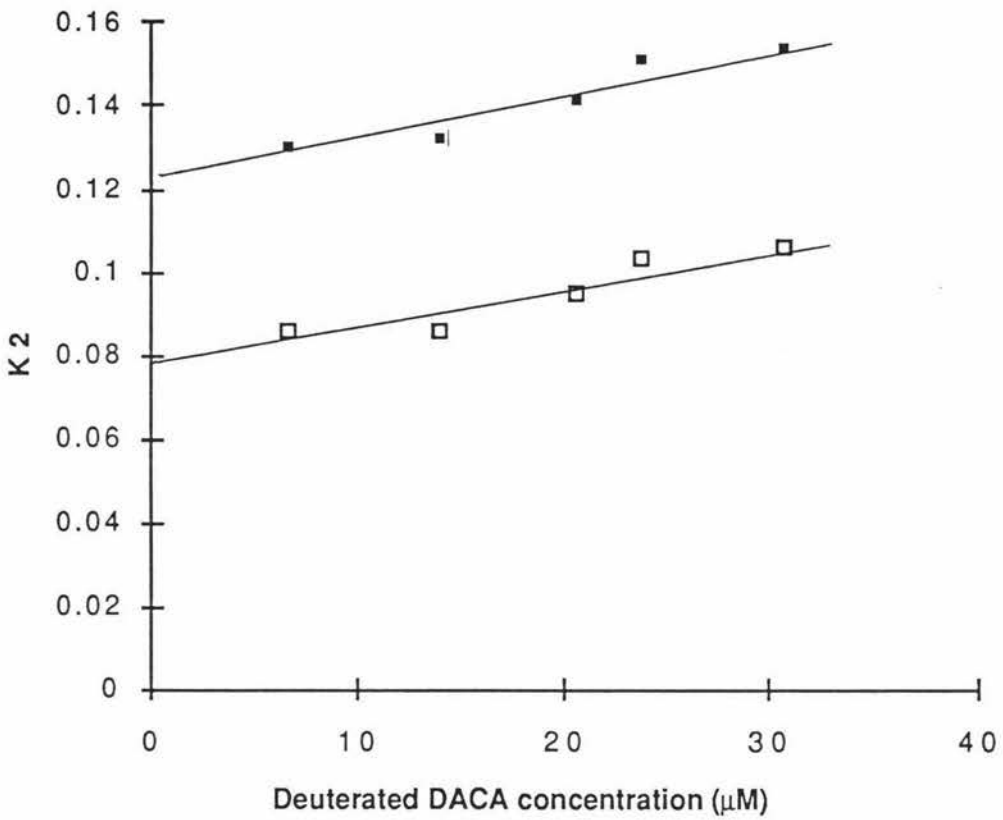

The data were fitted over 20 (■) and 30 (□) seconds at each detuerated DACA concentration.

Figure 1.4.3.8 Apparent rate constants for the slow process fitted over 15-20 seconds for non-deuterated DACA.

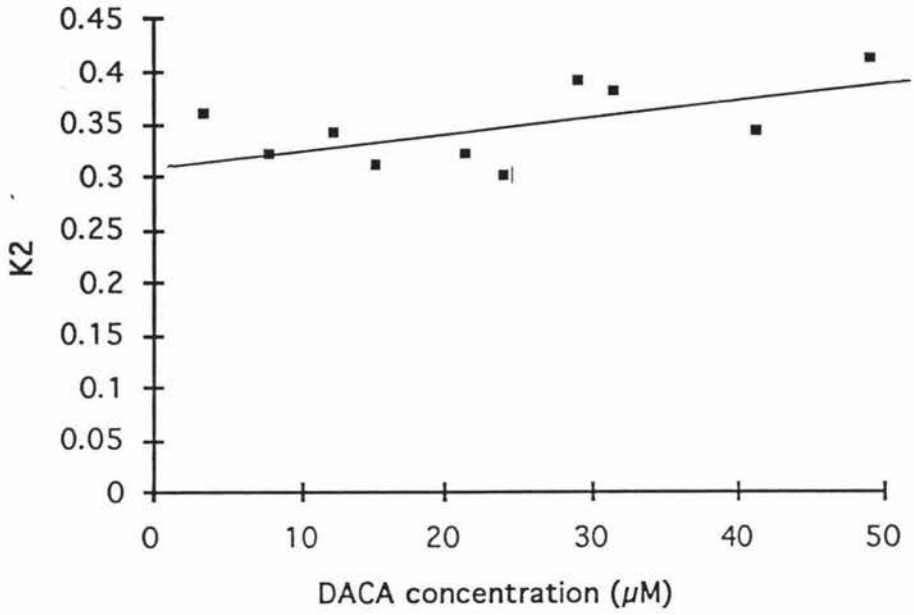

Data were provided by P. Buckley from preliminary experiments obtained with non-deuterated DACA.

As can be seen from Figure 1.4.3.7 and Figure 1.4.3.8 the slower phases for both DACA and deuterated-DACA appear to be virtually independent of concentration, although best fit lines indicate a small increase with increasing concentration. Using the deuterated-DACA data obtained for the 20 second fit (Figure 1.4.3.7, A) there was an apparent isotope effect on the slow phase of approximately 2.

There was also an observable isotope effect on the amplitudes of each of the fast (K1) and slow (K2) phases. For DACA the amplitude of the fast phase was approximately 91 % and the slow phase 9 % but for the deuterated-DACA data fitted over 20 seconds, the amplitude of the fast phase was only 60 - 70 % and was concentration dependent. This concentration dependence is shown in Figure 1.4.3.9.

Figure 1.4.3.9 Concentration dependence of the amplitudes of the fast and slow phases for deuterated DACA.

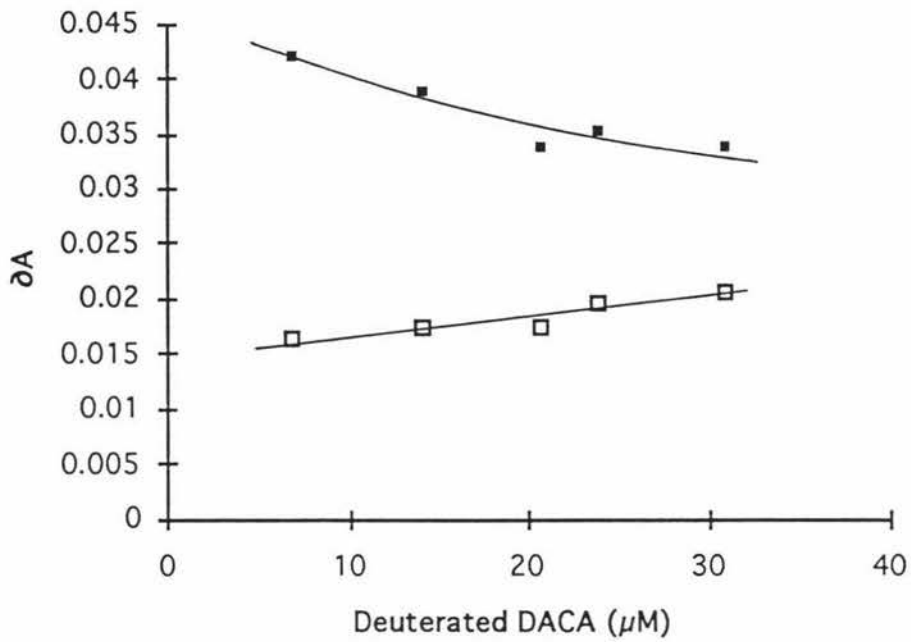

The DACA concentration dependence for the amplitude of the fast phase (■) had a slope of -0.0003668 and an intercept of 0.04370. The slow phase (□) had a slope of 0.0001738 and an intercept of 0.01480.

1.4.4 Kinetic modeling of the isotope effects on the pre-steady-state burst during the formation of the DACA acyl-enzyme intermediate

There are five important results from the present work, which must be accounted for in any kinetic model for ALDH.

1. Hydride transfer is a rate limiting step in the pre-steady-state oxidation of DACA.
2. The process is biphasic and the two phases are coupled.
3. Both phases have an apparent isotope effect.
4. The relative amplitudes of each phase have an isotope effect which is also dependent on the DACA concentration.
5, The fits to the experimental rate data depend on the time over which the computer analysis is carried out.

The currently accepted model (Scheme 1.4.4.1) for the aldehyde dehydrogenase catalysed oxidation of aldehydes involves a sequential mechanism in which the acyl enzyme is formed in a single step as hydride transfer takes place.

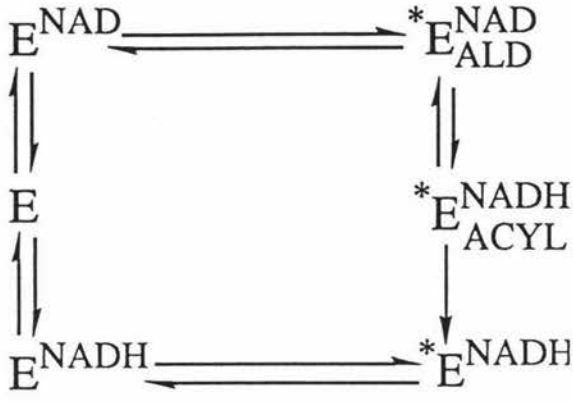

Scheme 1.4.4.1

It must be noted that the oxidation of DACA by NAD constitutes a special case in that the ALDH-acyl species formed is very stable, and hydrolysis of this species is considered to be rate limiting at pH 7.4. Hence, according to scheme 1.4.4.1, if NADH release can continue even when the enzyme is acylated then an extra acyl enzyme species will exist on the pathway for DACA oxidation as shown in scheme 1.4.4.2

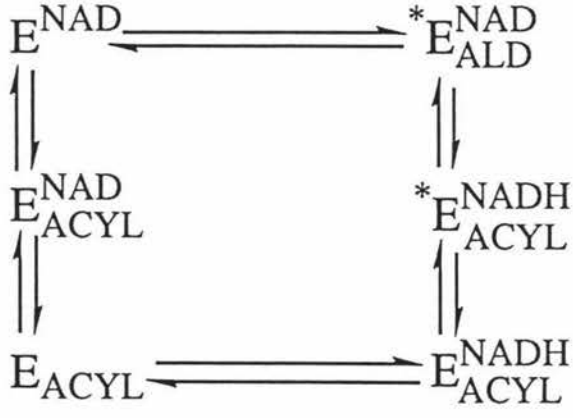

Scheme 1.4.4.2

Since at 475 nm it is the appearance of the acyl enzyme species that is being monitored, an isotope effect on the process is expected. Scheme 1.4.4.2 will only show biphasic behavior if the reverse of the hydride transfer step is rapid enough that not all of the enzyme exists in the acylated form during the transient phase of the reaction. Thus a second slower phase should result which is due to isomerisation (or displacement) of the NADH.

While scheme 1.4.4.2 would give rise to two transients one of which should show a large isotope effect it is difficult from computer modelling experiments to produce an isotope effect for the slower phase using rate constants which also give an isotope effect on the amplitudes of the fast and slow phases.

The problem then is to identify an additional step, the rate of which is coupled in some way to the rate of hydride transfer, and which will therefore show an isotope effect. The additional step must involve some other ALDH-DACA-NAD species, with the amount of the new species which is produced also depending on the rate of hydride transfer, so that the observed difference in amplitudes of the two processes shows an isotope effect.

Bennett (1981) proposed that ALDH-NAD like ALDH-NADH could exist in two possible conformations. If the ALDH-NAD species can exist in two possible conformations, and only one conformer is suitable for aldehyde oxidation, then the equilibrium between the two can be represented by scheme 1.4.4.3.

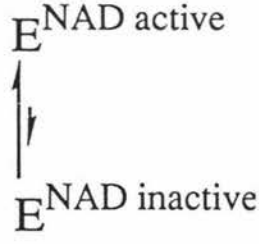

Scheme 1.4.4.3

In this model, the favoured ALDH-NAD conformer of the equilibrium is the active conformer, in the absence of aldehyde. When aldehyde binds to the ALDH-NAD species (either at the active site or some other site) the

equilibrium between the two ALDH-NAD species is perturbed (if hydride transfer does not occur) so that the inactive ALDH-NAD conformer is actually more favoured. Thus, in an experiment when a saturating concentration of NAD is premixed with ALDH and then mixed with an unreactive aldehdye such as DACA (so that acyl enzyme hydrolysis is slow, approximating to zero compared with the rate constants for the transients) the kinetic model becomes as shown in scheme 1.4.4.4

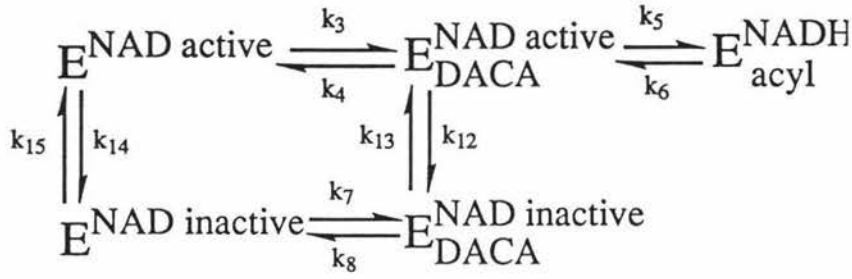

Scheme1.4.4.4

It is not possible to calculate the apparent rate constants for the transients assuming values for the rate constants of scheme 1.4.4.1. Therefore the scheme was simulated by computer analysis as outlined in Section 1.3.5. The kinetic parameters used in the simulations are listed in Table 1.4.4.1. Since there is also a DACA concentration dependence on the amplitudes of each phase, one concentration was chosen to test whether in principle the model was a viable explanation. It was assumed that the rate of hydride attack from NADH to the ALDH-acyl species was slow, just as nucleophilic attack from water is very slow for the ALDH-DACA-acyl species.

Table 1.4.4.1 Kinetic parameters for simulation of scheme 1.4.4.4

Initial parameters	Value
[DACA]	50 μM
k3	10 $\mu M.s^{-1}$
k4	200 s^{-1}
k5	19.6 s^{-1} for hydride, 2.04 s^{-1} for deuteride
k6	0.1 s^{-1} for hydride,0.01 s^{-1} for deuteride
k7	10 $\mu M.s^{-1}$
k8	200 s^{-1}
k12	1.3 s^{-1}
k13	0.35 s^{-1}
k14	0.0175 s^{-1}
k15	0.35 s^{-1}
X1 ($E^{NAD\ active}$)	0.95 μM
X2, X3, X7	0 μM
X8 ($E^{NAD\ inactive}$)	0.05 μM

A DACA concentration of 50 μM was chosen for the simulations, at this concentration all of the isotope effects are large (therefore more difficult to fit) while still staying in the approximate range of the experimental data.
It was assumed that the rate of hydride attack from NADH to the DACA acyl species was slow, in the same way that nucleophilc attack of the DACA acyl species from water is also slow.

The results are given in Table 1.4.4.2. Reasonable agreement was obtained between the experimental data and the computer fits.

Table 1.4.4.2 Summary of kinetic parameters obtained by computer fits to scheme 1.4.4.4

Experiment	K_1	K_2	A_1	A_2
H-measured	14.6	0.36	91%	9%
H-simulated	14.6	0.33	91%	9%
D-measured	2.58	0.17	52%	48%
D-simulated	2.52	0.20	52%	48%

The apparent isotope effect on the hydride transfer step for this model is 9.6. Thus scheme 1.4.4.4 does fit the experimental data for reasonable choices of the individual rate constants.

However it must be remembered that the values obtained from the simulation are not neccessarily unique. While agreement between the experimental values and the simulated values is reasonable scheme 1.4.4.4 predicts a simple biphasic system for which the values of K_1 and K_2 obtained by fitting experimental should be independent of the time over which the data is collected. Since in practice the data show a significant dependence on the time period chosen for fitting, scheme 1.4.4.4 still represents an over simplification. The true situation must be represented by more than two phases. The next most simple mechanism is tri-phasic.

Obviously the next difficult question then becomes, what is the third phase attibuted to? Since there is a large change in the apparent rates over time, the third phase must make a significant amplitude contribution to the slow phase. All changes after hydride transfer occurs can again be eliminated because they could not make any contribution to the measured isotope effects on the slow phase rate or on the amplitude. In the model already proposed, the dominant flux of enzyme starts in the active E.NAD species and then after the addition of DACA rapidly forms the active E.NAD.DACA species. If another step was included between these two species this may show triphasic behaviour, but again it could not

make any contribution to the measured isotope effects on the slow phase rate or amplitude.

Two mechanisms which could have the potential to show the observed isotope effect are shown in Scheme 1.4.4.5. Note that both these mechanisms have been simplified by only considering one E^{NAD} species.

Scheme 1.4.4.5

(A)

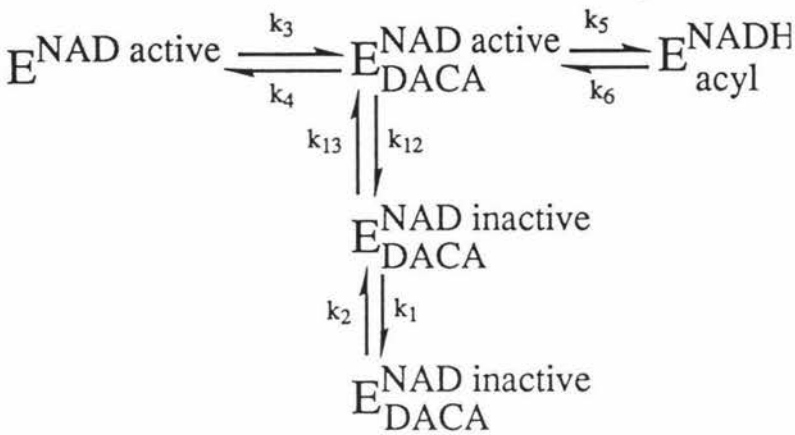

(B)

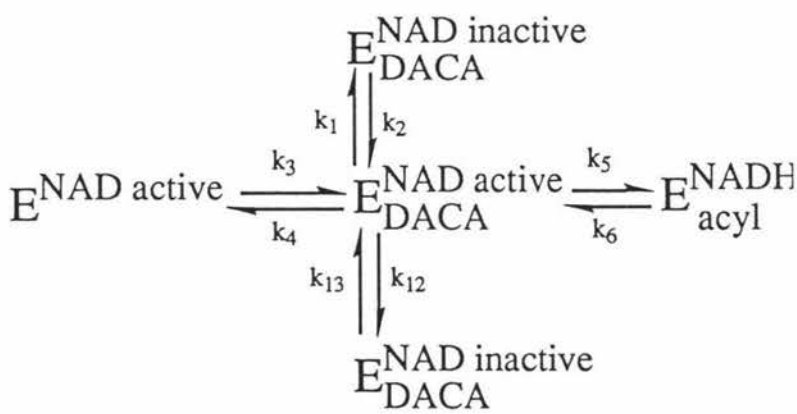

When (A) was investigated it was difficult to find combinations of rate constants that could fit the observed rates of the fast and slow processes and have a reasonable time dependence.

When (B) was simulated, time dependence on the apparent rates was very easy to achieve. The controlling rate constant for the slow phase of the

biphasic model was k_{13} (= 0.35 s^{-1}) in the new triphasic model (B) this was replaced by a combination of k_{13} and k_2. When k_{13} and k_2 are equal it is possible to produce identical behavour to the biphasic model and hence have no time scale dependence on the parameters required for fitting the data. As k_2 and k_{13} become very different a time dependence on the fast and slow phases is observed. Obviously the extent to which k_2 and k_{13} contribute is determined by the relative concentration of each of the E.NAD.DACA dead end complexes. This in turn is determined by the rates governing the formation and destruction of the dead end complexes. An example of this time dependent behaviour has been simulated and the rates for each process are shown in Table 1.4.4.3.

Table 1.4.4.3 Kinetic parameters for simulation of scheme 1.4.4.5 (B)

Initial parameters	Value
[DACA]	30 μM
k_3	10 μM.s^{-1}
k_4	200 s^{-1}
k_5	19.4 s^{-1} for hydride, 2.0 s^{-1} for deuteride
k_6	0 s^{-1}
k_1	1.55 s^{-1}
k_2	1.1 s^{-1}
k_{12}	1.1 s^{-1}
k_{13}	0.06 s^{-1}
X1 ($E^{NAD\ active}$)	1 μM
X2, X3, X7,X6	0 μM

Table 1.4.4.4 shows the apparent rate constants and amplitudes fitted to 20 seconds in comparison to the experimental results.

Table 1.4.4.4 Summary of kinetic parameters obtained by computer fits to scheme 1.4.4.5 (B).

Experiment	K_1	K_2	A_1	A_2
H-measured	12.33	0.335	91%	9%
H-simulated	12.34	0.328	91%	9%
D-measured	2.35	0.156	62%	38%
D-simulated	2.36	0.153	61%	39%

Again it must be remembered that this is far from being a unique solution, in that many combinations of rate constants can give rise to the same observed rates and amplitudes.The time dependence of K_1 and K_2 is shown in Figure 1.4.4.1.

Figure 1.4.4.1 Dependence of simulated rate constants on time interval of computer fits.

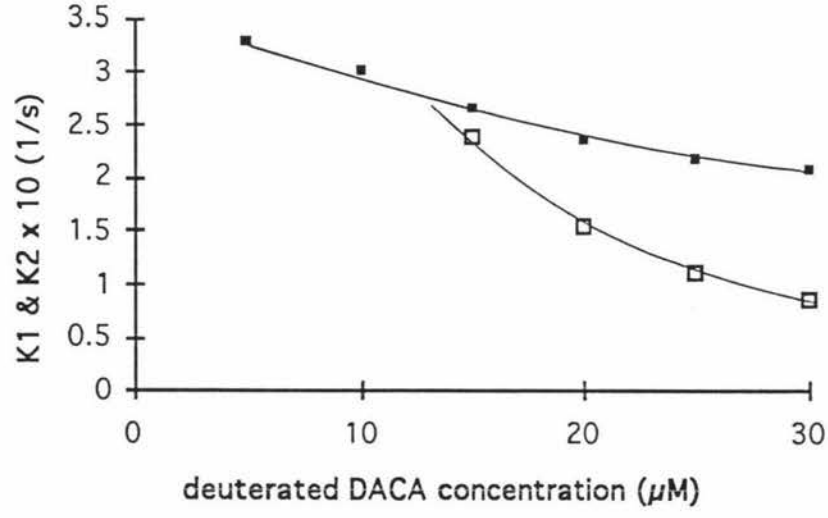

(■) Fast process *(□) Slow process*

In Figure 1.4.4.1 it can be seen by comparison with Figure 1.4.3.2 that for the simulated rate constants there is now too much time dependence on the apparent fast and slow rates, in particular with respect to the slow phase. It is possible in theory using this triphasic model to produce large

time dependence on the fitted parameters such as is shown in this example, right down to zero time dependence the same as in the biphasic model. Furthermore there is the flexibility to vary the slopes of the time dependant lines of the fast and slow phases relative to each other. Hence, it is likely with suitable combinations of rate constants that the triphasic model (B) could be a good approximation of the real mechanism. Data which fits this time dependent behaviour more exactly will be sought after the completion of this thesis, for the purpose of publication.

1.4.5 Ethanamoyl 4-*trans* (N,N-dimethylamino) cinnamoate

ALDH has been shown to catalyse the hydrolysis of anhydrides to the corresponding carboxylic acids (Motion, thesis). It has been suggested by Motion (thesis) that during catalysis that ALDH reacts with the anhydride forming an acyl intermediate. In order to study this reaction further it was decided to synthesis an anhydride that could undergo a colour change when reacting with ALDH. DACA has been shown to form a quasi-stable ALDH-acyl species which has an absorption spectrum that is considerably red-shifted, with a $\Delta\lambda_{max} \approx 64$ nm from the λ_{max} of DACA (Dunn and Buckley, 1982). Hence, if an anhydride of DACA was made it has the possibility of being a useful spectroscopic tool. The DACA anhydride that was synthesised was ethanamoyl 4-*trans* (N,N-dimethylamino) cinnamoate shown in Figure 1.4.5.1.

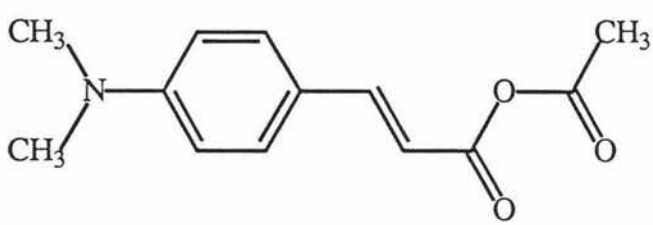

Figure 1.4.5.1 ethanamoyl 4-*trans* (N,N-dimethylamino) cinnamoate

Synthesis of Ethanamoyl 4-trans (N,N-dimethylamino) cinnamoate

Ethanamoyl 4-*trans* (N,N-dimethylamino) cinnamoate was successfully synthesised by the reaction of sodium 4-*trans* (N,N-dimethylamino) cinnamoate with ethanoic anhydride (scheme 1.4.5.1).

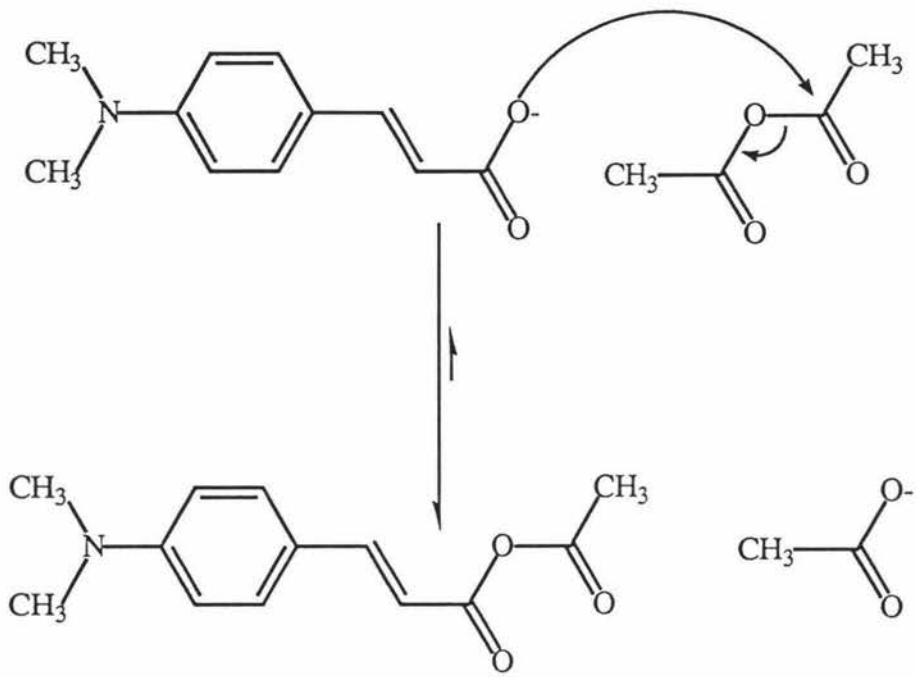

scheme 1.4.5.1

4-*trans* (N,N-dimethylamino) cinnamic acid (80 mg) was weighed into a 20 ml round bottomed flask and then NaOCH3 (23 mg) and 10 ml of analar methanol was also added. The mixture was stirred until the 4-*trans* (N,N-dimethylamino) cinnamic acid completely dissolved, (approximately 45 minutes). The solution was then evaporated to dryness on a roto-vac. Ethanoic anhydride (10 ml) was then added and the solution mixed for 30 minutes, during which time the colour changed from pale yellow to intense yellow. This mixture was then dried on a vacuum line. Dry dichloromethane (10 ml) was then added, and a small amount of white solid thought to be sodium acetate which was not very soluble settled to the bottom of the flask. The upper solution was decanted using a pipette into another flask and placed on the vacuum line. Separation of the products using chromatography was not possible due to the instability of the ethanamoyl 4-*trans* (N,N-dimethylamino) cinnamoate.

Figure 1.4.5.2 shows the n.m.r for ethanamoyl 4-*trans* (N,N-dimethylamino) cinnamoate.

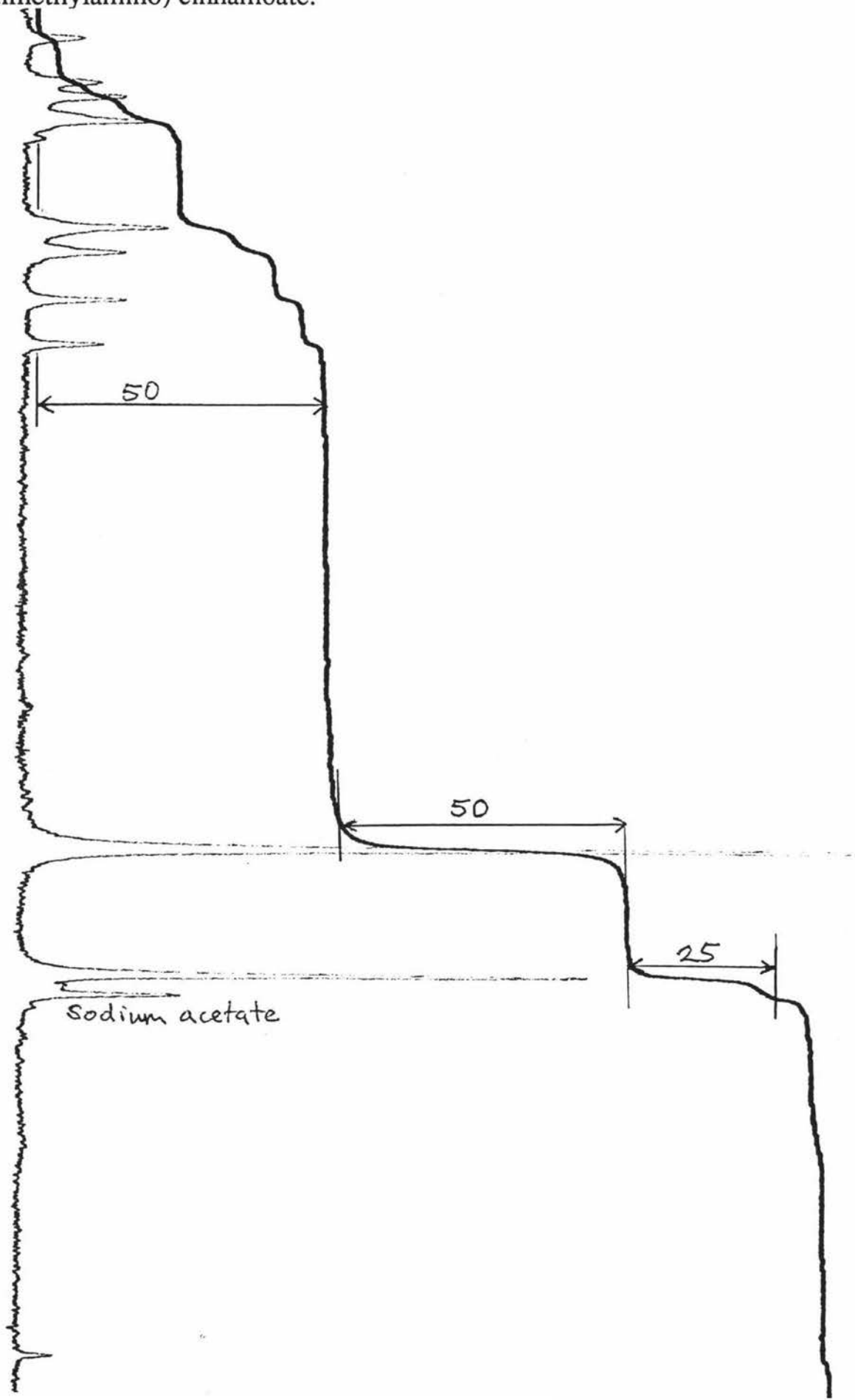

Figure 1.4.5.3 shows the reaction of ethanamoyl 4-*trans* (N,N-dimethylamino) cinnamoate with water .

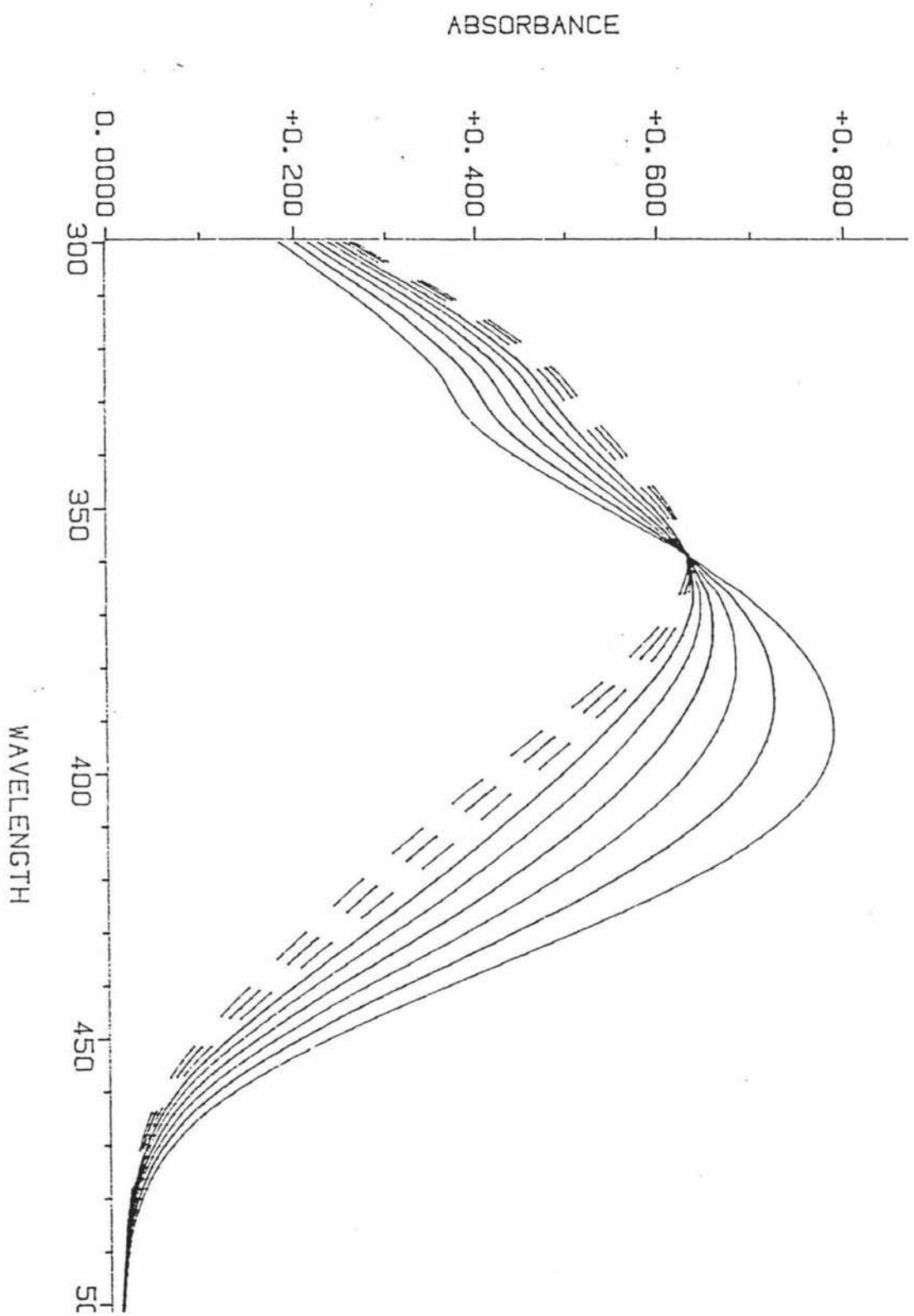

Kinetics of Ethanamoyl 4-trans (N,N-dimethylamino) Cinnamoate

When ethanamoyl 4-*trans* (N,N-dimethylamino) cinnamoate ($A_{398} \approx 0.8$) was mixed with phosphate buffer at pH 7.4 containing 1 μM ALDH a rapid decrease at 398 nm was observed corresponding to the hydrolysis of the anhydride. No appearance of a 464 nm DACA acyl species was observed and the spectral changes appeared to be the same as anhydride in buffer alone. This was an unexpected result and suggests that the active site of ALDH is unable to utilise ethanamoyl 4-*trans* (N,N-dimethylamino) cinnamoate as a substrate for steric reasons, or that the active site selectively attacks exclusively at the ethanamoyl carbonyl carbon.

1.4.6 Conclusion

Hydride tranfer is rate limiting step in the presteady state of ALDH catalysed oxidation of DACA (with NAD premixed). The currently accepted model certainly can not explain the apparent isotope effects. The results from the simulations of a model in which an inactive ternary E.NAD.DACA complexes were present on the pathway, indicated that such species might exist.

Chapter 2

Formation of 4-*trans* (N,N-dimethylamino cinnamaldehyde complexes as models for the acyl intermediate

2.1 Introduction

"Reporter groups", are molecules that can bind to an enzyme and in doing so they provide information about the micro-environment of the enzyme where they bind. "Reporter groups" are usually chromophores which exhibit environment dependent changes in their absorption or fluorescence spectra.

In this chapter use is made of an ALDH 4-*trans* (N,N-dimethylamino) cinnamoyl - cysteine moiety chromophore which is formed as an acyl intermediate in the ALDH catalysed oxidation of 4-*trans* (N,N-dimethylamino cinnamaldehyde (DACA) as a reporter group for the active site of aldehyde dehydrogenase.

Two spectrally red-shifted acyl species have been observed with DACA as a substrate, one at 484 nm and one at 464 nm, although when either are denatured a species absorbing at 408 nm is observed. The 484 nm species can be observed (Buckley, personal communication) by forming the 464 nm species at pH 7.6, then rapidly passing the enzyme solution though a short column of Pharmacia P60 biogel pre-equilibrated at pH 6.0 or pH 4.0. Figure 2.1.1.1 is an absorption spectrum of the 484 nm species.

Harvey (personal communication) has found from gel filtration HPLC studies, that passing ALDH through a gel column at pH 5.2 causes the tetrameric ALDH to totally dissociate.

The 464 nm species has been shown to be an ALDH 4-*trans* (N,N-dimethylamino) cinnamoyl - cysteine moiety, and there are two such

Figure 2.1.1.1 Absorption spectrum of the 484 nm ALDH 4-*trans* (N,N-dimethylamino) cinnamoyl - cysteine moiety

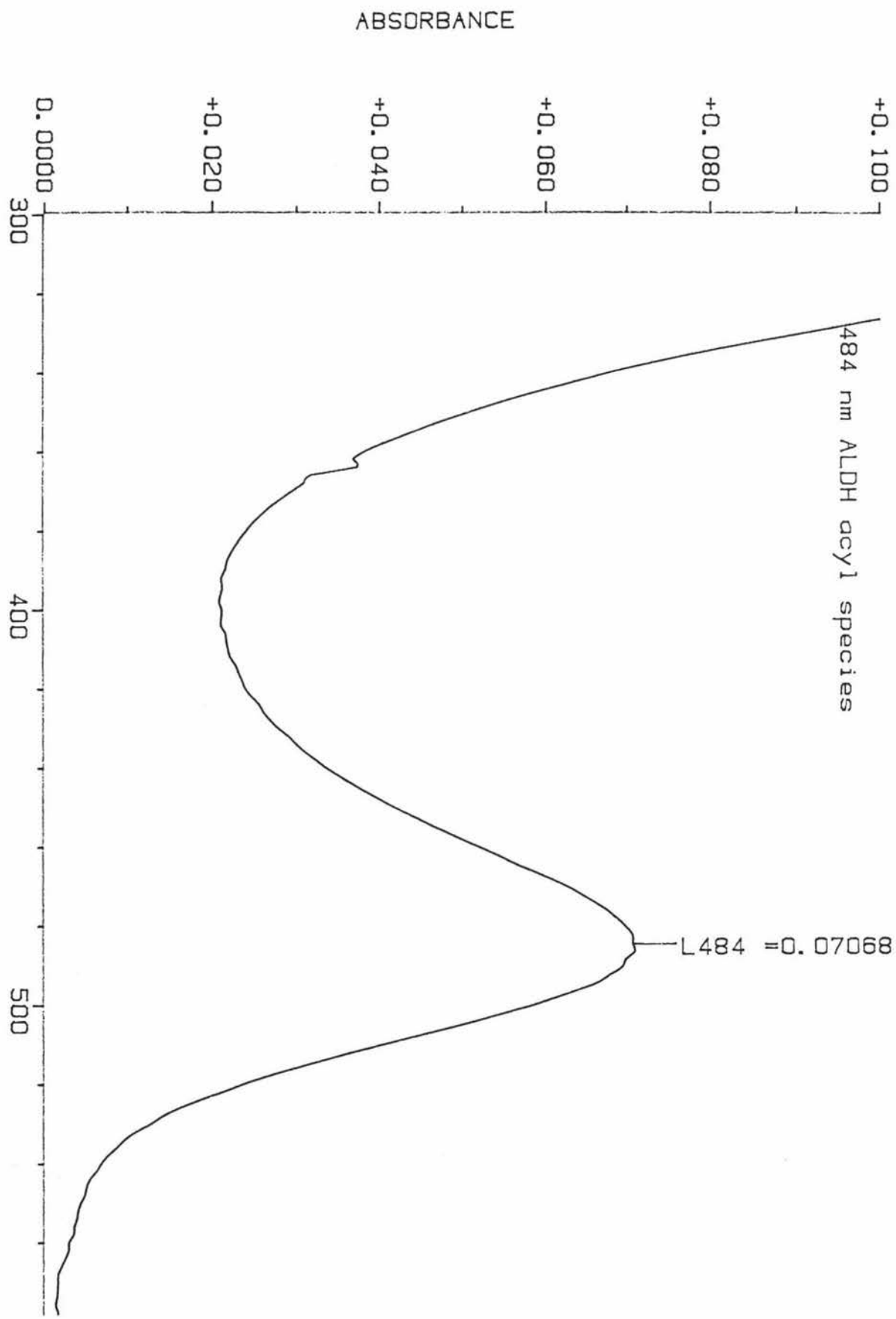

moieties present per ALDH tetramer (Pietruszko et al, 1990). The spectrum of the 464 nm intermediate appeared to be independent of pH over the range pH 4.1 to pH 10.5 (Buckley and Dunn, 1985).

2.2 Materials and Methods.

2.2.1 Formation of chromophore complexes

The commercially available compounds 4-*trans* (N,N-dimethylamino) cinnamaldehyde, furylacrolein, acetonitrile, acetic acid , imidazole, zinc chloride, cupric chloride, sodium fluoride, sodium chloride, sodium iodide, sodium hydroxide, sodium ethanoate, lithium sulphate, N,N,N,N-tetramethyl ethylene diamine and tetra n-butyl ammonium iodide were all analar grades and were used without further purification. Water was purified by reverse osmosis and followed by deionisation.

The UV-visible spectra of solutions of acetonitrile (or water, or chloroform) containing DACA (approximately 25 μM) and variable concentrations of complexing agents were measured in a Hewlet Packard 8452 diode array spectrophotometer. A blank was run in each case with acetonitrile or water containing just the complexing agent.

DACA (5 μl) was added to 1 ml of the solution being studied.
The complexing agents N,N,N,N-tetramethyl ethylenediamine dihydroacetate and imidazole hydroacetate were prepared *in situ*. This was accomplished by adding 95% of the theoretical amount of acetic acid to solutions containing N,N,N,N-tetramethyl ethylene diamine and imidazole respectively.

The concentration of the complexing agents used were as follows:-

Table 2.2.1.1 DACA complexing solutions

Complexing agent	Solvent	Concentration
chromium (III) chloride	acetonitrile	11.4 mM
cupric chloride	acetonitrile	33.4 mM
zinc chloride	acetonitrile	saturating
	acetonitrile	33.4 mM
	chloroform	saturating
sodium fluoride	water	0.5 M
sodium chloride	water	1.0 M
sodium Iodide	water	1.1 M
sodium hydroxide	water	1.0 M
sodium ethanoate	water	1.2 M
lithium sulphate	water	1.2 M
ethanoic acid	acetonitrile	4.2 M
	acetonitrile	33.4 mM
water	acetonitrile	1.1 M
ethanamide	acetonitrile	0.5 M
N,N,N,N-tetramethyl ethylenediamine dihydroethanoate	acetonitrile	0.6 M
Imidazole hydroethanoate	acetonitrile	2.6 M
tetra n-butyl ammonium iodide	acetonitrile	0.6 M
guanidinium chloride	water	0.7 M
ethanamide	water	1.0 M

This same procedure was repeated using furylacrolein as a chromophore, the complexing solutions are shown in Table 2.2.1.2

Table 2.2.1.2 Furylacrolein complexing solutions

Complexing agent	Solvent	Concentration
zinc chloride	chloroform	saturating
ethanamide	water	2 M
ethanoic acid	acetonitrile	4.2 M
guanidinium chloride	water	1 M

2.2.2 Determination of difference spectra

The spectrum of each DACA complex was determined in the following manner A spectrum of DACA with the complexing agent present (total) and of DACA without the complexing agent present (free DACA) was recorded. In acetonitrile as a solvent it was assumed that at 340 nm only free DACA absorbed, and there was negligible contribution from the complexed DACA (section 2.4.8, assumption 2).

Using the software of the diode array spectrometer, the "total" spectrum was multiplied by a scaling factor (F) so that the scaled spectrum (total x F) and the "freeDACA" spectrum had equal absorbance at 340 nm.

$$F = \frac{A_{340}\ \text{free DACA}}{A_{340}\ \text{total}}$$

$$\text{total} \times F = \text{total spectrum} \times F$$

The difference spectrum between the scaled DACA spectrum containing complexing agent (total x F) and the uncomplexed DACA spectrum

(freeDACA), was then calculated and is representative of the complexed DACA species (comDACA).
i.e.

total.F spectrum = freeDACA spectrum + comDACA spectrum

comDACA spectrum = Total.F spectrum - freeDACA spectrum

The red-shift in each case was then calculated by subtracting the absorption maximum of the free DACA spectrum (freeDACA) from the absorption maximum of the complexed DACA (comDACA) spectrum.

$$\text{Red-shift} = \lambda_{max}\ (\text{comDACA}) - \lambda_{max}\ (\text{freeDACA})$$

An example of this is shown in Figure 2.2.2.1 for the DACA complex formed with acetic acid. The red-shift was 408 nm (comDACA) - 380 nm (freeDACA) = 28 nm.

When the solvent used was water or chloroform, the spectra were equalised at 350 nm instead of 340 nm (for acetonitrile), because DACA absorbs at a longer wavelengths in water (λ_{max} 400 nm) and chloroform than acetonitrile (λ_{max} 380 nm). For furylacrolein the spectra were equalised at 280 nm when the solvent was acetonitrile and 290 nm when the solvent was water or chloroform.

Figure 2.2.2.1 The DACA complex formed with acetic acid

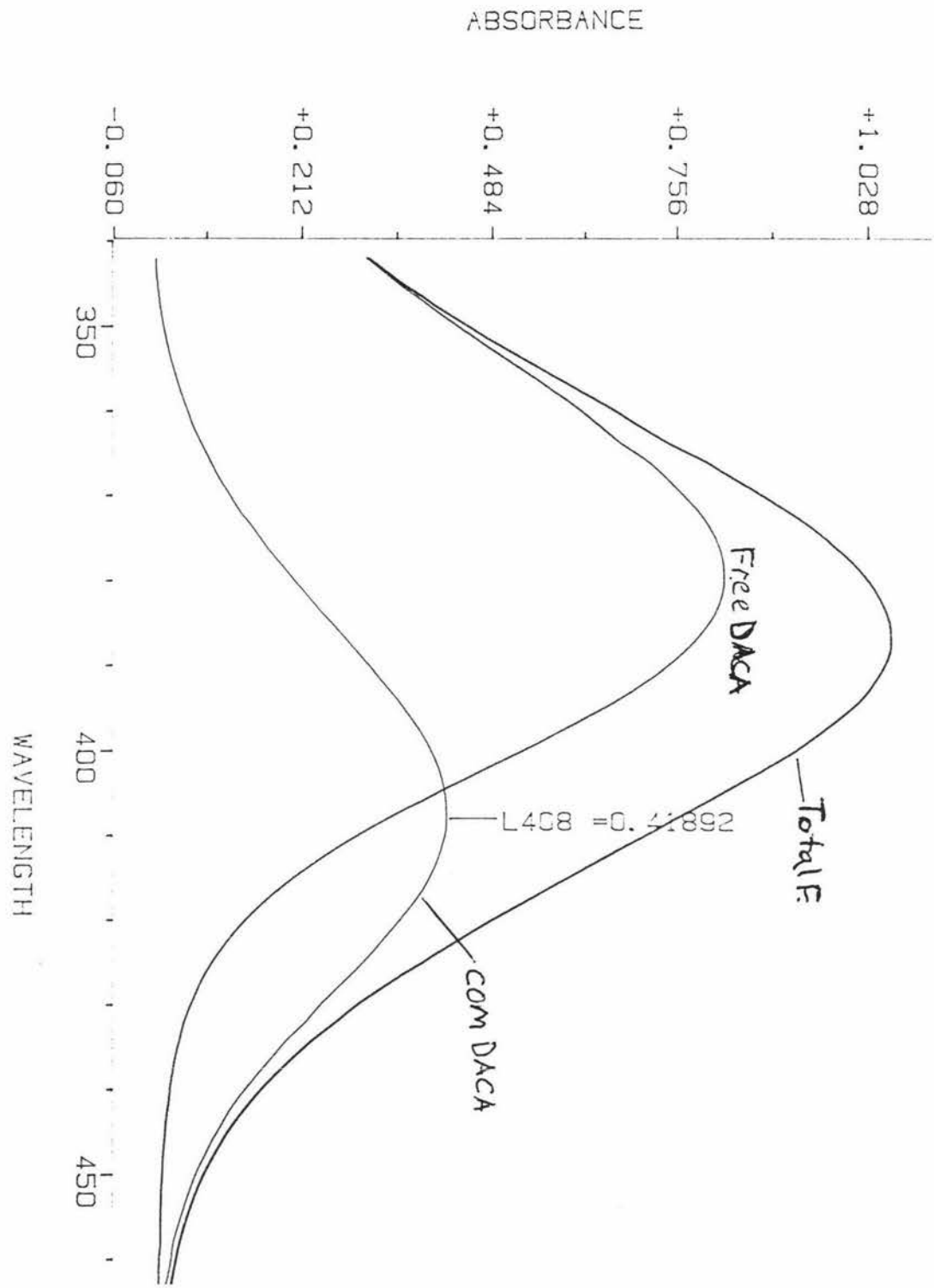

2.2.3 Formation of the ALDH furylacryloyl cysteine moiety using thioNAD

In ALDH (0.4 μM, final concentration) was added to pH 5.0 sodium ethanoate buffer (100 mM) with 70 μM thioNAD (1 ml total volume), and the solution was blanked. To this 10 μM of furylacrolein was added in 5 μl. After 30, 60, and 90 seconds the spectrum was recorded, and stored on to the hard drive. A spectrum of just furylacrolein in buffer was also recorded.
The spectrum of just furylacrolein alone (equalised at 324 nm) was subtracted from the spectra recorded at 30, 60 and 90 seconds (using the same method as described in methods 2.1), to give the spectrum of the ALDH furylacryloyl cysteine moiety and a small contribution from thioNADH. ThioNAD was used instead of normal NAD because the product formed with NAD absorbs at 340 nm, which would interfere with the assumption that at 324 nm the only absorbing species is furylacrolein.

2.3 Results

2.3.1 DACA complexes formed with non-metal electrophiles

Examples of the difference spectra obtained are shown below. Figure 2.3.1.1 shows the difference spectrum for the guanidinium chloride-DACA complex, Figure 2.3.12 shows the difference spectrum for the N,N,N,N-tetramethyl ethylenediamine dihydroethanoiate-DACA complex.

The results are summarised in Table 2.3.1.1

Table 2.3.1.1 Summary of the red-shifts induced in DACA by non-metal complexing agents.

Complexing agent	Solvent	Concentration	Red-shift
ethanoic acid	acetonitrile	4.2 M	28 nm
		33.4 mM	28 nm
ethanamide	acetonitrile	0.5 M	22 nm
N,N,N,N-tetramethyl ethylenediamine dihydroethanoate	acetonitrile	0.6 M	20 nm
imidazole hydroethanoate	acetonitrile	2.6 M	20 nm
tetra n-butyl ammonium iodide	acetonitrile	0.6 M	14 nm
guanidinium chloride	water	0.7 M	22 nm
ethanamide	water	1.0 M	12 nm

Figure 2.3.1.1 Difference spectrum for the guanidinium chloride-DACA complex.

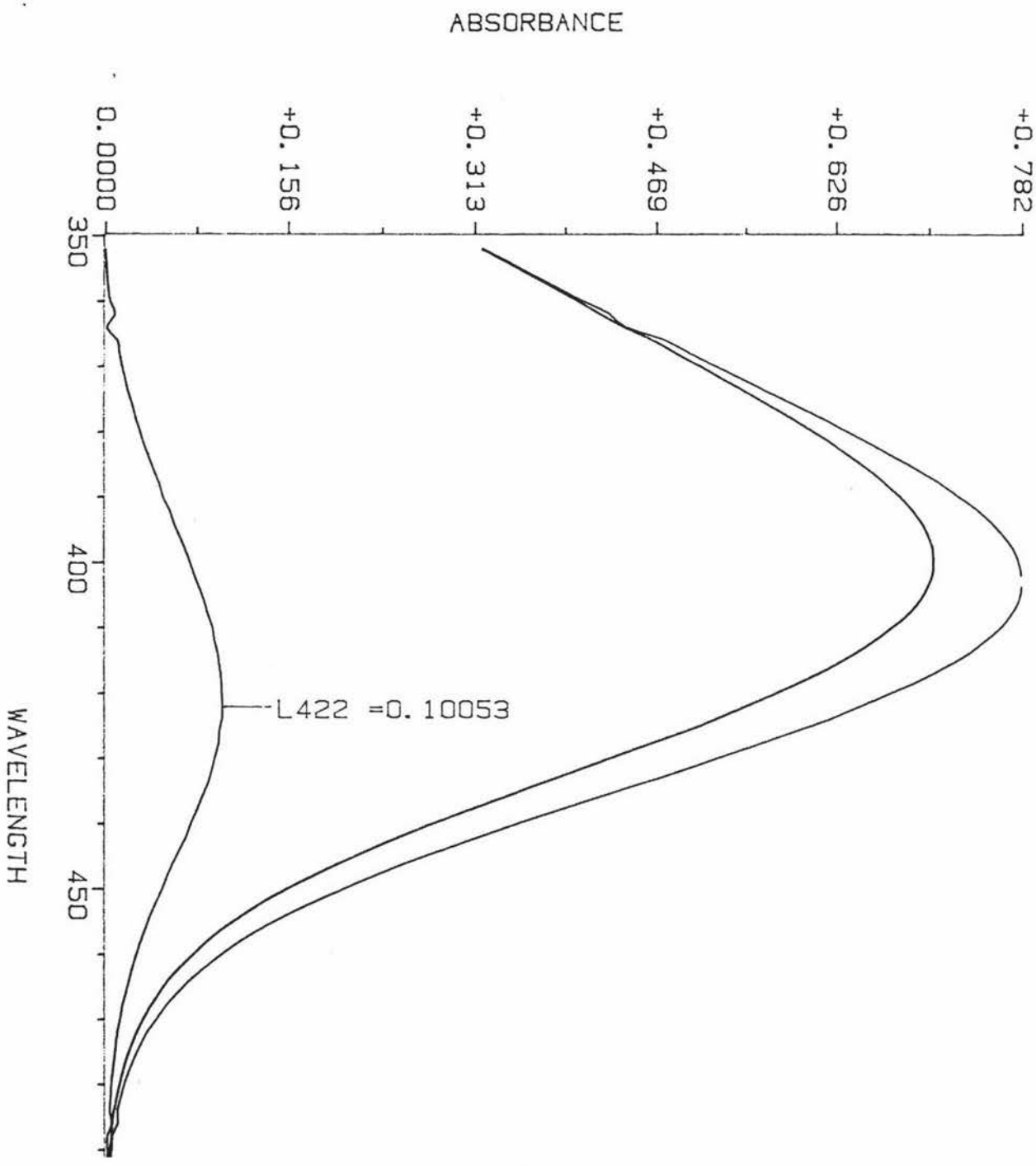

Figure 2.3.1.2 Difference spectrum for the N,N,N,N-tetramethyl ethylenediamine dihydroethanoiate-DACA complex.

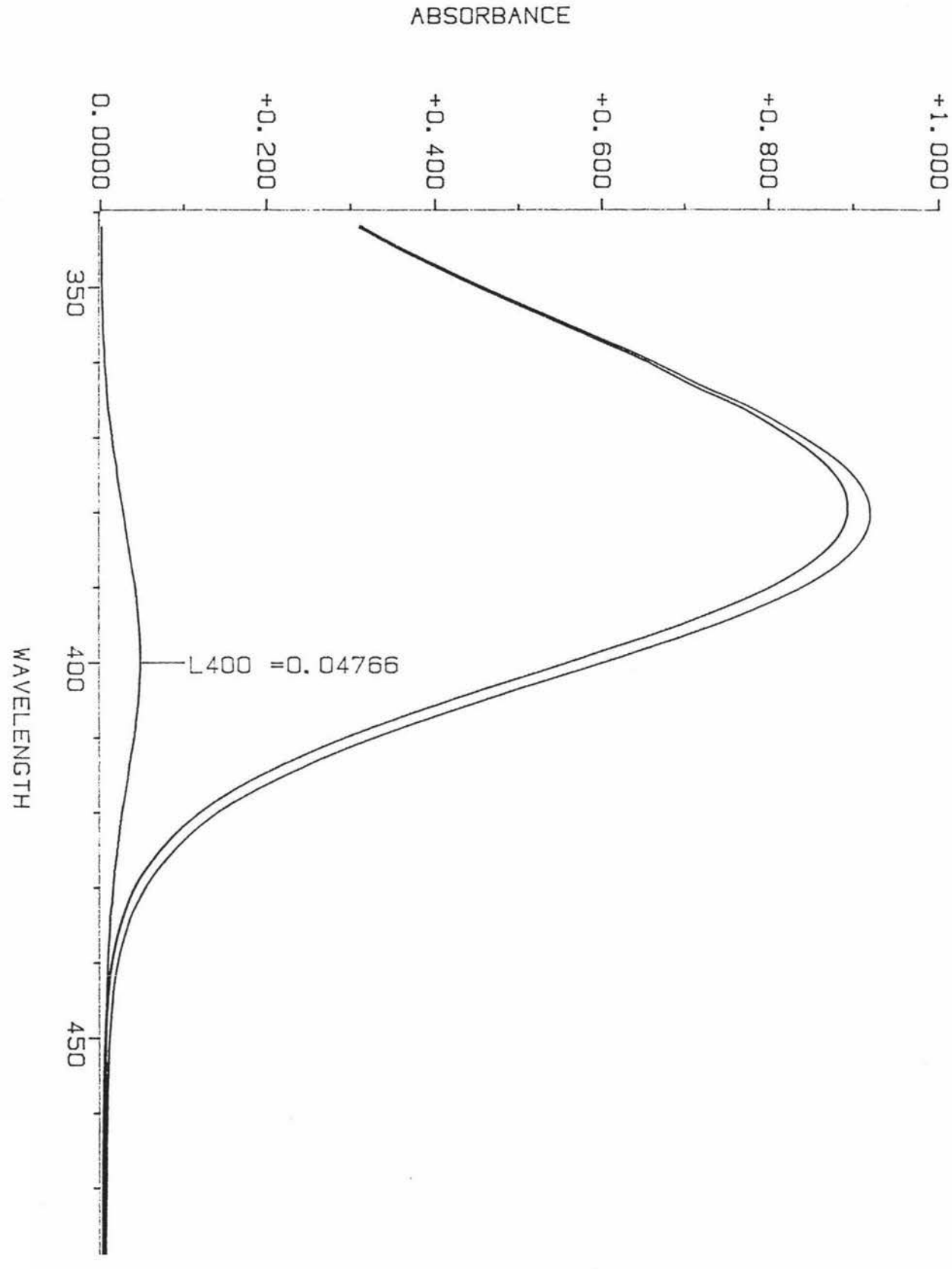

2.3.2 DACA complexes formed with metal electrophiles

Insolubility, instability, and overlapping absorption bands limited the divalent and trivalent metal ions studied to copper (II) chloride, chromium (III) chloride and zinc (II) chloride.
Other divalent or trivalent metal ions that were tried:-

Iron (II) chloride	-unstable, overlapping absorption bands
Iron (III) chloride	-unstable, overlapping absorption bands
Manganese (II) nitrate	-insoluble
Manganese (II) sulphate	-insoluble
Cobalt (II) chloride	-insoluble
Cobalt (II) ethanoiate	-insoluble
Cobalt (II) Cl_2 Py_2	-soluble, but no complex formation
Nickel (II) chloride	-insoluble
Zinc (II) ethanoiate	-insoluble

Examples of the difference spectra obtained with the metal electrophiles are shown below. Figure 2.3.2.1 shows the difference spectrum for the zinc-DACA complex. Figure 2.3.2.2 shows the difference spectrum for the sodium iodide-DACA complex.

Figure 2.3.2.3 shows the difference spectrum obtained for chromium-DACA complex, it is interesting to note the additional band observed at 380 nm which is possibly due to charge transfer between the chromium and either DACA or the chloride ion. An additional absorption band was also observed for the copper-DACA complex at 406 nm.

Figure 2.3.2.1 Difference spectrum for the zinc-DACA complex.

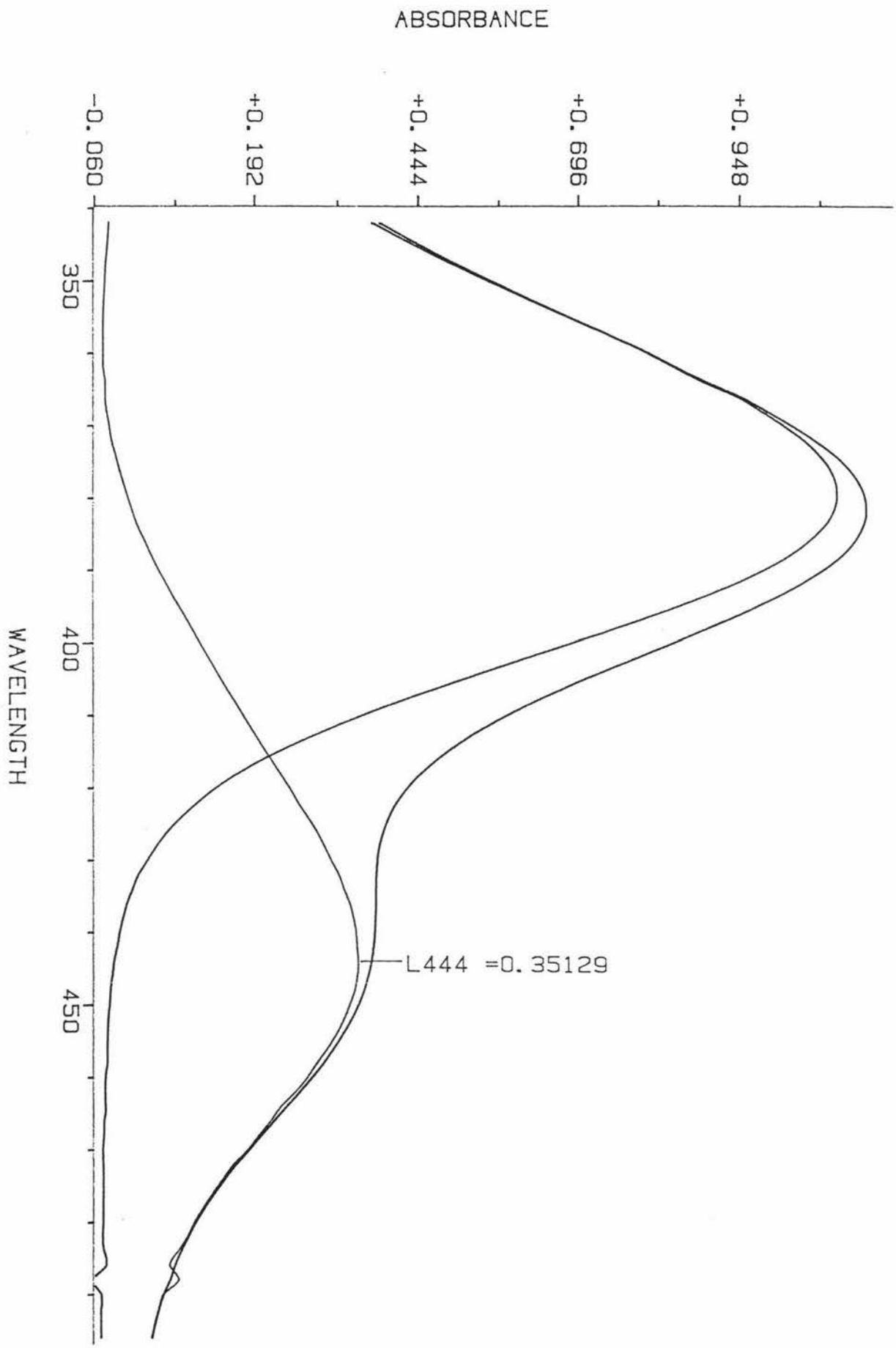

Figure 2.3.2.2 Difference spectrum for the sodium iodide-DACA complex.

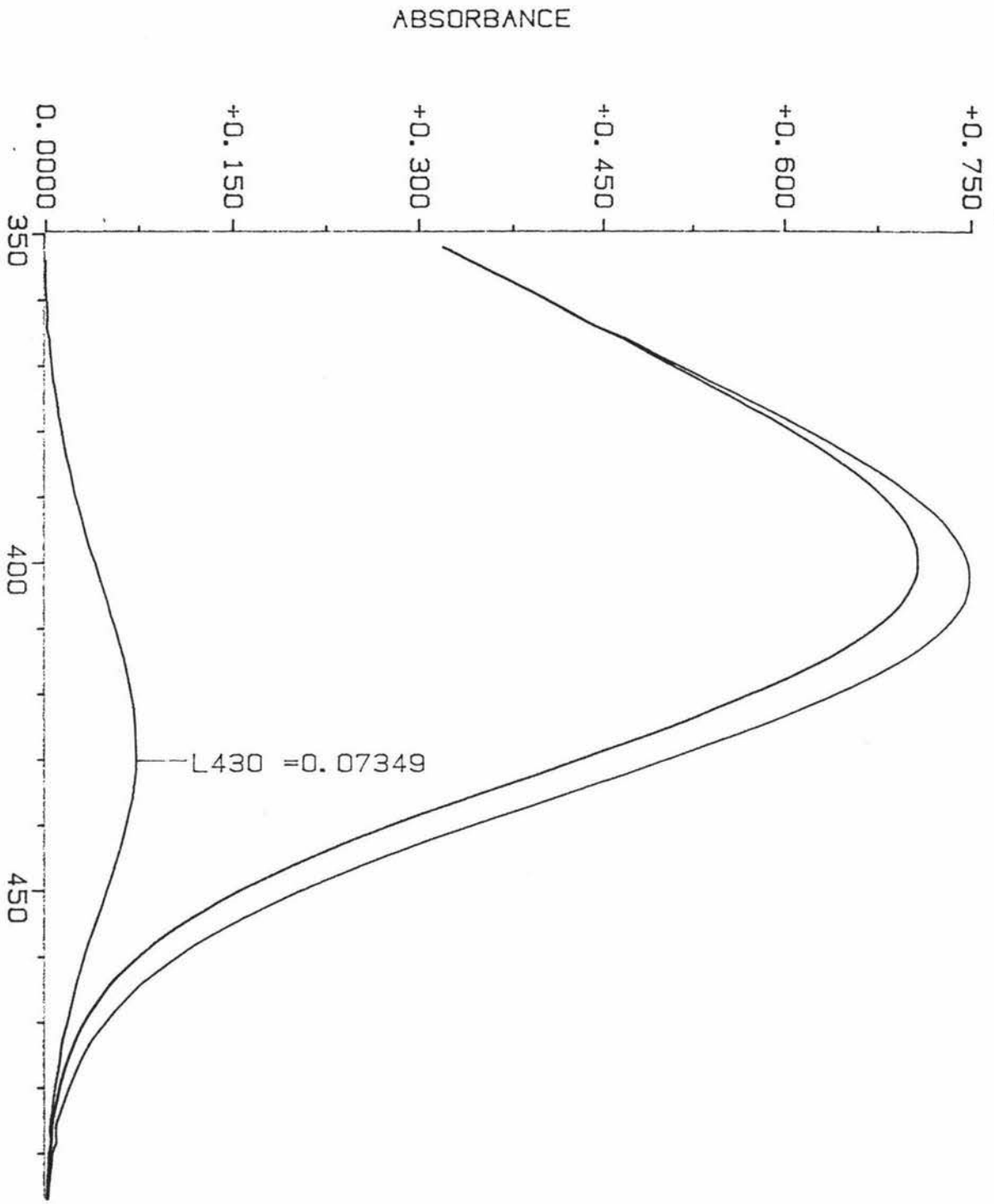

Figure 2.3.2.3 Difference spectrum for the chromium-DACA complex.

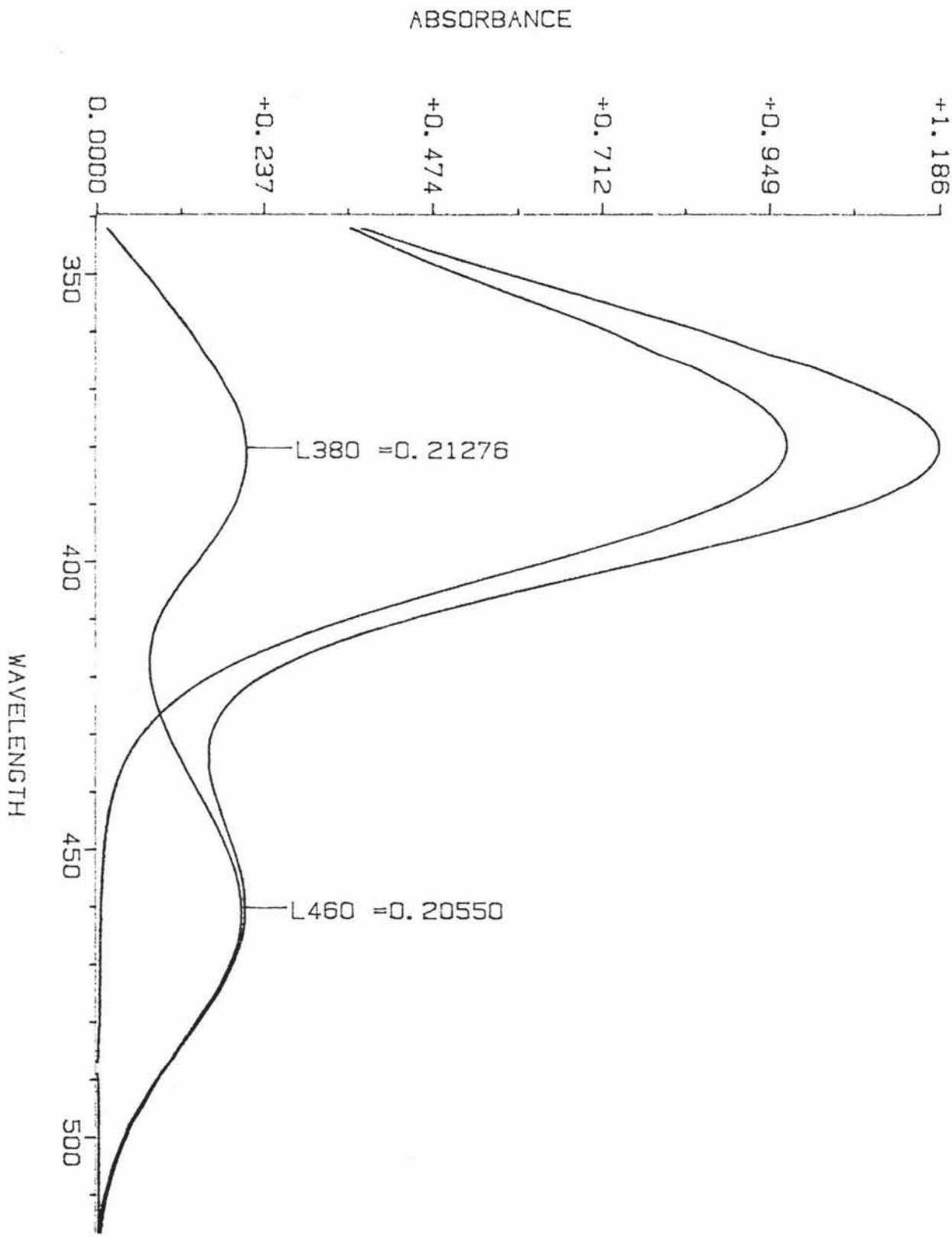

The results are summarised in Table 2.3.2.1

Table 2.3.2.1 Summary of the red-shifts induced by metal complexing agents in DACA

Complexing agent	Solvent	Concentration	Red-shift
chromium (III) chloride	acetonitrile	11.4 mM	80 nm
cupric chloride	acetonitrile	33.4 mM	74 nm
zinc chloride	acetonitrile	saturating	64 nm
		33.4 mM	64 nm
zinc chloride	chloroform	saturating	60 nm
sodium fluoride	water	0.5 M	44 nm
sodium chloride	water	1.0 M	34 nm
sodium iodide	water	1.1 M	30 nm
sodium hydroxide	water	1.0 M	30 nm
sodium ethanoate	water	1.2 M	28 nm
lithium sulphate	water	1.2 M	34 nm

2.3.3 Furylacrolein complexes formed with metal and non-metal electrophiles.

In general furylacrolein was difficult to form complexes with. In acetonitrile no divalent or trivalent complexes formed, presumably due to competition from the acetonitrile solvent. When chloroform was used as an alternative solvent a complex was formed with zinc, but neither chromium nor copper was soluble in chloroform. Table 2.3.3.1 shows the red-shifts induced in furylacrolein by complexing agents.

Table 2.3.3.1 Summary of the red-shifts induced by metal and non-metal complexing agents in furylacrolein.

Complexing agent	Solvent	Concentration	Red-shift
zinc chloride	chloroform	saturating	26 nm
ethanoic acid	acetonitrile	4.2 M	17 nm
guanidinium chloride	water	1 M	14 nm
ethanamide	water	2 M	8 nm

2.3.4 Absorption spectra of the ALDH furylacryloyl cysteine moiety.

Figure 2.3.4.1 shows the difference spectra obtained at 30, 60, and 90 seconds for the formation of the ALDH furylacryloyl cysteine moiety. From the results it can be seen that at pH 5.0 the acyl intermediate forms slowly, which is in good agreement with results shown by Buckley and Dunn (1985) for the formation of the DACA acyl species at pH 5.1. The ALDH furylacryloyl cysteine moiety was found to have a λ_{max} 368 nm, which is 30 nm red-shifted compared to the model compound furylacryloyl-S-acyl-N-acetyl cysteine (λ_{max} 338 nm). The zinc induces a red-shift in DACA (in chloroform) which is identical to the red-shift for the ALDH-DACA 464 nm species. Zinc under identical conditions induces a red-shift in furylacrolein which is only 26 nm, 4 nm less than the red-shift shown in the difference spectra obtained (Figure 2.3.4.1) for the ALDH furylacryloyl cysteine moiety (30 nm). The differences may in part be due to a small contribution from the thioNADH which is viewed in Figure 2.3.4.1 as an absorption shoulder at approximately 410 nm. However, observation of the time resolved UV-visible spectra for the reaction of ALDH-NAD with furylacrolein shown in Buckley and Dunn (1982, Figure 6.B), seems to indicate best agreement with a shift of 30 nm.

Figure 2.3.4.1 Absorption spectra of the ALDH-furylacryloyl cysteine moiety

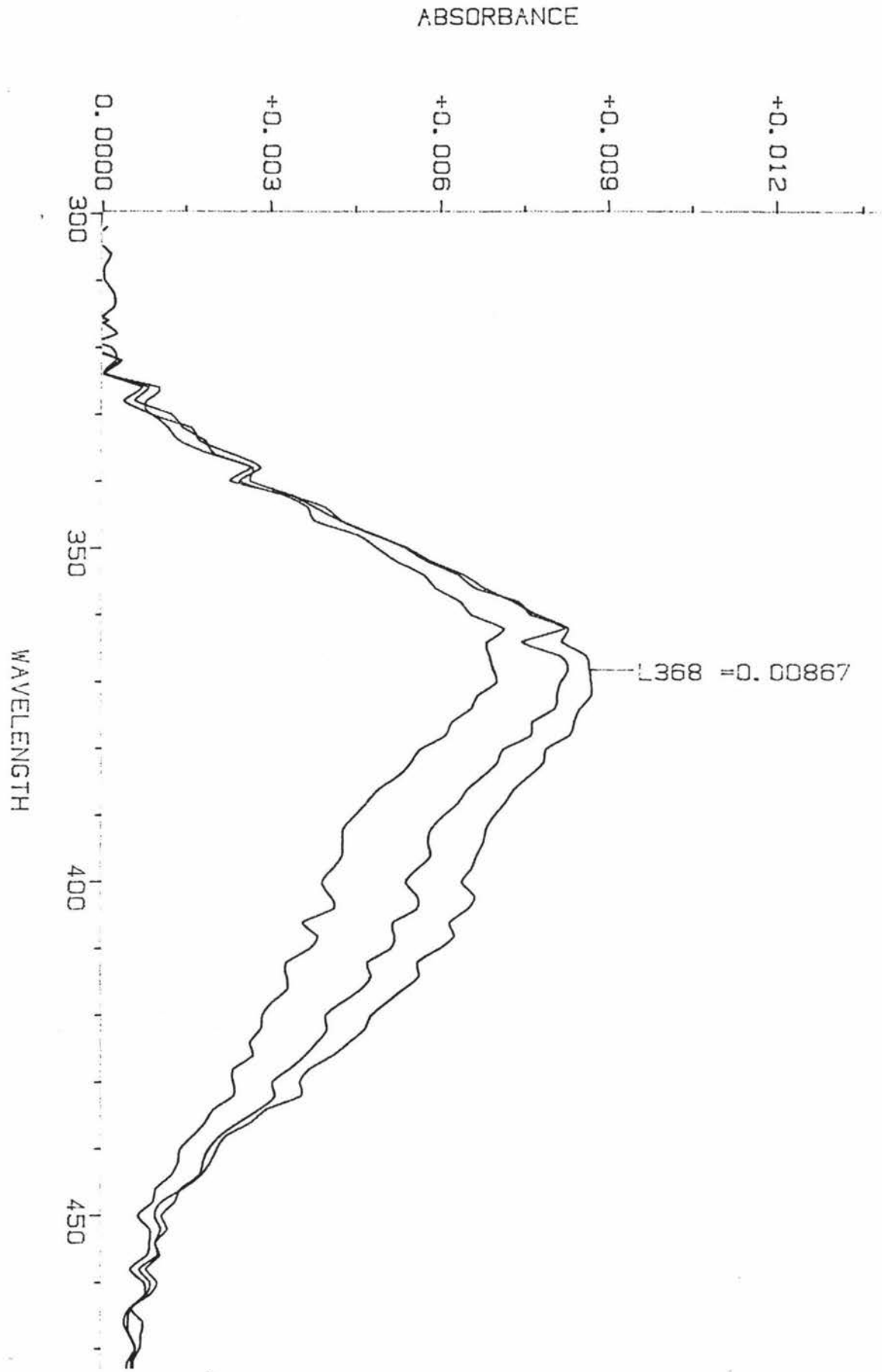

2.4 Discussion

2.4.1 Introduction to the discussion

It has been suggested by Dunn and Buckley (1985) that the red-shifted spectrum of the 464 nm species must result from a special active site microenvironment which "...almost certainly involves chemical activation of the acyl-enzyme...", and they proposed that this activation possibly arises via the interaction of a "strong electrophile" with the carbonyl oxygen of the acyl moiety.

The question of which possible "strong electrophiles" are biologically available and could bring about such a large red shifts is the focus of this chapter. To address this question DACA was used as a model chromophore to represent the ALDH 4-*trans* (N,N-dimethylamino) cinnamoyl - cysteine moiety, for the following three reasons.

1. In the modelling experiments the carbonyl carbon of DACA is activated to nucleophilic attack by complexation to strong electrophiles (Lewis acids). If 4-*trans* (N,N-dimethylamino) cinnamoyl-N,N-dimethylcysteamine (Figure 2.4.1.1) were used instead of DACA in the modelling experiments, the unstable thio-ester would on activation by a strong electrophile have a tendency to hydrolyse with trace water present, making spectroscopic determinations difficult. DACA however, is stable and amenable to study under these conditions.

Figure 2.4.1.1

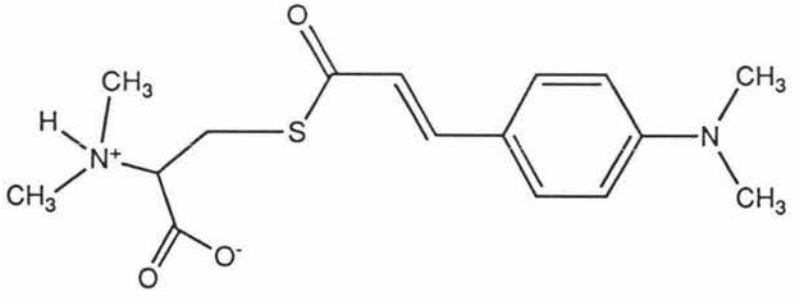

2. There are known biochemical examples that give characteristic red shifts for DACA, that are of the same order of magnitude as the ALDH-DACA acyl species. Dunn and Buckley (1982) commented that the red shifted spectrum of the intermediate was strikingly similar to the intermediate

found in the reaction of DACA with the horse liver alcohol dehydrogenase-NADH complex. This complex has been shown to arise from the direct co-ordination of the DACA carbonyl oxygen to the strongly electrophilic active site zinc ion (Angelis et al, 1977). Clearly spectral shifts with DACA can mimic those observed with aldehyde dehydrogenase.

3. DACA (λ_{max} 400 nm, in water) and the 4-*trans* (N,N-dimethylamino) cinnamoyl-N,N-dimethylcysteamine (λ_{max} 404 nm, in water) have similar chromophoric properties. This arises because the sulphur atom in the chemical analogue 4-*trans* (N,N-dimethylamino) cinnamoyl-N,N-dimethylcysteamine is neither very electron withdrawing or donating and the aldehyde hydrogen of DACA is also not very electron withdrawing or donating. The differences that do exist between 4-*trans* (N,N-dimethylamino) cinnamoyl-N,N-dimethylcysteamine and DACA will be discussed in more depth later in this chapter.

2.4.2 Basic concepts in colour chemistry

The purpose of the following discussion is to provide an introduction to the concepts commonly used in colour chemistry, but not generally discussed in chemistry textbooks.

In qualitative Valence Bond theory the ground state of a molecule is assumed to resemble that of the most stable valence bond structure, whereas the first excited state is crudely represented by a less stable, usually charge separated structure (Gordon and Gregory, 1983). This is represented schematically in Scheme 2.4.2.1 where the two forms are linked by hypothetical electron pair shifts using 'curly' arrows.

The ground state of DACA is regarded as a linear combination of canonical forms shown, but the neutral form (A) is the major contributor to the resonance hybrid since there is no charge separation. Hence the ground state is approximately represented by (A). When the molecule is excited is excited by absorption of a quantum of light structure (B) is the major contributor to the resonance hybrid. Hence the phenomenon of light absorption can be represented as shown in Scheme 2.4.2.1.

Scheme 2.4.2.1

(A)

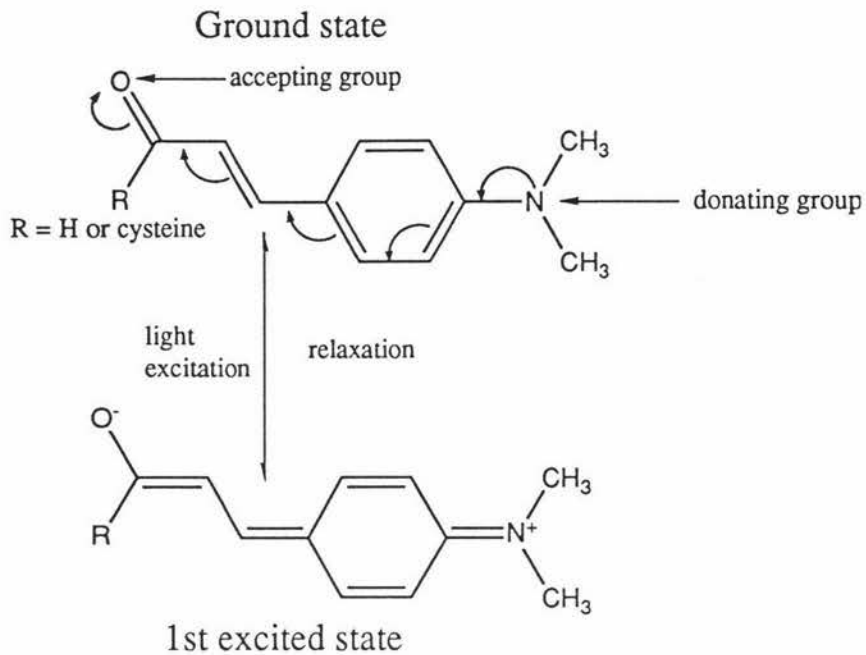

(B)

In each case there is direct conjugation between an electron donating substituent (+ M) and an electron withdrawing group (-M). Which structure contributes to the greatest extent will be influenced by interactions of the two functional groups with neighbouring electrophiles and nucleophiles. **As an electrophile is introduced near the carbonyl oxygen the charge separated form (B) will predominate more in the ground state resonance hybrid.** Or in other words, the basicity (donating ability) of the O^- group relative to the $-NMe_2$ group is reduced because the presence of the electrophile. Thus, the greater the interaction with an electrophile the more nearly equal will basicities (or the electron donating abilities or +M effects) of the two become.

In Figure 2.4.2.2 below are examples the absorption maximum of DACA when various electrophiles are complexed to the carbonyl oxygen. There is a progression starting with the carbonyl oxygen uncomplexed (I), through to a covalent bonding of the carbonyl oxygen atom with an ethyl group

(V). Each is represented in the most stable valence structure for the ground state.

Figure 2.4.2.2

(I) DACA in cyclohexane

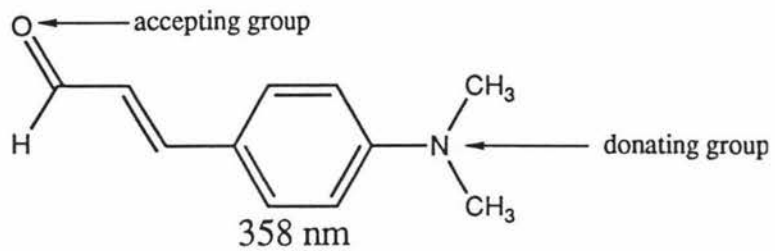

(II) DACA in water.

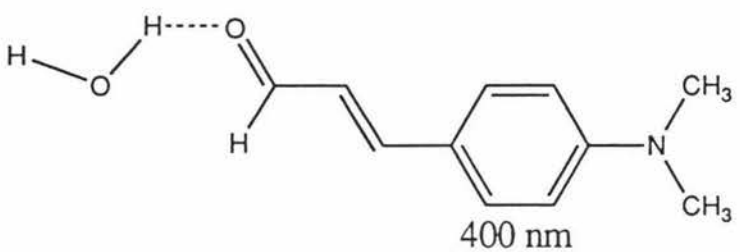

(III) DACA complexed to alcohol dehydrogenase (Dunn and Hutchinson, 1973)

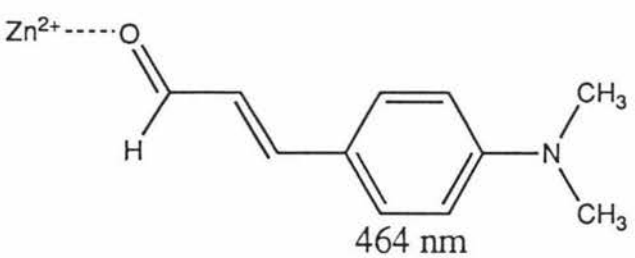

(IV) DACA complexed to alcohol dehydrogenase with NAD (Dahl and Dunn, 1984)

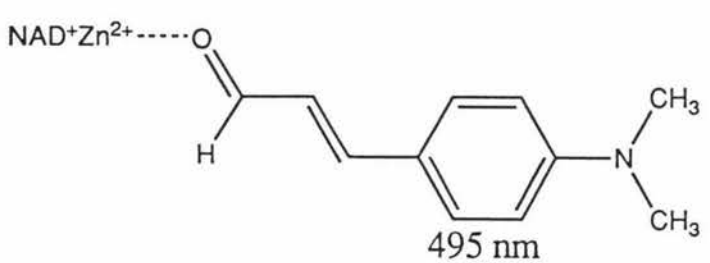

(V) The unsymmetric dye made by Angelis et al.(1977).

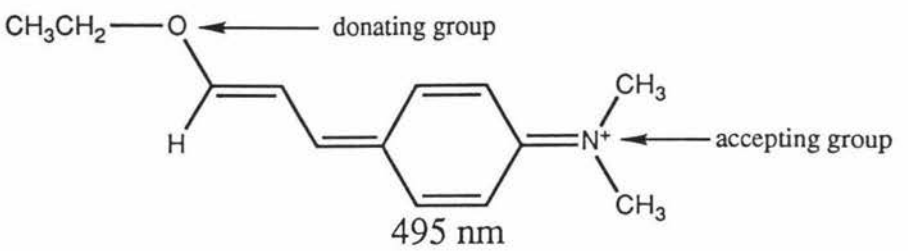

In the progression (I) through to (V) it is important to note that initially the nitrogen is the donor atom and the oxygen is an electron acceptor, eventually the oxygen becomes the donor and the positively charged nitrogen is the acceptor.

2.4.3 Calculation of the approximate maximum possible red-shift for a DACA moiety

The following discussion is to give a general understanding of what is the maximum red-shift an electrophile can ever induce in a DACA moiety. It is meant more for qualitative understanding than as a precise quantitative measurement.

If it is imagined that the progression (I) through to (V) is not represented by individual examples but rather by a continuum, then there is a position on the continuum where the basicities of the nitrogen and oxygen atoms are equal. In this situation there is complete delocalisation of the π-electrons: this leads, of course, to total bond uniformity (bond equalisation) within the chromophore(Gordon and Gregory, page 232).

Since at this point the basicity of the electrophile-oxygen group is exactly equal to that of the N,N-dimethyl amino group, then for calculational purposes it is possible to replace electrophile-oxygen with another N,N-dimethyl amino group (Figure 2.4.3.1) and the absorption maximum should be approximately the same: ignoring for the moment the differences in bathochromicity between oxygen and nitrogen.

The absorption maximum of the model unsymmetric chromophore is approximately equal to the mean of the two related symmetric dyes

(Figure 2.4.3.1 above), if the basicities are similar (Gordon and Gregory, pages 233-234).
i.e.

$$\frac{416\text{ nm} + 608\text{ nm}}{2} = 512\text{ nm}, \lambda_{max}$$

In reality because the bathochromicity of nitrogen is greater than oxygen, the longest wavelength at which a electrophile-DACA moiety can have an absorption maximum will be slightly shorter than 512 nm.

Figure 2.4.3.1

E = electrophile

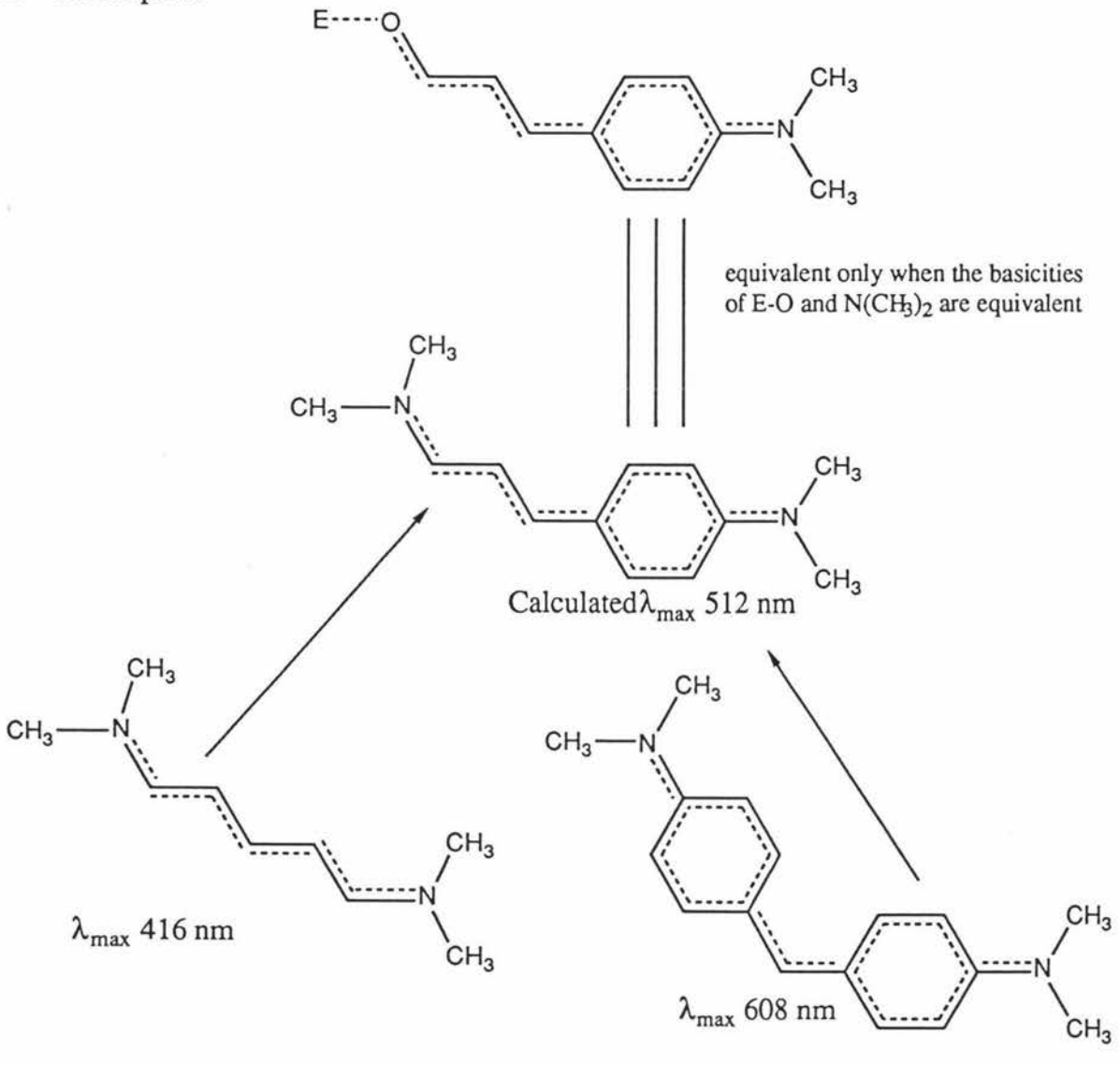

If the basicities of the oxygen and the nitrogen are not equal then the chromophore will absorb at shorter wavelengths than the theoretical

maximum. This decrease is known as 'Brooker deviation' (Gordon and Gregory, page 234).
In the case of example (V) the basicity of the neutral N,N-dimethyl amino group is greater than the ethoxy group (-NR_2 is more basic than -OR), hence structure (V) predominates in the ground state resonance hybrid of the molecule and absorbs at a wavelength (λ_{max} 495 nm) significantly shorter than 512 nm.

For alcohol dehydrogenase Dietrich et al. (1981) studied the dependence of DACA binding to alcohol dehydrogenase on the nature of the catalytic metal ion and related this to the complexed-DACA absorption spectra, as shown in Table 2.4.3.1.

Table 2.4.3.1

Catalytic metal electrophile	Wavelength max	Dissociation constant for DACA binding
Co^{2+}	478 nm	≤ 1 μM
Ni^{2+}	475 nm	1 μM
Zn^{2+}	464 nm	4.5 μM
Cd^{2+}	457 nm	15 μM

By examination of Table 2.4.3.1 it can be seen that as the wavelength maximum increased the dissociation constant decreased, hence the wavelength maximum is increasing with increasing binding strength of the catalytic electrophile (metal ion). For example, zinc alcohol dehydrogenase complexes DACA more weakly than cobalt alcohol dehydrogenase, and zinc alcohol dehydrogenase induces a smaller red-shift when complexing DACA than does cobalt alcohol dehydrogenase. Therefore, in the example (III) (zinc alcohol dehydrogenase DACA complex) it is certain that the basicity of the N,N-dimethyl amino group is less than the electrophile-oxygen (-NR_2 is less basic than E-O^-), since increasing the binding of DACA to the active site by substituting the more electrophilic cobalt decreases the Brooker deviation.

In the qualitative graph (Figure 2.4.3.2) examples (I) to (V) are plotted to summarise visually the Brooker effects for electrophile-DACA chromophores.

Figure 2.4.3.2

Qualitative graph showing the effect of Brooker deviation for electrophile-DACA chromophores

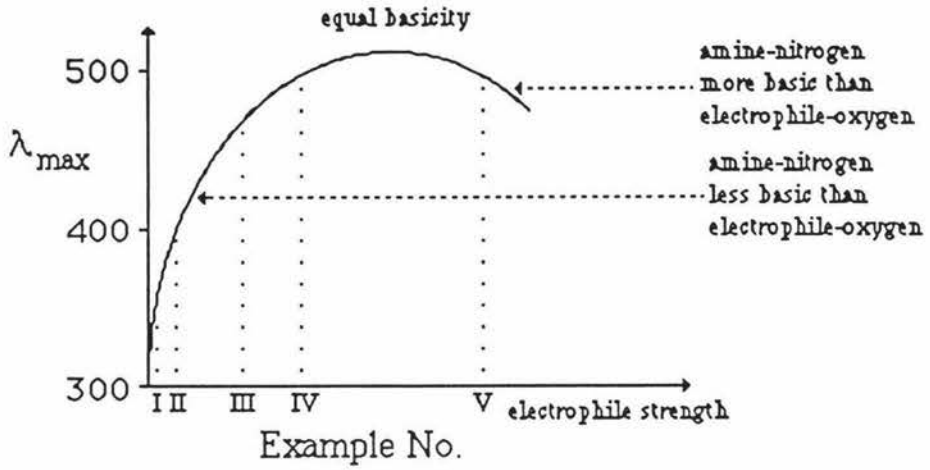

2.4.4 Consequences for DACA aldehyde dehydrogenase interactions

Since it is unlikely that aldehyde dehydrogenase or alcohol dehydrogenase have active site electrophiles that are strong enough to cause the electrophile-oxygen group to be less basic than the amine nitrogen group, discussion will be restricted to situations where the electrophile-oxygen is more basic than the amine nitrogen.

To bring about a red shift (an increase in the absorption maxima) it is necessary to reduce the energy required for excitation (since $\Delta E = hc/\lambda$) by making the basicities of the electrophile-oxygen and the amine nitrogen more equal. If an electrophile is complexed to the carbonyl oxygen this has the effect of reducing the basicity of the oxygen, and hence reducing the difference in basicities of the heteroatoms (oxygen and nitrogen). This allows the π-electrons to be more effectively delocalised and hence less light energy is required to perturbed the electrons into an excited state.

Consider again the acyl enzyme species formed at the active site of ALDH. The electrophile which caused a red-shift in the absorption maximum,

also has the effect of activating the carbonyl carbon to nucleophilic attack by withdrawing electronic charge from the carbonyl carbon.

Dunn and Buckley (1985) have also suggested that chemical activation of the acyl enzyme could possibly arise from interaction of a strong electrophile with the carbonyl oxygen of the acyl moiety.

Figure 2.4.4.1

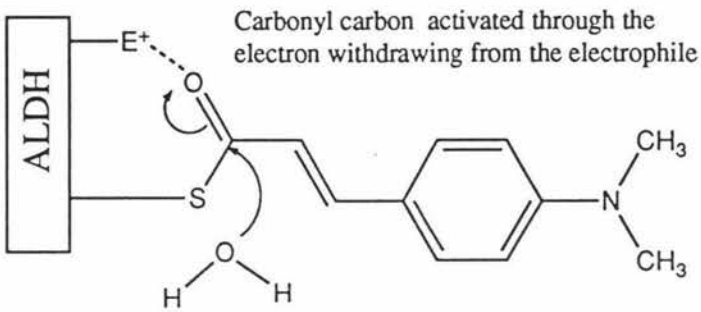

Similarly if there is an interaction between the amine nitrogen and a nucleophile this will allow the nitrogen to more easily donate electrons (be more basic) and hence lower the excitation energy required, resulting in a red-shift. But if the amine nitrogen is more basic this has the effect of deactivating the carbonyl carbon to nucleophilic attack by increasing the electron density in the carbonyl carbon.

If both heteroatoms are being complexed simultaneously this is known as dipolarisation. It should be noted that dipolarisation does not necessarily bring about activation of the carbonyl carbon.

In the introduction, three ALDH 4-*trans* (N,N-dimethylamino) cinnamoyl - cysteine moieties were reported. Table 2.4.4.1 (Buckley, personal communication) shows the approximate stabilities of the three species in 25 mM sodium phosphate buffer at pH 6.0.

Table 2.4.4.1 Stabilities of the ALDH 4-*trans* (N,N-dimethylamino) cinnamoyl - cysteine moieties.

ALDH DACA-acyl species	approximate time for 90 % hydrolysis at pH 6.0
464 nm	10 min
484 nm	70 min
408 nm (denatured)	days

From Table 2.4.4.1 it can be seen that both the 464 nm species and the 484 nm species are activated to hydrolysis, and that the 464 nm species is more activated than the 484 nm species. If the increased red-shift of the 484 nm species was associated with increased nucleophile strength about the amine nitrogen of the ALDH 4-*trans* (N,N-dimethylamino) cinnamoyl - cysteine moieties, then the carbonyl carbon would become less activated to hydrolysis, consistent with the data in Table 2.4.4.1.
For example, this could occur if the environment of the amine nitrogen of the ALDH 4-*trans* (N,N-dimethylamino) cinnamoyl - cysteine moiety changed from being hydrophobic to a more polar environment such as water (Figure 2.4.4.2).

Conversely if the increased red-shift is associated with increased electrophilic interaction with the carbamoyl oxygen, an increase in activation of the carbonyl carbon would be expected, which is not observed.

Figure 2.4.4.2

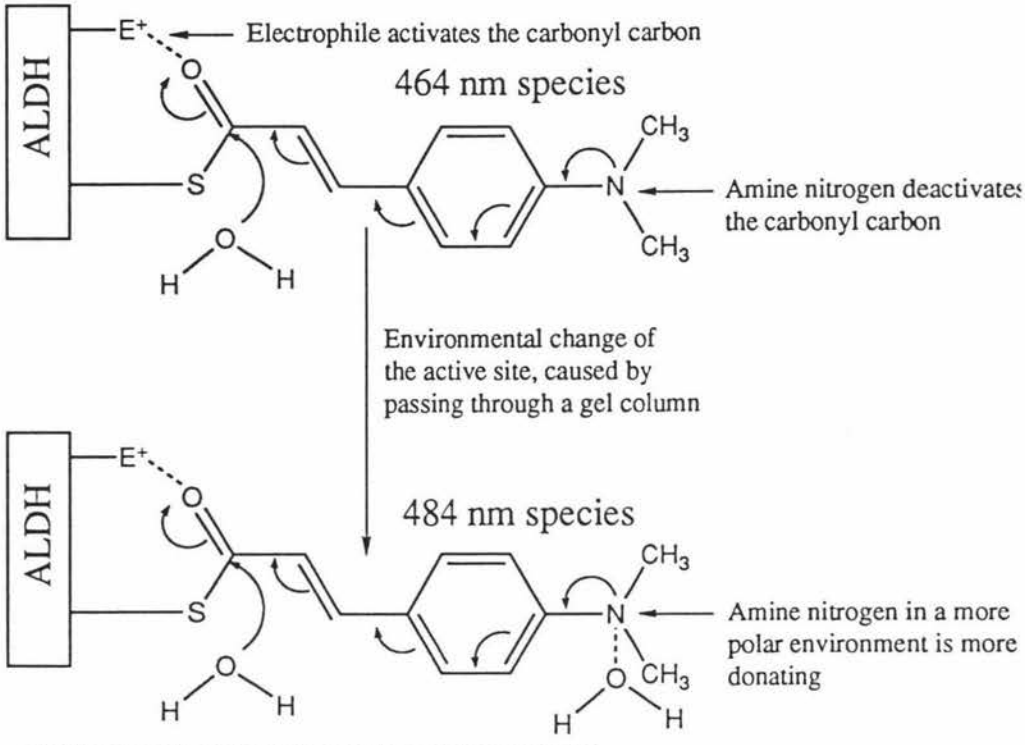

Carbonyl carbon less activated through the increased electron donating ability of the amine nitrogen

2.4.5 Modelling experiments

These experiments were designed to model spectral effects of a variety of electrophiles possibly available in the active site of ALDH. It is acknowledged that although instructive, they can not exactly represent the situation of ALDH active site. There are at least four reasons for this:-

1. In the modelling experiment, the red shift measured is representative of DACA carbonyl oxygen complexed at some average distance from an electrophile being investigated. The only factor holding the complex together is the electrostatic interaction between the carbonyl oxygen and the electrophile.

ALDH is commonly believed to have a hydrophobic active site, in which large hydrophobic aldehydes (such as retinal) can bind very much more strongly than small polar aldehydes (such as ethanal). For ALDH the 4-*trans* (N,N-dimethylamino) cinnamoyl moiety is held in a bonding position not only electrostatically by a putative electrophile, but also by hydrophobic interaction with the active site and covalent attachment to cysteine 302. Therefore it is possible that the average bonding distance between the carbonyl oxygen of the ALDH 4-*trans* (N,N-dimethylamino) cinnamoyl - cysteine moiety and the ALDH electrophile is shorter than for the modelling situation. This could lead to an underestimation of the red-shift inducible by the model electrophiles.

2. The chemical analogue of the acyl enzyme intermediate formed with DACA is 4-*trans* (N,N-dimethylamino)cinnamoyl-N,N-dimethylcysteamine (Figure 2.4.1.1), which has an absorption maximum of 404 nm in water. From this the extent of the red shift induced by an electrophile in the active site can be calculated .

e.g. 464 nm - 404 nm = 60 nm red shifted.

If in reality the 4-*trans* (N,N-dimethylamino) cinnamoyl chromophore in the ALDH active site exists in an environment which is less polar (more hydrophobic) than water, then the nucleophiles available to complex with the amine nitrogen would be less nucleophilic than water. Therefore the measurement of the absorption maxima of the chemical analogue 4-*trans* (N,N-dimethylamino)cinnamoyl-N,N-dimethylcysteamine in water (404 nm) may be not truly representative. Hence, the assumption that the active site is as polar as water can lead to an underestimation of the calculated red shift caused by the ALDH active site electrophile.

The 484 nm species has a larger red-shift and yet is more stable to hydrolysis than the 464 nm species. It is likely that the 484 nm species is in a more polar (less hydrophobic) environment than the 464 nm species (see section 2.4.4). For this reason the use of the spectral red-shift of the ALDH 484 nm species might be better represented by the measurement of the 4-*trans* (N,N-dimethylamino) cinnamoyl-N,N-dimethylcysteamine in water (404 nm) than the ALDH 464 nm species. In other words the observed 80 nm red-shift (of the 484 nm acyl species) is probably a better

representation of the active site electrophile strength than the observed 60 nm red-shift (of the 464 nm acyl species).

3) DACA is used as a model chromophore instead of 4-*trans* (N,N-dimethylamino)cinnamoyl-N,N-dimethylcysteamine on the assumption that the N-acetylcysteine sulphur has very similar chromophoric properties to the carbonyl hydrogen of DACA. This is not entirely correct when the carbonyl carbon becomes very activated. For 4-*trans* (N,N-dimethylamino)cinnamoyl-N,N-dimethylcysteamine in a dipolar environment such as water the carbonyl carbon is not very positive. In this situation the net effects of the electronegativety of the sulphur atom (which is greater than that of hydrogen) and the electron donating ability of sulphur (which is also greater than that of hydrogen) do not have much overall affect on the spectra of the 4-*trans* (N,N-dimethylamino) cinnamoyl moiety. When the carbonyl carbon becomes much more positive from activation by a strong electrophile, the sulphur atom will have a much greater net donating effect. An example of this effect is shown in Table 2.4.5.1 (Gorden and Gregory, 250-251).

Table 2.4.5.1 Comparative hypsochromicity of hydrogen, sulphur and oxygen.

Structure	Name	λ_{max} (nm)
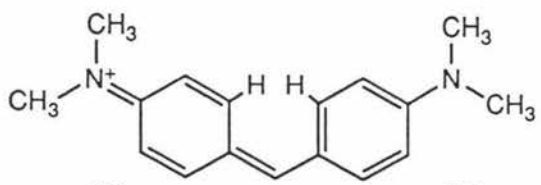	Michler's Hydrol Blue	607.5
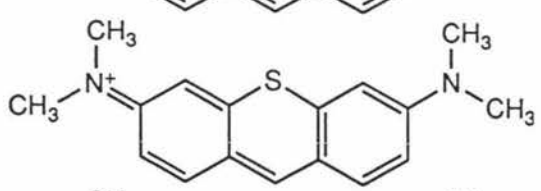	Thiopyronine	565
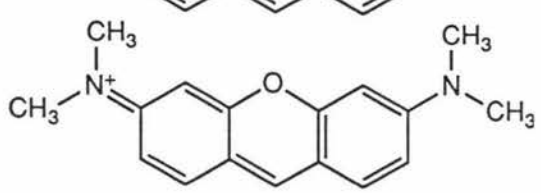	Pyronine	545

In this example the electron donating abilities of sulphur and oxygen are greater than that of hydrogen and because of this Thiopyronine and Pyronine absorb at shorter wavelengths than Michler's Hydrol Blue.

i.e. hypsochromicity (blue-shifting ability)

oxygen > sulphur > hydrogen

Hence when the carbonyl carbon atom of 4-*trans* (N,N-dimethylamino) cinnamoyl-N,N-dimethylcysteamine becomes activated by a strong electrophile a smaller red shift will result than in the model chromophore DACA, because of the hypsochromic effects of the adjacent sulphur atom. It is important to note therefore, that to bring about an 80 nm shift as observed in the ALDH 4-*trans* (N,N-dimethylamino) cinnamoyl cysteine moiety (the 484 nm species) a stronger electrophile is required than for the model chromophore DACA.

4. When an electrophile is added to complex with DACA a nucleophile is also unavoidably introduced. Hence the difference spectra obtained do not just represent the effects of complexation of an electrophile but possibility also a nucleophile as well.

2.4.6 Biological examples of red-shifted spectra induced by enzymes not containing metal electrophiles.

Red shifts have been reported for a variety of acyl-enzymes which do not have active site catalytic metal ions such as papain, chymotrypsin, novo subtilisin, glyceraldehyde 3-phosphate dehydrogenase (Hinkle et al., 1970) and elastase (Breaux and Bender, 1976).
In general the red-shifts reported were small (< 30 nm).With the exception of elastase the acyl-chromophores of the enzyme examples were not a 4-*trans* (N,N-dimethylamino) cinnamoyl moiety, making a direct comparison with the ALDH-DACA acyl species more difficult.

Glyceraldehyde 3-phosphate dehydrogenase is the enzyme which is thought to be the most similar to ALDH of all the enzymes previously mentioned.

When glyceraldehyde 3-phosphate dehydrogenase was acylated with a furylacryloylimidazole it formed a glyceraldehyde 3-phosphate dehydrogenase furylacryloyl cysteine moiety (λ_{max} 344 nm), which is only 6 nm red shifted compared to the model compound furylacryloyl-S-acyl-N-acetyl cysteine (λ_{max} 338 nm).

Figure 2.4.6.1

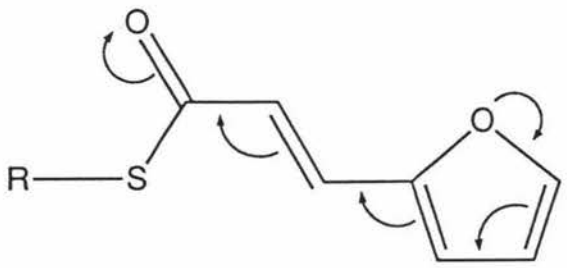

Furylacryloyl cysteine moiety

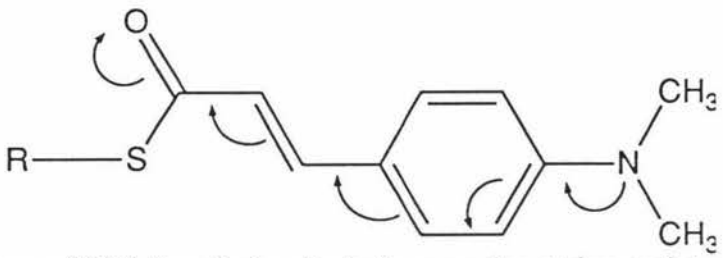

4-*trans*-(N,N-dimethyl amino) cinnamoyl cysteine moiety

where R = cysteine

When ALDH is acylated with furylacroleine in the presence of NAD, an ALDH - furylacryloyl cysteine moiety ($\lambda_{max} \approx 368$ nm) is produced which is approximately 30 nm red-shifted from the model compound furylacryloyl-S-acyl-N-acetyl cysteine (λ_{max} 338 nm). This can be compared with the ALDH 4-*trans* (N,N-dimethylamino) cinnamoyl cysteine moiety with a red-shift of 60 - 80 nm, hence it can be seen that the furylacryloyl cysteine moiety (Figure 2.4.6.1) is not as bathochromic as the 4-*trans* (N,N-dimethylamino) cinnamoyl cysteine moiety.

For papain, chymotrypsin and, glyceraldehyde 3-phosphate dehydrogenase the approximate red-shift induced by these enzymes for an enzyme 4-*trans* (N,N-dimethylamino) cinnamoyl moiety has been calculated by comparing the relative red-shifts induced in furylacrolein and DACA by different complexing agents. In Figure 2.4.6.2, the red-shifts obtained for the DACA complexes have been arbitrarily graphed as a linear relationship, and the relative positions of each of the complexed DACA species was then plotted on the horizontal axis. The red-shifts obtained by the same complexing agents with furylacrolein was then plotted on, which gave a curved line.

The relative position on the horizontal axis for the known red-shifts of the non-metallo enzymes was then plotted, and the corresponding red-shift induced by an enzyme 4-*trans* (N,N-dimethylamino) cinnamoyl moiety was read from the linear line.

Figure 2.4.6.2 Relative red-shifts induced in furylacrolein and DACA

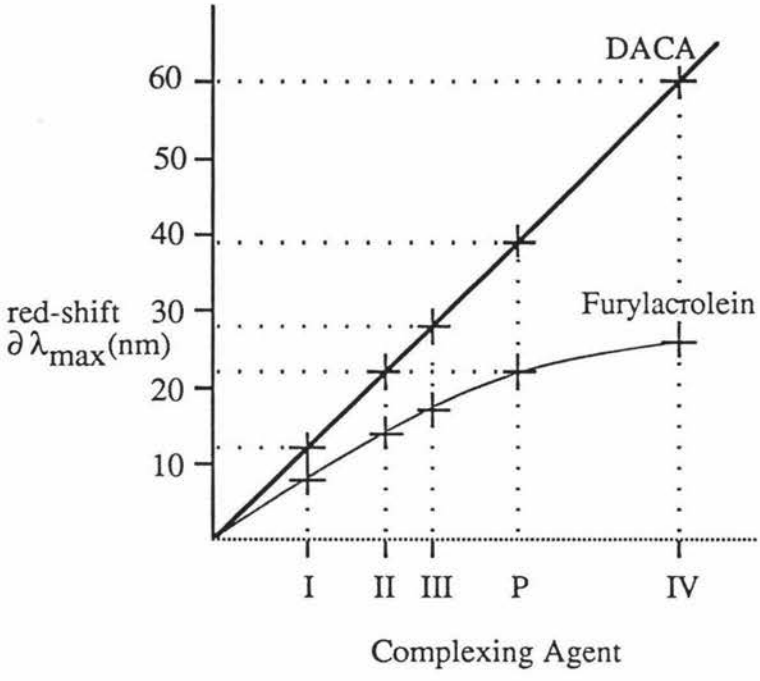

In Figure 2.4.6.2 the complexing conditions were; ethanamide/water (I), quanidinium chloride/water (II), ethanoic acid/acetonitrile (III) and zinc chloride/chloroform (IV). Papain (P) is shown as an example. The calculated red-shifts induced by non-metallo enzymes in a 4-*trans* (N,N-dimethylamino) cinnamoyl moiety are shown in Table 2.4.6.1.

Table 2.4.6.1 Calculated red-shifts induced by non-metallo enzymes in a 4-*trans* (N,N-dimethylamino) cinnamoyl moiety

Enzyme	Red-shift of the enzyme furylacryloyl moiety. (F)	Calculated red-shifts induced by an enzyme 4-*trans* (N,N-dimethylamino) cinnamoyl moiety
Glyceraldehyde 3-phosphate dehydrogenase [a]	6 nm	9 nm
Papain [a]	22 nm	39 nm
Chymotrypsin [a]	11 nm	17 nm

a Hinkle, 1970

Red-shifts induced by novo subtilisin have not been studied with either a furylacryloyl moiety or a 4-*trans* (N,N-dimethylamino) cinnamoyl moiety. However novo subtilisin has been shown to bring about a smaller red-shift than chymotrypsin for both trans-cinnamoyl and indoylacryloyl moieties (Hinkle, 1970). Hence it is likely that novo subtilisin would induce a less red-shifted spectrum than chymotrypsin for a 4-*trans* (N,N-dimethylamino) cinnamoyl moiety (i.e. < 17 nm).

Elastase (like alcohol dehydrogenase) has also been studied with a 4-*trans* (N,N-dimethylamino) cinnamoyl moiety (Breaux and Bender, 1976). Elastase was acylated with 4-*trans* (N,N-dimethylamino) cinnamoylimidazole at serine-195 forming a 4-*trans* (N,N-dimethylamino) cinnamoyl elastase moiety (λ_{max} 401 nm). The absorption maximum of denatured 4-*trans* (N,N-dimethylamino) cinnamoyl elastase moiety is 370 nm and the absorption maximum of the model related compound ethyl 4-*trans* (N,N-dimethylamino) cinnamate is 369 nm. Hence the active site of elastase has induced a red-shift in the spectrum of 32 nm.

Breaux and Bender (1976) offered two explanations for the red-shifted spectrum of elastase based on x-ray data for the related enzyme chymotrypsin.
1. The carbonyl group of the acyl derivative is hydrogen-bonded or protonated in the active site.
2. An "out of the plane" acyl-enzyme is formed. In an "out of the plane" acyl-enzyme, the lone pair orbitals of the alkyl oxygen are perturbed in such a way that they can not delocalize into the carbonyl group. The net result is that the acyl-enzyme is the electronic equivalent of an aldehyde or ketone.

Breaux and Bender (1976) had most support for the "out of the plane" acyl-enzyme model, substantiating this by the close similarity of the spectra of the aldehyde DACA (λ_{max} 400 nm) and the 4-*trans* (N,N-dimethylamino) cinnamoyl elastase (λ_{max} 401 nm).

For ALDH the "out of the plane" model can not explain the spectral red-shift observed because the spectra of the ALDH 4-*trans* (N,N-dimethylamino) cinnamoyl cysteine moieties (λ_{max} 464 and 484 nm) are considerably longer than that of the aldehyde DACA (λ_{max} 400 nm).

Of the five non-metallo enzymes so-far discussed, papain can produce the largest red-shifts, but the calculated red-shift for a papain 4-*trans* (N,N-dimethylamino) cinnamoyl cysteine moiety (39 nm) is still much less than red-shifts produced in the ALDH 4-*trans* (N,N-dimethylamino) cinnamoyl cysteine moieties (60 nm & 80 nm). Hence the red-shifted spectrum of the ALDH 4-*trans* (N,N-dimethylamino) cinnamoyl - cysteine moieties is not consistent with a non-metallo enzyme.

2.4.7 Model experiments for the non-metal electrophiles

Previous authors (Angelis et al., 1977; Bernhard et al., 1965) have modelled the effects of non-metal electrophiles on chromophores (such as DACA). Both Bernhard et al. (1965) and Angelis et al.(1977) formed the complexes by adding the chromophore to solutions containing saturating concentrations of the electrophile being tested. They then recorded the spectral wavelength maximum of the complexed solution, and calculated

the red-shift by subtracting the wavelength maximum of the same chromophore present in water alone.

In a complexing solution the DACA exists in an equilibrium between the complexed-DACA species and the uncomplexed DACA. Figure 2.4.7.1 represents the equilibrium between guanidinium complexed DACA and uncomplexed DACA.

Figure 2.4.7.1

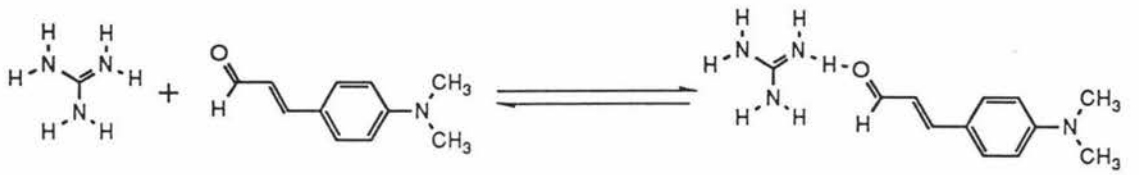

Presumably Bernhard et al. and Angelis et al. made the assumption that, because they had such a high concentration of electrophile, the equilibrium concentration of the complexed-chromophore was high compared to the equilibrium concentration of the uncomplexed chromophore. It is this over simple assumption that has led to a great deal of confusion about the ability of a non-metal electrophile to cause red-shifted spectra in a chromophore.

In the modelling experiments presented in this section three assumptions have been made:-

1. Even with saturating concentrations of a complexing agent, the equilibrium concentrations of complexed-chromophore are low compared with the concentration of the uncomplexed chromophore. In other words, the equilibrium constant K (for the equilibrium in Figure 2.4.7.1) is small for non-metal electrophiles. Hence, the measured absorption spectrum of the solution is mostly represented by the uncomplexed chromophore.
2. Because the spectrum of the complexed-chromophore is red-shifted relative to the uncomplexed chromophore there is a wavelength where the uncomplexed chromophore absorbs but the complexed chromophore does not, and vice versa.
3. That the complexing agent can act as both an electrophile to the carbonyl oxygen and a nucleophile to the donating group (i.e. amine nitrogen in DACA).

By making these assumptions it is possible to subtract the contribution from the uncomplexed DACA, which dominated the spectrum, leaving just the spectrum of the complexed DACA, see methods for details. By examination of the difference spectra obtained (Figure 2.3.1.1) it is quite clear that the spectrum of the complexed-chromophore only makes a small contribution to the total spectrum observed. When such a correction is not made, erroneous conclusions may be drawn from the data.

Bernhard et al (1965) on the basis of their methods for modelling amino acids as electrophiles, concluded that the unusual acyl-enzyme (either acylated chymotrypsin or acylated novo subtilisin) arises from an as yet undefined type of perturbation reflecting neither the polarity nor the hydrogen-bonding properties of the microscopic environment of the bound acyl group. Angelis et al. (1977) also rejected the possibility of a non-metal electrophiles being able to bring about significantly red-shifted spectra. Both sets of conclusions were based on the fact that using their modelling techniques they obtained very small red-shifts, if any at all.

For example, the largest red-shift observed (by Angelis et al., 1977 and Bernhard et al., 1965) when modelling a peptide, was for arginine, where saturating concentrations of guanidine salts were used as complexing agents. Even in this best case, the shifts obtained by using the modelling assumption that most of the chromophore exists in the complexed state are much smaller than the shifts obtained when using the assumption that most of the chromophore exists in the uncomplexed state. The difference between the two methods is illustrated clearly in Table 2.4.7.1

Despite the improvements that this modelling method offers it is still limited by assumption 3; that the complexing agent can act as both an electrophile to the carbonyl oxygen and a nucleophile to the electron donating group (e.g. amine nitrogen in DACA). Hence the spectra obtained do not merely represent the effects of an electrophile binding to DACA but also a nucleophile as well. This is well demonstrated in Table 2.3.2.1 by examining the difference in red-shifts induced by different anions of sodium. For example, sodium fluoride induces a red-shift 16 nm longer than sodium acetate.

Table 2.4.7.1 Comparison of modelling techniques

Chromophore	Complexing agent	Modelling Assumption	Wavelength change (red-shift)
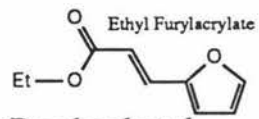 Ethyl Furylacrylate Bernhard et al.	guanidinium chloride 5 M	Most of the chromophore is complexed	3 nm
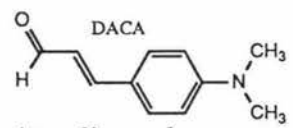 DACA Angelis et al.	guanidinium sulphate 4 M	Most of the chromophore is complexed	6 nm
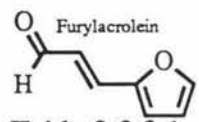 Furylacrolein Table 2.3.3.1	guanidinium chloride 1 M	Most of the chromophore is uncomplexed	14 nm
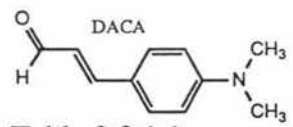 DACA Table 2.3.1.1	guanidinium chloride 0.7 M	Most of the chromophore is uncomplexed	22 nm

Therefore, the complexed DACA spectrum is made up of 3 species:-

1. A complex formed between the carbonyl oxygen atom of DACA and the electrophilic species.
2. A complex formed between the amine nitrogen and the nucleophile.
3. A complex where both the electrophile and the nucleophile are complexed to DACA. The probability of this is very low, since the probability of either 1 or 2 is low.

For the non-metal electrophiles an attempt to minimise the bonding interaction between the amine nitrogen and the nucleophile has been made by using weaker nucleophiles such as ethanoate where possible.

The non-metal complexing agents used in the modelling experiments in this thesis were designed to investigate the complexing properties of the side chain functional groups of peptides available in ALDH. It must be kept in mind that the electrophile must be able to act as an electrophile over the range pH 4.1 to pH 10.5, since the spectrum of the ALDH DACA acyl species appears to be independent of pH in this range.

From the results of the modelling study (Table 2.3.1.1) it would appear that the strongest non-metal electrophile was a proton of a carboxylic acid (aspartate, glutamate). However the magnitude of this shift (28 nm) is not close to the shifts actually observed for the ALDH 4-*trans* (N,N-dimethylamino) cinnamoyl - cysteine moiety (60 - 80 nm). Enzymes that utilise a carboxylic proton as an active site electrophile are well known (e.g. Pepsin, an acidic protease existing in the stomach membrane), although it is not normal for these enzymes to be active above pH 6. At pH 10.5 a carboxyl will not be protonated, therefore the active site electrophile of ALDH can not be a proton of a carboxylic acid.

At pH 10.5 only arginine and lysine can exist with a positive charge. Arginine is not normally considered a strong electrophile because its positive charge is very disperse being distributed over three nitrogen's, it's properties are most consistent with strong hydrogen bonding molecules such as urea. The red-shift obtained when using guanidinium as a model compound for arginine was only 22 nm.

N,N,N,N-tetramethyl ethylenediamine dihydroethanoate (representing lysine) was used as a model complexing agent in an attempt to model the possibility of simultaneously arranging two positive amines closely held together about the carbonyl oxygen of DACA. Only one absorption band was observed, which was attributed to DACA complexing to just one of the amines. In addition to this lysine is an unsuitable candidate as it can undergo schiff-base reactions with aldehydes.

Histidine was investigated using the model complexing agent imidazole hydroethanoate which induced a red-shift of 20 nm. Histidine (pK_a 7.6) is also unlikely to act as electrophile at pH 10.5.

Peptides that have amide functionality (such as asparagine and glutamine) were investigated with the model complexing agent ethanamide which can cause red shifts via hydrogen bonding and can also fulfil the requirements of being pH independent. The red-shifts induced were 22 nm in acetonitrile and 12 nm in water. The possibility of a water molecule bound in the active site acting as an electrophile via hydrogen bonding to the carbonyl oxygen atom of the chromophore was also investigated, and found to induce a 25 nm red-shift.

Other functional peptides such a tyrosine, cysteine, and serine were not investigated, but from the Table 2.3.1.1 it would appear that a single non-metal electrophile can induce a red-shift in a DACA moiety of up 30 nm.

For papain a red-shift larger than 30 nm (i.e. 39 nm) for a DACA moiety has been calculated. In serine and cysteine proteases the carbonyl oxygen is complexed to two amide groups (Ted Baker, personal communication). This is schematically shown in Figure 2.4.7.2.

Figure 2.4.7.2 Active site of non-metal proteases

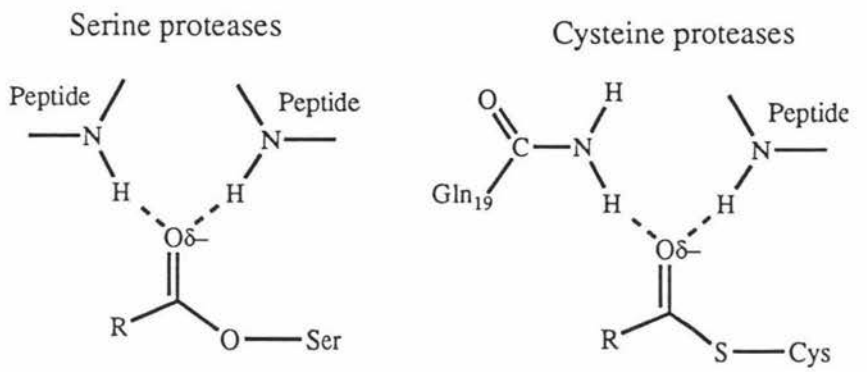

Hence by using a combinations of electrophiles such as amides it is possible to induce larger red-shifts than would be expected for a single electrophile. There also must be a limitation in the number of electrophiles that can be crowded around a single carbonyl oxygen without significant repulsion between the electrophiles occurring.

In glyceraldehyde-3-phosphate dehydrogenase the carbonyl oxygen is thought to be complexed to a proton of histidine 176 (Biesecker et al.,

1977). Figure 2.4.7.3 shows the active site of glyceraldehyde-3-phosphate dehydrogenase. Cysteine 149 is the active site thiol group.

Figure 2.4.7.3 Active site of glyceraldehyde-3-phosphate dehydrogenase

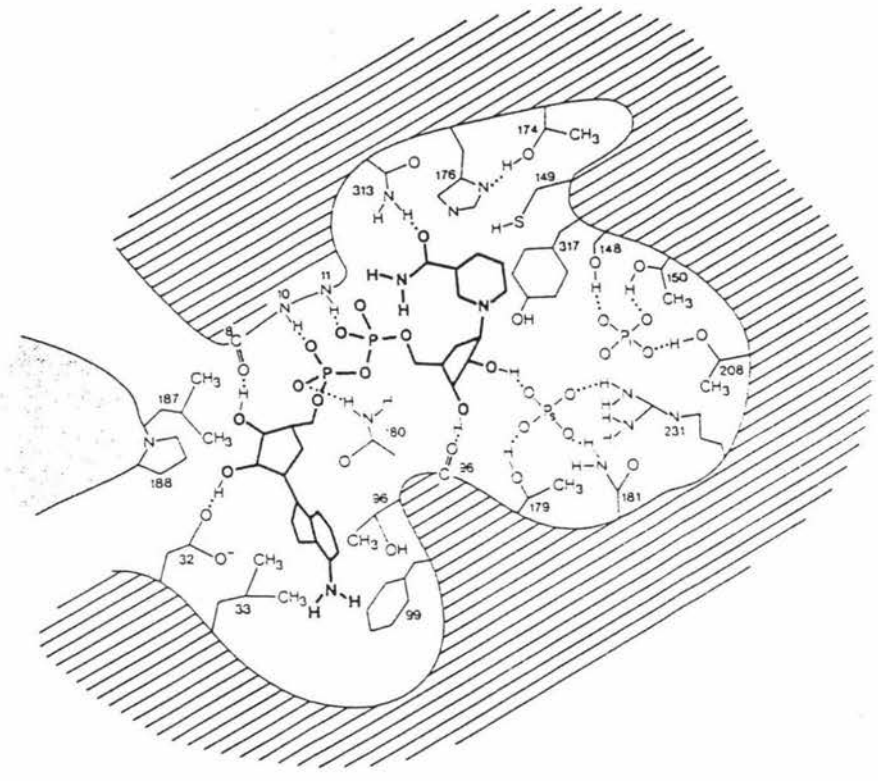

In contrast to previous authors this modelling experiment clearly demonstrates that non-metal electrophiles can induce significant red-shifts in acyl chromophores.

2.4.8 Possible improvements for modelling non-metal electrophiles.

A deficiency in this type of modelling experiment is the inability to separate the nucleophilic and electrophilic effects on the chromophore being studied. A way to avoid these problems is to have an effectively high concentration of electrophile with a low concentration of nucleophile, so that only the effects of the electrophile are observed. This is not possible using the methods so-far described in this chapter, but it is possible in principle.

Consider the chemical analogue synthesised by Dunn and Buckley (1982) 4-*trans* (N,N-dimethylamino) cinnamoyl-N,N-dimethylcysteamine.

Figure 2.4.8.1

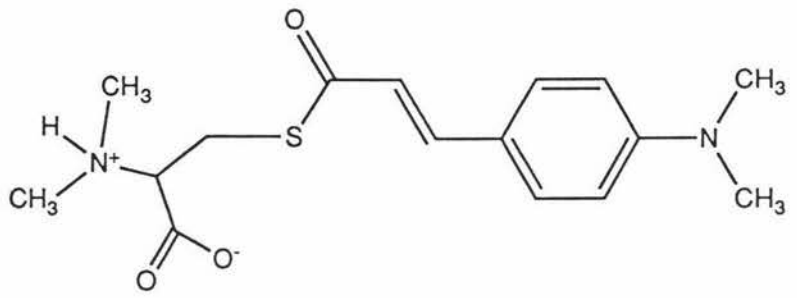

The N,N-dimethylcysteamine group contains both an electrophile and a nucleophile. It is possible for the electrophile (positive amine) to form an internal complex with the carbonyl oxygen, but the nucleophile (carboxyl) cannot form a complex with the amine nitrogen because they are too far apart.

Since the concentration of the chromophore normally measured is very low ($\approx$ 25 μM), the inter-molecular interaction between the nucleophile (carboxyl) and another DACA moiety is likely to be virtually non-existent as the bonding interactions are typically very weak (section 2.4.7) Hence there effectively high concentration of electrophile available via intramolecular interactions with a very low concentration of nucleophile available via intermolecular interactions.

Figure 2.4.8.2

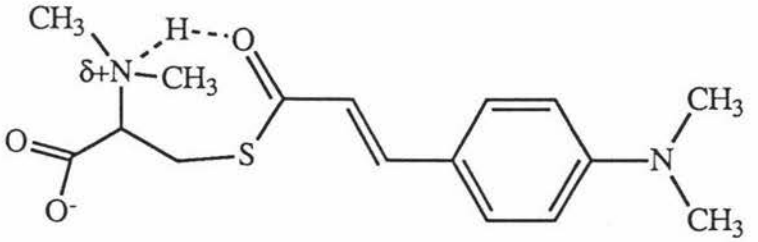

Because the internal complex is in equilibrium with the uncomplexed state it is necessary to subtract the spectrum of the uncomplexed DACA moiety. This can be achieved in a similar manner to the methods presented in this chapter, by comparing the 4-*trans* (N,N-dimethylamino) cinnamoyl-N,N-dimethylcysteamine with 4-*trans* (N,N-dimethylamino) cinnamoyl-S-ethanethiol.

Figure 2.4.8.3

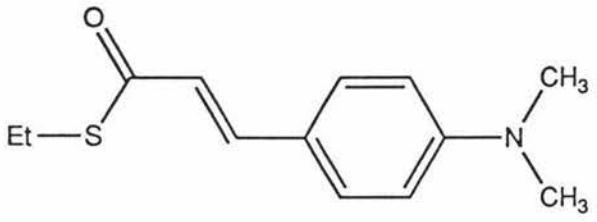

Another good example to study would be 4-*trans* (N,N-dimethylamino) cinnamoyl-S-thioethanoic acid.

Figure 2.4.8.4

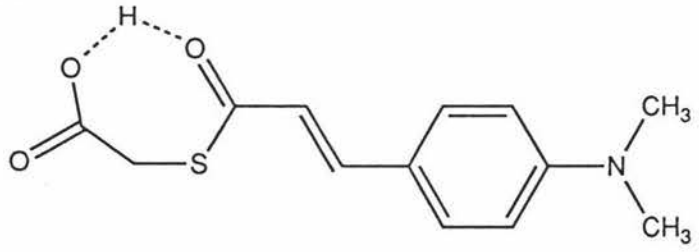

By forming the sodium salt of the analogue 4-*trans* (N,N-dimethylamino) cinnamoyl-N-acetyl cysteine fig 2.13 (made by Grunwell and Foerst, 1976) it would be possible to study the electrophilic effects of an amide.

Figure 2.4.8.5

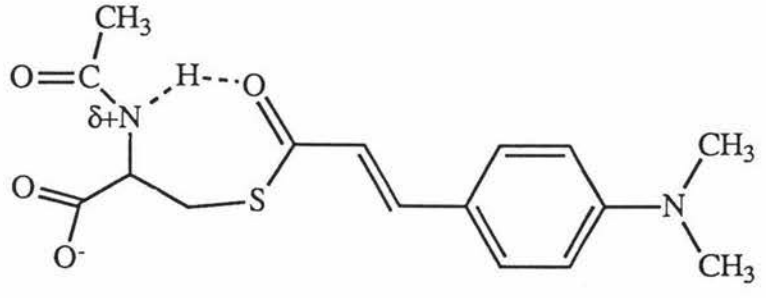

An added advantage with using these methods is that once the internal complex has formed it is likely to be more stable than the intermolecular complexes because the electrophile is covalently bonded to the DACA chromophore. Hence this is likely to be more representative of the real situation (see section 2.4.5 reason 1).

2.4.9 Metal electrophiles

The results obtained indicated that monovalent metal ions produced red-shifts in the spectrum of DACA typically about 30 nm (Table 2.3.2.1) which are much less than the shifts observed for the ALDH-DACA acyl species (60 and 80 nm), therefore it is unlikely that the active site electrophile is a monovalent metal ion such as sodium.

For the zinc, copper, and chromium modelling experiments, only the effects of the electrophiles binding to the carbonyl oxygen are spectrally observed for two reasons.
1. The required concentration of the complexing agents is very low because of the strong bonding interaction between the electrophile and the carbonyl oxygen. Therefore there are only very low concentrations of nucleophile (chloride) present and because there is only a weak interaction between a chloride ion and the amine nitrogen, very little of the DACA is complexed by a nucleophile.
2. Most of the nucleophile (chloride ion) added does not exist freely in solution but is complexed to the metal ions (zinc, copper, and chromium). Hence this reduces the available nucleophile concentration.

It is obvious from the results (Table 2.3.2.1) that divalent or trivalent metal ion electrophile complexing to DACA can cause large red-shifts in the range 60 - 80 nm, which are typical for what is observed for the ALDH-DACA acyl species (60 and 80 nm). These electrophiles exist independent of pH, and could easily bring about considerable activation by making the carbonyl carbon more electrophilic.

2.4.10 Comparison of the ALDH 4-*trans* (N,N-dimethylamino) cinnamoyl - cysteine moiety and Alcohol dehydrogenase - DACA intermediates.

In 1973 Dunn and Hutchinson studied the liver alcohol dehydrogenase catalyzed reduction of DACA. They found that DACA would rapidly bind to alcohol dehydrogenase forming a 464 nm intermediate which then very slowly underwent nucleophilic attack from the hydride of the NADH to finally release the products *trans*-4-N,N-dimethyl amino cinnamyl alcohol and NAD. For liver alcohol dehydrogenase Sloan *et al.* (1976) proposed (based on n.m.r data) that the DACA was not directly bound to the active site zinc but was hydrogen bonded to a zinc-bound water molecule.

Figure 2.4.10.1

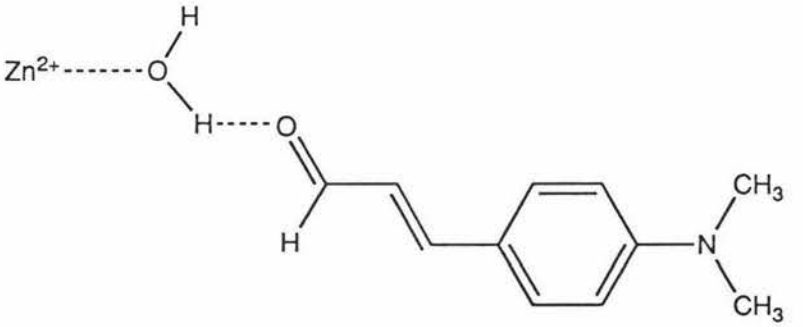

Angles *et al* 1977 did an extensive modelling study to determine whether DACA was directly bound to the active site zinc through inner sphere co-ordination or hydrogen bonded to the a zinc-bound water molecule. They concluded that the structure shown in Figure 2.4.10.1 could not account for the spectral properties of the 464 nm intermediate and their studies supported a structure for the enzyme-bound intermediate involving direct co-ordination of the carbonyl oxygen of DACA to the active site zinc ion. They also concluded that the pH-independent nature of both the spectrum of the intermediate and the kinetics of intermediate formation virtually eliminates any explanation for the intermediate based on protonation of DACA. In 1978 Plapp et al. (1978) using crystallographic techniques showed that the oxygen of the substrate 4-bromobenzyl alcohol was directly ligated to the active site zinc (2 Å). It is now generally accepted that substrates for alcohol dehydrogenase (aldehydes and alcohols) are directly ligated to the active site zinc through the oxygen.

Examples of DACA complexes with divalent metal electrophiles in the active sites of human and horse alcohol dehydrogenases are given in the Table 2.4.10.1.

Table 2.4.10.1 Red-shifts induced in DACA by human and horse liver alcohol dehydrogenase

complexing agent	Absorption change (red-shift)
cobalt(II) ADH-NADH(horse liver)/buffer [a]	80 nm
nickel (II) ADH-NADH(horse liver)/buffer [a]	77 nm
zinc (II) ADH-NADH(horse liver)/buffer [a]	66 nm
cadmium (II) ADH-NADH(horse liver)/buffer [a]	59 nm
cobalt(II) ADH-NADH(human liver)/buffer [b]	71 nm
zinc (II) ADH-NADH(human liver)/buffer[b]	60 nm

a - taken from Helmut et al, 1981
b - taken from Schnieder-Bernlohr et al, 1988

From Table 2.4.10.1 it can be seen that divalent metal electrophiles in alcohol dehydrogenases induce red-shifts in DACA in the range 59 - 80 nm which is in good agreement with the shifts predicted by the modelling experiments (Table 2.3.2.1) for divalent metal ions. For example in the case of zinc the predicted red-shift induced by the modelling experiment is 60 and 64 nm, and red shifts obtained for zinc-LADH were 60 nm (human) and 66 nm (horse).

The summary of the properties in Table 2.4.10.2 show remarkable similarity between the ALDH 4-*trans* (N,N-dimethylamino) cinnamoyl - cysteine moiety and alcohol dehydrogenase - DACA intermediates showing by analogy that the active site of ALDH almost certainly contains a metal electrophile. Furthermore it is likely that the active site metal electrophile of ALDH is more electrophilic than the active site zinc of liver alcohol dehydrogenase, because of the size of the red-shift and hypsochromic effects of the adjacent sulphur.

Table 2.4.10.1 Comparison of aldehyde dehydrogenase and alcohol dehydrogenase.

Enzyme intermediate	Alcohol dehydrogenase - DACA complex	ALDH 4-*trans* (N,N-dimethylamino) cinnamoyl - cysteine moiety
pH dependence of intermediate spectrum	None	None
Rate limiting step of catalysis	Nucleophilic attack of the carbonyl carbon by a hydride.	Nucleophilic attack of the carbonyl carbon by a water molecule.
Carbonyl carbon activated by	Electron withdrawing from the electrophile (Zn^{2+}).	Electron withdrawing from a putative electrophile (E^{n+}).
Carbonyl carbon deactivated by	Electron donation from the amine nitrogen.	Electron donation from both the amine nitrogen and the cysteine sulphur.
Chromophoric properties	Red-shift induced by electrophile complexed to carbonyl oxygen. 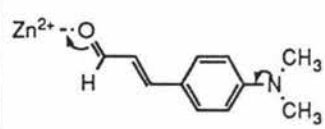	Red shift induced by a putative electrophile complexed to carbonyl oxygen. Electron donation from the cysteine sulphur reduces the red-shift. 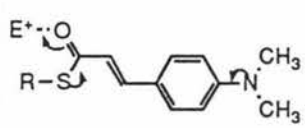
Overall bathochromic shift	60 - 66 nm	60 - 80 nm
Active site electrophile strength	= Zn^{2+}	≥ Zn^{2+}

2.5 Conclusion

In this chapter effects of both metal and non-metal electrophiles on the spectrum of DACA have been studied as models for the active site electrophile of ALDH. These studies indicated that the observed red-shifts for the ALDH 4-*trans* (N,N-dimethylamino) cinnamoyl - cysteine moieties (60 and 80 nm) were consistent with shifts induced by metal electrophiles, and that non-metal electrophiles can not account for the red shifted spectra.

Five examples of enzymes that do not contain metal electrophiles were discussed. None of these enzymes were able to induce a red-shifted spectrum of a similar magnitude to ALDH. Hence the red-shifted spectrum of the ALDH 4-*trans* (N,N-dimethylamino) cinnamoyl - cysteine moieties is inconsistent with an enzyme that does not contain a metal electrophile.

The red-shifts of two alcohol dehydrogenases with up two four different active site electrophiles have been reported. These have of a magnitude which is similar to the red-shift of the ALDH 4-*trans* (N,N-dimethylamino) cinnamoyl - cysteine moieties. Hence the red-shifted spectrum of the ALDH 4-*trans* (N,N-dimethylamino) cinnamoyl - cysteine moieties is consistent with an enzyme that contains a metal electrophile in the active site.

For ALDH, the "out of the plane" model can not explain the spectral red-shifts observed, because the spectra of the ALDH 4-*trans* (N,N-dimethylamino) cinnamoyl cysteine moieties (λ_{max} 464 and 484 nm) is considerably longer than that of the aldehyde DACA (λ_{max} 400 nm).

In conclusion the active site of ALDH must contain a strong electrophile that can complex to the carbonyl oxygen of an aldehyde which is almost certainly a divalent or trivalent metal ion.

Chapter 3

Effects of metal ions on ALDH

3.1 Introduction

Metallo-enzymes are enzymes which contain one or more metal atoms whose presence is required for catalytic activity or structural integrity. Venteicher et al (1977) showed that divalent and trivalent metal ions (Mg^{2+}, Ca^{2+}, Mn^{2+}, Co^{2+}, Ni^{2+}, Cu^{2+}, Zn^{2+}, Fe^{3+}, Y^{3+}, La^{3+}, Ce^{3+}, Pr^{3+}, Nd^{3+}, Sm^{3+}, Eu^{3+}, Gd^{3+}, Tb^{3+}, Dy^{3+}, Ho^{3+}, Er^{3+}, Tm^{3+}, Yb^{3+}, and Lu^{3+}) affected the activity of horse liver cytosolic and mitochondrial aldehyde dehydrogenases. Most of the metal ions produced dramatic activation at low concentrations (0.1- 10 μM) and inhibition at high metal ion concentrations (5 - 40 μM).

Divalent metal ions have been shown to promote dissociation of the sheep liver mitochondrial form of ALDH and in doing so activate the enzymes (Weiner and Takahashi,1985). However this was not the case for sheep liver cytosolic ALDH where magnesium ions favoured association (Hill et al., (1990) Enzymology of Carbonyl metabolism).

The metal ion content of ALDH was qualitatively examined by Motion (thesis, 1986) using a spark source emission spectrograph. From the data Motion found that ALDH contained copper, magnesium, aluminium and iron. After analysis of the copper and magnesium content using A.A. it was determined that these elements were present in considerably less than stoichiometric amounts, magnesium by a factor of 10 - 20 and copper by a factor of 20. The zinc content of ALDH was studied by MacGibbon (thesis) where it was found that the zinc content was only 20 % of the active site concentration. On the basis of this it was concluded that metal ions while not essential to the activity sheep liver cytosolic ALDH, did have structural and kinetic importance. This chapter further investigates the possible role of metal ions in aldehyde dehydrogenase.

3.2 Materials

The analytical reagents $MgCl_2$ (no company name), $CaCl_2$ (Unilab),Cu (no company name), Fe Zn (no company name) and $ZnCl_2$ (no company name) were used without further purification. All other reagents that were used in this chapter are outlined in chapter 1.

3.3 Methods

3.2.1 Determination of the number of magnesium binding sites using dialysis

The experiment was designed to investigate the magnesium binding properties of ALDH over the range of magnesium concentrations from 5 μM -1.2 mM. Solutions containing magnesium chloride were prepared in sodium phosphate (25 mM) buffer at pH 7.6. To 450 ml of each solution ALDH (1.2 ml, 30 μM) was added in dialysis sacking and allowed to swirl on a rotating platform for three days in the cold room. After this time the enzyme was removed from the dialysis sacking. An aliquot (20 μl) of the enzyme solution was used to measure the absorbance at 280 nm so that variations in enzyme concentration could be corrected for. 1 ml of each of the dialysed enzyme samples was placed in a 10 ml flask, and evaporated to dryness on a water bath. To each concentrated nitric acid (2 ml) was added and again the sample was evaporated to dryness. The solid was redissolved in 1 M HCl and made up to 10 ml in a volumetric flask. The magnesium concentrations were measured by atomic absorption spectroscopy at 285.2 nm using deuterium background correction for the molecular absorption. The more concentrated magnesium solutions were diluted to a concentration which was in the working range of the standard magnesium solutions. The analar acids used in the experiment were checked for magnesium but did not contain measurable amounts of this ion. The concentration of magnesium in the bulk dialysate solution was subtracted from the concentration of magnesium in the enzyme solution, so that the concentration of enzyme bound magnesium could be determined.

3.2.2 Effect of calcium, magnesium and zinc ions on the ALDH activity at pH 5.22

Sodium acetate buffer (0.85 ml, pH 5.22) was added to a 1 ml cuvette with 50 µl of ALDH (0.2 µM, final concentration) and NAD (50 µl, 1mM final concentration). The reaction was then started by the addition of propanal (50 µl, 20 mM final concentration) and then followed using the (334 to 346 nm) -(470 to 490 nm) mode on the HP8452 diode array spectrophotometer for 60 seconds. The metal ion solution (50 µl) of the appropriate concentration was then added. After thorough mixing the absorption changes were followed from 90 seconds to 150 seconds. This was then compared with a control assay in which 50 µl of buffer was added after 60 seconds instead of a metal ion solution and the reaction was followed further until 150 seconds. The first 60 seconds of the assay was used as an internal comparison to correct for small variations in the enzyme and substrate concentrations. The results for the metal ion assays were then expressed as a percentage of the enzyme activity with no metal ion added.

$$\% \text{ Act} = \frac{\text{rate(60 - 90s) x 100\%}}{\text{rate (0 - 60s) x F}}$$

The factor 'F' was obtained from the control assay which had no added metal ion.

$$F = \frac{\text{rate (0 - 60 s)}}{\text{rate (60 - 90 s)}}$$

This factor corrects mostly for dilution, but when using very low substrate concentrations it also corrects for a minor amount of substrate depletion and NADH inhibition over the time period of the assay.

The mode employed for following the reaction allows the average absorption changes over the range 470 to 490 nm to be subtracted from the average absorption changes over the range 334 to 346 nm. Using this mode corrects for non-specific absorption changes due to dust contamination, as can be seen in Figure 3.2.2.1.

Figure 3.2.2.1. Background correction of steady state assays

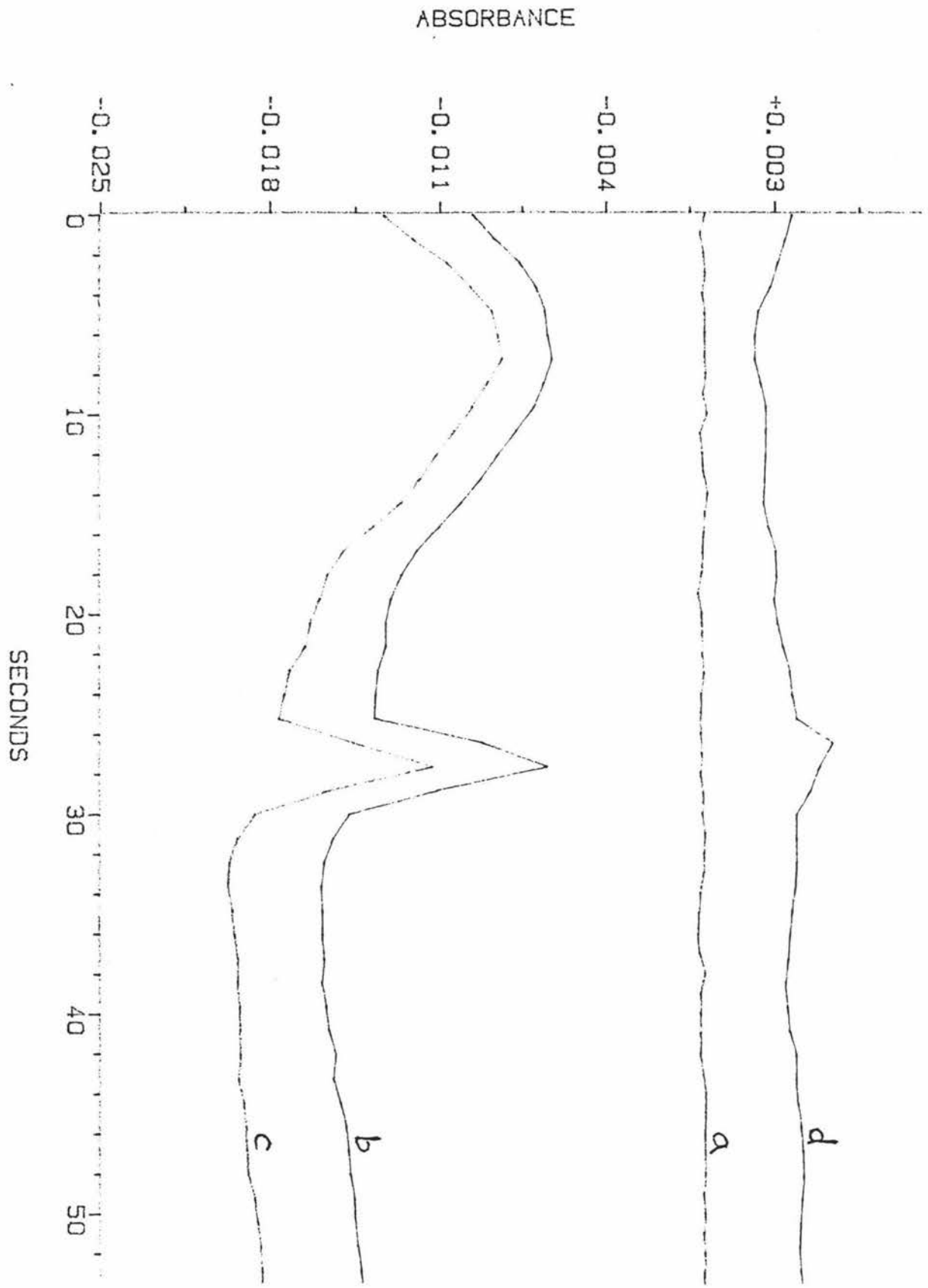

For line a (340 nm) there is no sample in the sample holder and hence this just represents the machine noise. Lines b (340 nm) and c (480 nm) were obtained by measurements on an aqueous sample containing some tissue paper fibers. The difference between b (340 nm) and c (480 nm) is shown as d. Note that despite the improvements not all of the background absorption has been removed. This is because more light is scattered at short wavelengths than at long wavelengths. Therefore, it is better not to have any particulates in the solutions than to correct for them.

However, since perfection is difficult to attain, having the spectrometer in a background correcting mode can improve the accuracy of the experimental measurements. Thus, if the spectrometer being employed has a background correcting facility it is advisable to make use of it, but it is clearly important to still maintain the best practically possible quality for the assay solutions.

For magnesium the background correction mode was not used, but at least one repeat was done at each concentration point. The effects of magnesium and zinc on ALDH activity were only studied using 1 mM NAD and 20 mM propanal. The effects of calcium on the ALDH activity was studied at variable concentrations of both NAD and propanal.

3.2.3 Determination of the Metal ion content of highly purified ALDH

An aliquot (2.5 ml) of ALDH (32.5 μM, measured from A280) which had been purified using the affinity column (see chapter 1, methods) was evaporated to dryness using a steam bath. Concentrated nitric acid (2 ml) was added and evaporated to dryness and then repeated with a further 2 ml of nitric acid. The solid was then redissolved in 1 M HCl (new bottle of RP Pronalys A.R. grade) and made up to 10 ml in a volumetric flask. This solution was then analysed for Zn, Cu, and Fe in an Instrumental Laboratory atomic absorption spectrometer using deuterium background correction. The acids used were also analysed but did not contain significant concentrations of iron, zinc or copper.

3.2.4 Examination of the iron profile of ALDH from the pH gradient column

ALDH was eluted from a pH gradient column (chapter 1, methods) and collected in approximately 10 ml fractions. With these fractions the aldehyde dehydrogenase activity and the absorbance at 280 nm were measured. The iron content of each tube was then measured by directly aspirating into an Instrumental Laboratory atomic absorption spectrometer using deuterium background correction.

3.2.5 Time dependent effects of EDTA

Three 1 ml enzyme samples (18 μM) were placed in double ended dialysis tubes and then into 100 ml solutions of 50 mM EDTA pH 6.5, containing 50 μl of mercaptoethanol. These were allowed to dialyse at 4 C. After 26, 50 and 120 hours one was removed and the activity and A^{280} were recorded. The EDTA buffer was changed for each of the dialysis tubes at 26 and 50 hours.

3.2.6 The pH dependence of EDTA inhibition

ALDH (0.1 ml, 18 μM) was placed in 8 dialysis buttons. The buttons were then sealed with a sheet of dialysis membrane and fastened with a 1.5 ml tube of silicone rubber. Either 50 mM EDTA or 50 mM bistris (1 ml) at the appropriate pH was then added to each of the tubes. All of the buffers contained 0.1 % mercaptoethanol. The buttons were then left to dialyse in the fridge. After 24 hours the activity and the absorbance at 280 nm of the enzyme in each of the buttons was measured.

3.3 Results

3.3.1 Number of metal binding sites

The concentration of magnesium bound to ALDH is equal to the total concentration of magnesium in the enzyme solution minus the concentration of magnesium that is free (represented by the dialysate solution).

$$[\text{ALDH } Mg^{2+}] = [\text{total } Mg^{2+}] - [\text{free } Mg^{2+}]$$
$$= [Mg^{2+}, \text{enzyme solution}] - [Mg^{2+}, \text{dialysate solution}]$$

The number of magnesium ions bound per ALDH tetramer is then given by the ratio [ALDH, Mg^{2+}]/[ALDH]. A graph of the number of magnesium ions bound per ALDH tetramer vs magnesium concentration was plotted and shown in Figure 3.3.1.1.

Figure 3.3.1.1

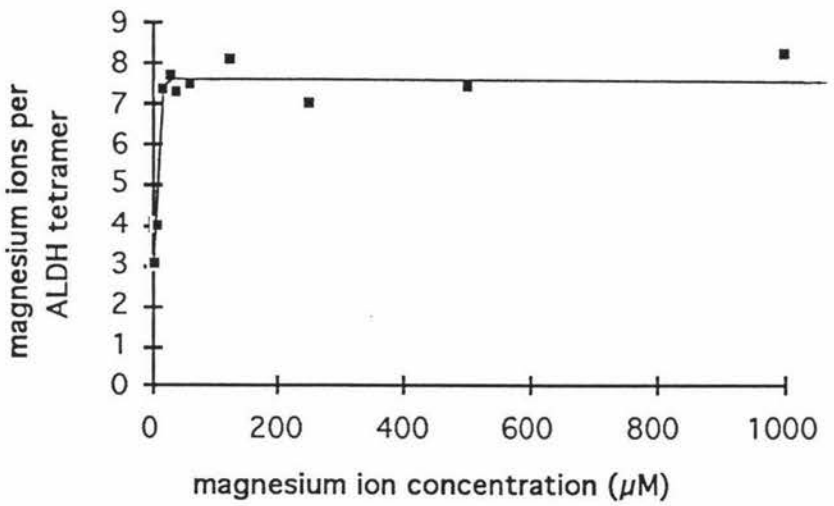

From Figure 3.3.1.1, it can be seen that at a magnesium concentration of ≈ 20 μM ALDH is saturated with ≈ 7.6 magnesium ions and no significant increases occur at higher magnesium concentrations. Under these conditions ALDH binds either 7 or 8 magnesium ions. However

since ALDH is a tetramer it is most likely that the enzyme actually binds 8 magnesium ions rather than 7.

3.3.2 Effect of Calcium Magnesium and Zinc on ALDH activity at pH 5.22.

Figure 3.3.2.1 shows the effect of increasing magnesium concentrations on the steady state activity of ALDH using 20 mM propanal and 1 mM NAD at pH 5.22. As at pH 7.6 (Bennett, thesis) there was a marked inhibition of the steady state at high magnesium concentrations. However, unlike the effects at pH 7.6 there was activation (22%) of the steady state activity at lower concentrations of magnesium (≈ 175 μM).

Figure 3.3.2.1 Effect of Mg^{2+} on ALDH activity

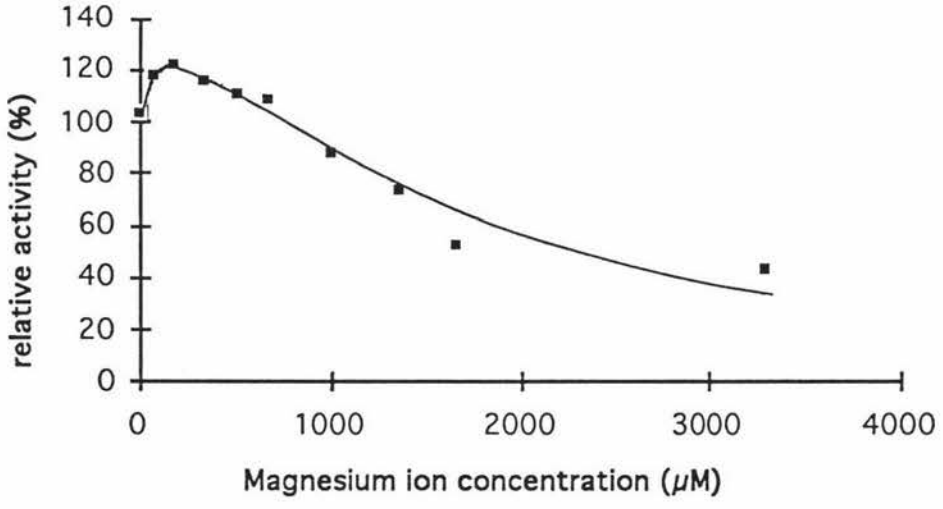

Similar effects were observed with $ZnCl_2$ (Figure 3.3.2.2) and $CaCl_2$ (Figure 3.3.2.3). In both cases low concentrations of the divalent metal ion stimulated the steady state activity, 60 % for $ZnCl_2$ (≈125 μM) and 46 % for $CaCl_2$ (200 μM) before marked inhibition occured.

Figure 3.3.2.2 Effect of Zn^{2+} on ALDH activity

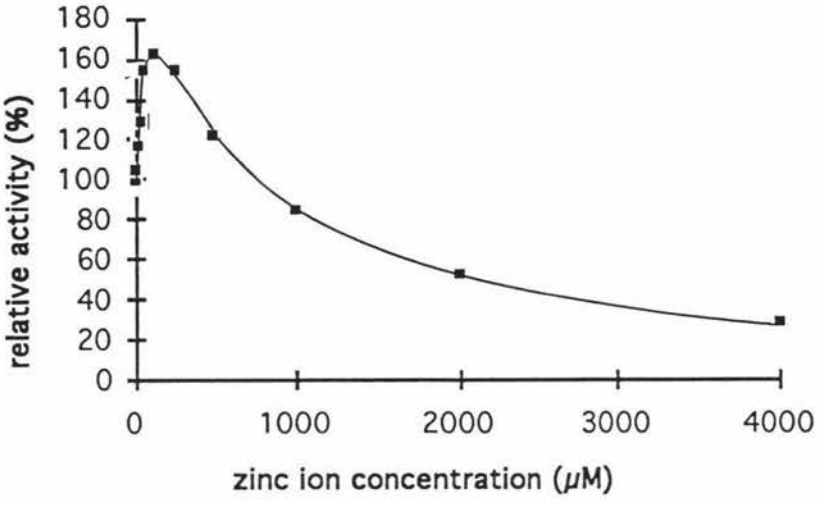

Figure 3.3.2.3 Effect of Ca^{2+} on ALDH activity

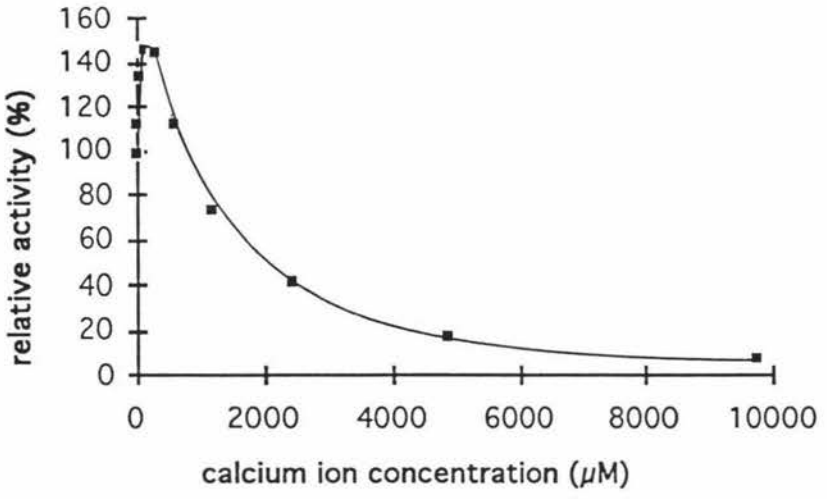

Figure 3.3.2.4 (a) - (d) show the activation and inhibition of the dehydrogenase reaction as a function of calcium ion concentration at propanal concentrations of 20 mM (a), 2 mM (b), 200μM (c), and 20 μM (d). The NAD concentration was 1 mM and the pH was 5.22. Note that the calcium ion concentration is a $\log_2$ scale so that differences can more easily be observed.

Figure 3.3.2.4

(a) 20 mM propanal

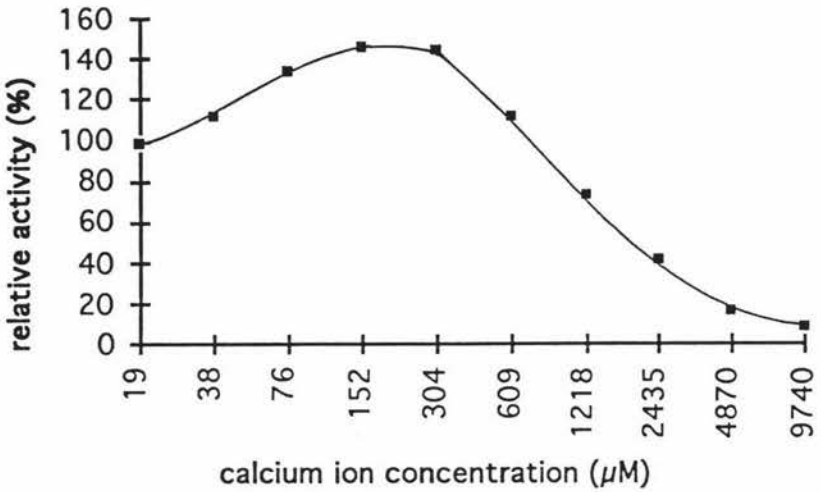

(b) 2 mM propanal

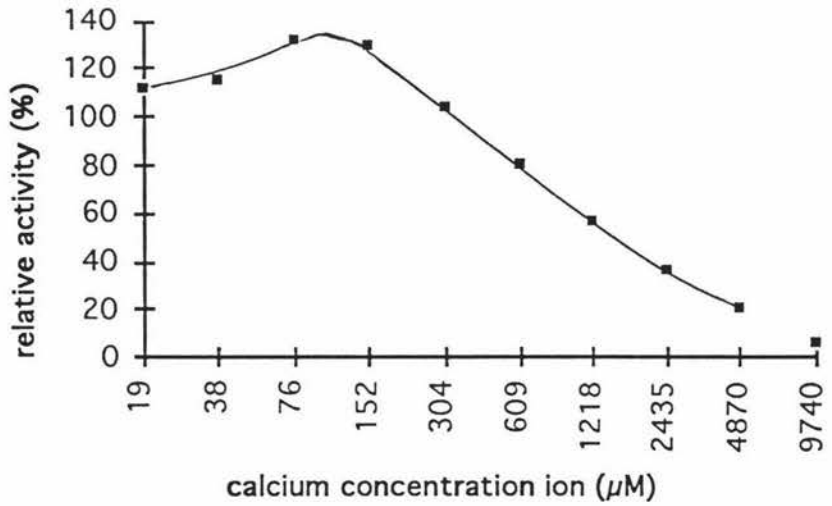

(c) 200 μM propanal

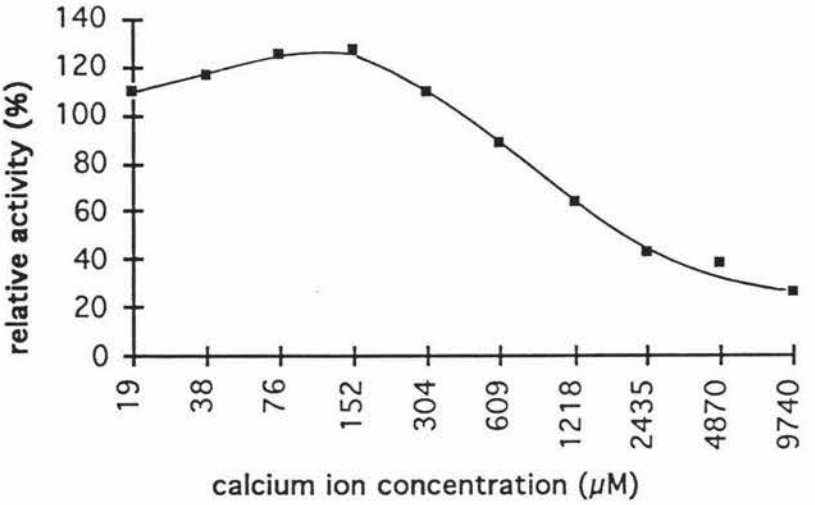

(d) 20 μM propanal

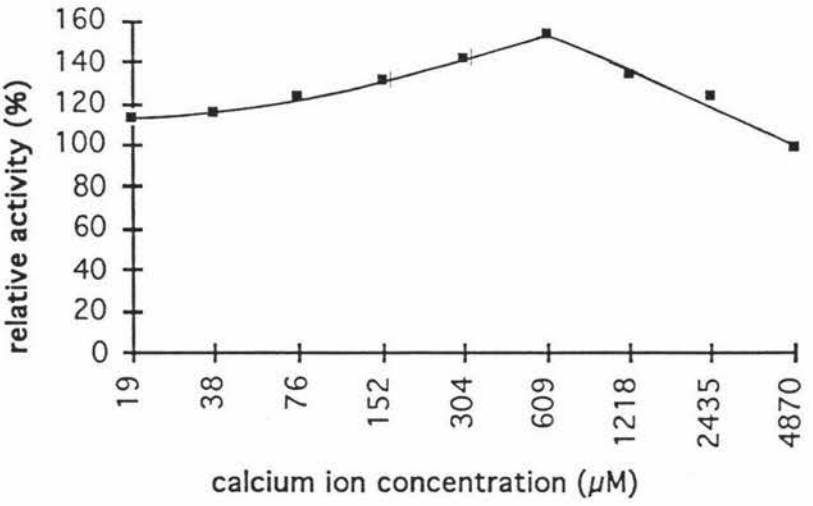

A significant point to note from this data was the highest activation (53%) occured at 20 μM propanal (i.e. close to physiological concentrations) and reasonably high Ca^{2+} concentrations (609 μM).

The activation and inhibition of ALDH as a function of calcium at 100 μM NAD (Figure 3.3.2.5 (a)), 1mM NAD (Figure 3.3.2.4 (a)) and 10 mM NAD (Figure 3.3.2.5(b)) was also studied. In all cases the propanal concentration was 20 mM and the pH was 5.22.

Figure 3.3.2.5

(a) 100 μM NAD

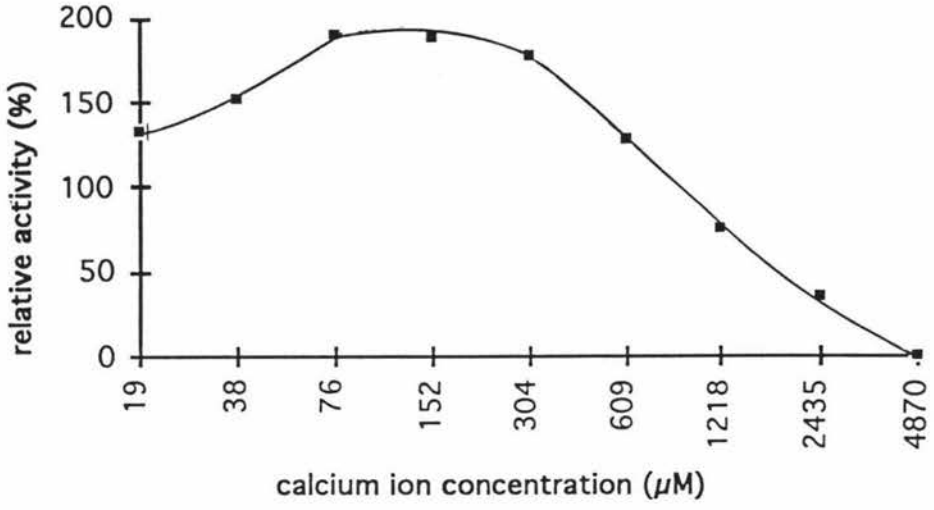

(b)

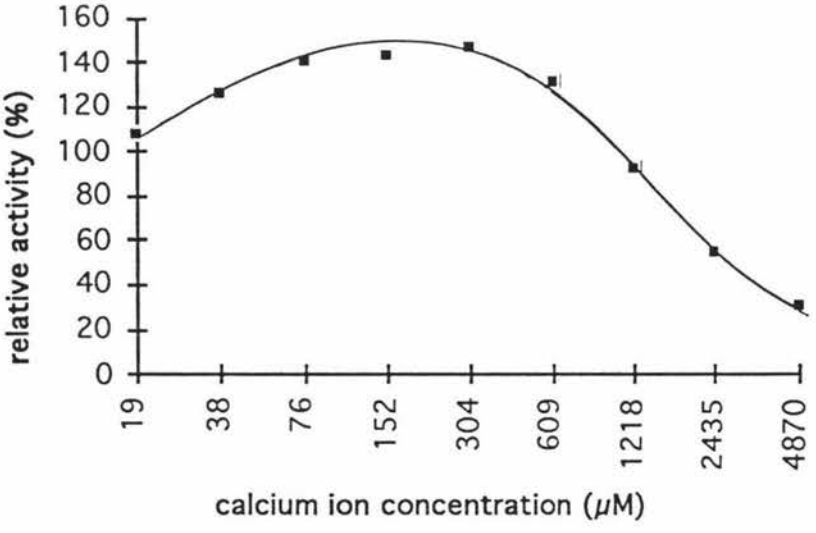

The activation induced by the presence of calcium is highest (90 %) at lower concentrations of NAD (100 μM), reaching a maximum at 76 μM Ca^{2+}.

3.3.3 Iron, copper and zinc determination of highly purified ALDH using atomic absorption

The enzyme solution used in this study was purified using affinity chromatography (see methods section 1.3.1). A gel of the enzyme used in this preparation is shown in Figure 1.3.1.2. It should also be taken into account that the affinity column buffers all had 1 mM EDTA present. The measured amount of iron was found to be 1.94 mols of iron per mole of ALDH tetramer (measured from the A_{280}). ALDH has been reported to have an active site concentration between 1 and 1.5 active sites per ALDH tetramer (Hart and Dickinson, 1982). In this enzyme preparation the active site concentration was 1.3 active sites (from the measured activity) per tetramer (measured from the A_{280}), the highest recorded active site concentration for the enzyme used in this thesis was 1.87 active sites per ALDH tetramer. Thus, it can be seen that iron concentration was equal or greater than the number of active sites per tetramer. Copper and zinc were also measured and found to be present in a concentration of 0.19 mols and 0.47 mols per ALDH tetramer respectively. These levels are not sufficient to account for the active site concentration and were in agreement which the conclusions of Motion (thesis) and MacGibbon (thesis).

3.3.4 Examination of the iron profile of ALDH from the pH gradient column

During the elution from the pH column (see methods section 1.3.1 for details) the profile of the active site, the protein concentration and the iron concentration were determined across the main peak.

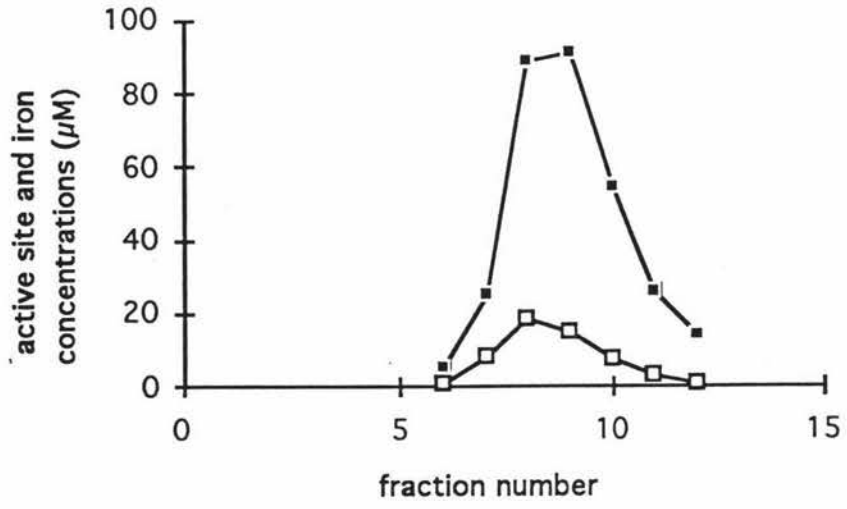

Figure 3.3.4.1(a) shows the active site concentration (□) and the iron concentration elution profiles (■), from the pH gradient column.

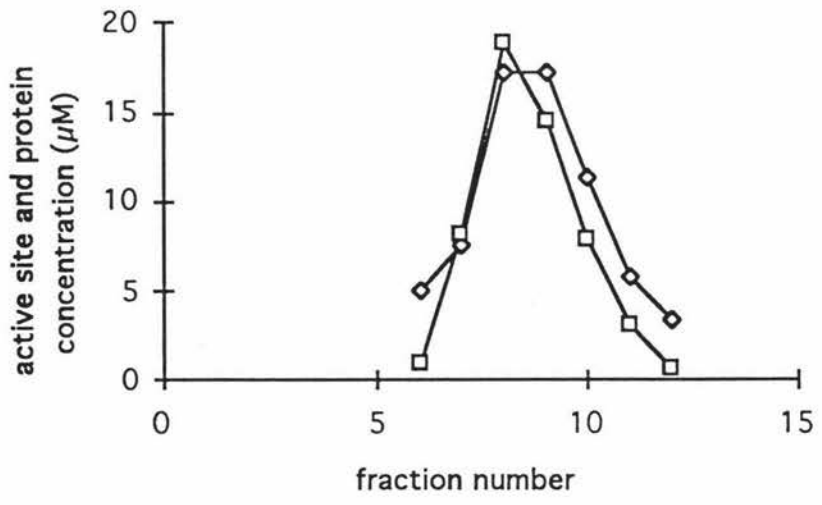

Figure 3.3.4.1(b) shows the active site concentration (□) and the protein concentration elution profiles (◇ , calculated using the extinction coefficient for ALDH at 280 nm), from the pH gradient column.

It can be seen that fraction 6 exhibited a high protein concentration, a low active site concentration and a low iron concentration. In fraction 7 the active site concentration had dramatically increased with a corresponding increase in the iron and protein concentrations. Fraction 8 reached a maximum for the enzyme activity, but both the peak iron and protein concentrations did not occur until slightly later in the elution profile. Fraction 12 contained only 0.3 μM enzyme active sites but 14.3 μM iron

content, i.e. 48 times more iron than the active site concentration. Hence, it is likely that there is significant contaminating iron containing proteins present which elute slightly later in the pH gradient.

3.3.5 Time dependent effects of EDTA

In this experiment, the decrease in the aldehyde dehydrogenase activity (Figure 3.3.5.1 (a)) and increase in the protein A_{280} (Figure 3.3.5.1(b)) due to the presence of EDTA (50 mM pH 6.5) was followed as a function of time.

Figure 3.3.5.1 (a) Decrease in the ALDH activity as a function of time, in EDTA buffer (50 mM, pH 6.5)

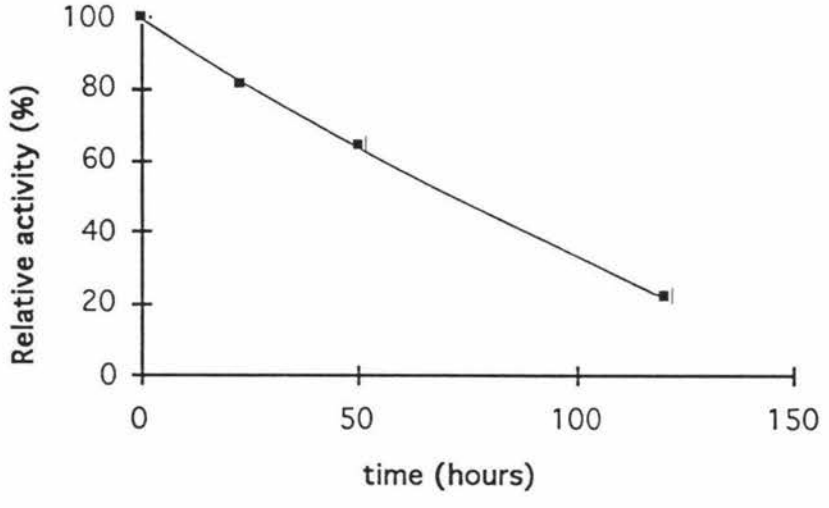

Figure 3.3.5.1 (b) Increase in the ALDH absorbance (280 nm) as a function of time, in EDTA buffer (50 mM, pH 6.5)

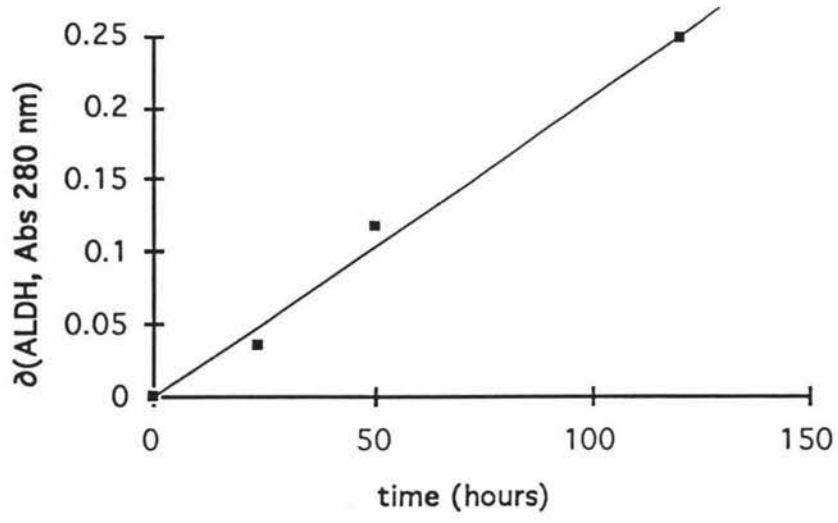

It can be seen that the decrease in the activity had also a corresponding increase in the A_{280}. EDTA is a strong metal ion chelator, hence the most obvious cause for the observed decrease in the activity would be removal of essential metal ions necessary for activity or structural stability. It is a mystery why the absorbance at 280 nm had increased. It might be due to colloidal protein formation which causes an apparent absorption of light through scattering, though the increase was so large that one might have expected to see precipitation of the protein.

3.3.6 pH dependence of the ALDH inactivation by EDTA.

In this experiment, the time dependent decrease in enzyme activity due to EDTA buffer was compared to a control buffer (50 mM Bistris, which is not a strong metal ion chelator) over a pH range 5.5 to 7.0.
Figure 3.3.6.1 shows a graph of enzyme activity dialysed with bistris (A) and EDTA (B) compared with the undialysed activity, over 24 hours. The enzyme sample in EDTA at pH 6.0 had only a very small A_{280} and activity, due to a leak in the dialysis membrane and was therefore not included.

Figure 3.3.6.1 Dependence of pH on the EDTA inactivation of ALDH

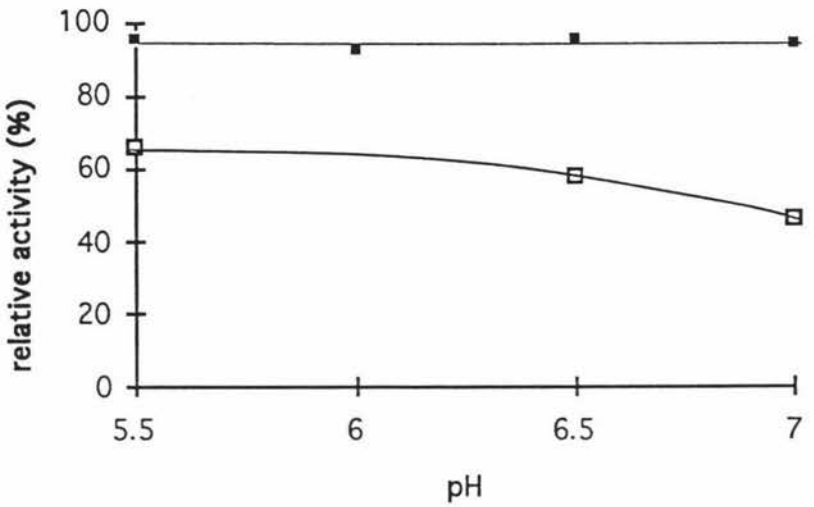

It can be seen that the decrease in activity for samples dialysed with bistris was only very small, but for the sample dialysed into EDTA a substantial activity decrease was observed, with a maximum decrease occuring at pH 7.0.

3.4 Discussion

3.4.1 Effects of metal ions on ALDH

It has been shown that at physiological pH approximately 8 magnesiums can bind to ALDH at a magnesium concentration of 20 μM. The concentration of magnesium in the liver is approximately 833 μM (Soman et al.,1970), although free magnesium would only constitute a small part of this. For example in human erythocyte cells, the free magnesium content represents only approximately 20 % of the total magnesium (Henrotte et al.,1990). The rest of the magnesium usually exists bound to a host of molecules such as NAD, ATP and ADP (Henrotte et al.,1990). Therefore the free magnesium content available to ALDH is likely to be only about 170 μM. In either case it is certain that ALDH is saturated with approximately 8 magnesiums.

Bennett (pg 105, thesis) commented that he observed no effect on the enzyme activity below 20 μM magnesium content at pH 7.6, suggesting that the binding of the eight magnesiums to ALDH did not have an adverse affect on the activity of the enzyme. Venteicher et al (1977) have shown for horse liver ALDH that low concentrations of magnesium caused activation of the enzyme. For sheep liver ALDH at pH 5.2, low concentrations of magnesium (33 μM) have also been shown to cause activation (≈ 20 %) of the enzyme. At pH 5.0 the k_{cat} measured by NADH displacement off ALDH with saturating NAD has been shown to be 20 % activated in the presence of a low concentration of magnesium, 30 μM (Paul Buckley, personal communication).

At high magnesium concentrations (3.3 mM) dramatic inhibition was observed (80 %) at pH 5.22. Bennett also observed dramatic inhibition of ALDH at pH 7.6 with high magnesium concentrations. At pH 5.0 the k_{cat} measured by NADH displacement off ALDH with saturating NAD has been shown to be 80% inhibited in the presence of a high concentration of magnesium, 3.3 mM (Paul Buckley, personal communication).

At magnesium concentrations up to 1 mM at pH 7.4 there appears to be no increase in the number of magnesium binding sites, yet there is a dramatic change in the enzyme activity. Presumably there must be an interaction between the enzyme and the magnesium which is not accounted for from the magnesium binding study. One possibility is that more magnesium is binding in the presence of NADH or NAD, perhaps in a site which makes use of the pyrophosphate part of the coenzyme as part of the magnesium binding site, as Venteicher et al (1977) has proposed. The outcome of this additional magnesium binding appears to greatly increase the binding of both NAD and NADH to the enzyme (Bennett, thesis).

The use of magnesium ions in growing crytstals of ALDH is vital (Baker personal communications), and are thought to be important for structural stability of the enzyme. Buckley et al. (1990) has shown that the presence of magnesium causes ALDH to be present predominantly in the tetrameric state, which is the active form.

Hence it can be seen that at low magnesium concentrations (20 μM) ALDH is completely saturated with 8 magnesium ions and that the presence of these ions appears to have no adverse effects on the activity, and under some conditions (pH 5.22) low concentrations of magnesium ions activate the enzyme (this work and Bennett thesis). Therefore it is likely that the presence of these ions are only of structural importance. At high magnesium concentrations (0.83 mM) dramatic inhibition has been observed (this work and Bennett thesis), yet from the binding study results no further magnesium binding has occured. It appeared that Ca^{2+} and Zn^{2+} also had a similar effect to Mg^{2+}.

3.4.2 Effects of EDTA on the ALDH activity

EDTA is commonly used in enzyme preparations because EDTA is an inhibitor of many metallo-proteases which can potentially damage the enzyme of interest (Gill Norris, personal communication), unfortunately it also appears to be an inhibitor of ALDH. For ALDH, EDTA was also added by workers in the field because there was a concern that even minute concentrations of metal ion impurities present in the preparation buffers might reduce the activity of the ALDH being prepared. The results from this study and Bennett's (thesis) indicate that minute concentrations of metals ions do not have any adverse effect on the activity of sheep liver ALDH.

The results from this study indicate that addition of EDTA to preparative buffers would have quite an adverse time dependent effect on the activity of ALDH and certainly cannot be considered at all beneficial. Fortunately the decrease in the ALDH activity due to the presence of EDTA occurs very slowly even at EDTA concentrations of 50 mM.

The ultimate purpose of kinetic studies on ALDH is the understanding of the physiological role of the enzyme in situ. In situ, there certainly is an abundance of metal ions present (such as magnesium), rather than EDTA. Therefore one would wonder whether for normal study of the enzyme, metal ions should be added in a concentration which is representative of the free metal ion content of the liver cells, as this would certainly be more representative of the real situation.

3.4.3 What is the active site metal electrophile?

The results from acyl enzyme modeling study (chapter 2) indicate that an electrophile which is greater than, or equal to, the electrophilc strength of Zn^{2+}, is an important feature of the active site. Of the metal ions examined using atomic absorption spectroscopy only iron was present in sufficient quantity to be equal to the active site concentration.

Iron is normally present in biological systems in the oxidation states (II) or (III). Dietrich et al. (1981) proposed that, as the ionic radius of a metal ion decreased, the red-shift inducible in a alcohol dehydrogenase DACA moiety increased. This observation is in good agreement with the findings of the metal ion modelling experiments outlined in chapter 2. However making predictions about the oxidation state of the iron based on the ionic radii and the observed red-shift requires a detailed description of the environment the active site iron. A tetrahedral metal environment (e.g. alcohol dehydrogenase) should induce a larger red-shift in DACA than would a octahedral metal environment, because the ionic radius of a tetrahedral metals is smaller than the ionic radius of the corresponding octahedral metal (Shannon and Prewitt, 1969). Therefore, while it is possible from the modeling study to make predictions about whether the catalytic electrophile is a metal or a non-metal it is not possible to predict the oxidation state of the metal.

3.5 Conclusion

ALDH has been shown to contain up to eight magnesium binding sites per tetramer (at 20 μM) which appear to be of structural significance at physiological pH. All enzymes involved in carbonyl chemistry that this author has observed have an electrophile which stabilises the carbonyl oxygen of the substrate, which is either a non-metal electrophile such as imidizolium ion (glyceraldehyde 3-phosphate dehydrogenase) or a metal electrophile such as zinc (carboxypeptidase). Therefore it is likely that the active site of ALDH must also fit in to one of these catagories. The conclusions of chapter 2 indicated that the active site electrophile was either a divalent or a trivalent metal ion.

Atomic absorption of very pure ALDH has indicated that iron is present in sufficient quantity to account for the observed number of ALDH active sites. The activity requirement for a divalent anion such as carbonate (Motion, thesis) shows striking similarity to lactoferrin which is an Fe (III) metalloenzyme. Dialysis with EDTA showed a dramatic, time dependent decrease in the activity of ALDH, which might be attributed to removal of a metal ion essential for activity.

In conclusion the active site of ALDH certainly contains a strong electrophile which is most likely Fe (II) or Fe (III).

Chapter 4

The Interactions of NADH on the ALDH Pathway

4.1 Introduction

Two research groups have undertaken to study sheep liver cytosolic ALDH. One of them based here at Massey University, and the other at Hull University in the United Kingdom. Over the last 23 years each group has made a significant contribution to the understanding of the kinetic mechanism of this enzyme. However, there has been a number of differences in the research observations of the two groups. This has lead to mistrust between the two research camps, each camp being sure of their own experimental observations which on initial inspection should have been in agreement. In this chapter these apparent differences in what is observed experimentally have been addressed.

In the original studies of the pre-steady-state kinetics of ALDH, MacGibbon, Buckley and Blackwell demonstrated that NADH was displaced from ALDH in a byphasic manner. A model for this was proposed, in this model NADH is bound to ALDH in two enzyme isomeric forms. Hence the displacement of NADH from ALDH with NAD can be represented by Figure 4.1.1.1

Figure 4.1.1.1 Equilibrium between enzyme and NADH

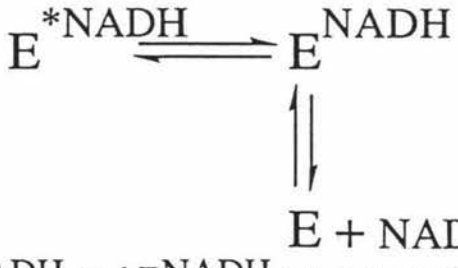

where E^{*NADH} and E^{NADH} are not equivalent species

It was also proposed that both of these E^{NADH} species were kinetically significant in the normal dehydrogenase pathway, hence an understanding of the involvement of these two species in the kinetic pathway might be important.

NADH has been spectrally followed both in absorption and fluorescence. Fluorescence is very useful in that it is very sensitive to its environment, but is often very difficult to quantitate because the fluorescence of a molecule can vary greatly depending on the environment which it is in. Absorbance, although less sensitive than fluorescence has the advantage that shifts in the absorption maximum of a molecule are rarely accompanied by large changes in its extinction coefficient.

From measurements of fluorescence changes after excitation at 340 nm (with emission monitored at 460 nm), MacGibbon et al. (1978) have argued that the fluorescence of the two complexes are the same. Otherwise it appears to have been implicitly assumed that the two E.NADH complexes have identical absorption and fluorescence properties. However because the ability to spectrally study these two species independently of each other is potentially useful, it seemed worthwhile to attempt to identify spectral differences between the two species.

4.2 Materials

The reagents tetra-sodium pyrophosphate (BDH), NADH (Sigma) and boric acid (no company label) were analytic grade and used without further purification. N,N-dimethylethanolamine (bulk supply) was purified by refluxing with ethanoic anhydride (to remove primary and secondary amines), then vacuum distillation. All other reagents are outlined as in chapter 1.

4.3 Methods

4.3.1 Spectral properties of NADH bound to ALDH

The spectrum of NADH (≈ 100 μM) was recorded ('unbound NADH') using buffer alone to blank the spectrophotometer.
The spectrum of ALDH (active site concentration, 7 μM) with NADH (≈ 100 μM, added in 5 μl) was recorded ('total NADH') using ALDH alone to blank the spectrophotometer. The pH for these measurements was 5.8, made from a mixture of 10 mM sodium acetate buffer pH 4.6 and 10 mM bistris buffer pH 6.5.
From Motion's (thesis) difference spectrum it can be seen that the ALDH-NADH species must only have a small absorption contribution at 328 nm because the difference spectrum is at a minimum at 328 nm. Since unbound NADH absorbs well at 328 nm the spectrum of just the ALDH-NADH species can be calculated in a similar manner to the calculated difference spectra in section 2.2.2

The 'total NADH' spectrum was then multiplied by a factor F, where

$$F = \frac{A^{328}\ \text{'unbound NADH'}}{A^{328}\ \text{'total NADH'}}$$

The spectrum of the NADH bound to ALDH was then calculated by subtracting the unbound NADH spectrum from the newly calculated spectrum (F x 'total NADH').

ALDH-NADH spectrum = (F x 'total NADH') - 'unbound NADH'

This was repeated using solutions containing :
-1 mM magnesium nitrate
-2 mM propanal
-1 mM magnesium nitrate and 2 mM propanal
In each the spectrum of the ALDH-NADH species was calculated.

The spectrum of the ALDH-NADH species was calculated for enzyme that had been dialysed into the following buffers :

-50 mM sodium phosphate pH 7.4
-50 mM sodium pyrophosphate pH 9.0
-50 mM sodium borate pH 9.0

4.3.2 Effect of pyrophosphate on ALDH activity

The assay conditions were as follows:

Buffer	=	40 mM N,N-dimethylethanolamine/HCl (pH 9.35)
NAD	=	400 μM
propanal	=	200 μM
pyrophosphate	=	variable concentration (pH 9.35)
Temp	=	25 C

The reaction was initiated with addition of propanal and followed as outlined in section 3.2.2.

4.3.3 Activation and inhibition of ALDH by NAD

The assay conditions were as follows:

Buffer	=	50 mM sodium acetate (pH 5.22)
ALDH	=	0.64 μM (active site concentration)
NAD	=	variable concentration (the pH of the stock was ≈ 5.2)
Propanal	=	variable
Temp	=	25 C pre-incubated 3 minutes

After the ALDH was added to the buffer the A280 was recorded so that small errors in the amount of enzyme added could be corrected for. NAD was subsequently added followed by a 3 minute incubation period. The reaction was initiated with addition of propanal and followed as outlined in section 3.2.2

4.4 Results and Discussion

4.4.1 Spectral properties of NADH bound to ALDH

Using the software applications available on the spectrophotometer, difference spectra of ALDH bound NADH were calculated for a variety of conditions and are shown in Figures 4.4.1.1 (A) and 4.4.1.1 (B).

Figure 4.4.1.1 (A) shows the ALDH bound NADH difference spectra at pH 5.8 under the following conditions:
a. In the presents of magnesium and propanal.
b. In the presents of propanal
c. In the presents of magnesium
d. ALDH-NADH species alone

Figure 4.4.1.1 (B) shows the ALDH bound NADH difference spectra under the following conditions:
e. In borate buffer pH 9.0
f. In phosphate buffer pH 7.4
g. In pyrophosphate buffer pH 9.0

It can be seen that the spectra of NADH bound to ALDH have a maximum at 364 nm are therefore red-shifted ≈ 24 nm from the spectrum of NADH (Figure 4.4.1.3)

Figures 4.4.1.1 (A) E^{NADH} difference spectra

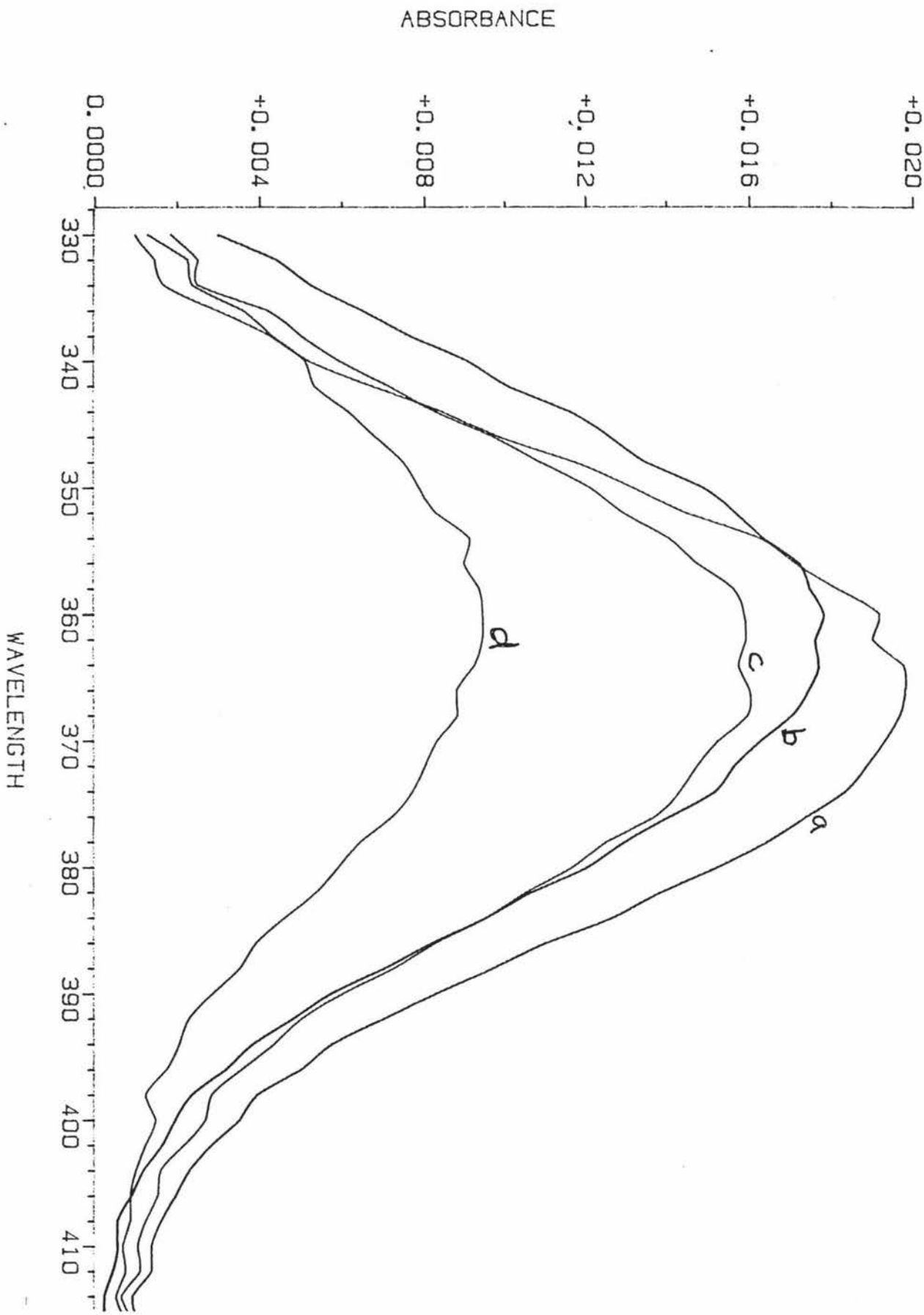

Figures 4.4.1.1 (B) E^{NADH} difference spectra

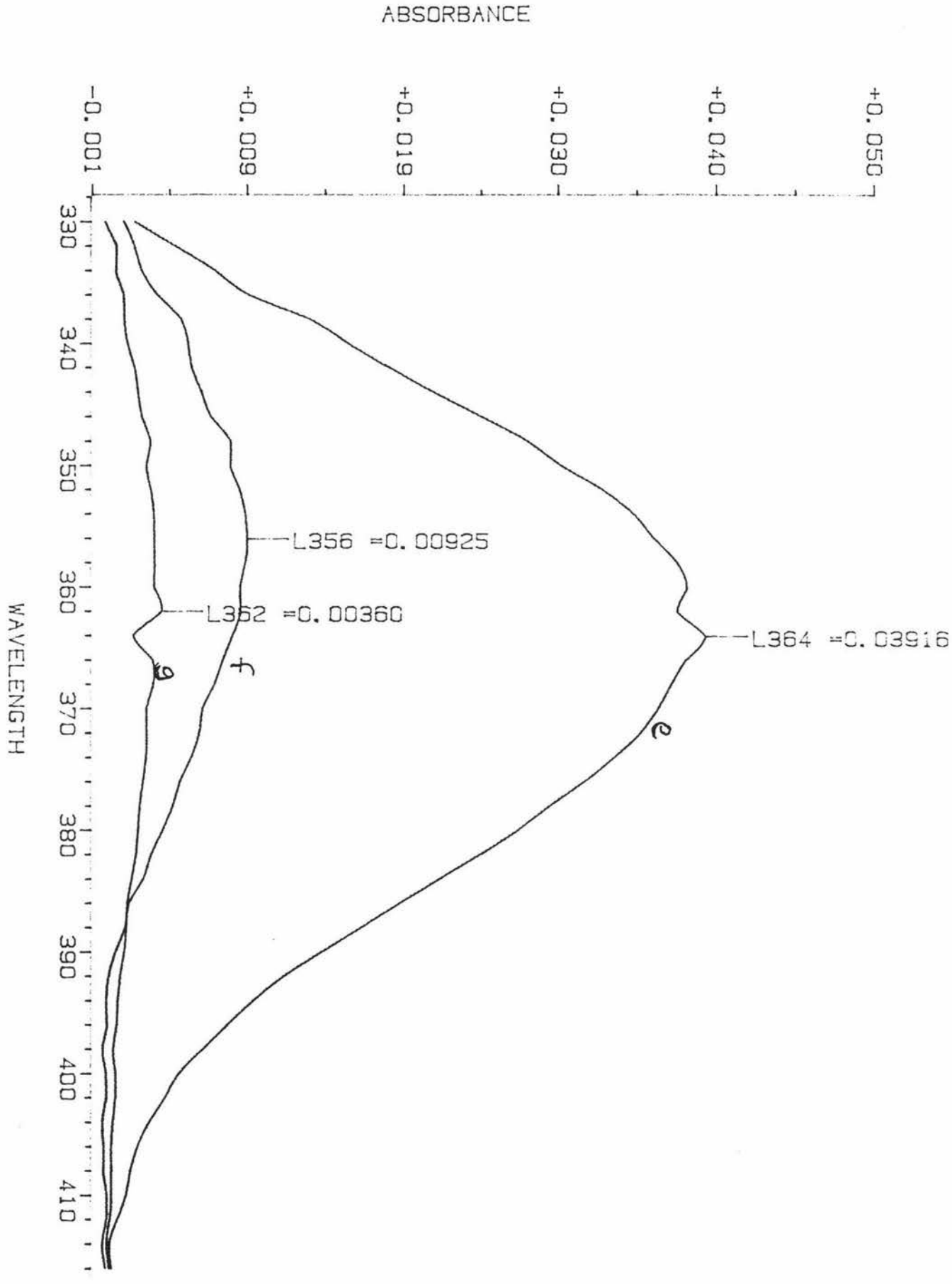

Figures 4.4.1.2 The spectrum NADH in sodium phosphate buffer (pH 7.4)

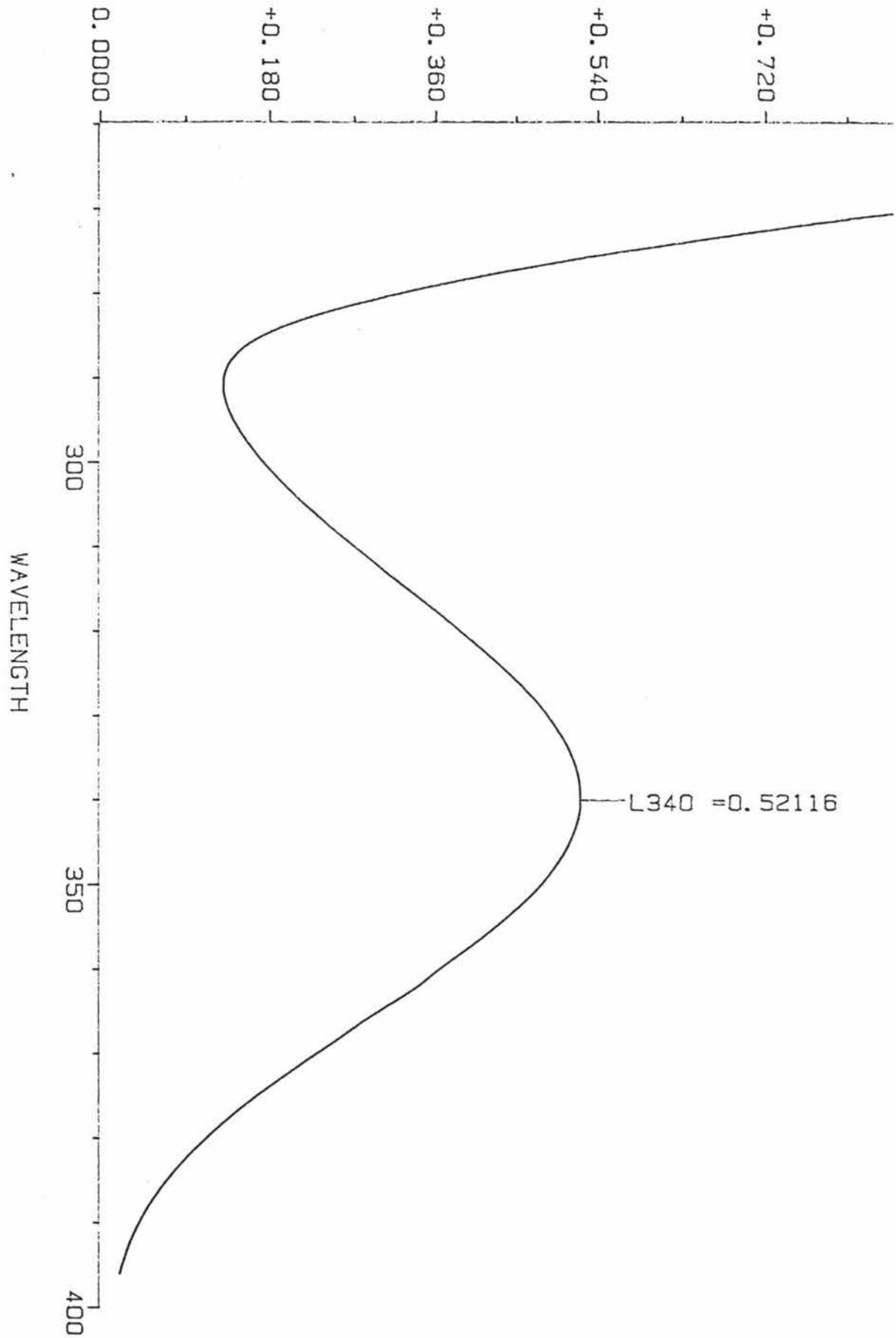

4.4.2 Probable cause of the E^{NADH} red-shifted spectra

When NADH absorbs light its π-electrons are perturbed to an excited state. Once in the excited state the π-electrons lose this energy by vibrational energy losses and by fluorescence in which light is emitted at a longer wavelength (Figure 4.4.2.1).

Figure 4.4.2.1

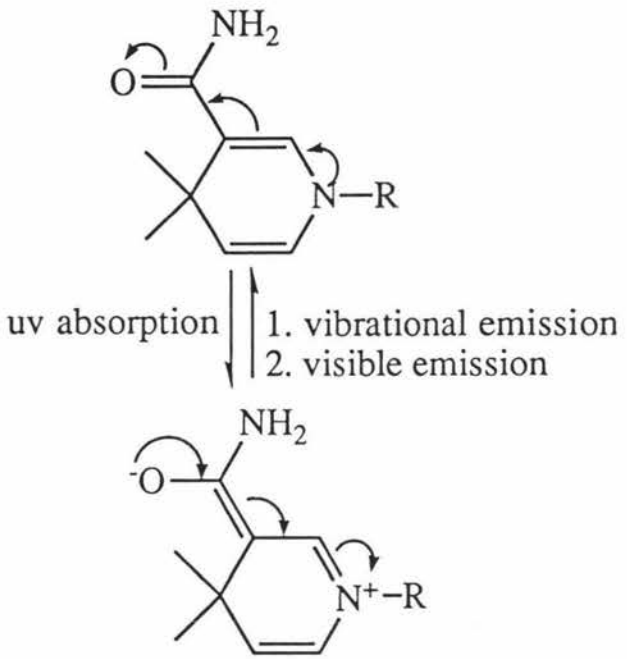

Two obvious ways a red-shift can occur in the absorption spectrum of NADH are:

1. A nucleophile complexes with the amine nitrogen, increasing the nitrogens electron donating ability.
2. An electrophile complexes with the amide oxygen, increasing the oxygens electron withdrawing ability.

Since the amide oxygen can withdraw electrons from both the amide nitrogen and the nicotinamide nitrogen it will carry the most stable negative charge. Hence it is most likely that an electrophile complexes (possibly hydrogen bonding) with the amide oxygen, increasing the oxygen's electron withdrawing ability, and bringing about a spectral red-shift Figure 4.4.2.2)

Figure 4.4.2.2

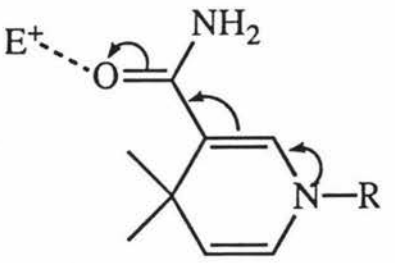

4.4.3 Calculation of the equilibrium constant for the two E^{NADH} species.

From the ALDH-NADH dissociation constant it can be seen that at 100 μM NADH, ALDH would be completely saturated with NADH.
If the extinction coefficient of the ALDH-NADH species at the maximum absorbance (364 nm) is approximately the same as that of free NADH at its maximum (340 nm) then from the active site concentration the approximate absorption of the 364 nm species can be calculated, assuming that all of the NADH bound to ALDH is also complexed to an electrophile.

max Abs = e . c . L
max Abs(364 nm) = 6220 (L.cm.mol^{-1}) x 7 x 10^{-6} (mol.L^{-1}) x L(cm)
max Abs(s64 nm) = 0.04354 (a)

For the ALDH-NADH spectrum (a) (with propanal and Mg^{2+}) the absorption maximum of the 364 nm species was only 0.0198 and in spectrum (d) (alone) the absorption maximum was only 0.0092 . In both cases the ALDH is completely saturated with NADH, hence on the enzyme the NADH is only complexed to the electrophile only some of the time and the rest of the time the NADH exists bound to the ALDH but not complexed to the electrophile.

The method used for observing the ALDH-species can only detect species that are spectrally different from the free NADH, therefore NADH present bound in a binding site which do not electronically perturb the nicotinamide, are not detected, but are present, since saturating conditions apply.

The question then becomes, how many E^{NADH} species are there and what is their relationship to the two E^{NADH} species already predicted by MacGibbon et al (1978)? Applying the principle of Occam's Razor, there are two spectrally different E^{NADH}, which are the same species predicted by MacGibbon et al (1978). The two conformer model will be further developed for the remainder of this chapter. However the possibility of three E^{NADH} species can not be excluded, indeed the outcome of the simulations in chapter 1, which indicated the presence of at least three kineticaly significant E^{NAD} species, would support the possibility of three E^{NADH} species.

Assuming for simplicity sake that there are only two major favourable binding conformations, then most of the time the NADH is bound in an conformation where its absorption spectra is unperturbed (i.e. $\lambda_{max} \approx$ 340 nm) and some of the time the NADH will be bound in an orientation where the λ_{max} is red-shifted (i.e. $\lambda_{max} \approx 364$ nm) relative to free NADH.

Figure 4.4.3.1 represents the equilibrium of the NADH on ALDH

$$E^{NADH}\ 340\ nm \rightleftharpoons E^{NADH}\ 364\ nm$$

An equilibrium constant (K) for this process can be crudely calculated by assuming that complexed-NADH has the same extinction coefficient at 364 nm as free NADH at 340 nm as discussed above..

K = measured Abs / (max Abs - measured Abs)

where

max Abs = 0.4354 see (a) above

The equilibrium constants for each of the difference spectra at pH 5.8 are summarised in Table 4.4.3.1.

Table 4.4.3.1 Calculation of the approximate equilibrium constant of the E^{NADH} species.

ALDH-NADH species, pH 5.8, 7 μM ALDH	λ_{max}(nm)	Absorption	K
(a) With Mg^{2+} & propanal	366	0.0198	0.84
(b) With propanal	362	0.0175	0.67
(c) With Mg^{2+}	366	0.0160	0.58
(d) Alone	362	0.0092	0.27

The equilibrium constants for each of the difference spectra using variable pH are summarised in Table 4.4.3.2, where max Abs = 0.0597.

Table 4.4.3.2 Calculation of the approximate equilibrium constant of the E^{NADH} species in different buffers.

ALDH-NADH species, 9.6 μM ALDH	λ_{max} (nm)	Absorption	K
pyrophosphate pH 9.0	362	0.0036	0.06
borate pH 9.0	364	0.0392	1.91
phosphate pH 7.4	358	0.0090	0.18

Bennett (thesis) showed that the fluorescence of the ALDH-NADH species in the presents of magnesium (1.6 mM) was significantly enhanced (18 fold). Bennett also observed increased binding of NADH to ALDH in the presents of magnesium (K_D without added magnesium 1.1 μM K_D with magnesium 0.2 μM). He also showed that addition of citrate (6.6 mM) deceased the fluorescence of the ALDH-NADH species and decreased the binding of NADH to ALDH (K_D with citrate 1.8

μM). Similarly addition of EDTA also resulted in decreased fluorescence of ALDH bound NADH. Dickinson (1985) showed that the ALDH-NADH species had increased fluorescence in the presents of up to 2 mM propanal.

Increased NADH fluorescence observed by both Bennett and Dickinson correlates well with an increase in the absorption of a 364 nm species, hence it can be hypothesised the ALDH-NADH 364 nm species is strongly fluorescent while the ALDH-NADH 340 nm species is less fluorescent.

This is supported by the observed fluorescence of ALDH-NADH species (ALDH was in excess, phosphate pH 7.6) which is maximised when the excitation frequency is 355 nm (MacGibbon, thesis). From the absorption spectrum of the intermediate at pH 7.4 it can be seen that the measured absorbance at 356 nm (0.009) represents only 15 % of the theoretical absorbance (0.060) of NADH on the enzyme. Clearly 356 nm (15 % of total) much closer to the maximum fluorescent excitation (355 nm) than is the 340 nm (85 % of total), this indicates that the 356 nm species is more fluorescent than the 340 nm species. Why the difference spectrum indicates that the ALDH-NADH species absorbs at 356 nm in phosphate buffer (pH 7.4) and not ≈ 364 nm is unclear

The apparent fluorescence of ALDH bound NADH is 5.8 times free NADH when excited at 340 nm (Bennett, thesis). However when excitation is at 366 nm there is an apparent enhancement of approximately 10.5 (Kitson, 1989) suggesting the presence of a longer wavelength absorbing species with good fluorescent properties. In addition to this Kitson was using enzyme which had EDTA added to its preparation buffers, which Bennett (thesis) has been shown to decrease the fluorescence of the E^{NADH} species (when excited at 340 nm). Therefore, for enzyme which has not been modified by the presence of EDTA, the fluorescence enhancement at 366 nm could be even higher than 10.5.

4.4.4 Effects of propanal on the E^{NADH} species

Dickinson (1985) showed that the ALDH-NADH species had increased fluorescence in the presence of propanal at concentrations up to 2 mM , and decreased fluorescence at much higher propanal concentrations (50 - 130 mM). Clearly there are at least two observable effects occurring, which must be due to at least two aldehyde binding site. The effects of propanal concentrations up to 2 mM will be discussed, as these appear to correlate with aldehyde binding at the active site.

Kitson (1991) showed that modification of ALDH with p-nitrophenyl dimethylcarbamate gave a stable ALDH-dimethylcarbamoyl acyl species. By using radioactive labelling Kitson showed that the acyl species had been incorporated at cysteine 302, which is considered to be the active site nucleophile for propanal. Propanal is thought to react with cysteine 302 and form a thiohemiacetal.

Figure 4.4.4.1 (a) represents the ALDH-dimethylcarbamoyl acyl species. Figure 4.4.4.1 (b) represents the ALDH thiohemiacetal formed by binding of propanal. In these diagrams it the electrophile present in the active site is shown as Fe^{n+} where n is either 2 or 3 (See section 3.5).

Figure 4.4.4.1

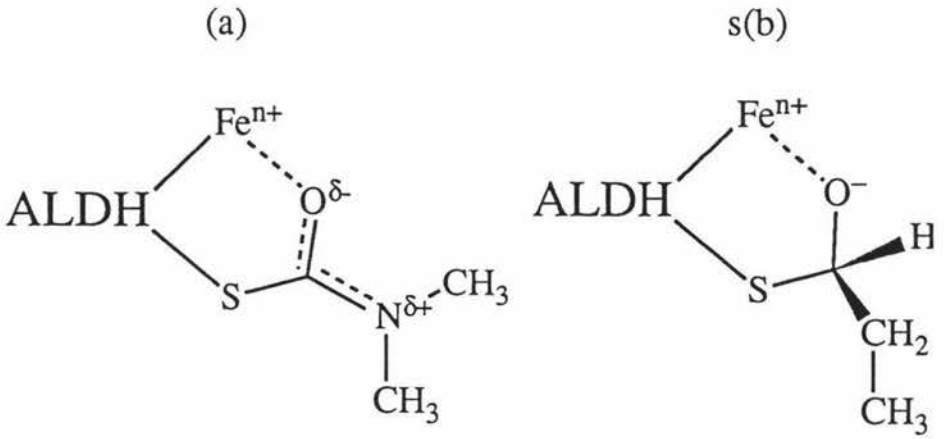

Kitson (1989) found that this ALDH-acyl species had dramatically increased NADH fluorescence (when excited at 366 nm) and decreased NADH dissociation. These effects were further amplified by the

presence of 10 mM Mg^{2+}. A comparison of the properties of ALDH in the presence of propanal (2 mM) and Mg^{2+}, and p-nitrophenyl dimethylcarbamate modified ALDH are shown in Table 4.4.4.1.

Since propanal and p-nitrophenyl dimethylcarbamate are both known to react with cysteine 302 then it is reasonable that they might induce changes to the equilibrium shown in Figure 4.4.3.1 between the E^{NADH} species in a similar manner. Both acylation with p-nitrophenyl dimethyl carbamate and thiohemiacetal formation on the pathway for propanal oxidation encourage binding of NADH in the 364 nm orientation. At higher concentrations of propanal (up to 100 mM) there appear to be addition effects which can not merely be associated with propanal binding to the active site. Dickinson and Hart (1985) have proposed that the binding of this second propanal molecule dramatically increases the rate of NADH dissociation from ALDH and hence results in an activation of the steady-state-rate.

Table 4.4.4.1 Correlation between ALDH-NADH-acyl and ALDH-NADH-aldehyde.

NADH	Fluorescence (420 - 435 nm)	Absorption (362 - 364 nm)	NADH Dissociation, K_D native ALDH, 1.1 μM
ALDH & Mg^{2+}	Increased [a]	Increased	Decreased [a] K_D 0.2 μM
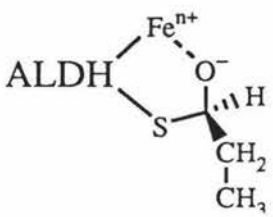	Increased [b]	Increased	———
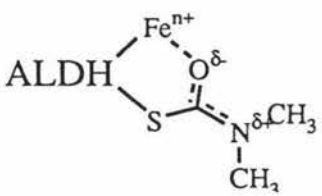	Increased [c]	———	Decreased [c] K_D 0.36 μM
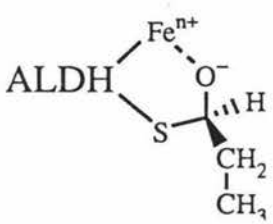 &Mg^{2+}	———	Increased further	———
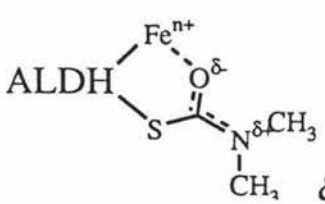 &Mg^{2+}	Increased [c] further	———	Decreased [c] further K_D 0.087 μM

a : Bennett (thesis)
b : Dickinson (1985)
c : Kitson (1989)

4.4.5 The 364 nm species in the kinetic pathway.

To determine the kinetic significance of the 364 nm species it is necessary to consider the pre-steady-state for the burst in production of NADH. Pre-steady-state data in theory can give information about a single turnover of the enzyme, particularly if the rate limiting step occurs late on the catalytic pathway.

Dickinson and Hart (1982) studied the pre-steady-state NADH burst in both absorbance and fluorescence (excitation 320-380 nm) when ALDH (5 mM, final concentration) was rapidly mixed with propanal (33 mM, final concentration) which had been pre-mixed with NAD (400 mM, final concentration). The initial burst in 340 nm absorption was followed by a lag in absorbance lasting about 300 ms (Figure 4.4.5.1). The burst in fluorescence was followed by a lag starting at about 280 ms and lasting about 800 - 1000 ms (Figure 4.4.5.2).

Dickinson and Hart (1982) commented that the change in the absorbance rate seemed to correspond to completion of the first transient in fluorescence. When these experiments were repeated this time with propanal and NAD pre-mixed, a slower burst in NADH absorption and fluorescence was observed.

Note, that when enzyme/propanal is mixed with NAD, the burst behaviour is identical to the experiments where enzyme is mixed with propanal/NAD (Dickinson and Hart, 1982).

Figure 4.4.5.1 NADH burst in absorbance (340 nm). In the upper trace enzyme/NAD was mixed with propanal. For the lower trace, enzyme was mixed with NAD/propanal.

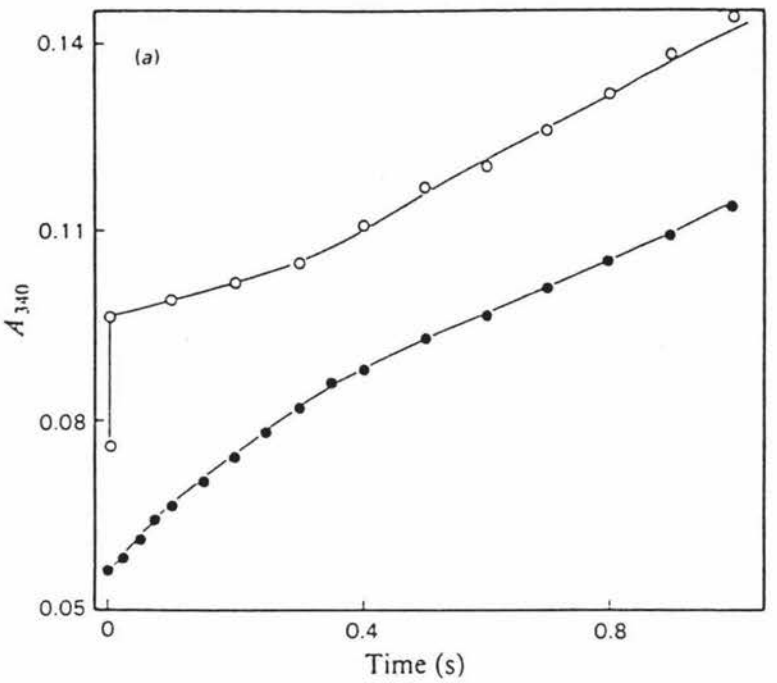

Figure 4.4.5.2 NADH burst in fluorescence (excitation 320 nm - 380 nm, detected at 430 nm). In the upper trace enzyme/NAD was mixed with propanal. For the lower trace, enzyme was mixed with NAD/propanal.

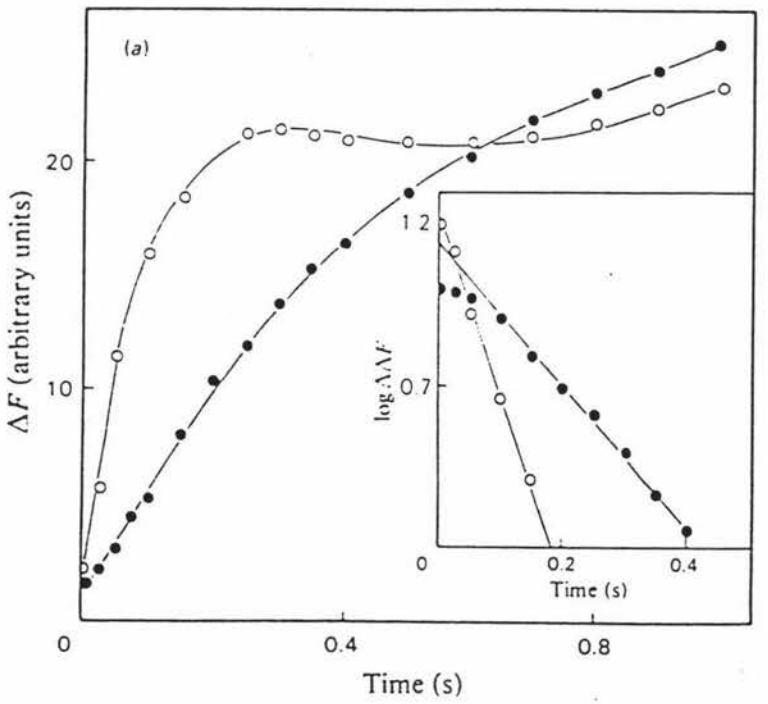

Dickinson and Hart commented that this experiment was too complex to allow a detailed interpretation, but such an interpretation will be attempted in this chapter.

Essentially the model which will be used is nearly identical to that commonly accepted for the pre-steady phase of the reaction, accept for when enzyme is not premixed with NAD. It is proposed that in the presence of propanal the NAD does not bind directly in a comformation in which hydride transfer can occur, but rather the NAD binds initially in an inactive conformation (a suggestion also made by Dickinson and Hart, 1982). The other difference is that rather than assuming that both of the E.NADH conformers have identical spectral properties advantage will be taken of the knowledge that conformers with different spectral properties do exist. At high aldehyde concentrations when NAD is premixed with enzyme the mechanism can be crudely represented by Scheme 4.4.5.1. Note not all of the aldehyde binding equilibria have been shown.

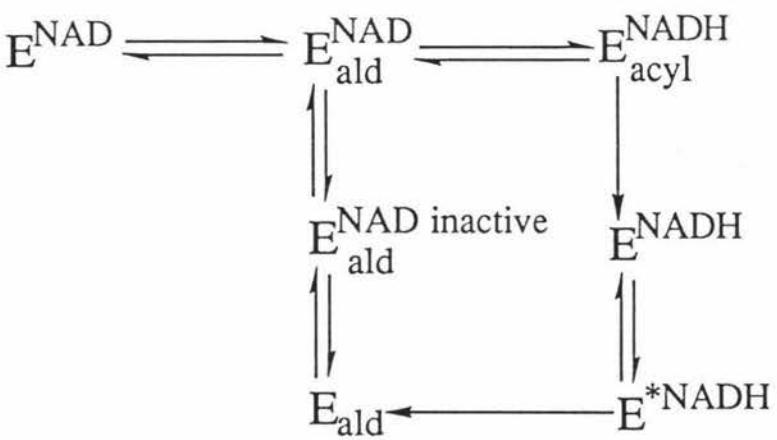

Scheme 4.4.5.1

The hypothesised model is as follows. After hydride transfer has occurred there is an initial 340 nm absorbance burst due to the production of NADH at the active site. After the NADH has formed at the active site the enzyme undergoes a conformational change and the NADH absorbs at 364 nm, in doing so there must also be a decrease in absorption at 340 nm because the 364 nm NADH species only has small absorption at 340 nm. Therefore a lag in the absorption increase (lasting

≈ 300 ms) can be accounted for by the a conformational rearrangement of the enzyme.

During this time (first 300 ms) the NADH fluorescence must still be increasing, since NADH bound in the inactive conformation fluorescence well. The increase in fluorescence can only continue until the ALDH-NADH has reached an equilibrium between the two conformations. Hence the change in the absorbance rates which Dickinson and Hart thought corresponded to completion of the first transient in fluorescence, can be rationalised in terms of the ALDH-NADH reaching equilibrium between the 340 nm and 364 nm absorbing forms.

It has been shown by Bennett (thesis) and Kitson (1989) that the fluorescence of NADH bound to ALDH is significantly enhanced (5.8 & 10.5 times, respectively). Therefore, if at 280 ms most of the ALDH is present with NADH bound then when the NADH dissociates from the enzyme the NADH fluorescence enhancement caused by the enzyme will be lost. If it is imagined that each enzyme can only turnover once, a substantial fluorescence decrease would occur when NADH dissociates from the enzyme. In the real situation, after the NADH has been lost into solution more NADH can form on the enzyme. However, on the second catalytic turnover the product NADH forms at a much slower rate since it is no longer in premixing conditions that were initially experienced. The result of this is because more NADH forms on the enzyme only a lag in fluorescence with a small decrease is observed.

For the purpose of simulating this model, the mechanism was simplified further to Scheme 4.4.5.2. while still maintaining the important features. NAD binding and subsequent isomerisation to the active form is controlled by a single rate constant (k_{12}). For the experiment where NAD is premixed with ALDH, all the enzyme is started in the X1 form. Conversely when NAD is not premixed with enzyme, all the enzyme is started in the X6 form.

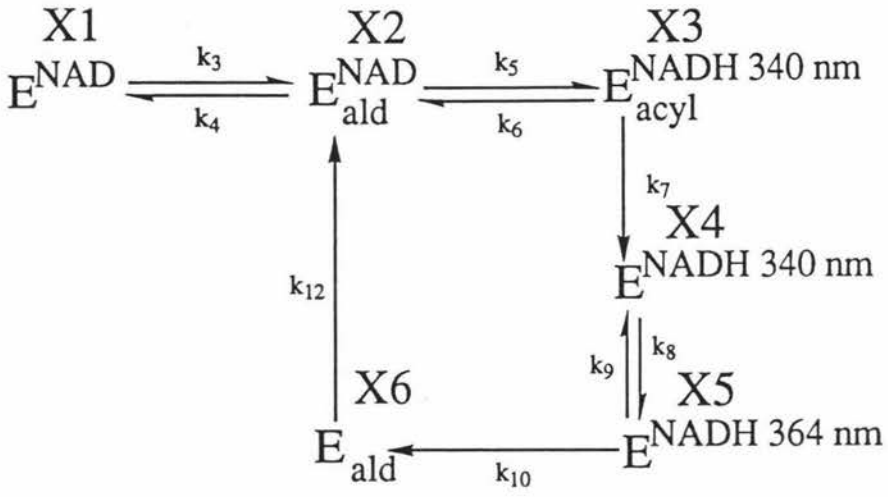

Scheme 4.4.5.2

Figure 4.4.5.3 and Figure 4.4.5.4 are the simulated bursts in absorbance and fluorescence respectively. The top trace in each corresponds to the experiment where NAD is pre-mixed with the enzyme, and the bottom trace in each represent the experiment where NAD is not pre-mixed with enzyme.

Figure 4.4.5.3 Simulated NADH burst in absorbance

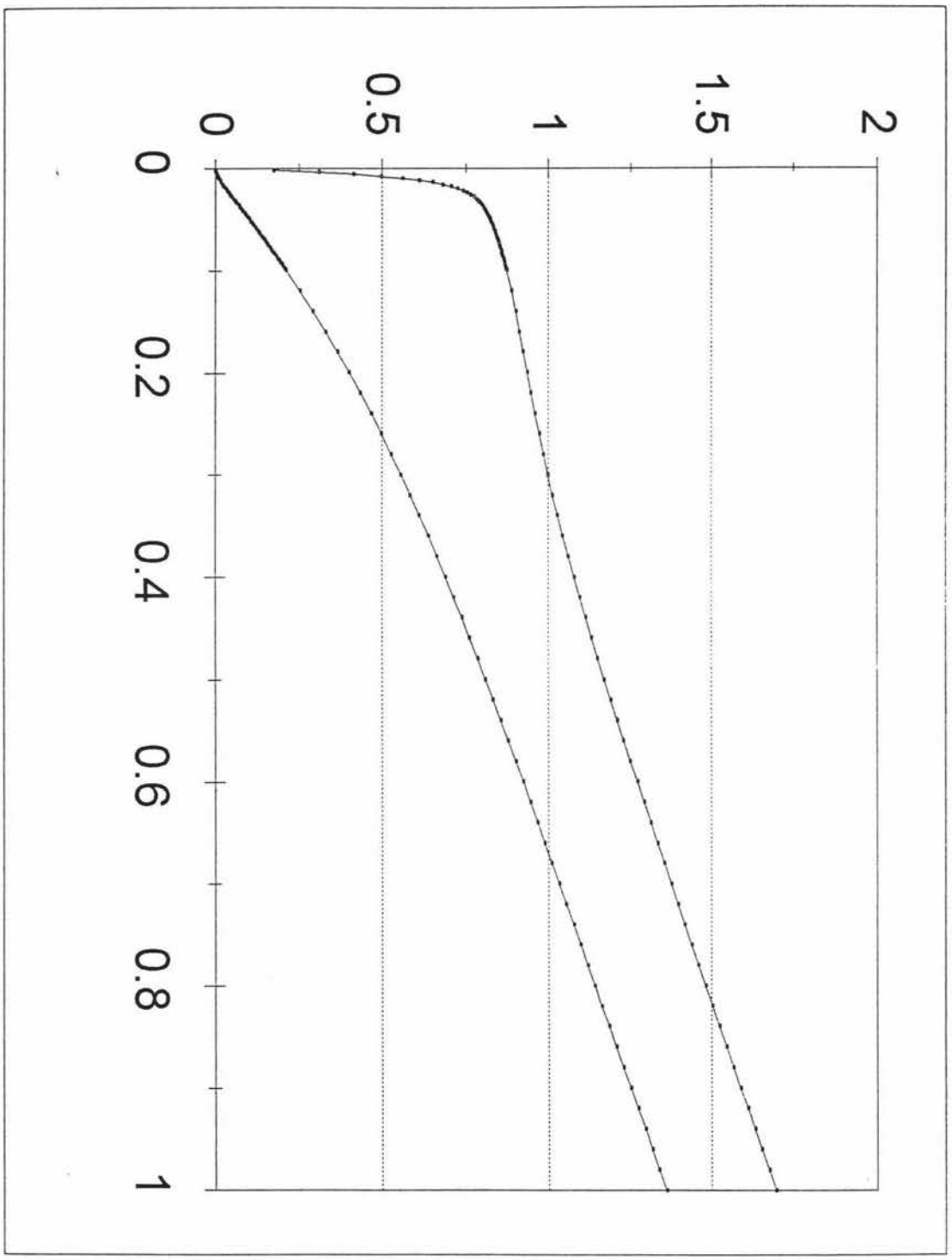

Figure 4.4.5.4 Simulated NADH burst in fluorescence

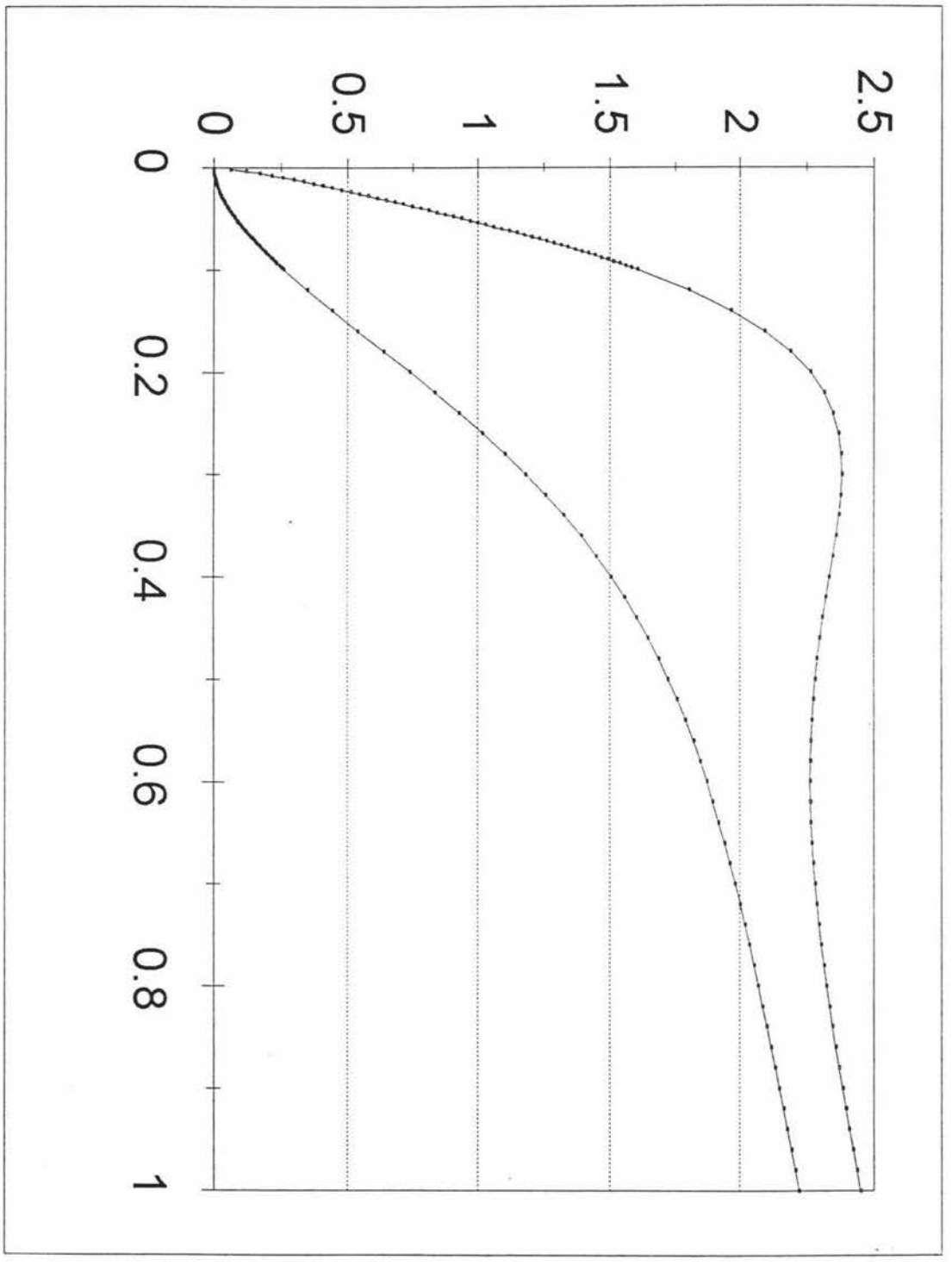

The parameters for the simulated bursts are shown in Table 4.4.5.1

Table 4.4.5.1 Parameters used for the NADH burst simulations

parameter	value
k3	1 $\mu M.s^{-1}$
k4	50 s^{-1}
k5	100 s^{-1}
k6	30 s^{-1}
k7	12 s^{-1}
k8	2.3 s^{-1}
k9	0.05 s^{-1}
k10	20 s^{-1}
k12	3.2 s^{-1}
A340 X3,X4,NADH	1
A^{340} X5	0.4
Fluorescence X3	0.5
Fluorescence X4	3
Fluorescence X5	20
Fluorescence NADH	1
	initial concentration
X1	0 μM, or 1 μM if NAD is premixed
X2,X3,X4,X5	0
X6	1 μM, or 0 μM if NAD is premixed

The features demonstrated in these simulations are as follows :

(1) For the simulation with NAD premixed with enzyme.
-a burst in 340 nm absorbance
-a burst in fluorescence which is slower than the burst in 340 nm absorbance

-a lag in 340 nm absorbance lasting ≈ 300 ms
-an apparent correlation between change in the absorbance rate and the completion of the first transient in fluorescence.
-a lag (with a slight decrease) in the fluorescence starting at about 280 ms, reaching a local minimum at 600 ms, and lasting 800 - 1000 ms.

(2) For the simulation with NAD not premixed with enzyme.
-Slower burst in absorbance with an amplitude of only 0.3 M of NADH per mol of enzyme, reaching the steady-state after 800-1000 ms
-Slower burst in fluorescence reaching the steady-state after approximately 400 ms

The simulated traces, while not exactly identical to the experimental, well demonstrate the principle of the model, and the usefulness in terms of fitting a wide range of experimental conditions of not assuming that all of the E^{NADH} species have identical spectral properties.

The simulated data does not predict that the fluorescence of the enzyme/NAD premixed experiment be less than the unpremixed data at 1000 ms. It is likely that this is due to experimental error for two reasons. (1) that when these same experiments are repeated using 40 μM propanal, this behaviour was not observed (Hart & Dickinson, 1982). (2) that if in the experiment where NAD is not pre-mixed with ALDH the production of NADH was less rapid, then it is very unlikely that at 1000 ms there apparently is more NADH present.

It has been assumed that in the experimental absorbance burst (when NAD premixed with ALDH) that the initial burst was so rapid that much of it occurs during the mixing time, causing an apparent reduction in the observed burst amplitude, (however if this assumption is incorrect see section 4.4.7)

A feature which became apparent while simulating the NAD pre-mixed reaction conditions was that the E.NADH.ACYL (340 nm) species must have poor fluorescence compared to the E.NADH (340 nm) species otherwise a rapid increase is observed in fluorescence trace is observed corresponding to the rapid formation of NADH.

It is seldom that in presteady-state kinetics that experiments are designed that reveal so many changes in the presteady-state. I would therefore like to congradulate Dickinson and Hart for their fine experimental work which well demonstrates the usefulness of presteady-state studies.

4.4.6 Effect of the acyl species on the absorption and fluorescence lag phases.

Dickinson and Hart (1984) studied the pre-steady-state NADH burst in both absorbance and fluorescence when enzyme/NAD was mixed with *trans*-cinnamaldehyde (20 mM, final concentration), and compared the with the data they obtained using 33 mM propanal, Dickinson and Hart (1982).

Unfortunately the lag phase in absorbance also had a contribution from the decrease in absorption due to hydrolysis of the ALDH-*trans*-cinnamoyl cysteine moiety, which also absorbs at approximately 340 nm. Hence the lag phase in absorbance for the burst using *trans*-cinnamaldehyde as a substrate can not be directly compared with the lag phase in absorbance for the burst using propanal as a substrate.

It is possible that the fluorescence data might be useful, but that depends vastly on the fluorescent properties of the ALDH-*trans*-cinnamoyl cysteine moiety, which are unknown. Dickinson and Hart (1984) observed a lag in fluorescence when using cinnamaldehyde as a substrate that lasted about 20 s, though the lag did not appear so dramatic as their earlier work using propanal.

Because the increased lag in fluorescence appeared to correlate with increased acyl stability, Dickinson and Hart (1984) describe the lag in fluorescence as being due to hydrolysis of the acyl species relieving a severe quenching effect caused by the presence of the acyl species. The likelihood of fluorescence quenching by the acyl species has been validated by the simulations in this chapter. However, Hart and Dickinson are attributing a very much later part of the fluorescence burst as being due to this acyl quenching, which is incorrect for a very good reason.

As the acyl species is produced at exactly the same time as the NADH, presumably 'quenching' occurs when the NADH is formed on the enzyme. If this is true, then for the fluorescence burst using propanal (NAD/enzyme pre-mixed, Figure 4.4.5.2), a local maximum at 300 ms with a local minimum following at about 600 ms can not occur. This is because at 300 ms there should be more of the unhydrolysed acyl species still present quenching the fluorescence than at 600 ms. Therefore Dickinson and Harts conclusions on this matter are inconsistent with their experimental work, but their observations of the correlation between the stability of the acyl species and the apparent fluorescent lag time may still be true.

It has been proposed in section 4.4.5 that the fluorescent lag phase is simply due to loss of fluorescent enhancement when NADH dissociates from the enzyme. Kitson (1989) demonstrated for the stable acyl enzyme generated by reaction with p-nitrophenyl dimethylcarbamate, that the dissociation constant was markedly decreased (K_D 0.36 μM) relative to the native enzyme (K_D 1.1 μM, Bennett thesis). Also more importantly, the rate of NADH displacement from the enzyme with NAD was greater reduced by 1-2 orders of magnitude. If this is also true for other acyl enzymes, then after formation of the NADH, the NADH dissociation from the enzyme might be inhibited by the presence of enzyme acyl species. Hence, for more stable acyl enzyme species such as the ALDH-cinnamoyl acyl species, the NADH will dissociate from the enzyme more slowly. Thus the fluorescence lag will occur over a longer time. Also, the time dependent contribution of the decrease in fluorescence (due to NADH dissociation) of the total fluorescent changes will be less, hence, the observed lag will be less dramatic.

This explanation requires that the 364 nm E^{NADH} species does not experience fluorescence quenching from the acyl species. The validity of this assumption must be considered. MacGibbon et al (1978) proposed a sequential model (see Figure 4.1.1.1) where NADH is formed in one enzyme conformer and then the E^{*NADH} species undergoes a conformational rearrangement forming another conformationaly different ENADH species before dissociating fully from the enzyme.

The simulations in section 4.4.5 indicate agreement with this mechanism. Note however, that only the first E^{*NADH} species is in a conformation (orientation) where hydride transfer can occur. For hydride transfer to occur in forming the E^{*NADH} species, the nicotinamide ring of NAD must be approximately 2 Å away from the thiohemiacetal (bound aldehyde). The same is also true for the reverse hydride transfer process. Hence, it can be understood that for the E^{*NADH} species, the NADH must be environmentally very close to the acyl species. Because the fluorescence of a chromophore is very sensitive to its environment, it is no surprise that the fluorescence of the E^{*NADH} species is quenched.

However, when NADH is present in the E^{NADH} conformer (i.e. the 364 nm species) hydride transfer does not occur, hence the NADH species must be environmentally more distant from the acyl species. In addition to this the red-shifted spectrum of the E^{NADH} species suggests that the nicotinamide ring of the E^{NADH} species is orientated differently from the E^{*NADH} species so that an electrophile is complexed (possibly hydrogen bonding) to the amide oxygen. Thus, because the acyl species is environmentally separated from the NADH (of the E^{NADH} species), it is reasonable to suggest that acyl quenching will not occur.

4.4.7 Relationship between decreased amplitudes and the observed rate.

In enzyme kinetics it is common to observe decreased amplitudes for processes. This can occur in five ways:

(1) The spectral properties of the observed species have changed in such a way that a decrease in sensitivity is observed. In this situation the observed burst rate will still be the same.
(2) The reverse reaction of the formation of the observed species is rapid enough so that reaction does not go to completion. In this situation the observed rate is more rapid than the rate constant governing formation of the observed species, and is equal to the sum of the forward and reverse rates.
(3) Some of the enzyme can become involved in a dead end complex, reducing the active site concentration of the enzyme species and hence

reducing the observed burst. In this situation the observed rate is also more rapid than the real rate. Since this appears to not be commonly understood by enzyme kineticists a example will be given. Consider a very simple model for the oxidation of aldehydes by ALDH. NAD is premixed with ALDH and then mixed with saturating aldehyde (the formation of NADH is being observed). In this model there is a dead-end complex which is also formed and for simplicity no reverse reactions are considered. Hence the example can be represented by Figure 4.4.7.1.

Figure 4.4.7.1 Reduced amplitude through formation of a dead end complex.

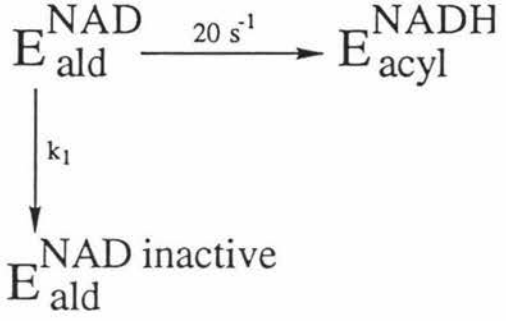

When k1 is set equal to 0 s^{-1} the observed rate constant is 20 s^{-1} and the amplitude is 100%, as expected. However when k_1= 47 s^{-1}, the observed rate constant is 67 s^{-1} and the amplitude is 30% (see Figure 4.4.7.2). So in this example also, the observed rate is equal to sum of the two rates constants.

observed rate = 20 s^{-1} + 47 s-1
= 67 s^{-1}

The simulations for this are shown in Figure 4.4.7.2

Figure 4.4.7.2 Simulated reduced amplitude through formation of a dead end complex.

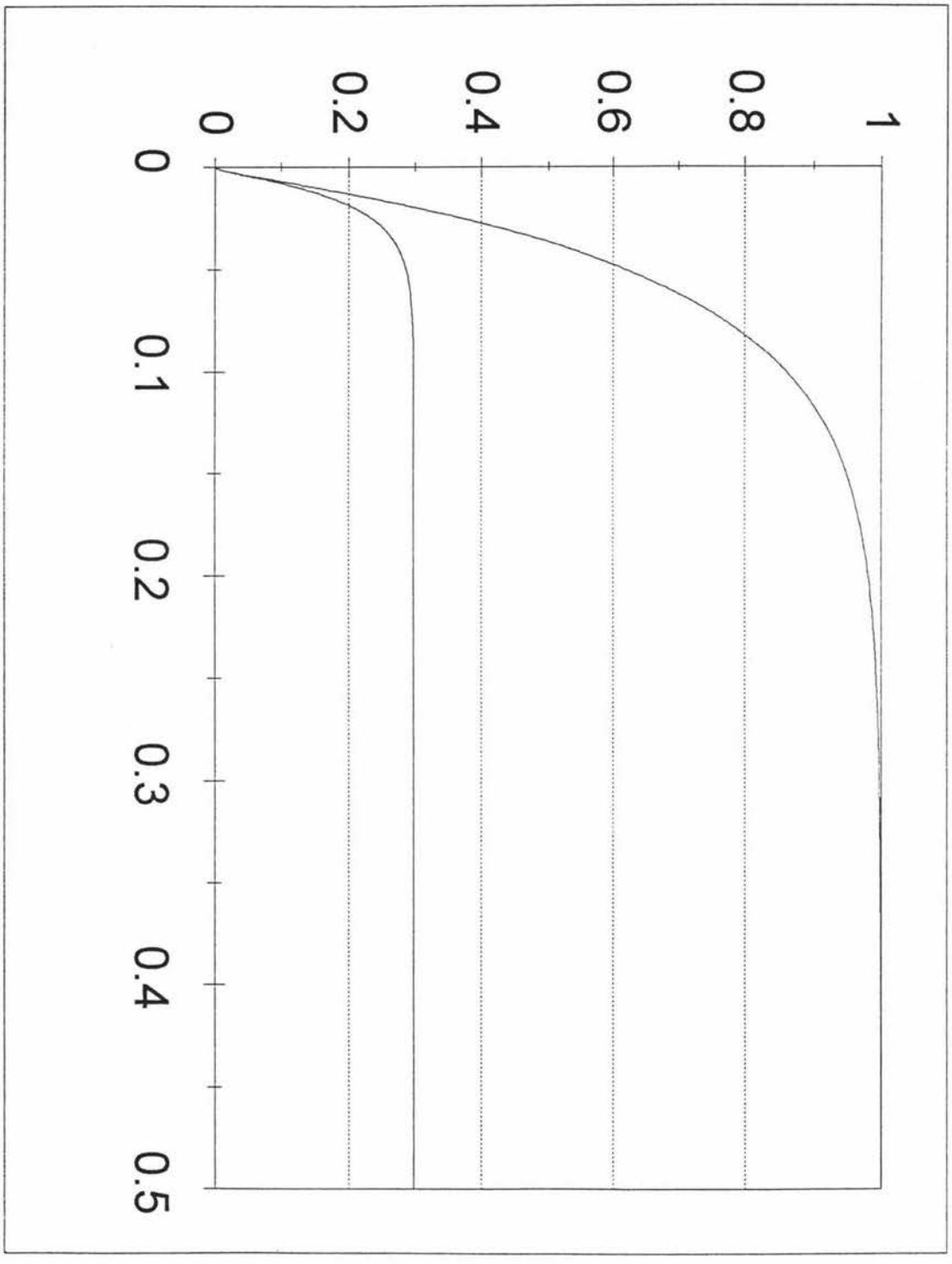

(4) A rate governing the formation of the observed species is partly rate limiting. In the extreme situation where the formation of the observed species is rate limiting, no burst amplitude will be observed, only a steady-state. However when this rate of formation of the observed species is only partly rate limiting, reduced amplitude is observed and the rate of the process is again slower than the observed rate.

(5) A reaction that is so rapid that a significant amount occurred during the mixing time of the stopped-flow spectrometer. Hence only the later part of the change is recorded by the spectrometer, giving the appearance of a reduced amplitude for the process.

It had been assumed earlier (section 4.4.5), regarding the pre-steady-state data by Dickinson and Hart (with enzyme/NAD premixed and observing absorbance at 340 nm) that the observed reduced amplitude was due to much of the burst taking place during the mixing time. A dominating feature for rejecting the possibility that for both the enzyme/NAD premixed experiment and the unpremixed experiment the amplitudes were identical, is that Dickinson and Hart's data for the same experiment only at lower propanal concentrations (40 μM) exhibited much smaller amplitude for the unpremixed experiment than the enzyme/NAD premixed experiment. The possibility that at one concentration of propanal (40 μM) the amplitude is very much reduced by not premixing with the enzyme with NAD, and at a higher concentrations of propanal (33 mM) the amplitudes are both identically reduced would appear mechanisticaly irreconcilable. Only non-identical reduced amplitudes for 33 mM propanal experimental are mechanistically acceptable. Furthermore Hart and Dickinson (1982) were uncertain of the exact active site concentration (they only knew the enzyme concentration) used in their experimental work, making it impossible to know what the exact amplitudes are.

Despite all these uncertainties, it is in principle possible to account for this pre-steady-state data by allowing the possibility of spectrally non-identical E.NADH species.

4.4.8 Explanation for the difference results observed by the two research groups.

In the past there have been a number of differences in the experimental observations of the two main research groups studying sheep liver cytosolic ALDH. How some of these problems arise will be illustrated with an example of one of the observational difference. MacGibbon (thesis, 1976) did a study on the burst dependence on propanal concentration in fluorescence. MacGibbon's results showed a clear hyperbolic dependence on the aldehyde concentration with a V_{max} of 11 s^{-1}. However when this was repeated by Dickinson, less dependence on the propanal concentration was observed Also the apparent maximum rate was $\approx$ 4 s^{-1}. When he studied the same experiment in absorbance he observed a linear dependence on the propanal concentration, with an observed rate at 10 mM of about 70 s^{-1}.

To understand this difference it is necessary to again consider the spectral properties of the E^{NADH} species which were being monitored. The most rapid burst observed was in absorbance, with the second most rapid being in fluorescence by the Massey group, and the slowest burst was by the Hull group using fluorescence. To explain this behaviour it was hypothesised that slower bursts in fluorescence could be attributed to species further down the mechanistic pathway, with the fluorescence burst by the Hull group being even further down the pathway than the Massey group.

From the simulations of the model proposed it was evident, that was an initial burst in 340 nm absorbance which was controlled by hydride transfer. The initial burst in fluorescence however was more controlled by acyl enzyme hydrolysis. Further down the mechanism still was a more fluorescent species which had a maximum absorption of $\approx$ 364 nm, controlled by an isomerisation step.

It seemed likely that the Hull group were observing a fluorescence burst that was mainly dominated by the formation of the more fluorescent 364 nm species, and hence were probable exciting at a longer wavelength than the Massey group who excite at 340 nm. On inquiry

Mark Dickinson confirmed that the excitation wavelength that was used at Hull was in fact a broad band of excitation wavelengths from 320 nm to 380 nm. Clearly this would excite both the 340 nm species and the more fluorescent 364 nm species, and could easily lead to an apparent difference in the observed rates.

Another experimental difference that generally exists between the two groups is the use of EDTA in the preparation buffers. Bennett (thesis) reports decreased fluorescence of the ALDH.NADH species in buffers containing EDTA. This raises a number of questions such as: Do both of the E^{NADH} species have proportionally the same decrease in their fluorescence properties, or does one species decrease in it's fluorescence more than the other? Alternatively, can the decreased fluorescence be due some perturbation of the equilibrium constants between the two species? Or is the decreased fluorescence due to the removal of metal ions which are bound to the enzyme, hence reducing the fluorescence enhancement induced by such metal ions ?

Obviously more experimental is required to gain understanding of all the implications of modifying ALDH with EDTA. Experimental differences such as different excitation wavelengths or the use metal ion chelators should not be shunned because in doing so they often provide a fresh perspective from which to gain understanding. However they should be accompanied with control experiments so that any differences may be properly exploited. Another important feature is that if a different parameter (such as excitation wavelength) is used then it should be reported so that the exact differences may be understood by all. Measures such as this would greatly improve the understanding of the kinetics of ALDH, providing the links that would allow the puzzle to be solved.

4.4.9 Effects of pyrophosphate on activity of ALDH

The activity of ALDH has been shown to be increased in pyrophosphate buffers (Motion, thesis). Since pyrophosphate (and structural variants) occur naturally in the liver, it is of interest to understand how the reputed activation of the steady-state occurs. Two theories can be proposed to account for this behaviour:

1, The enzyme has been chemically modified by the pyrophosphate producing a more active enzyme
2, The pyrophosphate binds on the enzyme at a site which activates the enzyme.

It was hypothesised that pyrophosphate binding to the enzyme in some site was a more reasonable explanation. To investigate the hypothesis that pyrophosphate was binding to a site on the enzyme without chemically modifying the enzyme, it was decided to study the activity of ALDH as a function of pyrophosphate concentration. The results of this study are shown in Figure 4.4.9.1.

Figure 4.4.9.1 Pyrophosphate activation of the steady-state

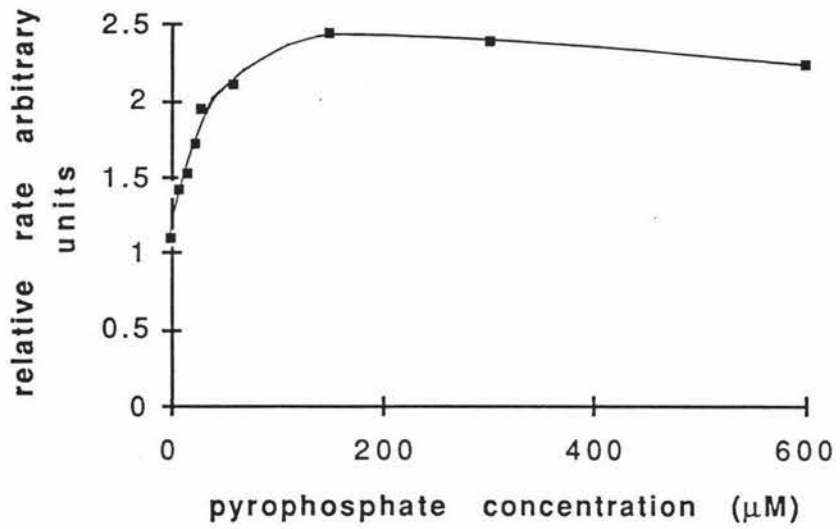

The results show a saturating binding curve supporting the hypothesis that pyrophosphate binds to the ALDH in a site which causes activation of the steady-state rate. To Motion (thesis) has shown from stopped-flow studies that the activation is primarily due to an increase in the rate of NADH dissociation from the enzyme.

The question then becomes, how does pyrophosphate increase the rate of NADH dissociation? To address this question arguments will be presented that attribute the observed activation, to pryrophosphate (Figure 4.4.9.2 (2)) binding in the ALDH coenzyme-pryrophosphate (Figure 4.4.9.2 (1)) binding site.

Figure 4.4.9.2

(1) Pyrophosphate of the coenzymes NADH and NAD at pH 9.3

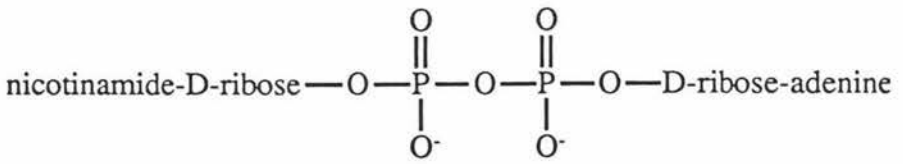

(2) Pyrophosphate at pH 9.3

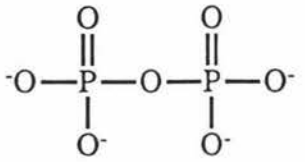

Many enzymes bind the coenzymes NAD and NADH through the coenzyme-pyrophosphate. This is because the coenzyme-pyrophosphate has two negative charges in close proximity which can bind to an electrophile to form a complex. For example, in the glyceraldehyde 3-phosphate dehydrogenase the coenzyme-pyrophosphate is bound to three amide hydrogens on the enzyme (Biesecker et al., 1977) (Figure 2.4.8.3).

If pyrophosphate binds in the NADH-pyrophosphate binding site, this prevents the NADH from being properly bound, and therefore the NADH dissociates from the enzyme more easily. The result of this is that the steady-state is activated in the presence of pyrophosphate. The difference spectra of the ALDH bound NADH in the presence of pyrophosphate buffer (pH 9.0) showed a dramatic decrease in the absorption of the 364 nm compared to borate buffer (pH 9.0), indicating a change in the equilibrium between the two conformers in favour of the 340 nm species.

4.4.10. Steady-state kinetics.

The steady-state kinetics of ALDH where studied at pH 5.22 using variable NAD and variable propanal. The results are summarised in Figure 4.4.10.1.

Figure 4.4.10.1 Steady-state data for ALDH at pH 5.22

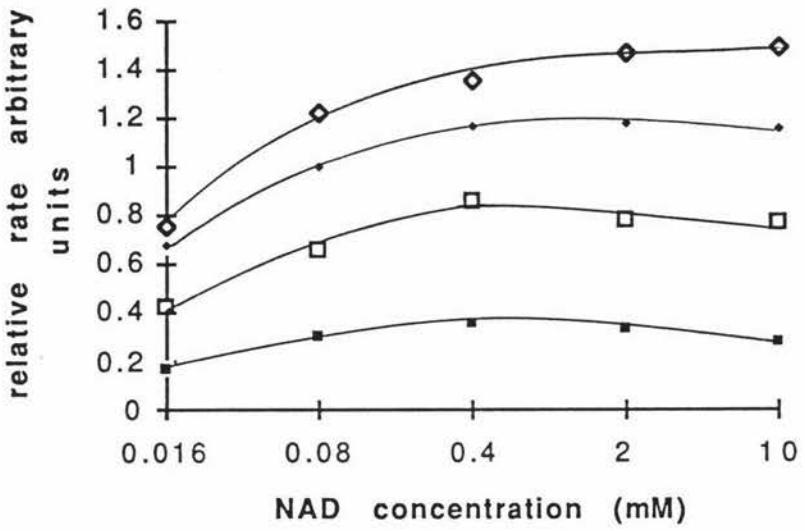

The propanal concentrations used in Figure where (■) 0.4 mM, (□) 2 mM, (◆) 10 mM and (◇) 50 mM

A striking feature of these is that at medium aldehyde concentrations (0.4 - 10 mM) the steady-state activity was first activated by NAD then at higher concentrations inhibited. While the activation of steady-state rate by NAD is expected (since NAD is a substrate of the reaction) inhibition of the steady-state by higher concentrations of NAD is not expected, but this does typify the behaviour of ALDH. For example Bennett (thesis) has shown that low concentrations of NAD activate the esterase reaction with 4-nitrophenyl ethanoate, but higher concentrations of NAD cause inhibition again. In both these situations it would appear that a minimum of two NAD binding sites are required to explain this behaviour.

For high concentrations of propanal (50 mM) inhibitory effects of high concentrations of NAD are not observed. Dickinson and Hart (1982) showed with steady-state data at pH 7.0, that at low NAD concentrations, propanal activates the ALDH activity at low propanal concentrations and inhibits the enzyme at higher propanal concentrations. When both substrates were present in high concentrations activation was observed. Hence, high concentrations of either substrate can be inhibitory if the other substrate is not present also.

4.5 Conclusion

The allocation of the different spectral properties of the ALDH bound NADH is consistent with the experimental results, although a more thorough investigation is recommended to a best exploit any potential differences in the spectral properties the ALDH-NADH species.

Chapter 5

Synthesis of a sensitive substrate for use in homogeneous enzyme immunoassays

5.1. Introduction

In the past much of the skill of the analytical chemist has been employed measuring atomic and simple molecular quantities. For the determination of atomic composition, the analytical chemist has met this challenge exceedingly well, with the introduction of atomic absorption, inductively coupled plasma, mass spectrometry etc. With these and many other techniques the analytical chemist can measure atomic composition even at very low levels with a high degree of accuracy.

There is now an increasing demand for rapid inexpensive methods for measuring quantities of specific molecules present in foodstuffs, bodyfluids etc. with very high accuracy. This poses a problem in that separation of specific trace organics from complex molecular soups using techniques such as chromatography are often very difficult, expensive, and above all time consuming.

Immunoassays were first developed in the late 1950's (Yalow and Berson, 1959) and since then the field has been expanding extremely quickly. There are now many different types of immunoassay systems used to detect a broad range of analytes. All immunoassay systems have one fundamental feature; that they all make use of the vertebrate immune system to produce macromolecules (antibodies) which specifically bind a particular molecule (antigen or hapten which is usually the analyte).

Of the enzyme immunoassay techniques which have been designed, homogenous enzyme immunoassay (EIA) is the most easy and rapid to use, but it is the most difficult to design. This is because homogenous EIA relies on the inhibition of the enzyme activity which results when

the antibody binds to the enzyme -hapten conjugates (Rubenstein et al., 1972) as shown in scheme 5.1.1.1 (A). Free hapten (or antigen) competes with the enzyme-hapten for a limited number of antibody binding sites. Therefore the more hapten present from a sample being analysed, the greater the observed enzyme activity will be (see scheme 5.1.1.1 (B)). No separation steps are required, hence the simplicity of the procedure makes it suitable for do it yourself technologies.

Figure 5.1.1.1 The principle of homogeneous enzyme immunoassays

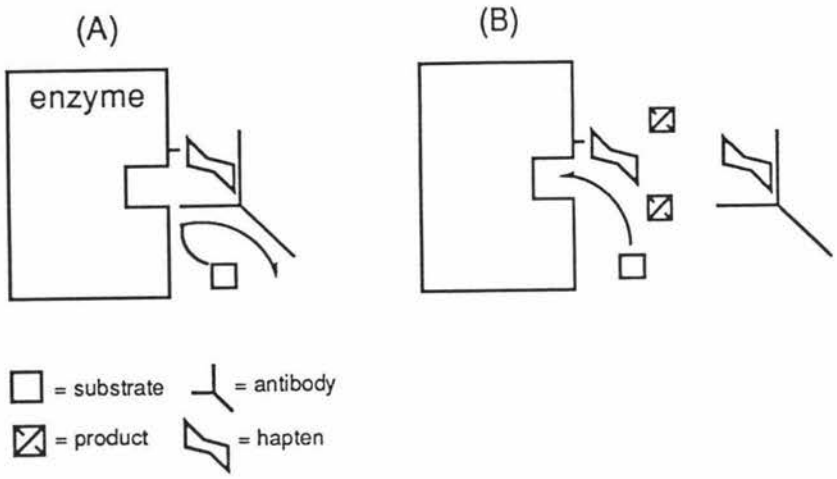

These assays are very simple and often rapid, taking only 2 - 5 minutes. Homogeneous EIA was first employed by Syva Co. in America (Rubenstein et al., 1972) using lysozyme as the enzyme for the detection of morphine metabolites in urine. Several other enzymes have also been used including β-galactosidase, β-glucuronidase and malate dehydrogenase.

The requirement that the anti-hapten (antibody) must inhibit the enzyme activity is a demanding challenge. Of the homogenous EIA systems designed, the assays utilising lysozyme have given the greatest degree of inhibition by the antibodies (which bind to the conjugated hapten).

Homogenous EIA have been used for the home monitoring of estrone glucuronide and pregnanediol glucuronide concentrations in daily urine samples of woman (Brown et al., 1989). A woman can determine from this information when her fertile period is occurring. In this system the enzyme (lysozyme) activity is very effectively inhibited by the anti-hapten (antibody) (≈ 97 %). A significant feature of this assay is that the substrate is a suspension of micrococcus cells, which of course are very large and hence easy to occlude from the active site.

At present one of the most significant disadvantages of homogeneous EIA is that they are less sensitive than their counterparts utilising phase separation (non-homogeneous EIA). For some applications decreased sensitivity is not important because of high analyte concentrations, an example of this is in the measurement of pregnanediol glucuronide in urine (Brown et al., 1989). This is an assay developed in Melbourne, which has sufficient sensitivity after only 5 minutes reaction, with the required precision. However, other applications for which increased sensitivity is required such as the accurate determination of estrone glucuronide either have assay times which are long, or do not have the required precision.

The major reason why homogenous EIA have decreased sensitivity is because the enzymes being used are not as active as the non-homogeneous alternatives or they do not catalyse an easily detectable reaction without the use of expensive equipment. Ideally to compete favourably with the non-homogeneous EIA systems designed the homogeneous enzyme system should have high catalytic turnover and catalyse a reaction which is easily detectable.

5.1.2 Desirable features when designing a substrate for a homogeneous EIA

The following factors need to be considered when designing a substrate enzyme system suitable for use in a home assay.

a. The reaction on the substrate must be catalysable by many enzymes to optimise the chances of finding an enzyme for which the anti-hapten (antibody) has good inhibition properties.

b. The reaction on the substrate must be detectable using absorption. Reactions which are detectable by fluorescence can only be followed in solution and require expensive equipment to follow the reaction. Luminescent reactions are catalysed by a very limited number of enzymes. It is also very difficult to design a molecule that will undergo a luminescent reaction.

c. The substrate must undergo a very sensitive colour change on catalysis with the enzyme i.e. the change in extinction coefficient must be very high.

d. The colour change must be detectable in the visible region so that the system may be mounted on a paper strip similar to those used for the detection of blood sugar in diabetics.

e. Ideally the visible change should be from one colour to another colour, rather than coloured to colourless (and vice versa). This feature is important if the system is to have the versatility of being detectable by the human eye and well as by machine. For those who are not colour-blind, the human eye is more capable of detecting colour changes, than detecting different intensities of the same colour.

f. The substrate must be very reactive so that a high catalytic turnover can be achieved.

g. The substrate must be stable under the conditions required and have a very low non-catalytic reaction rate. This is a difficult requirement because often highly coloured molecules have poor aqueous stability and are light sensitive. The substrate must be stable to long term storage on a solid phase such as a paper strip.

h. The substrate should be bulky to optimise the chances of the anti-hapten (antibody) precluding access to the active site. A disadvantage of having a bulky substrate is that the potential number of enzymes that can catalyse a reaction is reduced if the substrate becomes too bulky to allow easy access to the active site.

i The substrate must have good solubility. Many large highly conjugated organic molecules have poor solubility in aqueous solutions.

j. The substrate must be non-toxic if possible so that it could used with complete safety by the general public.

k. The substrate must be synthesisable. It is easy to design molecules which should have desirable properties, but it is another matter to be able to synthesis them in sufficient quantities at a suitable price.

5.2 Materials

Porcine and rabbit esterase's were bought commercially from Sigma chemical company. Phenol and 4,4-bis(dimethylamino) benzophenone were purchased from May & Baker and Aldrich respectively. All other chemicals were as outlined in sections 1.2 and 3.2.

5.3 Methods

5.3.1 Synthesis of 4-((bis 4-N,N-dimethylaminophenyl) methylinium ethanoate) phenol

The mechanistic scheme for the synthesis of 4-((bis 4-N,N-dimethylaminophenyl) methylinium ethanoate) phenol from 4,4-bis(dimethylamino) benzophenone and phenol is shown in Scheme 5.3.1.1. Zinc (II) is required as a Lewis acid because the carbonyl carbon of 4,4-bis (dimethylamino) benzophenone is very deactivated by the two N,N-dimethylaminobenzene rings.

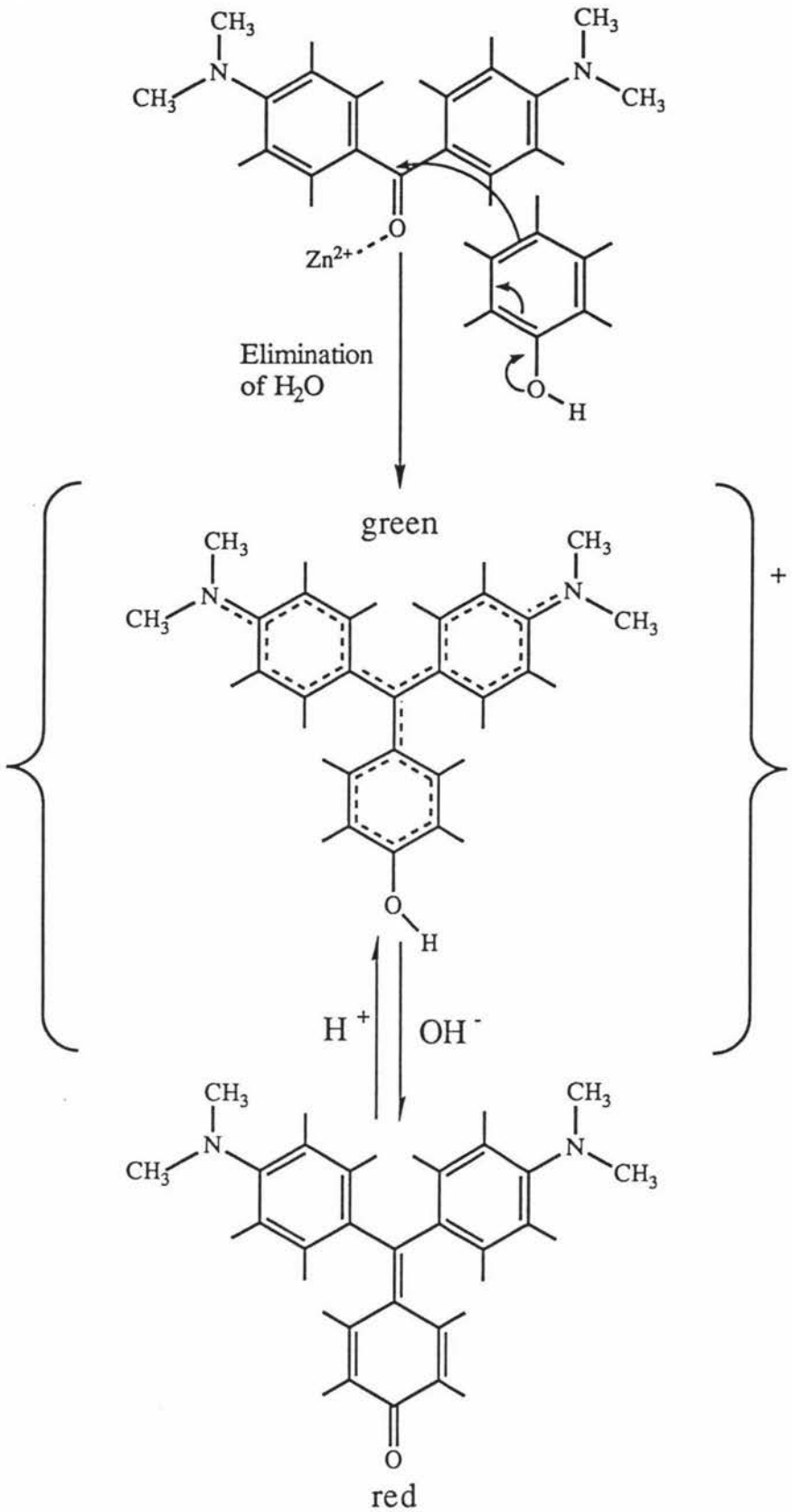
CH3
N
CH3
CH3
N
CH3
O
Zn2+
Elimination
of H2O
O
H
green
CH3
N
CH3
CH3
N
CH3
+
O
H
H +
OH -
CH3
N
CH3
CH3
N
CH3
O
red

Scheme 5.3.1.1

In a 10 ml round bottomed flask, was placed 0.3 g of 4,4-bis (dimethylamino) benzophenone, 1.0 g of phenol and 1.5 g of zinc chloride. A reflux condenser was fitted and the mixture was heated until the phenol had completely melted (m.p. 41 C). H_2SO_4 (100 µl) was then added with stirring. The whole mixture was heated with stirring at 90 C for 3 hours and the solution gradually became a deep red colour. After allowing the mixture to cool the viscous material was tranferred to a 150 ml flask by washing with acetone. Ammonium hydroxide was added dropwise until the solution became green (see Scheme 5.3.1.1, green species) and the mixture was then tranferred to a 1 litre beaker and 300 ml of water was added. The acetone was boiled off and chloroform (200 ml) was added and stirred vigorously to extract the product.

The chloroform was removed and the extraction was repeated. The combined chloroform extract was red in colour (see Scheme 5.3.1.1, red species). The chloroform was removed using a rotary-evaporator. The residue was then redissolved in the minimum quantity of ethyl acetate, and loaded on to a silica column. The column was then washed with ethyl acetate to remove the starting materials, as the product remained at the top of the column. The product was then eluted with 1:1 methanol / ethyl acetate and dried under vacuum. After redissolving in the minimum quantity of CCl_4 the product was loaded on to a $CaCO_3$ column and eluted with CCl_4. Some purple coloured material remained bound to the column. The eluent was rotary evaporated to dryness.

The name 4-((bis 4-N,N-dimethylaminophenyl) methylinium ethanoate) phenol (acronym **DMP**) refers to the green protonated species and the deprotonated **DMP** species will be referred to as **dDMP**.

5.3.2 Synthesis of 4-((bis 4-N,N-dimethylaminophenyl) methylinium ethanoate) phenyl ethanoate.

The synthetic scheme for the production of 4-((bis 4-N,N-dimethylaminophenyl) methylinium ethanoate) phenyl ethanoate (acronym **DMPE**) from dDMP is shown in Scheme 5.3.2.1

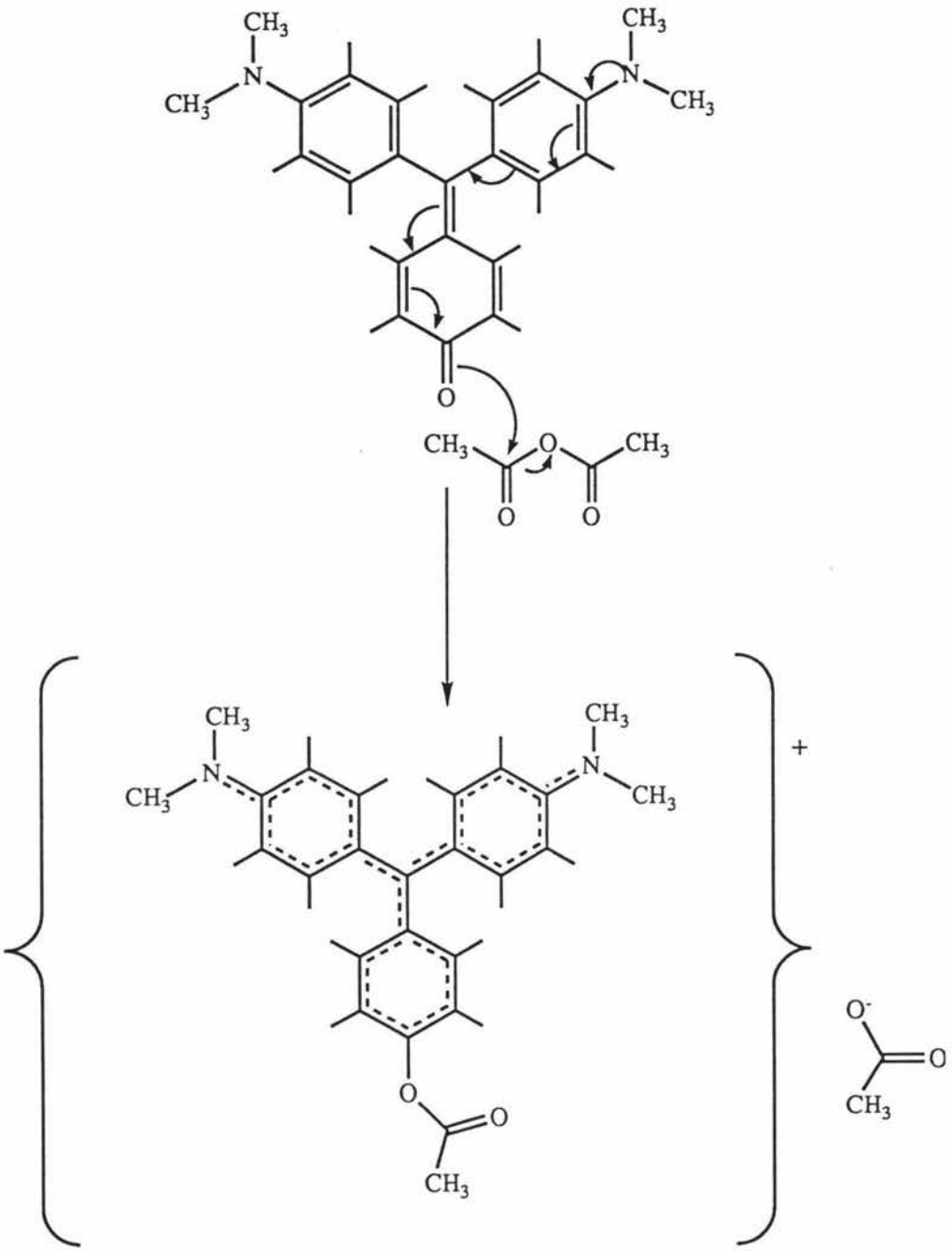

Scheme 5.3.2.1

The black-red solid dDMP was dissolved in 2 ml of acetic anhydride over a few minutes and the colour changed to black-green. After 30 minutes the acetic anhydride was removed using a vacuum line. Finding conditions to purify the product salt was difficult because of the polar nature of the salt. Eventually a carboxymethyl cellulose column was used. This column was used as a cation exchanger, since the product has a positive charge and hence has an affinity to the column. A column was

pre-equilibrated at pH 6.0 using 100 mM sodium acetate buffer and then washed with a 20 % solution of ethanol. A portion of the product was then loaded on to the column and then further washed with a 50 % solution of ethanol. This washed off a tiny amount of green coloured material which was identified spectrophotometrically as DMP. The product was then eluted using a 10 % solution of ethanol containing 1% of acetic acid.

5.2.3 Measurement of the rate of hydrolysis of DMPE with rabbit liver esterase and porcine liver esterase.

The activity of both porcine (15 nm, final) and rabbit (100 nm, final) esterase's was assayed using 30 μM DMPE (assuming $\varepsilon^{622} = 105000$, see Table 5.4.4.1) in 50 mM phosphate buffer, pH 7.4. The non-enzymatic hydrolysis rate was also recorded. The porcine esterase activity was also assayed using 30 μM DMPE in 50 mM pyrophosphate buffer pH 9.3. All of the assays were followed at the less sensitive wavelength of 428 nm so that the absorbances would be in a range which was less than one.

5.3.4 Measurement of the rate of hydrolysis of DMPE with ALDH

ALDH (4.3 nM final concentration) in 50 mM phosphate buffer (pH 7.4) was assayed with variable DMPE concentration using the (622,628) - (548,558) kinetics mode of the Hewlett Packhard diode array spectrometer (see section 3.2.2). The path length used was 4.1 mm. The ALDH used was predialysed against buffer to remove the mercaptoethanol.

5.3.5 Inhibition of the DMPE esterase reaction by ALDH 4-trans (N,N-dimethylamino) cinnamoyl - cysteine moiety.

Sodium phosphate buffer (0.8 ml, 50 mM, pH 7.4) was added to a 1ml quartz spectrometer cell. To this NAD (50 μl, 2 mM), DACA (50 μl, 2 mM), and ALDH(50 μl,80 nM) were added and allowed to react for 5 seconds.

4-((bis 4-N,N-dimethylaminophenyl) methylinium ethanoate) phenyl ethanoate (50 µl, 615 µM) was then mixed thoroughly and rapidly transferred to the spectrometer. After the addition of the ester (5 seconds) the absorbance at (500-520 nm) - (720-730 nm) was measured in the kinetics mode for 60 seconds. This was compared with a blank containing 0.85 ml buffer and no DACA.

5.4 Results and Discussion

5.4.1 Synthesis of dDMP

dDMP was produced in 67% yield as described in methods and characterised by its nmr spectrum in $CDCl_3$ (Figure 5.4.1.1) as follows: 3.12 ppm (12H, s, $-N(CH_3)_2$); 6.56 ppm (2H, d, J=9.52 Hz, quinone meta protons); 6.71 ppm (4H, d, J =8.79 Hz, ortho protons); 7.20 ppm (4H, d, J=8.79 Hz, meta protons); 7.35 ppm (2H, d, J=9.73 Hz, quinone ortho protons). The spectrum shows the $-N(CH_3)_2$ protons and the two sets of ortho protons and two sets of meta protons as expected from the structure shown in Scheme 5.3.1.1. The four meta protons in the two 4-N,N-dimethylaminophenyl rings are deshielded by the electron withdrawing effect of the quinoid ring carbonyl group as are the two ortho protons of the quinoid ring itself. These two ortho protons occur at the most deshielded position (7.35 ppm) as they are closest to the carbonyl group. On the other hand, the four ortho protons in the two 4-N,N-dimethylaminophenyl rings are each shielded by a single $-N(CH_3)_2$, but the two meta protons in the quinoid ring are even more shielded (6.56 ppm) since two $-N(CH_3)_2$ groups are conjugated to these positions. Thus, the n.m.r spectrum is consistent with the product structure shown in scheme 5.3.1.1.

The extensive conjugation of the molecule was shown clearly by the fact that it was coloured and the colour was pH dependent. At pH 7.4 the spectrum showed a single peak at 570 nm, whereas at pH 5.2 two visible absorptions peaks were observed (λ_{max} 456 nm; λ_{max} 604 nm) with the maximum occurring at 604 nm (Figure 5.4.1.2). The structural changes giving rise to these spectral changes are summarised in Scheme 5.3.2.1.

Figure 5.4.1.1 The n.m.r. of dDMP

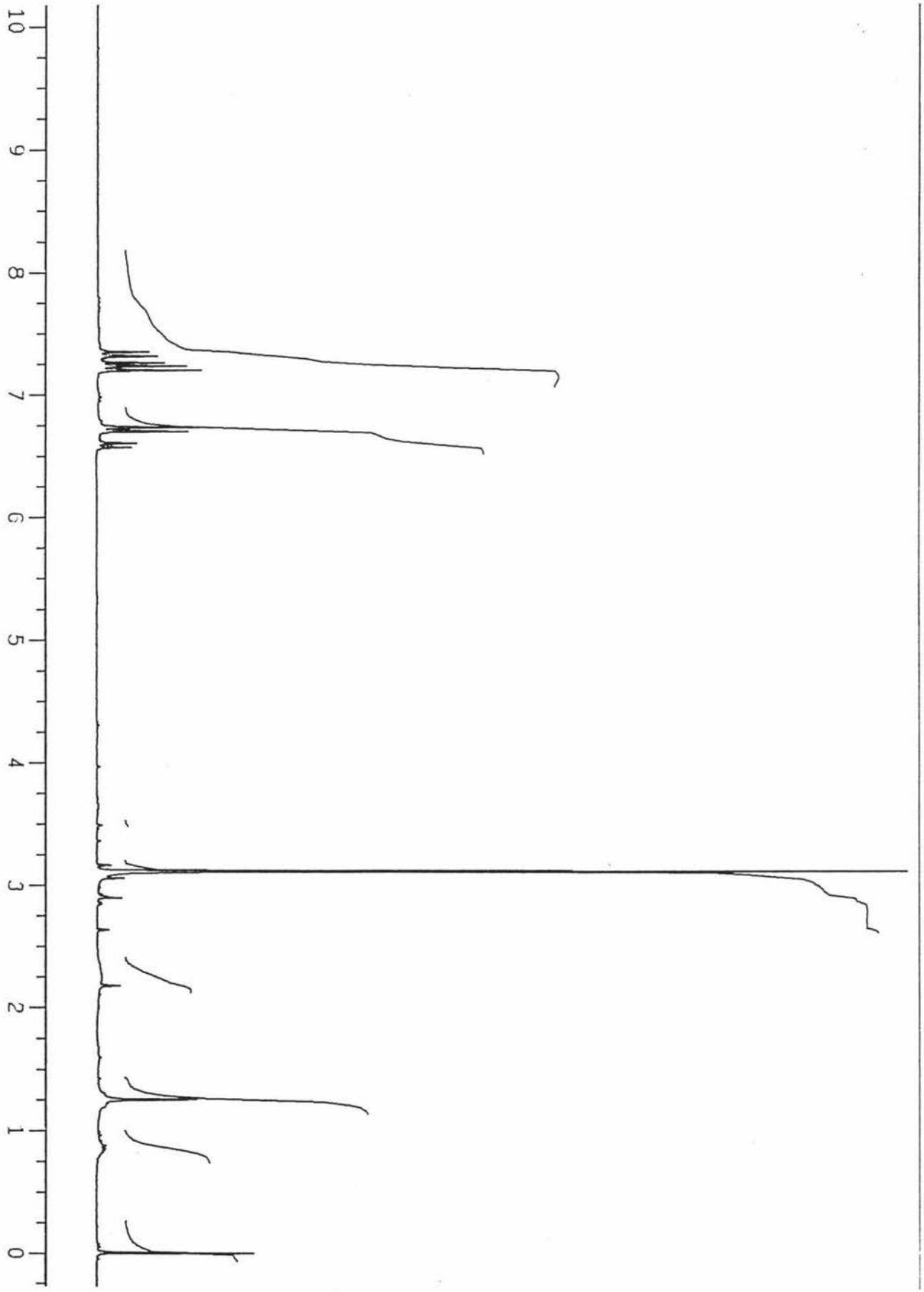

Figure 5.4.1.2. The visible absorption spectra of dDMP (visually crimson) is shown at pH 7.4 and DMP (visually green) is shown at pH 5.2.

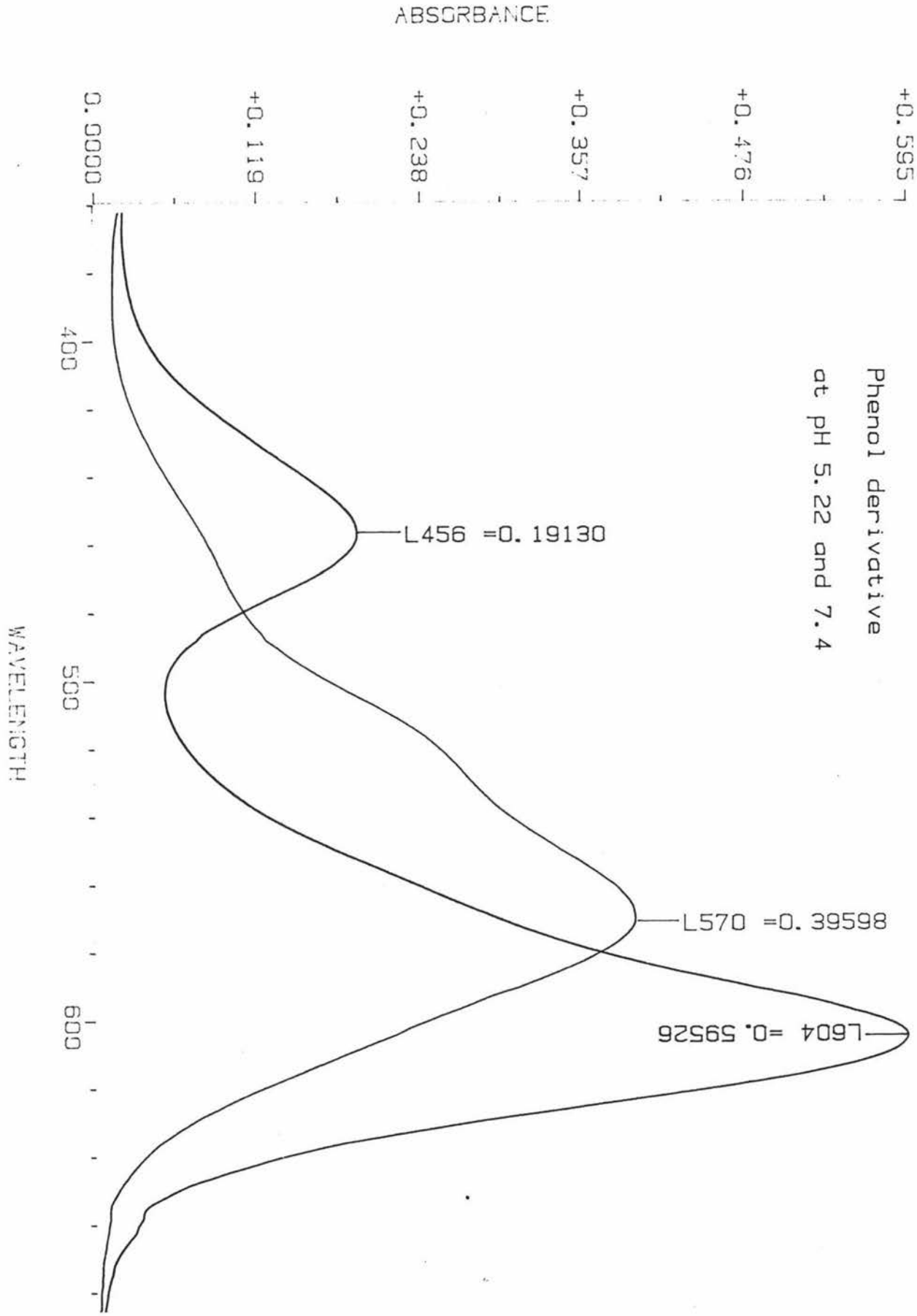

5.4.2 Synthesis of DMPE

DMPE was successfully synthesised as described in methods (section 5.3.2). A yield for the product DMPE was not recorded because the purification method using the ion exchange column gave yields which were greater than 100 % due to the co-elution of sodium acetate from the ion exchange column. The mass spectrum of DMPE (Figure 5.4.2.2) was consistent with the assigned structure with a $M^+ = 388$ compared with an expected value of 387.5. Other assignments are 344 = (M^+ - $N(CH_3)_2$); 329 = (M+ - $OCOCH_3$); 267 = (M^+ - $C_6H_5N(CH_3)_2$); 253 = (M+ - $C_6H_5OCOCH_3$). Both DMPE and DMP were pure as shown by t.l.c. (Figure 5.4.2.1).

Figure 5.4.2.1 is a t.l.c. of purified DMPE (r.f. 0.47) on the left and DMP (r.f. 0.58) on the right. The solvent used was 1 : 1, methanol : ethanoic acid.The ethanoic acid was dried off prior to taking the photograph so that the colour of the two species would appear different.

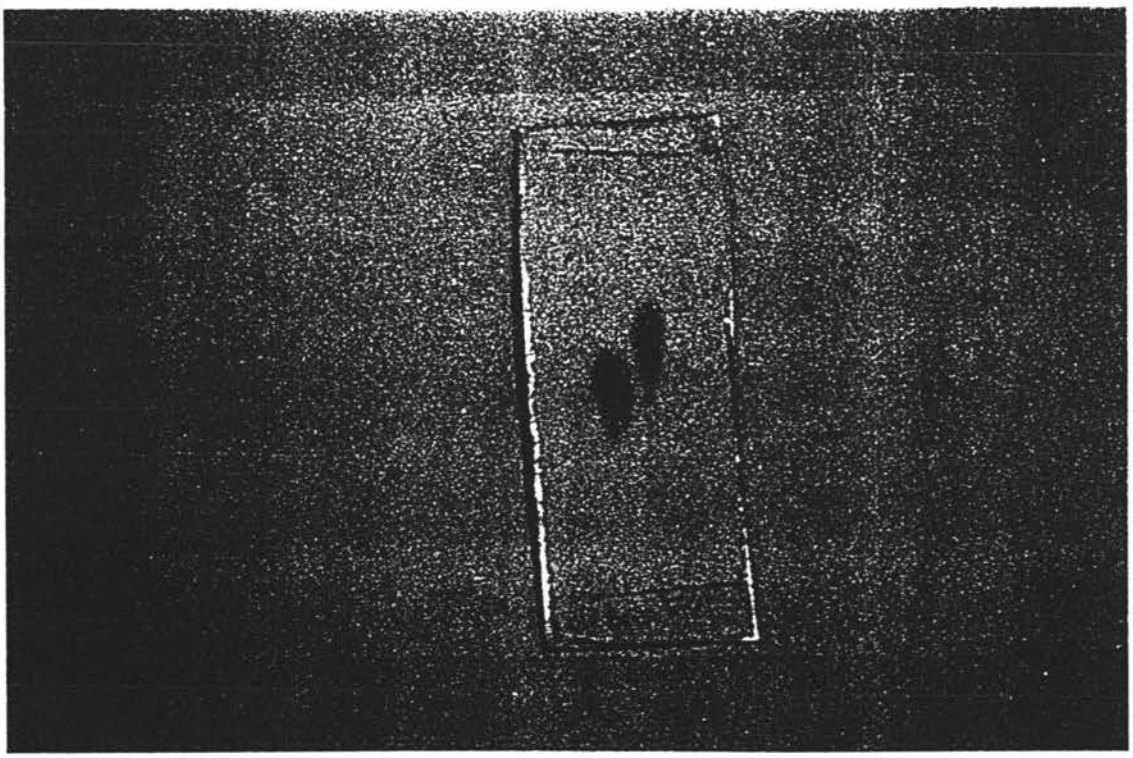

Figure 5.4.2.2 Mass Spectrum of DMPE

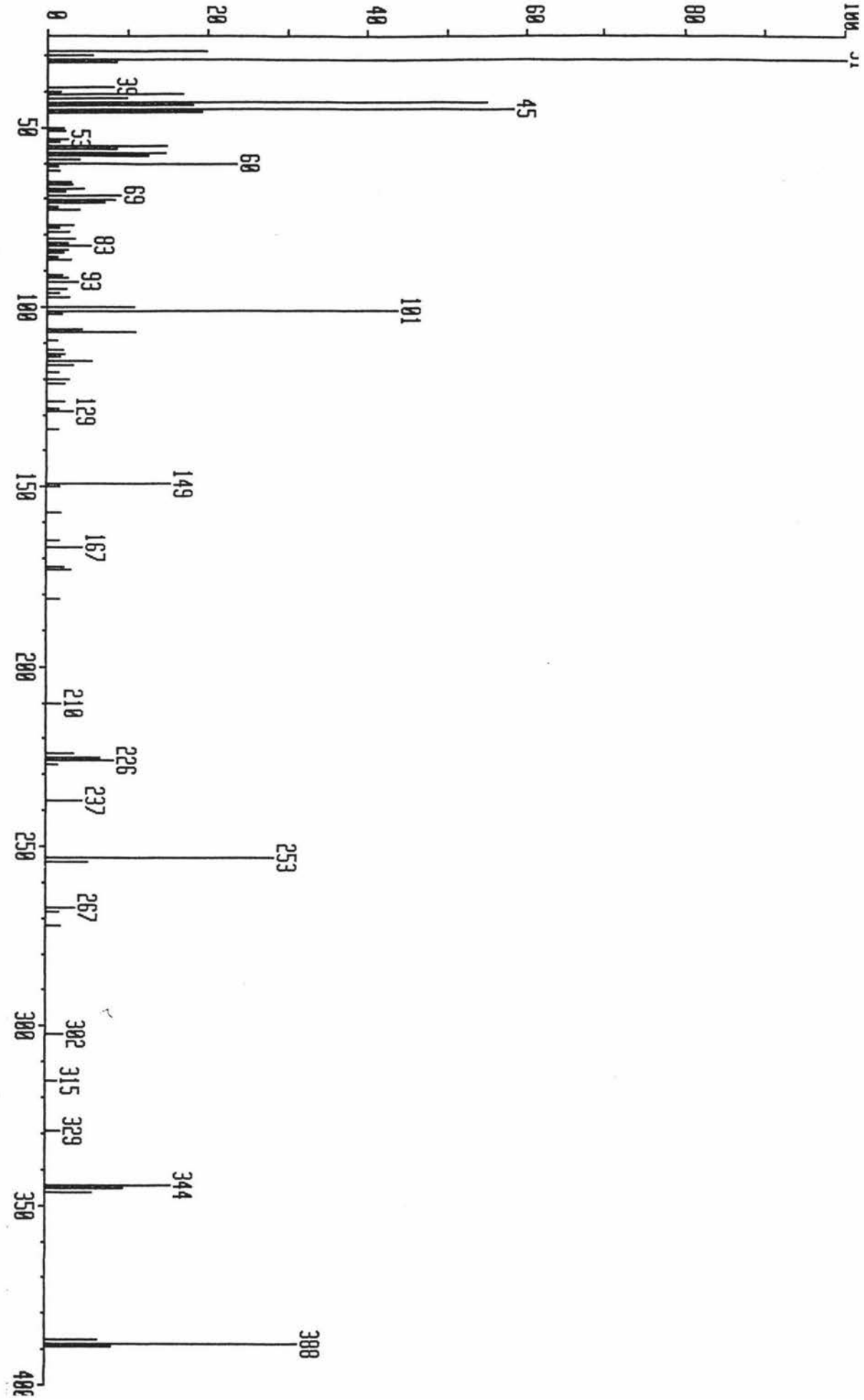

The most important feature of DMPE from the point of view of its possible use as a substrate in enzyme immuno assays is it's u.v./visible absorption spectrum. Figure 5.4.2.3 shows the visible absorption spectrum of DMPE in pH 9.3 pyrophosphate buffer (50 mM). The absorption maximum for the ester (DMPE) was at 620 nm with minor peaks at 428 nm and 318 nm.

Figure 5.4.2.3 DMPE pH 9.3 pyrophosphate buffer (50 mM)

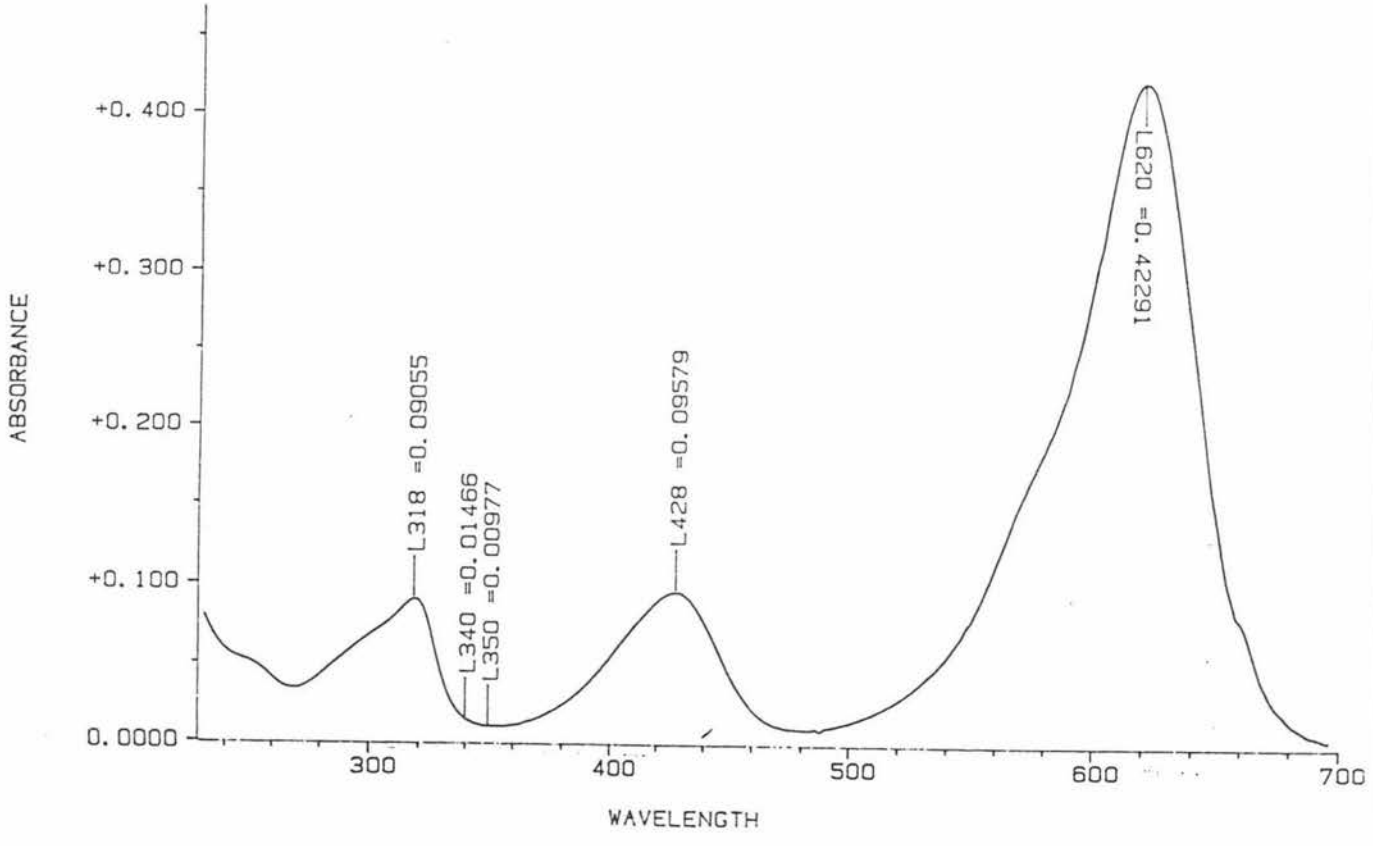

Figure 5.4.2.4 shows the product of hydrolysis of DMPE (dDMP) with porcine esterase at pH 9.3. The product of the enzymatic hydrolysis has an absorption maximum at 566 nm (pH 9.3), 54 nm blue-shifted from DMPE.

Figure 5.4.2.4 DMPE that has been hydrolysed with porcine esterase at pH 9.3

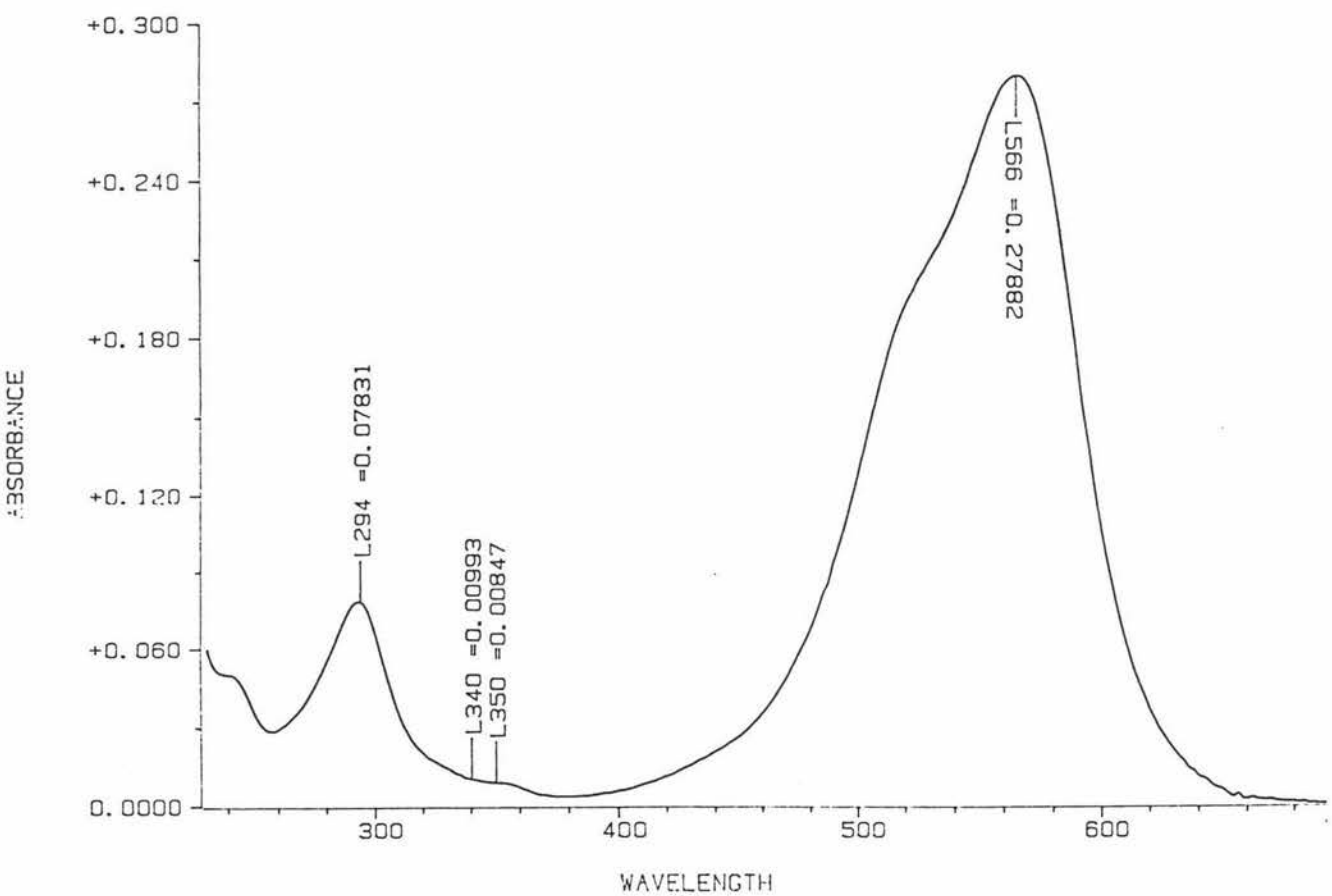

Figure 5.4.2.5 shows the visible absorption spectral changes during the hydrolysis of DMPE in pH 9.3 pyrophosphate buffer using porcine esterase. Inflexion points are found at 302 nm, 350 nm, 454 nm, and 588 nm. During the hydrolysis of DMPE the colour changed during the reaction from green, to blue, to indigo, to purple, and finally to crimson.

Figure 5.4.2.5 Hydrolysis of DMPE

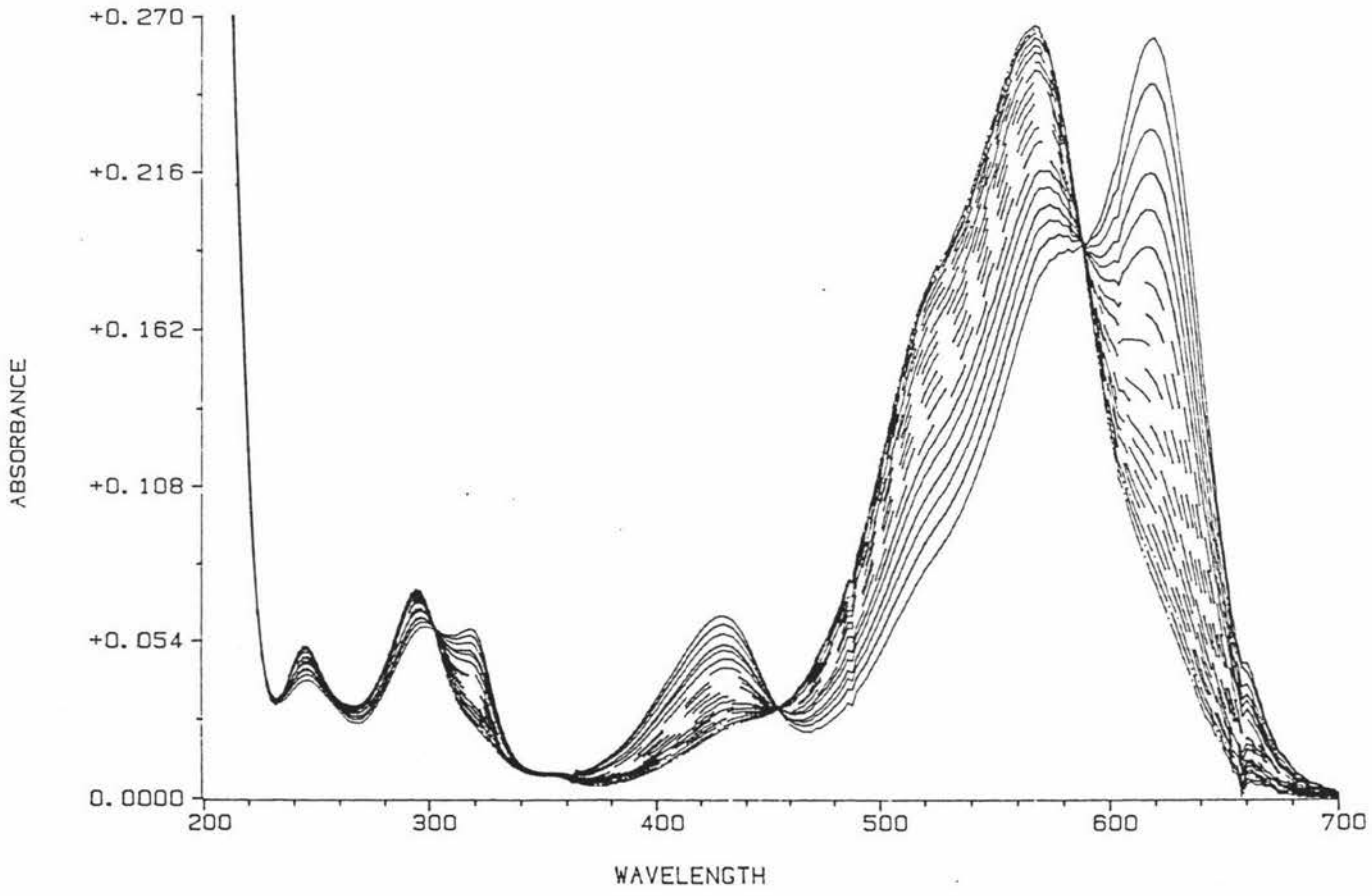

5.4.3 The comparison of the spectral properties of DMPE with other structurally related compounds

The spectral properties of DMPE are shown with comparison with other related chromophores in Table 5.4.3.1

Table 5.4.3.1 Spectral properties of tri-aryl carbonium dyes

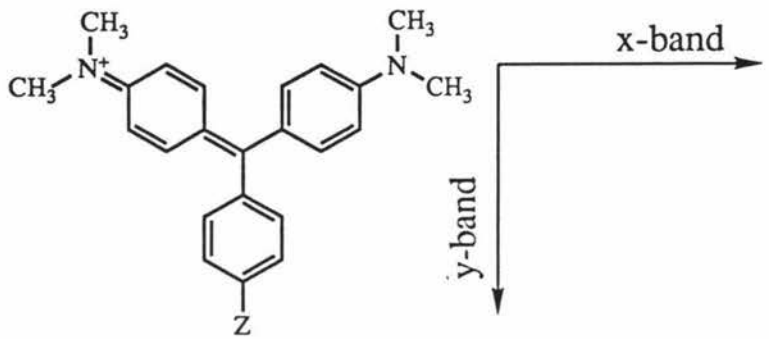

substituent (z)	x-band λmax	εmax	y-band λmax	εmax
O-	566	___	___	___
NMe2 *	589	117000	___	___
OH	604	___	456	___
OMe *	608	107000	465	33900
OCOCH3	620	___	428	___
H *	621	104000	427.5	20000
CN *	643	87100	429	15900
NO2 *	645	83200	425	17000

*Taken from Gorden and Gregory

By examination of Table 5.4.3.1 it can be seen that the x-band λmax increases with increasing electron donating ability of the substituent group on the chromophore; the y-band in general shows this same behaviour but not as well. For DMPE the ethanoate group has a similar effect on the spectral properties of the chromophore as a hydrogen atom

does. Hence the ethanoate group like a hydrogen must be neither very electron withdrawing or very electron donating. By way of contrast the negatively charged oxygen of dDMP must be even more electron donating than a N,N-dimethylamino group.

An accurate extinction coefficient of DMPE could not be determined because of the added mass of sodium acetate in the preparation procedure. Hence an extinction coefficient of 105000 was assumed (at 620 nm) in later calculations.

5.4.4 Measurement of the rate of hydrolysis of DMPE with rabbit liver esterase and porcine liver esterase.

DMPE was examined as a substrate for both rabbit and porcine esterase's. The kinetic rates were measured at the less sensitive absorption maximum (to keep the Abs<1) at 428 nm and then related back to maximum sensitivity at 622 nm. The results are shown in Table 5.4.4.1. The calculated rate at 622 nm was equal to 5.7 times the measured rate at pH 7.4 and 5.0 times at pH 9.3. These factors were determined by comparing the measured rate of decrease at 428 and 622 nm for a single assay at the appropriate pH.

Table 5.4.4.1 Measurement of k_{cat} for porcine esterase and rabbit esterase

Assay solution	measured rate at 428 nm	calculated rate at 622 nm	calculated k_{cat} with 30 μM DMPE (s^{-1})
porcine esterase 15 nm, pH 7.4	2.217×10^{-3}	1.264×10^{-2}	8.0
rabbit esterase 100 nm, pH 7.4	8.306×10^{-5}	4.735×10^{-4}	0.04
phosphate buffer pH 7.4	6.358×10^{-6}	3.624×10^{-5}	____
porcine esterase 15 nm, pH 9.3	1.906×10^{-2}	9.532×10^{-2}	60.5
pyrophosphate buffer pH 9.3	2.305×10^{-4}	1.150×10^{-3}	____

$\Delta\varepsilon^{622}$ was taken as 105000
These results are discussed in section 5.4.9

5.4.5 Measurement of the rate of hydrolysis of DMPE with ALDH

ALDH is known to catalyse the hydrolysis of unstable esters such as 4-nitrophenyl ethanoate (MacGibbon, thesis). Hence it was of interest to investigate the DMPE esterase activity of ALDH. In Figure 5.4.5.1 the DMPE concentration dependence of the esterase activity has been represented using a Lineweaver-Burk plot.

Figure 5.4.5.1 Lineweaver-Burk plot of DMPE esterase activity of ALDH at pH 7.4.

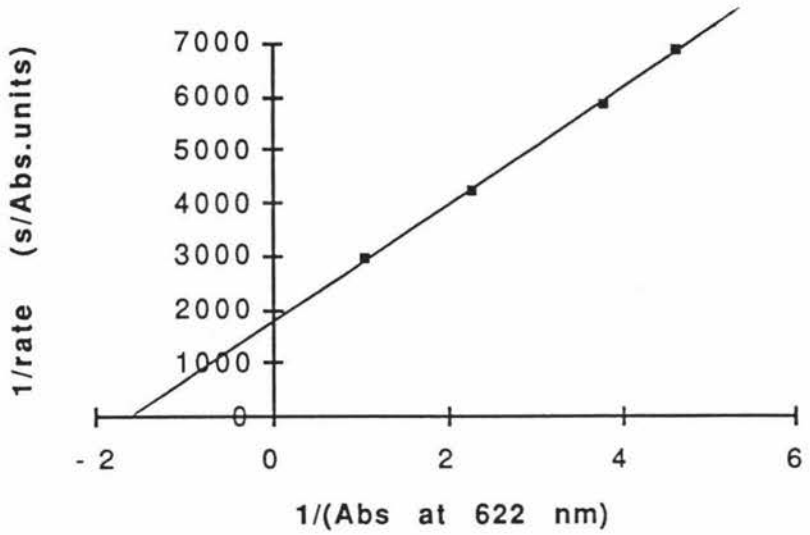

The reaction obeys Michaelis Menten kinetics with a saturating k_{cat} value of $\approx 2.5\ s^{-1}$ and a K_m value of $\approx 15\ \mu M$. At a DMPE concentration of 30 μM the apparent k_{cat} was $\approx 1.7\ s^{-1}$. Note the pathlength was 4.1 mm. These values were calculated using the linear regression function in the computer application "ENZ-FIT".

5.4.6 Inhibition of the DMPE esterase reaction by ALDH 4-trans (N,N-dimethylamino) cinnamoyl - cysteine moiety.

Since DMPE is a good esterase substrate for ALDH the question may be asked whether the formation of an ALDH-acyl intermediate (of the aldehyde dehydrogenase activity) is an inhibitor of the DMPE esterase activity. In this experiment the quasi-stable acyl-enzyme species of DACA was formed (at pH 7.4), then DMPE was added. The rate of formation of dDMP was then spectrally observed (Figure 5.3.6.1). Because of the mixing time it was not possible to measure the esterase activity at zero time. However it would appear by extrapolation that the ALDH 4-trans (N,N-dimethylamino) cinnamoyl - cysteine moiety is initially almost totally inhibitory of the esterase activity. After 1 minute the esterase activity rose to a steady rate of approximately 6 % of its uninhibited activity (Figure 5.4.6.1). **Note: In the absence of NAD,**

DACA is a poor inhibitor of the DMPE esterase activity of aldehyde dehydrogenase.

Figure 5.4.6.1 Inhibition of the esterase reaction by ALDH 4-trans (N,N-dimethylamino) cinnamoyl - cysteine moiety

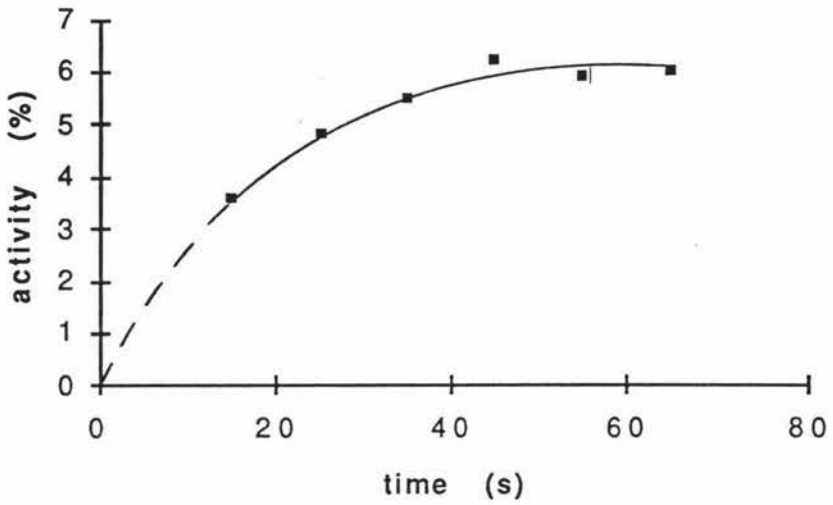

After the addition of DACA and NAD nearly all of the active site cysteines of the ALDH are rapidly acylated, since initially there is no competition from the ester. Subsequent addition of the ester competes with DACA for the active sites as they become available. Since it takes nearly one minute to reach an equilibrium, it is almost certain that hydrolysis of the ALDH 4-trans (N,N-dimethylamino) cinnamoyl - cysteine moiety is limiting at physiological pH. Thus, either both the esterase reaction and the dehydrogenase reaction utilise the same active site, or both reactions occur in a similar region of the enzyme, so that mutual steric inhibition occurs.

5.4.7 Long term stability of DMPE

In solution DMPE gradually hydrolyses over time because DMPE is a reactive unstable ester. Figure 5.4.7.1 shows the spectral changes in purified DMPE after 7 months in the ion exchange column elution solution at 4 C (the measurement was made in phosphate pH 7.4), by comparison with the initial spectrum (Figure 5.4.2.3) some hydrolysis

has occurred (note the larger absorption from 480 nm to 540 nm), however it is clear that the ester is still mostly unhydrolysed. The visual colour in phosphate buffer pH 7.4 had changed from green to blue.

Stability when absorbed on the solid phase has not yet been studied, but the ester was inadvertently spilled onto cloth making a green stain. It was thought that the green stain would gradually change to a crimson stain, however, after 7 months the green stain was still green, indicating that the rate of hydrolysis is slower in the absence of water.

Figure 5.4.7.1 DMPE after 7 months in solution

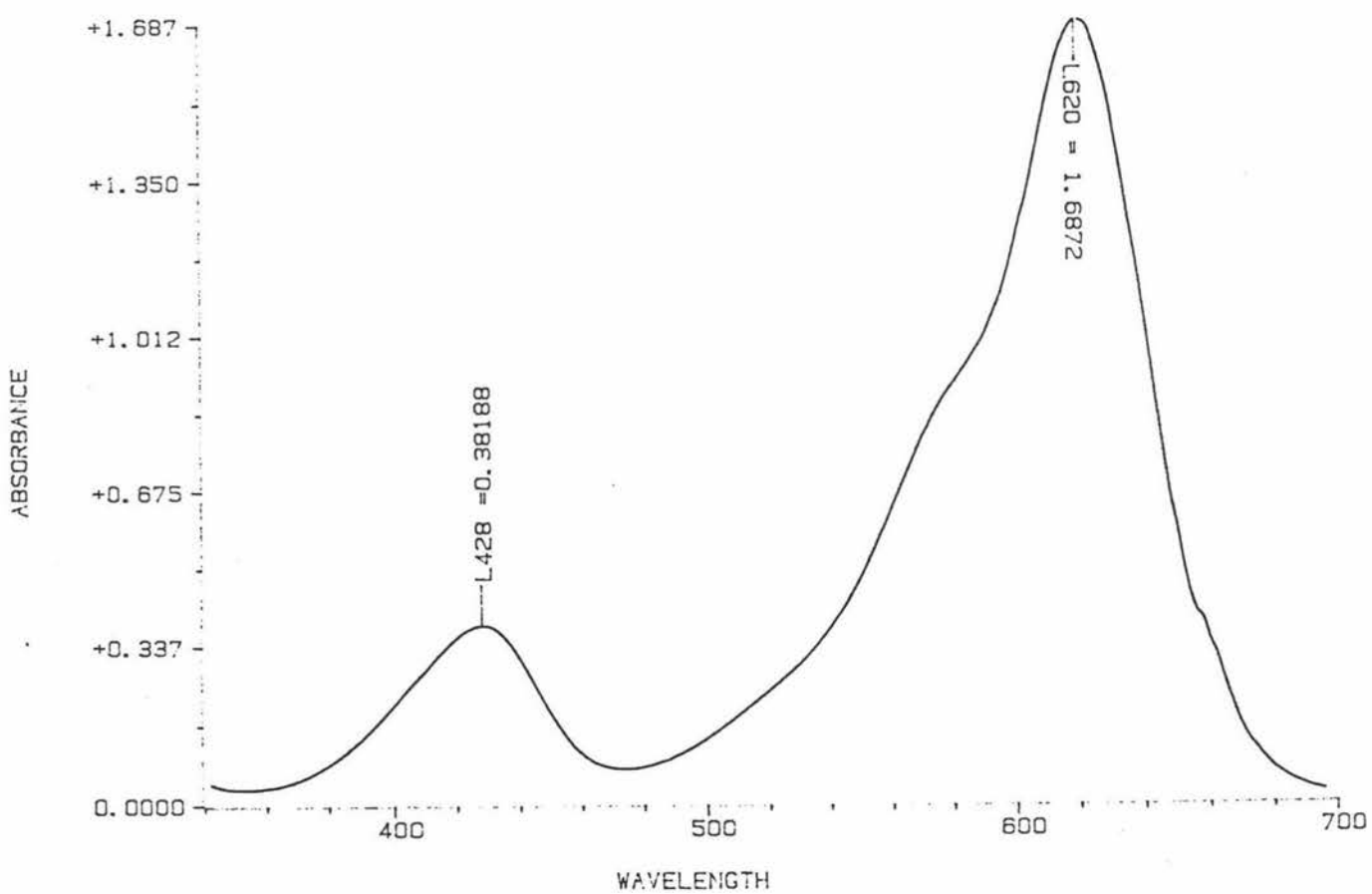

5.4.8 Safety of DMPE

DMPE is derived from a similar basic structure to C.I Food Green 3, shown in Figure 5.4.8.1.

Figure 5.4.8.1

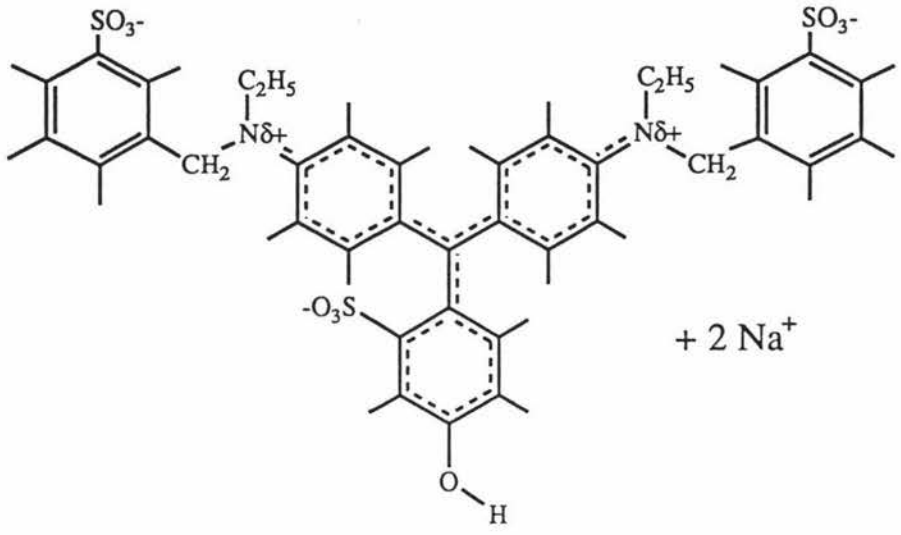

It was hoped that the substrate DMPE and the product dDMP would have the same low toxicity that is characteristic of many of the tri-aryl carbonium dyes such as C.I Food Green 3.

C.I. Food Green 3 was not used as a starting material to make an acylated C.I. Food Green 3 because of the sulphonate group meta to the phenolic oxygen. The presence of the sulphonate group twists the plane of the aromatic ring relative to the rest of the conjugated system, reducing the effect of any changes in the phenolic ring on the whole conjugated system. In other words if the ester of C.I. Food Green 3 was used, the visual colour of the product of hydrolysis (i.e. base form of C.I. Food Green 3) is blue, hence the visual colour change on hydrolysis would only be from green to blue, which is visually less sensitive to the eye than green to crimson.

5.4.9 Potential of DMPE in homogenous enzyme immunoassays

DMPE certainly has the potential to be a very sensitive substrate, as can be seen by comparing the activity of porcine esterase with a known assay utilising lysozyme. Hen egg white lysozyme (24 nm) when lysing micrococcus cells (0.21 $mg.ml^{-1}$) produces an absorption change of 0.6 in twenty minutes using a 1 cm path length. Porcine esterase (24 nm) can hydrolyse DMPE (30 μM) at pH 9.3 producing the same absorption change at 622 nm in 3.9 seconds. The non-catalytic reaction rate under these conditions is 0.7 % of the porcine esterase catalysed rate.

DMPE also has the versatility of being able to visually quantify the reaction rate according to the colour. Once an enzyme immunoassay has been initiated, the colour that has developed after a set time can be compared to a colour series chart, and hence related to the approximate rate and the analyte concentration.

Another encouraging feature is that rabbit esterase had very poor DMPE activity (200 times less than porcine esterase). Rabbit esterase normally has very good esterase activity, which is similar to the activity of porcine esterase. The fact that the DMPE activity of rabbit esterase is very poor suggests that DMPE is too bulky to gain access to the active site of the rabbit enzyme. As was mentioned earlier the substrate must be bulky if the anti-hapten (antibody) is to have the best the chance of occluding the substrate from access to the active site. If even more bulkiness is required then it is relatively easy to attach more groups which will increase the size of the substrate still further (e.g. similar to C.I. Food Green 3).

The next stage in the development of this project is to investigate enzymes which have known 4-nitrophenyl ethanoate esterase activity and test them for DMPE esterase activity. There are a very large number of enzymes which have been reported in the literature with 4-nitrophenyl ethanoate esterase activity. To the enzymes with good DMPE esterase activity a hapten can be attached and with these enzyme-hapten conjugates measure the activity with and without the presence of

anti-hapten antibody. In addition to this there is a crystal structure library facility available on the network. It has been suggested (L.F. Blackwell, personal communication) that a search for enzymes that have a lysine residue (for the purpose of conjugation) near the active site might prove beneficial in the choice of appropriate enzymes for use in homogeneous enzyme immunoassays.

5.5 Conclusion

A bulky substrate was designed, for which the formation of the product should be catalysable by many enzymes. The reaction is very sensitive and may be monitored either visually or with a spectrophotometer. The substrate and product are likely to have similar low toxicity like many of the related tri-aryl carbonium dyes. The stability of the substrate appears acceptable for the function for which it was designed.

Chapter 6

ALDH as biological model for the effects of electromagnetic fields

6.1 Introduction

For some years there has been concern about the effects of non-ionizing electromagnetic radiation on biological systems, however historically popular opinion of many in the science community has maintained that such radiation is harmless. Unfortunately this opinion had been largely devoid of scientific data.

Due to the prompting of some of the more recent studies which indicated health risks associated with electromagnetic radiation, several countries have now undertaken to review the evidence. In 1990 the British National Radiation Board appointed Sir Richard Doll, the eminent scientist who established the link between smoking and cancer, to chair the committee on electromagnetic fields. His report, published in 1992, concluded that there was no firm evidence of a health hazard (Consumer, 13 July 94).

However, just last year Sir Richard Doll was quoted (Consumer, 13 July 94) as saying: **"Two years ago I would have said that I am pretty confident that there really isn't any association. Now I'm not confident of that at all. I think there is a possibility that there is, and we must therefore investigate it very urgently"**. This turn-around typifies the recent change in the attitude of the science community regarding this issue. Much of the difficulty in determining whether or not effects of electromagnetic radiation are significant, is that many of the studies were done on people. For example, Goldhaber et al. (1988) reported a 100 % increase in miscarriages (sample size 1593) was found for VDU operators when compared with non-working pregnant women (sample size 1593). However one wonders how much of this is due to added stress from working, or could it be due to the posture of the VDU operator, or differences in eating habits? Despite these difficulties, the

sheer multitude of recent reports have raised a lot of concern, particularily those reports showing effects on the cellular level for which control experiments are much more certain.

In the past electromagnetic radiation public safety levels were based on macroscopic thermal effects. In other words, the amount of electromagnetic radiation that a person could be exposed to before they start cooking. The United States National Academy of Sciences, National Research Council, which now accepts non-thermal effects stated that "Abundant fragmentary evidence has been presented in support of possible biological effects from non-ionizing radiation, at both transmission and microwave frequencies. These effects often appear to be unaccompanied by macroscopic thermal changes."

Many of these effects have been recently reported in journals such as 'Bioelectromagnetics' and 'The Journal of Bioelectricity'. There are also many books written on the subject (see reference section). By way of contrast, many physiotherapists claim beneficial effects of electromagnetic fields on health. Hence, magnetic field therapy is a common physiotheraputic technique and is funded in New Zealand by the Accident Compensation Corporation.

Despite the multitude of these reported effects, the mechanisms by which these reputed effects occur are not clear. Many of the studies have been done on complex physiological systems (such as humans, plants, or cells). In 1991 Lednev proposed a mechanism (ion parametric resonance) for the effects of magnetic fields on charged particles (e.g. Ca^{2+}) bound to macromolecules such as proteins. In this theory ion binding to proteins is influenced by a combination of aligned d.c. and a.c. magnetic fields, via a perturbation of the vibrational energy levels of the ion. A modified version of this theory was published in mid 1994 by Blackman & Blanchard.

To investigate these theories, ALDH was used as a model biological system. ALDH is an ideal biological system for investigating these theories because the catalytic activity is influenced by the binding of metal ions such as Ca^{2+} (see chapter 3). It was anticipated that by

studying a relatively simple system, further insight into the effects of magnetic fields on complex physiological processes would be gained.

6.1 Methods

A geographical site was found which was sufficiently separated from iron-containing objects (such as steel reinforced buildings) that the distortion of Earth's magnetic field was minimal. A three person tent was then erected under a willow tree, using the tree as the support for the tent The tent had aluminium poles and plastic pegs.

A Shimardzu u.v.160 spectrophotometer was placed in one corner and in the diagonally opposite corner a thermally insulated container was placed. At opposite ends of the thermally insulated container there were two Hewlett Packhard spectrophotometer cell holders which had the ferromagnetic components replaced with non-ferromagnetic components.

Arranged spacially around (but not in contact with) one of the cell holders were two coils in a 'Helmholtz' configuration, with the cell holder located in the centre of the coils. The coils were directed parallel to Earth's magnetic field. A thermocouple was used to monitor the temperature in the thermally insulated container and spot checks were also done on the sample holders as well. The coils themselves produce negligible heating effects when active because they are only 2 mW, i.e. 0.002 % the power output of a standard 100 W lightbulb. A function generator was used to power the coils and two multimeters were used to monitor the frequency and the current in the coils.

The first experiment was done during November 1993. The assay conditions were as follows:

Buffer	= 50 mM sodium ethanoate, pH 5.22
ALDH	= 62 nM, final active site concentration
NAD	= 1 mM, final concentration
Ca^{2+}	= 600 μM, final concentration
propanal	= 20 mM, final concentration

The reaction was initiated by the addition of propanal. The total volume was 6 ml.

The second experiment was done during December 1994. The assay conditions were as follows:

Buffer	= 50 mM sodium ethanoate, pH 5.22
ALDH	= 19.2 nM, final active site concentration
NAD	= 0.5 mM, final concentration)
Ca^{2+}	= 600 μM, final concentration
propanal	= 20 mM, final concentration

The reaction was initiated by the addition of propanal. The total volume was 6 ml.

Each assay solution was divided (after mixing) into two unused 4 ml plastic cuvettes. Both cuvettes were then placed in the spectrophotometer and blanked relative to each other. After this, they were rapidly transferred to the cuvette holders in the thermally insulated container. When 15 minutes had elasped the samples were transferred back to the spectrophotometer, with each cuvette being placed into same holder of the spectrophotometer from which it came. The absorption difference was then recorded.

To correct for any bias in the spectrophotometer, the cuvette that was placed in the coils was alternated with each repetition of the assay. In other words, in the first assay the cuvette from holder 1 of the spectrophotometer was placed in the coils and in the next assay the cuvette from holder 2 of the spectrophotometer was placed in the coils and so forth.

6.3 Results and Discussion

In our original experiment in November 1993 the Lednev theory was tested. The basics of this theory suggest that the combined interaction of aligned a.c. and d.c fields can perturb the vibration energy levels of a charged particle. The probability (p) of ion transition from an excited vibrational state to the (ground) vibrational state is shown below.

$$p = A_1^2 + A_2^2 + 2A_1A_2(-1)^n J_n(nB_{ac}/B_{dc})$$

$$= K_1 + 2K_2(-1)^n J_n(nB_{ac}/B_{dc}) \quad \text{since } A_1 \text{ and } A_2 \text{ are constants}$$

B_{ac} is the applied a.c. magnetic field amplitude
B_{dc} is Earth's d.c. magnetic field
J_n is the 'Bessel' function of order n
$n=f_c/f_{ac}$

where f_c is the characteristic frequency for the ion and f_{ac} is the applied a.c. frequency of the coils. Note : $f_c = (q. B_{dc}/m)$ where 'q' is the charge on the ion and 'm' is the mass of the ion (f_c for $^{40}Ca^{2+}$ = 43.0 Hz).

In chapter 3 it was shown that the binding of Ca^{2+} dramatically affected the activity of ALDH. The Lednev theory predicted an increase in the Ca^{2+} binding via an increase in the probability of transition from an excited vibrational state to the ground. In the experiments the activity of two identical samples, one placed within an a.c. magnetic field and the other separated from the a.c. field (the reference) were compared. In the absence of an a.c. field the probability of an ion vibrational transition is:

$$p = K_1 \qquad \text{when } B_{ac}=0$$

Hence by comparing with a reference sample, only changes in the probability 'p', which are due to the combined effects of the a.c. and d.c. fields are observed. Lednev's theory was tested in November 1993 using conditions which should have resulted in a maximum decrease in 'p'. A decrease in 'p' would decrease the binding of Ca^{2+}, and hence an increase in enzyme activity should be observed.

The Blanchard and Blackman (B&B) theory was proposed in mid 1994. It was claimed by B & B that the original Lednev theory was mathematically incorrect. The B & B expression (shown below) is subtly different in that the factor 2 is included in the 'Bessel' expression rather than outside the Bessel expression as Lednev had proposed.

$$p = K_1 + K_2.(-1)^n.J_n(n.2.B_{ac}/B_{dc})$$

The B & B theory was tested in December 1994 using two conditions, one which should show a maximum increase in 'p' and the other which should show a maximum decrease in 'p'.

The results of the experiments investigating both Lednev's and B & B theories are summarised in Table 6.3.1.1

Table 6.3.1.1 Effects of parallel combinations of a.c. and d.c. magnetic fields on the activity of ALDH

Theory	peak field strength a.c (μT)	r.m.s current a.c. (mA)	frequency a.c. (Hz)	sample size	activity change (%) P=0.05
Lednev maximum decrease in p	101	31.4	43.2	5	0.4±0.9
B & B maximum decrease in p	50.3	15.8	43.0	7	2.4 ± 1.3
B & B maximum increase in p	43.3	13.6	21.5	10	5.3 ± 1.0

The observed changes in the activity were small. However because the experiments were a comparison of identical solutions with both in the same thermally insulated environment, small differences in activity could be confidently measured.

When using the conditions prescribed by the Lednev theory a null result was achieved, the change in the activity being 0.4 ± 0.9% (P=0.05). The B & B theory predicts that under these conditions a null result would be achieved. However, under the conditions prescribed by the B & B theory which predicted a maximum increase in 'p', hence a maximum decrease in the activity, it also failed in that increased activity was observed 5.3 ± 1.0 % (P=0.05). The B & B theory did do better using conditions for which a maximum decrease in 'p' was expected, with an observed 2.4 ± 1.3 % (P=0.05) increase in activity.

The theory proposed by B & B did fit their own experimental data on the effect of combined a.c. and d.c fields on the neutrite outgrowth of PC-12 cells. An example of this is shown in Figure 6.3.1.1

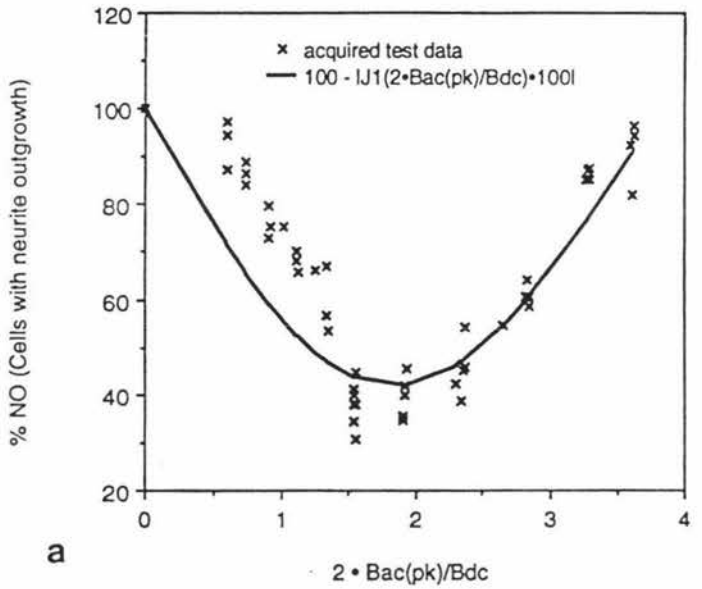

Figure 6.3.1.1 General fit of n=1 prediction of the IPR model to the experimental data (f_{ac}=45 Hz, B_{dc}=366mG, exposure time 23 hours).

Two important experimental outcomes that can be observed from the B & B results were that effects are exhibited in broad resonant patterns, requiring certain combinations of field strengths (B_{ac}/B_{dc}) and frequencies to interfere with the biological process. For ALDH this also appears to be true. It can be seen that the largest change in the activity was at 21.5 Hz. When the frequency was doubled the activity change was

approximately halved. When the ratio of fields (B_{ac}/B_{dc}, i.e. a.c. current doubled) was also doubled a null result was observed.

A difficulty in interpreting the B & B experimental results was that they claim the observed effects could have been related to any one of at least nine different cations. Certainly the B & B experimental data is very impressive, in that their proposed theory approximately fits the experimental data. However, since their introduction of this new theory, a number of other theoreticians (Engstrom and Pettis,1994 ; Polk and Wu, 1994) have examined the B & B and Lednev theories. In both cases these theoreticians support the Lednev theory as being mathematically correct and B & B theory as being mathematically incorrect. However, Engstrom and Pettis (1994) did acknowledge that the impressive experimental data by B & B could not be reconciled with the Lednev model.

This poses a problem, Lednev's theory is mathematically correct but has no experimental data in its support. The B& B theory is mathematically incorrect, but their own experimental data does fit their incorrect theory. Our experimental work supports neither theory.

Another possibility for the increased activity, might be related to the protein rather than the Ca^{2+} metal ions. Enzymes have natural oscillations (conformational changes) and the rates of these natural oscillations is often associated with rate limiting processes in the enzymatic pathway. There seems to be a remarkable correlation between the frequencies that are reported in the literature and the process rates that are observed for many enzymes. B & B have suggested that alteration of the conformational changes **of the protein** might increase the rates of association or dissociation of metal ions. One step further in this proposition, would be to suggest that not only could these forces **on the protein** affect the rates of metal binding and dissociation but also other species (such as NADH). For ALDH the k_{cat} under these conditions is approximately 1.3 s^{-1}, hence if this hypothesis were correct a maximum change in the activity might be expected at a frequency slightly faster than the k_{cat} (i.e. 2 - 5 s^{-1}).

6.4 Conclusion

The preliminary outcomes of this study while not showing direct support for the ion parametric resonance theories, did indicate some small but statistically significant effects. At this stage little is known regarding the mechanisms by which magnetic fields interact with biological systems. However, with 23 years accumulation of detailed kinetic knowledge of aldehdye dehydrogenase, we are well positioned to give vital insight into this difficult and very controversial problem.

The future objective of the research here at Massey University, is to further the present studies with the purpose of finding conditions where a maximum change in ALDH activity is observed. In particular we will be investigating the frequency range close to the k_{cat} of ALDH. The metal ion dependence of the activation associated with magnetic fields will also be examined.

Table of abreviations

abreviation	formal name
ALDH	Sheep liver cytosolic aldehyde dehydrogenase
NAD	β-nicotinamide adenine dinulcleotide
NADH	β-nicotinamide adenine dinulcleotide, reduced form
EDTA	ethylenediamine tetra acetic acid
VDU	vidio display unit
SDS	sodium dodecyl sulphate
EIA	enzyme immunoassay
A^{280}	Absorbance at 280 nm
DACA	4-*trans*-(N,N-dimethylamino) cinnamaldehyde
DMPE	4-((bis 4-N,N-dimethylaminophenyl) methylinium ethanoate) phenyl ethanoate
DMP	4-((bis 4-N,N-dimethylaminophenyl) methylinium ethanoate) phenol
dDMP	deprotonated 4-((bis 4-N,N-dimethylaminophenyl) methylinium ethanoate) phenol

References

Angelis C.T., Dunn M.F., Muchmore D.C. and Wing R.M. (1977) *Biochemistry*, **16**, No. 13, 2922 - 2931

Bennett A.F. (1981) Thesis, M.Sc., Massey University

Bernhard S.A., Lau S.J. and Noller H. (June, 1965) *Biochemistry*, **4**, No. 6, 1108 - 1118

Biesecker et al. (1977) *Nature, Lond.*, **266**, 328

Blackwell L.F., Motion R.L., MacGibbon A.K.H., Hardman M.J. and Buckley P.D. (1987) *Biochemical J.*, **242**, 803 - 808

Blanchard and Blackman (1994) *Bioelectromagnetics*, **15**, 217 - 238

Blatter E.E., Abriola D.P. and Pietruszko R. (1992) *Biochemical J.*, **282**, 353 - 360

Breaux E. J. and Myron L.B. (1976) *Biochemical and Biophysical Research Communications*, **70**, No. 1, 235 - 240

Brown J.B., Blackwell L.F., Holmes J. and Symth K. (1989) *Int. J. Gynecol. Obstet.*, **suppl. 1**, 111-122.

Buckley P.D. and Dunn M.F. (1982) *Enzymology of Carbonyl Metabolism*, **1**, 23 - 35

Buckley P.D., Motion R.L., Blackwell L.F. and Hill J.P. (1990) *Enzymology of Carbonyl Metabolism*, **3**, 31 - 41

Crow K.E. (1975) Thesis, Ph.D., Massey University

Crow K.E. and Hardman M.J. (1989) *Human metabolism of alcohol*, **2**, 3 - 12

Dietrich H., Maret W., Kozlowski H. and Zeppezauer M. (1981) *J. Inorganic Biochemistry*, **14**, 297 - 311

Dickinson M.F., (1986) *Biochemical J.*, **238**, 75 - 82

Dunn M.F. and Buckley P.D. (1985) *Enzymology of Carbonyl Metabolism*, **2**, 15 - 27

Henrotte et al. (March 1990) *Proc. Natl. Acad. Sci. USA*, **87**, 1894-1898

Hinkle et al. (1970) *Biochemistry*, **9**, No. 24, 4636

Kitson T.M. (1989) *Biochemical J.*, **257**, 585 - 590

Kitson T.M. (1989) *Human metabolism of alcohol*, **2**, 117 - 129

Kitson T.M., Hill J.P. and Midwinter G.G. (1991) *Biochemical J.*, **275**, 207 - 210

Konig W., Schramek W. and Rosch G. (1928) *Chemische Berichte*, **61**, 2074 - 2080

Lednev V.V. (1991) *Bioelectromagnetics*, **12**, 71 - 75

MacGibbon A.K.H (1976) Thesis, Ph.D., Massey University

MacGibbon A.K.H., Buckley P.D. and Blackwell L.F. (1976) *Biochemical J.*, **165**, 455 - 462

Motion R.L. (1986) Thesis, Ph.D., Massey University

Plapp et al. (1978) *J. Mol. Biol.*, **122**, 23-32

Rubenstein K.E., Schneider R.S., and Ullman E.F. (1972) *Biochem. Biophy. Res. commun.*, **47**, 846

Schneider-Bernlohr H., Formicka-Kozlowska G., Buhler R., von Wartburg J. and Zeppezauer M. (1988) *Eur. J. Biochem*, **173**, 275 - 280

Sloan D.L., Young J.M. and Mildvan A.S. (1975) *Biochemistry*, 14, 1998

Weiner H. (1989) *Human metabolism of alcohol*, **2**, 147 - 160

Weiner H. et al. (1985) *Enzymology of Carbonyl Metabolism,* **2**

Wiberg K. (1955) *Chem. Revs.*, **55**, 713 -720

Yallow R.S. and Berson S.A (1959) *Nature*, **184**, 1648 -1649

The following textbooks are reference material (available at Massey) on the biological effects of electromagnetic fields.

Magnetic Fields : Health and Safety Guide' written by the World Health Organisation, in conjunction with the United Nations Environmental Programme and the International Radiation Protection Association (Geneva 1989).

Bioelectromagnetism : Principles and Applications of Bioelectric and Biomagnetic Fields (Oxford University Press, 1994).

Electromagnetic Interaction with Biological Systems (Pub. Plenum Press, 1989).

On the Nature of Electromagnetic Field Interactions with Biological Systems (Pub. Landes, 1994).

CRC Handbook of Biological Effects of Electromagnetic Fields (Pub. CRC press, 1986).

Biological Effects of Exposure to Non-ionising Electromagnetic Fields and Radiation (National Radiological Protection Board, U.K., 1991).

Emerging Electromagnetic Medicine (Spinger-Verlag, 1990)

Biological Effects and Medical Applications of Electromagnetic radiation (Pub. Prentice-Hall,1990)